Influence of alloying elements, testing solution and surface roughness on corrosion behaviour of stainless steel reinforcing bars

by

Ibrahim Ogunsanya

A thesis
presented to the University of Waterloo
in fulfilment of the
thesis requirement for the degree of
Doctor of Philosophy
in
Mechanical and Mechatronics Engineering

Waterloo, Ontario, Canada, 2019

Examining Committee Membership

The following served on the Examining Committee for this thesis. The decision of the Examining Committee is by majority vote.

Supervisor	Carolyn M. Hansson, PhD. Professor, Mechanical and Mechatronics Engineering, University of Waterloo
External Examiner	Burkan Isgor, PhD Professor, Civil and Construction Engineering, Oregon State University
Internal-External Examiner	Michael Fowler, PhD Professor, Chemical Engineering, University of Waterloo
Internal Examiner	Adrian Gerlich, PhD Professor, Mechanical and Mechatronics Engineering, University of Waterloo
Internal Examiner	Hamid Jahedmotlagh, PhD Professor, Mechanical and Mechatronics Engineering, University of Waterloo

Author’s Declaration

This thesis consists of material all of which I authored or co-authored (See attachment of contributions included in the thesis).

This is a true copy of the thesis, including any required final versions, as accepted by my examiners.

I understand that my thesis may be made electronically available to the public.

Statement of contributions

The following co-authors have contributed to the current work:

Professor Carolyn M. Hansson supervised all the work completed in this PhD thesis and provided both technical and editorial feedback in the preparation of the work.

Mr. Colin Van Niejenhuis performed equal amount of work in preparation of the first journal paper, “Analysis of pore solution of different cements with and without admixed chlorides” featured in this manuscript-based thesis. In the experimental work, Mr. Van Niejenhuis was involved in the casting of cement paste cylinders and expression of their pore solution. He also co-wrote and edited all sections in the first journal paper.

The balance of the research and published journals was carried out by the author. The link to the published journals in this work has been provided in a footnote of each chapter in the thesis.

Acknowledgement

It has taken the support of many to complete this degree and, I would like to express my appreciation to the cast who have, in one way or the other, contributed to this project. First, all praise to Allah for his grace and mercy and for bringing these amazing people my way.

I would like to thank Professor Carolyn M. Hansson for providing me an opportunity for a graduate school experience and for the supervision. She has not only provided me a career opportunity, but also tremendous mentoring. Prof. Hansson showed great enthusiasm towards my ideas and helped me maximize them. Under Prof. Hansson's supervision, I have earned MASc, PhD and unofficial English language degrees – the latter was the toughest!

I would also like thank my PhD examination committee members; Prof. Adrian Gerlich and Prof. Hamid Jahedmotlagh, both of whom were also my MASc. committee members, thank you very much! A big thank you to Prof. Michael Fowler and Prof. Burkan Isgor for their constructive contributions and comments.

I would like to appreciate colleagues who supported my graduate school work: Dr. Nermein Khattab, Victoria Strong, Timothy Bandura, Dr. Michael Benoit, Colin Van Niejenhuis, Leah Kristufek, Peter Loudfoot, Adam Felinczak, Marc Johnson. To the technicians that assisted in some aspect of this work: Mark Griffet, Yuquan Ding, Richard Morrison, Douglas Hirst, Peter Volcic, Joy Hu, thank you! I also appreciate the administrative work of the departmental and faculty staffs: Allison Walker, Connie Slaughter, Karen Schooley, Jian Zou.

This research would not be possible without the funding support provided by the Ministry of Transportation of Ontario (MTO), Ontario government (as Queen Elizabeth II Graduate Scholarship in Science and Technology (QEII-GSST)), University of Waterloo (as President's Graduate Scholarship (PGS)) and the Natural Sciences and Engineering Council of Canada (NSERC). The kind donations of steel reinforcing bars supplied from Harris Rebar, Contractors Materials Company (CMC) and Salit Specialty Rebar (SSR) and cement donation from Dufferin Cement are greatly appreciated.

To my wife Omobolanle Rukayat Ogunsanya, this would be not be possible without your love and support. The data entry you helped with, although grumbling sometimes, and the tremendous mental stability you provided are hugely appreciated. We agreed that we co-own both the thesis and degree and I love you so much. To my lovely kids, Adnan Dolapo Ogunsanya and Maryam Busayo Ogunsanya, both of whom taught me how to smile in difficult times, this is for you. We all own this achievement.

To my parent, Muniru Oriyomi Ogunsanya and Bilikisu Atilade Ogunsanya, I know you both are proud of me in this moment and I say a massive thank you for doing all you can to help me get here. To my siblings, Yusuf Ololade Ogunsanya, Munirat Abisola Ogunsanya, Jubril Kolapo Ogunsanya, Dare Rufai, I say a big thank you to you all for the support during these long years of my studies.

To myself, thank you for believing and hanging on in difficult moment. Remember, this is only an achievement, the dream is to make the world better.

To the readers of this thesis, I hope you'll enjoy this piece of work. I leave you with this Nigerian quote:

SUFFRI DO LIFE OOO, BECAUSE NA WHO FES BUY MOTOR, BUY OLD MODEL & NEW ARRIVAL FOR STORE TODAY, GO TURN SALES TOMORROW

Abstract

The province of Ontario has moved from applying rock salt crystals, predominantly impure sodium chloride, to locally available anti-icing brine solutions with chloride amounts as high as 21%. At the same time, the specified design service life of highway structures has increased from 50 years to 75 years. The exposure to aggressive chloride brines has increased the need for more corrosion resistant reinforcing bar (rebar) than the traditional carbon steel rebar. However, the high cost of many stainless steel rebar alloys made them a last resort when concrete reinforcement options are considered. A major factor for their high cost is the price of their major alloying elements. Therefore, the contributions of these elements towards passive film properties, pitting corrosion resistance, critical chloride threshold (C_{CRIT}) values and overall corrosion performance in the presence of deleterious species in concrete, such as chlorides, must be ascertained.

This research aimed to provide a critical evaluation of the various parameters affecting long term corrosion performance of different grades of stainless steel rebar in concrete exposed to anti-icing brines. The first step to achieving this was to determine the variation in pore solution compositions of different concrete mixes so that bars can be tested in a similar environment. To do this, cement pastes of varying admixed chloride content, cementitious materials and water-to-cementitious ratio (w/cm) were cast and their pore solutions were analyzed for ionic composition and pH. The results revealed increasing dissolution of sulphate ions with increasing admixed chloride ions in the pore solution. These actual solutions were used in subsequent assessment procedures involving electrochemical techniques such as Mott-Schottky analysis, potentiostatic linear and non-linear polarization resistance and cyclic potentiodynamic polarization techniques. The goal was to determine the passive film properties, pitting characteristics, critical chloride threshold (C_{CRIT}) and relative corrosion performance of carbon steel and five grades stainless steel rebar. Results showed the addition of sulphates to testing solutions suppressed the damage from chloride ions on steel passive films, by forming iron and nickel sulphides in passive films that provided additional protection. Results also showed that testing in lower pH solution, as done by many researchers, is conservative and underestimates corrosion resistance.

The influence of the expensive stainless steel alloying elements (Cr, Ni, Mo, Mn) on the corrosion parameters listed above were then investigated. Chromium significantly improved these properties by decreasing passive film defects and increasing C_{CRIT} values of the rebar. Molybdenum did not improve the corrosion resistance in the austenitic alloys but was beneficial in duplex alloys by concentrating in the ferritic component. Nickel was found to improve the outer layer of passive films properties by forming an Fe-Ni spinel, while manganese improved the inner passive layer.

It is necessary for these observations in corrosion behaviour of rebar to be consistent. Consequently, other factors potentially leading to variations in corrosion performance of stainless steel rebar alloys were examined. These included the influence of variability in composition, microstructure and surface roughness between batches of stainless steel alloys from different manufacturers, and results showed surface roughness to be the major and overwhelming factor in corrosion resistance.

The most important observation has been that, for the particular concrete mixture used in this research, the critical chloride threshold concentration, found by extrapolation of the experimental data, was greater than the solubility limit of chlorides in cement pores. This implies that chloride induced corrosion of the stainless alloys would not be possible in this concrete in the absence of cracks or major flaws.

Table of Contents

List of Figures

List of Tables

List of Equations

List of symbols/abbreviations/acronyms

Symbols/Abbr.	**Standard Units**	**Definitions**
ASTM		American Society for Testing and Materials
B		Tafel constant
CALPHAD		Calculation of phase diagram
C_H or C_{dl}	A.s/V	Double layer capacitance
C_{SC}		Capacitance of the space charge
CE		Counter electrode
C_{CRIT}		Critical chloride threshold
CH		Calcium hydroxide
CP		Cyclic polarization
E	V	Electrochemical potential
E_0	V	Electrochemical potential at standard state
E_{corr}	V	Corrosion potential
EDS		X-ray energy dispersive spectroscopy
EMF	V	Electromotive force
EIS		Electrochemical impedance spectroscopy
E_p	V	Passive potential
E_{pit}	V	Pitting potential
E/pH		Potential versus pH diagram
F	A.s/mol	Faraday's constant (96500)
FA		Fly ash
G	J	Gibbs free energy
GGBFS		Ground granulated blast furnace slag
HDL		Helmholtz double layer
I_{corr} (i_{corr})	A (A/m^2)	Corrosion current (corrosion current density)
LPR		Linear polarization resistance
M-S		Mott-Schottky
MTO		Ministry of Transportation of Ontario

OPC		Ordinary Portland cement
PS		Pore solution
PS+S		Pore solution with increasing sulphate
RE		Reference electrode
RST		Rapid screening test
R_p	Ω	Polarization resistance
R_Ω	Ω.m	Ohmic/solution/electrolyte resistance
SCE		Saturated calomel electrode
SCL		Space charge layer
SF		Silica fume
SHE		Standard hydrogen electrode
SPEIS		Staircase potentio electrochemical impedance spectroscopy
St. St.		Stainless steel
t	S	Time
T	K	Temperature
W	Ω.s-1/2	Warburg impedance
WE		Working electrode
w/c (w/cm)		Water to cement (water to cementitious) ratio
XRF		X-ray fluorescence
x	M	Length / distance / depth
ε		Permittivity
ε_0		Permittivity of free space
ϕ	(rad)	Phase shift
ω	l/s (in rad/s)	Angular frequency

1. Introduction

1.1. Background

The readily available raw materials, low cost and ease of forming at room temperature makes concrete one of the most widely used materials today. Concrete is weak in tension and, therefore, is usually reinforced with steel bars. Concrete is also a porous material, majorly because the cement particles hardens under water (i.e. hydration) to produce porous solid components [1]. The solution in these pores has a high pH (~12.5 – 13.8) that allows a protective film (passive film) to form on the most common rebar - plain carbon steel (commonly called black steel) [2]. However, chloride sprayed on concrete infrastructures during winter season or from marine environment, can migrate through these pores and, in sufficient quantities, break down the passive film formed on the steel, resulting in very high corrosion rates [2]. The corrosion products of carbon steel are expansive and cause tensile stresses in the concrete cover, eventually cracking and spalling of the concrete [2]. Consequently, corrosion of the reinforcing bars (rebar) in concrete exposed to de-icing salts and/or marine atmospheres is the major cause of deterioration of highway infrastructure, parking garages and marine structures [2].

It is economically beneficial for any active corrosion on steel reinforcement to be detected and remediation steps taken prior to the deterioration of their surrounding concrete and several companies have produced instruments to measure rebar corrosion non-destructively in the field (such as GalvaPulse®, Gecor®, iCOR®, etc.), with varying success [3]. Also, many laboratories have investigated the corrosion deterioration process of reinforced concrete. However, most laboratory tests are constrained by time of testing and the need for non-destructive testing. For example, there are two major limitation of testing rebar in non-cracked concrete [3]. The first is the time for diffusion of chlorides from the surrounding through the capillary pores in the concrete to the rebar in sufficient quantity to degrade the passive film. The second is underestimation of severity of corrosion from averaging the measured corrosion rates over the entire exposed area, thus assuming general corrosion, despite local passive film breakdown in some cases, as will be discussed later. The former limitation is typically remedied by adding chlorides to the mixing water (admixed chloride) during casting which significantly reduces the time to corrosion but no longer represents field conditions [4].

In order to observe the location and extent of corrosion, bars can also be tested in “simulated pore solution”, a solution of similar composition and pH as found in concrete pores. The bars are given time to form stable passive film before introducing chlorides to solution. Concrete pore solution compositions can be obtained by applying compressive loads to hardened cement pastes cast with known admixed chloride to express their solution, which is then analysed for ionic concentration and pH [5]. This ionic compositions and pH will vary with type of cement or cementitious materials (Portland cement, fly ash, silica fume, blast furnace slag), water-to-cementitious ratio, etc. used to make the cement paste [6]. Consequently, corrosion properties of any rebar are expected to vary from one ionic composition and pH to another and, unfortunately, this has not been taken into account in many corrosion tests.

One strategy to satisfy the Canadian Bridge Code design service life requirement of 75-100 years [7] is the use of more corrosion-resistant reinforcement. Over the last few decades, the superior corrosion performance of stainless steel rebar compared with that of carbon steel rebar is attributed to the more compact and adherent passive films formed on stainless steel alloys resulting from their higher alloying content. These passive films are semiconductors [8] and understanding their electronic properties can reveal the corrosion resistance properties of the steel. The Mott-Schottky (M-S) analysis [8] has been used in the present work to understand this electronic properties of different alloys. The electronic and electrochemical properties of these stainless steel bars must be translated to a more useful engineering parameter such as critical chloride threshold value, C_{CRIT}. The C_{CRIT} value of a bar is the chloride amount sufficient to initiate active corrosion on the steel and, it is an important input parameter to life cycle cost and service life analysis which helps the user to make decisions on choice of steel reinforcement, among other things. Unfortunately, values of this parameter reported in the literature vary significantly because they are dependent on a wide range of concrete and environmental factors, as well as on the method of testing. An assessment procedure involving potentiodynamic and potentiostatic polarization techniques has been further developed to investigate some of the variable affecting this parameter.

1.2. Objectives and innovation in approach and outcomes

The objective of this research was to provide a critical evaluation of the various parameters affecting the long term performance of different grades of stainless steel rebar in concrete exposed to de-icing salts. In order to achieve this objective, the research was conducted in the following sequence: (a) determination of concrete pore solution composition from different cement mixes and its impact on passivation of the steel; (b) evaluation of the influence of these compositional variations on passive films formed in the mixes and, hence, the critical chloride threshold values of the bars; (c) investigation of the role of the major stainless steel alloying elements (Cr, Ni, Mo, Mn) on electronic structure and electrochemical properties of passive films formed and the critical chloride threshold of bars in the highly alkaline environment in concrete; (d) assessment of influence of variation in microstructure, alloying compositions and surface roughness of batches of stainless steel bars from different manufacturers on their corrosion resistance.

Parts a, b and c of the research projects mostly contribute to fundamental knowledge with outcomes that provides input parameter to life cycle and service life analysis of reinforced structures. The results reflect possible under- or over-estimation of corrosion properties by testing reinforcing bars in inappropriate pH and ionic concentration and show the contributions of the different alloying elements to corrosion resistance of stainless steel in this medium. These projects are innovative in that they combine extensive analysis of electronic properties of semiconducting passive films with the electrochemical and corrosion properties of current stainless steel reinforcing alloys to predict the long term behaviour of the bars when exposed highly aggressive ionic species. Part d of the research contributes to engineering application of stainless steel as a reinforcement option. The results from this section will inform steel producers, users and researchers of the typical range of properties that can be expected from a single rebar grade with varying composition, microstructure and surface roughness. The research contributions are expanded upon in the following chapters.

1.3. Thesis Structure

The following contents of this manuscript-based thesis are organized as shown in Figure 1-1. Chapter 2 provides relevant literature review on the current research presented in other chapters. Chapters 3 to 8 are published journal papers that provide contributions to fundamental knowledge and engineering application in the field. Copies of necessary copyright permissions for the manuscripts are provided at the end of the thesis. Chapter 9 presents summaries and conclusions of the findings from Chapters 3 to 8 and recommendations for future work.

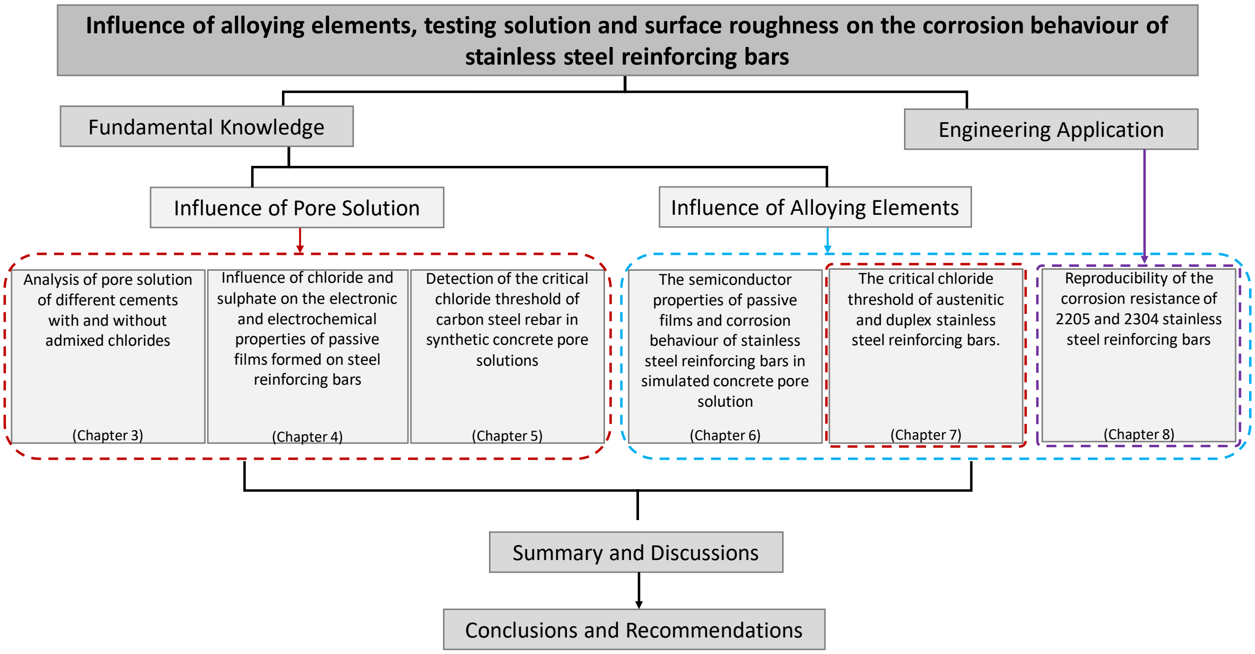

Figure 1-1. Thesis structure and contributions of fundamental knowledge and engineering applications.

Chapter 3 details the only investigation on complete compositional analysis of expressed pore solution from varying supplementary cementitious materials, water-to-cementitious ratio, and admixed chlorides in the range that initiates corrosion on stainless steel (2.5 – 7.5% by mass of cementitious materials). Previous expressed pore solution compositions were either reported for a single cement, multiple cementitious materials or single water-to-cementitious ratio with admixed chlorides in the range that initiates corrosion on carbon steel (0.1 – 0.5% by mass of cementitious materials). Similar work varying all three parameters was not found in the literature prior to this research. A major finding in this chapter was the increasing sulphate in pore solution with increasing admixed chlorides in the cement paste, which had not been taken into account in previous simulated pore solutions used to test rebar for corrosion resistance.

Based on the outcome in Chapter 3, Chapter 4 further investigates the influence of increasing sulphates with chlorides in simulated pore solutions on electronic and electrochemical properties of passive film formed on carbon and stainless steels. Three types of testing solution were employed in the study which represent: (i) the expressed pore solution with increasing sulphates as observed in Chapter 3 (initial pH ~13.5); (ii) same pore solution as (i) but without sulphate, which allows comparison with previous work (pH ~13.6); and (iii) the commonly used saturated calcium hydroxide (pH ~12.6). The influence of increasing sulphate in alkaline solutions on the passive film and corrosion properties of carbon- and stainless-steel bars had not previously been reported. Chapter 5 details the translation of the observed influence of sulphate on passive film properties to determination of critical chloride threshold value of the bars through a potentiodynamic polarization technique, developed by the present author.

Chapters 6 and 7 also detail similar electronic and electrochemical properties of passive films and critical chloride threshold values as Chapters 4 and 5, respectively, but in investigating the influence of major stainless steel alloying elements such as Cr, Ni, Mo, Mn. The tested bars were austenitic 304L, 316LN and 24100 and duplex 2205 and 2304 reinforcing bars. This was considered important because Mo and Ni are the most expensive alloying elements in stainless steel rebar costing 8 - 30 times more than other elements. A section of Chapter 7 also reported the influence of testing solution composition on stainless steel.

Following the passive film and corrosion properties observed in previous chapters, it was important that rebar is consistent in performance between batches and between manufacturers. Chapter 8 investigated the reproducibility of three batches of 2205 and 2304 stainless steel alloys from each of three different manufacturers. Similar work detailing the influence of variation in composition, microstructure, and surface roughness on corrosion resistance between batches of stainless steel bars from different manufacturers was not found in the literature. The influence of Mo on the ferrite and austenite phases of the 2205 was also investigated in this chapter.

2. Literature review

2.1. Concrete

Concrete is a composite material which consists primarily of cement, fine aggregate (sand), coarse aggregates (stone) and water. It is one of the most commonly used materials because its components are readily available, cheap, and easy to form at ambient temperature.

2.1.1. Portland Cement

The most widely used type of cement is Portland cement, an hydraulic cement that sets and hardens by a chemical reaction with water, a process called hydration. The manufacturing process begins with grinding and mixing certain proportions of raw materials, typically clay and limestone, in a rotary kiln at a temperature as high as 1450ºC to form cement clinker. The clinker is then cooled, mixed with gypsum ($CaSO_4.2H_2O$) to control the setting time, and ground to fine power to produce the commercial ordinary Portland cement (OPC), formerly known in Canada as Type 10 but, currently, as General Use (GU) cement. As shown in Table 2-1, each clinker particle contains 4 major compounds and several minor compounds. The term "minor" refers to their quantity and not their importance [1], [9], [10].

Table 2-1. Bogue composition of normal Portland cement clinkers [9].

Compound name	**Compound formula**	**Abbreviation**	**Compound composition (%)**
Tricalcium silicate (alite)	$3CaO.SiO_2$	C_3S	50 - 70
Dicalcium silicate (belite)	$2CaO.SiO_2$	C_2S	15 - 30
Tricalcium aluminate	$3CaO.Al_2O_3$	C_3A	5 - 10
Tetracalcium aluminoferrite	$4CaO.Al_2O_3.Fe_2O_3$	C_4AF	5 - 15
Calcium sulphate (gypsum)	$CaSO_4.2H_2O$	CS-	1-5
Other minor compounds present are CaO and oxides and sulphates of Mg, Na, K			

The products of hydration are a porous solid known as cement paste. The pores are filled, partially or completely, with a solution rich in hydroxide compounds of Ca, K and Na. The pore solution is saturated with $Ca(OH)_2$ which buffers the pH to ~12.6, while the NaOH and KOH increase the pH to above 13. As recently shown by the author [11], for cement pastes with admixed chlorides, sulphates are released into the cement pores and increase with admixed chlorides. Several types of 'pore solution' have been simulated and used for testing by many authors and some of the compounds employed are highlighted in Table 2-2.

It is the cement pore solution that determines the composition, stoichiometry and stability of passive film formed on the embedded rebar and, it is also through these pores that deleterious species from the environment penetrate the concrete to breakdown the passive film. Therefore, as explained in Section 2.2, pore solution simulated in the laboratory can under- or over-estimate the protective nature of steel passive film in the presence of deleterious species.

Table 2-2. Compounds in many simulated pore solutions found in literature.

	Pore solution types				pH
Commonly Use [12]–[18]	$Ca(OH)_2$				~12.6
ASTM A955		KOH	NaOH		~13.7
Tri-hydroxide [19], [20]	$Ca(OH)_2$	KOH	NaOH		~13.6
Expressed pore solution [2], [20]–[22]	$Ca(OH)_2$	KOH	NaOH	$CaSO_4.2H_2O$ (without Cl-)	~13.5
Expressed pore solution [11]	$Ca(OH)_2$	KOH	NaOH	$CaSO_4.2H_2O$ (increasing with Cl-)	~13.5

Over the past decades, many cement supplements such as blast furnace slag, fly ash, silica fume etc. have been used to replace some portion of OPC for many reasons. These supplementary cementitious materials, SCMs, are typically waste by-product that possess pozzolanic and/or hydraulic properties that can be activated when used together with OPC. Pozzolans are alumino-siliceous materials that in themselves possess little to no cementitious properties but will chemically react with the calcium hydroxide present in cement pores to form solid hydrate phases. Reducing the amount of OPC through replacement with SCMs, the amount of CO_2 emissions produced in the production of OPC can be reduced. Short descriptions of some SCMs employed in this research is discussed next.

2.1.2. Ground Granulated Blast Furnace Slag (GGBFS)

Ground granulated blast-furnace slag (GGBFS) or, as commonly called, blast furnace slag (BFS), is obtained by quenching molten iron from a blast furnace to produce a granular product than is then dried ground to the same fineness as OPC. The primary components of the slag are SiO_2, MgO, and Al_2O_3 which are similar components to those in OPC. The replacement amount of GGBFS beneficial to concrete has been well studied in the literature. The most common replacement amount in Ontario Canada is 25% of OPC, which is known to improve strength and reduces permeability [23], especially at a later age. However, study on its effect on pore solution chemistry, which in turn affects rebar passive film, has not been documented.

2.1.3. Fly Ash (FA)

Fly ash (FA) is a bi-product from coal fired power plants with composition and reactivity range based on coal type, boiler type and operation, as well as collection method [ref]. Various pollution control technologies employed in different plants also affect ash composition [ref]. A typical FA contains high levels of SiO_2, Fe_2O_3, and Al_2O_3 and limited amount of CaO, similar to compounds found in OPC. The variation in compositions of these compounds results in the different classes of FA. ASTM C618 defines two classes: low-calcium Class F, containing $SiO_2+Al_2O_3+Fe_2O_3$ greater than 70% and high-calcium Class C, containing $SiO_2+Al_2O_3+Fe_2O_3$ greater than 50%. The replacement amount of FA with OPC has also been well studied in the literature and the most common amount in Ontario Canada is 25%, which has been reported to reduce permeability and increase strength, especially at a later age of the concrete.

2.1.4. Silica Fume (SF)

Silica fume (SF) is a by-product of silicon and ferrosilicon alloy production with composition > 90% SiO_2 and particles about 100 times smaller than OPC. Due to the fineness and carcinogenic nature of sub-micrometer particles, they are usually inter-ground with OPC in a typical replacement amount of 8% OPC and, this is called blended cement. The OPC-SF cement has been shown [24] to improve strength and permeability of concrete more than OPC, OPC-GGBFS and OPC-FA because the OPC in the OPC-SF mix develops high pH (through the $Ca(OH)_2$) that is consumed by the SiO_2 in the early hydration hours to form more calcium silicate hydrate phase, the solid component in hardened cement paste. Larbi et al. [25] showed that more than 80% of the calcium released in the pore solution during the onset of hydration was consumed after 4 hours.

2.2. Corrosion of steel in concrete

Steel reinforcing bars and concrete are good match. Rebar provides concrete with strength for tensile applications, while concrete protects rebar against corrosion by first providing the high pH environment for the formation of a stable passive film that significantly lowers corrosion rate and then acting as physical barrier against aggressive species in the environment [2]. There are three common cases where passive films on rebar can be compromised: i) chloride attack: Cl^- from seawater or de-icing agents locally breakdown passive film, resulting in pitting corrosion; ii) carbonation: CO_2 from the atmosphere penetrates the concrete pores to react with $Ca(OH)_2$ in the pore solution, thereby reducing the pH and resulting in general corrosion; iii) anaerobic conditions: structures submerged or underground may lack the oxygen needed to maintain the passive film, again resulting in general corrosion [2]. This research focusses on the first case.

Chlorides can be intentionally or unintentionally introduced in concrete either at the time of mixing (i.e. admixed chloride) as a set accelerator or in contaminated aggregate, or can penetrate from the concrete surrounding, i.e. from seawater or de-icing agents. Some of these chlorides can take part in the hydration reactions and are chemically bound to the hydrate (solid) phases formed [26]. Chlorides can also become physically bound, being “trapped” in the hydrate phases. The remaining chloride in the concrete pore solution and are called “free chloride” or “soluble chloride”. It is the free chloride that poses a threat to steel reinforcing material. Keeping the salts away from steel reinforced concrete would reduce, significantly, the likelihood of corrosion. However, this solution may be unrealistic in Northern climates because of the harsh winter season. Thus, other methods of protecting reinforced structures from corrosion are typically adopted, such as the use of a more corrosion resistant alloy discussed in the next heading.

2.3. Stainless steels

Corrosion resistant reinforcing bars are used in those structures or parts of structures that are highly susceptible to chloride attack, such as marine and highway structures. Other corrosion resistant reinforcement includes galvanized steel, epoxy coated rebar (ECR), fibre reinforced polymer (FRP), solid stainless steel and stainless steel clad black steel, and proprietary products like MMFX [27]. Table 2-3 compares these reinforcing materials in terms of their reported properties. The focus of this research is the solid stainless steel bars.

Table 2-3. Comparison between most common reinforcing materials [27].

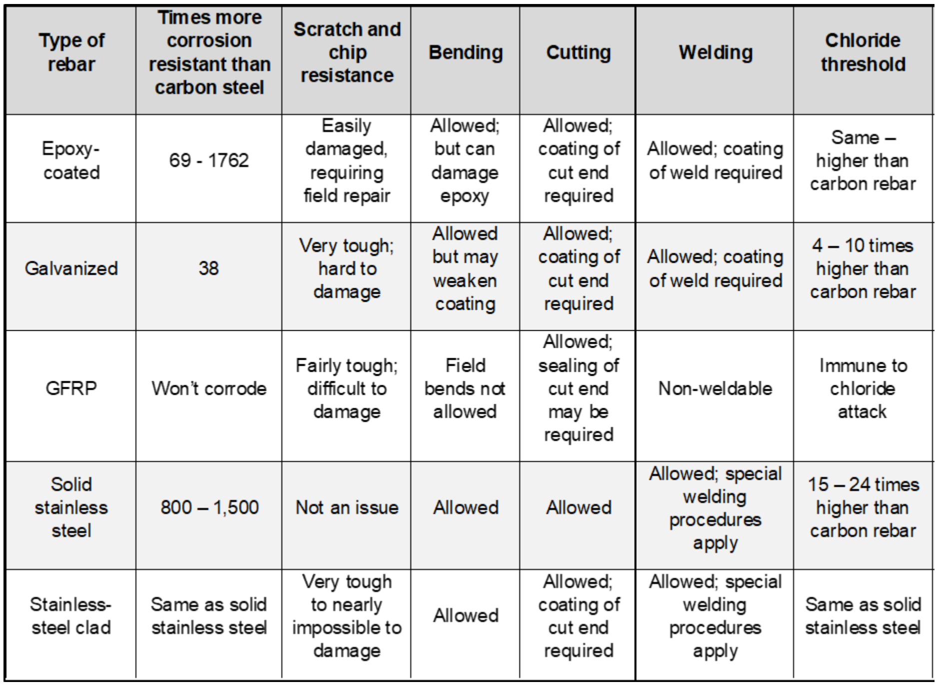

Type of rebar	Times more corrosion resistant than carbon steel	Scratch and chip resistance	Bending	Cutting	Welding	Chloride threshold
Epoxy-coated	69 - 1762	Easily damaged, requiring field repair	Allowed; but can damage epoxy	Allowed; coating of cut end required	Allowed; coating of weld required	Same – higher than carbon rebar
Galvanized	38	Very tough; hard to damage	Allowed but may weaken coating	Allowed; coating of cut end required	Allowed; coating of weld required	4 – 10 times higher than carbon rebar
GFRP	Won't corrode	Fairly tough; difficult to damage	Field bends not allowed	Allowed; sealing of cut end may be required	Non-weldable	Immune to chloride attack
Solid stainless steel	800 – 1,500	Not an issue	Allowed	Allowed	Allowed; special welding procedures apply	15 – 24 times higher than carbon rebar
Stainless-steel clad	Same as solid stainless steel	Very tough to nearly impossible to damage	Allowed	Allowed; coating of cut end required	Allowed; special welding procedures apply	Same as solid stainless steel

2.3.1. Background

Despite its high initial cost, stainless steel is one of the most viable options for reinforced concretes in environments prone to chloride attack because of its significantly higher chloride threshold resulting from its more stable passive film. The first recorded successful use of stainless steel as concrete reinforcement is the 2100-metre-long pier built between 1937 – 1941 in the Port of Progreso, Mexico [28]. In the first 75 years of its service life, the stainless steel reinforced pier showed little corrosion per a visual inspection and chloride penetration analysis [29]. In comparison, a carbon steel reinforced pier built in the early 1970's already deteriorated by 1999, Figure 2-1.

Figure 2-1. Pier in Progresso, Mexico built with 304L stainless steel and carbon (black) steel [29].

In today's market, two classes of stainless steel alloys are commonly used for construction, namely; single phase austenitic; and duplex, containing both ferrite and austenite phases. The constituents of each rebar grade under these categories are shown in Table 2-4.

Table 2-4. Mill composition of carbon steel and stainless steel rebar used in this project.

Class		Grade (ASTM)	In text	Composition (wt.%)							
				Cr	Ni	Mo	Mn	C	N	Si	Cu
Austenitic	**High Mo, high Ni**	UNS S31653	316LN	16.6	9.5	**2**	1.6	0.03	0.14	0.7	0.4
	Low Mo, high Ni	UNS S30403	304L	17.4	8.2	**0.5**	1.3	0.03	0.1	1	0.6
	Low Ni, low Mo, high Mn	UNS S24100	24100	17.1	0.9	0.19	**12.7**	0.04	0.34	0.9	0.14
Duplex	**High Mo, low Ni**	UNS S32205	2205	22.7	4.4	**3**	1.4	0.02	0.14	0.6	0.3
	Low Ni, low Mo	UNS S32304	2304	22.4	3.2	**0.3**	1.8	0.02	0.14	0.7	0.3
	Low Ni, low Mo, mid Mn	UNS S32101	2101	21.4	1.5	0.2	**5**	0.02	0.2	0.7	0.2
Carbon steel		400W	Carbon	0.17	0.16	0.04	0.92	0.02	0.2	-	0.46

A minimum of 10.5 wt.% chromium content is needed in stainless steel to form the adherent and self-healing chromium oxide layer that protects against atmospheric corrosion. However, a higher amount is typically needed in alloys used in more hostile environment. Since all stainless steel grades contains chromium (Cr), comparing the price between different grades is best achieved by comparing the relative contents of other, more costly, elements such as nickel (Ni) and molybdenum (Mo), because their price per unit can range between 8 - 30 times as much as Cr. For example, Figure 2-2 shows that the austenitic 316LN and duplex 2205 are the most expensive stainless steel grades, and the main difference in composition when compared with the austenitic 304L and duplex 2304, respectively, is the Mo content. Similarly, the major difference between the more expensive 304L grade and the cheaper 24100 grade is the Ni replacement with Mn in the latter alloy. Thus, for economical reasons, it is important to understand the role of these elements in the corrosion resistance of stainless steel alloys.

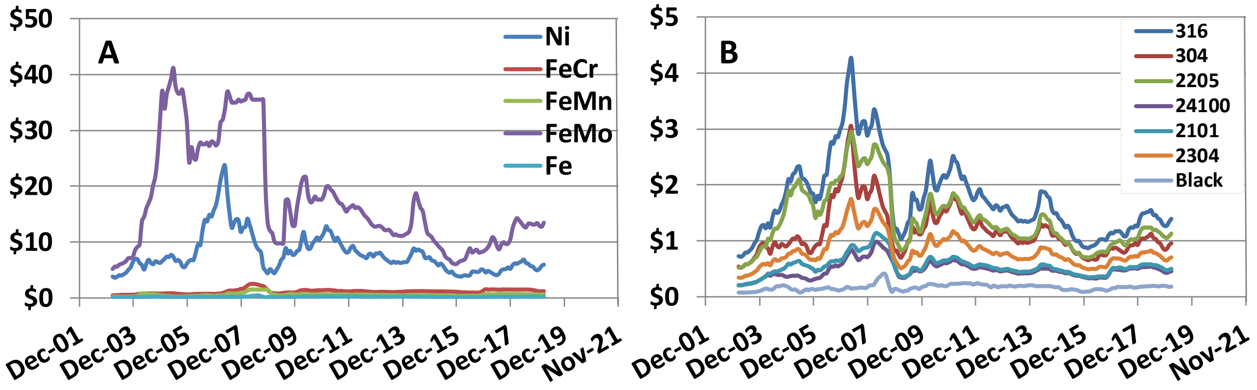

Figure 2-2. Raw material costs of stainless steel alloying elements (A) and bars (B) in US $/lb.

2.3.2. Pitting corrosion and pitting resistance equivalent number (PREN)

Despite possessing superior properties to many other types of rebar, stainless steel is still susceptible to pitting corrosion in the presence of chloride ions. Pitting is a form of localized attack that is autocatalytic, often difficult to detect and can cause severe decrease in the cross-section of the rebar, reducing its load bearing capability. Generally, pits are initiated at surface discontinuities or flaws (e.g. scratches), regions with deposits (e.g. dust, mud, sand) [30] and regions affected by steel inclusions (e.g. impurities such as phosphorus (P) [31], manganese sulphide (MnS) [32], etc.

Although the Fe-Cr system forms the basis for all stainless steel grades, many grades contain additional elements to enhance specific properties in the alloy. For example, Ni and Mo are typically added to give the alloy an austenitic phase and enhance pitting resistance, respectively. In some alloys, the Ni content is reduced, due to its high cost, and Mn is added as substitute, although its role in stabilizing the austenitic phase is debatable. Manganese was reported to be: (i) a ferrite stabilizer [33]; (ii) an austenite stabilizer [34] [35]; (iii) a ferrite stabilizer at higher content and an austenite stabilizer at lower content [36]; (iv) possessing role dependent on other alloying elements - a ferrite stabilizer at high Cr, and an austenite stabilizer at low C and N [37]. Most stainless steels have a low carbon content (typically less than 0.03%) to reduce their susceptibility to "sensitization" and nitrogen is sometimes added to provide interstitial strengthening to compensate for the lower carbon content [38]. Sensitization occurs when, at inadequately rapid cooling from the hot working or annealing temperature, carbon combines with the Cr to form an intermetallic chromium carbide, $Cr_{23}C_6$, along the grain boundaries of the alloy, leaving a Cr-depleted layer adjacent to the boundaries. This area is then susceptible to stress corrosion cracking. Molybdenum can reduce sensitization because it has a greater affinity for carbon than does chromium.

Recent efforts on the prediction of the quantity of the elements needed to balance a specific phase in any stainless steel grade have led to the development of many 'equivalent number' formulae. The traditional equivalent numbers are those of nickel and chromium, being the primary constituents of stainless steel alloys, and several formulae were proposed for them [36], [39]–[41]. These formulae changed with the compositions of different stainless steel alloy. For example, Post et al. (mentioned in [42]) in 1940 suggested the nickel equivalent to be $Ni_{eq} = \%Ni + 0.65\%Cr + 0.98\%Mo + 1.05\%Mn + 0.35\%Si + 12.6\%C$ and a more recent study by Takemoto et al. [43] in 1990 suggested the formula to be $Ni_{eq} = \%Ni + 0.6\%Mn + 0.18\%Cr + 9.69(\%C + \%N) - 0.11\%Si$.

In the 1960s, a pitting resistance equivalent number (PREN) was developed for quantifying the influence of alloying constituents on the critical pitting temperatures of stainless steel alloys used in the nuclear industry for which the environment ranges from acidic to neutral and the temperature ranges between $300 - 400^{O}C$. This environment (pH and temperature) is significantly different from that found in concrete. Consequently, the published PREN formulae are not applicable to the current research and should be considered qualitative where found in published journals present in this work. Like other equivalent numbers, the PREN formula has since been changing [44]. The two most widely used formulae are $PREN_{16} = \%Cr + 3.3\%Mo + 16\%N$ and $PREN_{30} = \%Cr + 3.3\%Mo + 30\%N$ [44]–[47]. As mentioned earlier, stainless steel grades with high Mo content are shown to be highly resistance to pitting corrosion in acidic to neutral environment. Sukimodo and Shiwada [48], [49] proposed that it is due to the formation of a metal molybdate ($xMoO_4^{2-}$) that occupies interstices in passive films. It is importance to mention that some authors [46], [50]–[52] believe Mo and N act synergistically in enhancing pitting resistance. The role of Cu in enhancing pitting resistance in stainless steel is not concluded – some authors believe it to be positive [53]–[55], while others found no contribution [56]. Silicon is found to improve corrosion resistance in austenitic stainless steel alloys if the amount is kept low so that ferrite does not form [57]. Thus, today's PREN formulae may incorporate many more of these elements, but it remains to be determined how these elements influence the pitting corrosion resistance in highly alkaline concrete environment.

2.3.3. Critical chloride threshold (C_{CRIT})

The superiority of stainless steel alloys over carbon steel is their ability to withstand a significantly higher chloride concentration before initiation of pitting corrosion. The critical chloride threshold (C_{CRIT}) value of a bar is the concentration of chloride at the steel surface necessary to break down its passive film and initiate active corrosion. To determine this value for any rebar, different experimental systems have been employed, including but not limited to [58], [59], [60]:

- Environment: Pore solution; mortar; concrete;
- Exposure: laboratory atmosphere (approximately constant temperature and relative humidity); outdoor exposure (variable temperature, relative humidity and precipitation).
- Chloride: admixed, ingressed through the mortar/concrete
- Measurement techniques: visual inspection; potential mapping; linear polarization resistance, cyclic polarization; electrochemical impedance spectroscopy; potentiostatic tests; galvanostatic tests etc.

The ranking of different rebar grades from one C_{CRIT} test can vary significantly with different tests, making comparison difficult. For example, as shown in Figure 2-3 [61], a C_{CRIT} test conducted on concrete may vary with: cement type and origin; supplementary cementitious material (SCM) type and replacement amount, water-to-cementitious ration (w/cm), curing time, concrete age, type of chloride, rebar surface condition. Table 2-5 shows the C_{CRIT} value from different authors for different stainless steel grades tested in pore solution with a wide range of values for the same rebar grade. An additional reason for variation in C_{CRIT} value of a rebar grade is the surface condition of the tested bars. This is discussed in detail in Chapter 8.

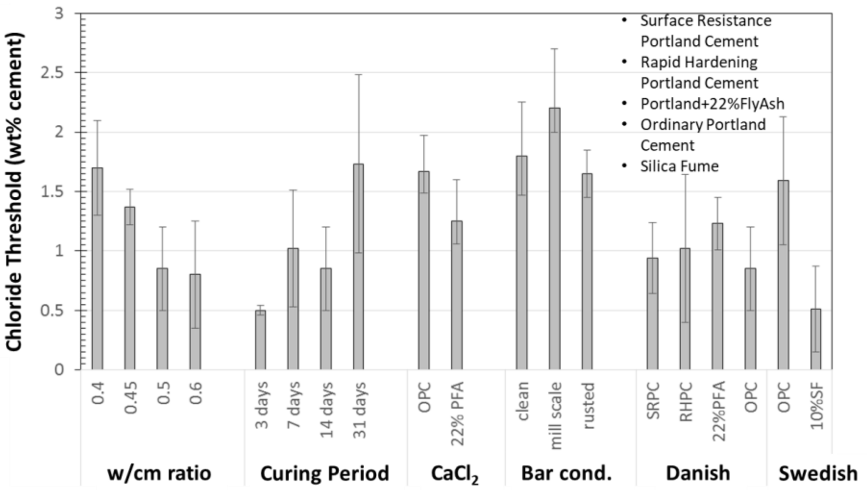

Figure 2-3. Influence of w/cm ratio, curing, cement type, SCM type, surface condition of black steel chloride threshold [61].

Table 2-5. The C_{CRIT} values in wt.% for stainless steel rebar alloys tested in simulated pore solutions [19].

Stainless steel Product	**Randström et al. 2010** [19]	**Bertolini et al. 1996** [62]	**Bertolini et al. 2009** [63]	**Hurley and Scully 2006** [64]
pH (after test)	12.8 - 13.3	12.6	12.6	12.6
304L	2.8 - 10.6	5	6.5 - 10	-
316L	5.7 - 6.8	5.5	>10	2.8 - 11.3
LDX 2101	5.7 - 10.6	-	3.5 - 6	1.1 - 1.4
2304	4.6 - 10.6	>10	7.5 - 8	-

2.4. Passivity and Passive film characteristics

A passive film is an oxide or hydroxide film, usually only a few nanometers in thickness, formed on a metal's surface by exposure to the environment and protects the metal from high rates of corrosion. The passive corrosion rate is dependent on the stoichiometry, compactness, ionic defectivity and electrical conductivity of the passive film formed on the rebar. Thus, it is essential to understand the nature of the passive film, especially in the presence of deleterious species such as chlorides, and the potential/pH range for which passive film is stable on rebar used in concrete.

2.4.1. Semiconductor nature of passive film

Passive films formed on steels have been described as semiconductors. Therefore, understanding the behaviour of semiconductors and the passive film-electrolyte interface is essential to characterising the corrosion behaviour of different stainless steel grades of interest in this study.

A solid material contains large number of atoms or ions, each having several electrons that exist in discrete energy levels, closely packed together. Since those electrons are closely packed, their energy levels overlap and so they form bands called energy bands [65]. Depending on the amount of overlap, the band widths are defined, such that those bands closer to the nucleus of an atom are narrow compared to those in the outermost shell [65]. The valence band, typically occupied, contains energy levels of the valence electrons of atoms present in the solid. The top part of the valence band has a potential E_V associated with it, which can be thought of as a measure of ionization potential of the bulk material [65]. The conduction band, typically unfilled at zero kelvin, contains energy levels at which excited electrons from the valence band can move freely within the material. This lower level of the conduction band has a potential E_C, which can be thought of as a measure of electron affinity of the bulk material. The gap between the lower part of the conduction band (E_C) and the upper part of the valence band (E_V), where no electron is permitted, is called band gap (E_g).

The conduction of a solid material requires electrons to be present in the conduction band. In a metal, the valence band and the conduction band of metal overlap and, therefore, electrons can move freely within the conduction band. In an insulator, there is a large gap between the valence and the conduction band, and as a result, electrons have many energy levels to overcome before aiding conduction. The gap between the valence and the conduction band in a semiconductor is smaller (1 – 4 eV [66]) than that of an insulator. Therefore, small thermal activation can result in conduction of the material. When electrons are transferred into the conduction band, they leave vacant sites, called holes. These holes are considered positive charge carriers and can move throughout the material (i.e. energy band) in the direction opposite to the free electrons. Thus, both electrons and holes contribute to conduction in a semiconductor solid.

An important concept when describing the electronic nature of a semiconductor is the Fermi energy level (E_F). Since electron energy value is not definite, but rather defined by wave functions, there is a probability (greater than zero) that an electron can exist in the band gap [67]. The Fermi level is defined as an energy level within the band gap with a 50% chance of being occupied by an electron at any time [68]. The Fermi function f(E), Equation 2-1, shows the relationship between applied potential (E) and the position of the fermi level (E_F). In an intrinsic semiconductor, the E_F is located halfway between the E_C and E_V, but the position varies with impurities. For a p-type semiconductor, where impurities result in holes, E_F lies just above the E_V, whereas in an n-type semiconductor, where impurities result in extra electrons, E_F lies just below E_C. The E_F changes with applied potential to the semiconductor. For example, with a positive (anodic) applied potential, E_F moves downward in the direction of E_V.

$$f(E) = \frac{1}{e^{\left(\frac{E-E_F}{kT}\right)} + 1}$$

Equation 2-1. f(E) = Fermi function, E = applied potential, E_F = Fermi energy, k = Boltzmann's constant, T = temperature [68].

2.4.2. Semiconductor-electrolyte (S/E) interface

During the formation of a stable passive film, charge transfer occurs continuously until the electrochemical potential of both the semiconducting passive film and the surrounding electrolyte are equal. Due to this charge transfer, a region that differs in energy from the bulk of the semiconducting passive film and from the electrolyte is formed adjacent to the S/E interface. The region on the semiconductor side of this interface is called the *space charge layer* (SCL), while that on the electrolyte side is the *Helmholtz double layer* (HDL) [68]. The equilibrium electrochemical potential of the SCL in the semiconductor is determined by the Fermi level (E_F) – obtained from the Fermi function in Equation 2-1 [68], while that of the HDL in solution is determined by the redox potential (E_{redox}) - obtained from Nernst equation shown in Equation 2-2.

$$E_{red} = E^0_{red} + \frac{RT}{nF}\ln\left[\frac{C_{oxi}}{C_{red}}\right]$$

Equation 2-2. E_{red} = redox potential, E^0_{red} = standard redox potential, R = gas constant, T = temperature, n = number of moles, F = faraday's constant, 96,500 C, C_{oxi} = concentration of the oxidized species, C_{red} = concentration of the reduced species [30].

2.4.2.1. Space charge layer (SCL)

The potential at which E_F is equal to E_{redox} is called *flatband potential* (E_{FB}) because the charge transfers are in equilibrium and there is no bending of the band edges. Bending of a band edges is caused by a potential difference between band (valence and conduction) edges closer to the S/E interface (i.e. in the SCL) and the bulk of the bands in the semiconductor [69], as shown in Figure 2-4. In other words, at E_{FB}, there is no space charge layer (bent region of the bands) in the semiconductor. The E_{FB} is crucial in determining the electronic behaviour of the semiconductor passive film as it considers the physical phenomena occurring at and on both sides of the S/E interface. The potential of the flatband in Equation 2-3 [70] shows the relationship between the potential of the SCL in the semiconductor and that of the HDL in electrolyte.

$$E_{FB}(SHE) = (x + \Delta E_F - E_H) - 4 \cdot 5$$

Equation 2-3. E_{FB} = flatband potential with respect to SHE, X = electron affinity of the semiconductor, ΔE_F = potential difference between the fermi level and the charge carrier band, E_H = Helmholtz potential.

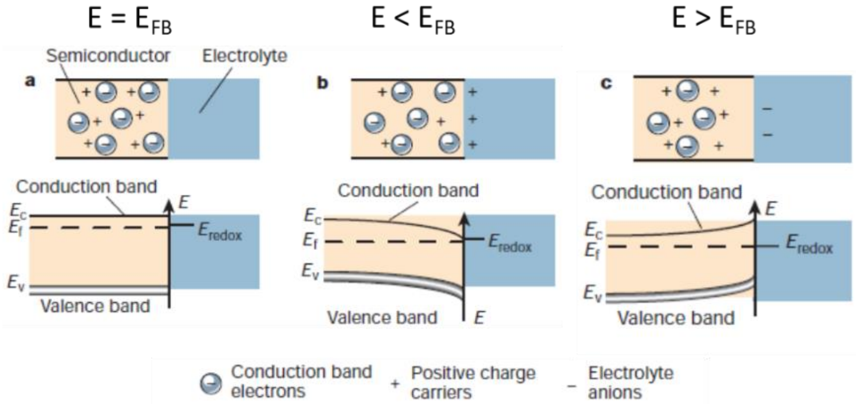

Figure 2-4. The behaviour of the band edges (i.e. space charge layer) in an n-type semiconductor under applied potential [68].

A space charge layer can be an electron depletion region or an electron accumulation region depending on the direction of charge transfer under applied potential [68]. The behaviour of an n-type semiconductor under applied potential is shown in Figure 2-4. At an applied potential more negative than E_{FB} (i.e. $E < E_{FB}$), there is transfer of electrons from the electrolyte into the semiconductor which causes a downward bending of the band edges. Since there are now extra/excess electrons in the space charge layer, the SCL is an *accumulation layer*, Figure 2-4b. At an applied potential more positive than E_{FB} (i.e. $E > E_{FB}$), there is transfer of electrons from the semiconductor into the electrolyte which generates a positively charged region in the space charge layer and an upward bending of the band edges. Since majority of the electrons, which are responsible for conduction in an n-type semiconductor, are transferred from this region, the SCL is a *depletion layer*, Figure 2-4c. These accumulation and depletion concepts are similar to the application of an anodic and cathodic potential to an electrode during polarization. At potential application more negative than the corrosion potential (i.e. cathodic polarization), electrons are supplied to the steel (or its passive film), while at potential more positive than corrosion potential (anodic polarization), electrons are being stripped off steel (or its passive film).

2.4.2.2 Helmholtz double layer (HDL)

Water is a polar molecule with positively charged hydrogens and a negatively charged oxygen. The positively charged end is attracted towards the negatively charged metal surface as shown in Figure 2-5. As a result, a layer of water is adsorbed on the metal surface, and this region forms the inner Helmholtz double layer (IHDL). The region extending to the solvated ions attracted towards the adsorbed water layer forms the outer Helmholtz double layer (OHDL) [69]. The HDL behaves as a capacitor [65] just like the SCL in the semiconductor that forms on a passivated metal. The HDL can result in a significant drop in measured potential and this drop, unlike the SCL, is independent of the direction of charge transfer across the interface or applied potential [69]. It should be noted that the HDL is one of the electric double layer theory model, including others such as Gouy-Chapman, Stern and Grahame.

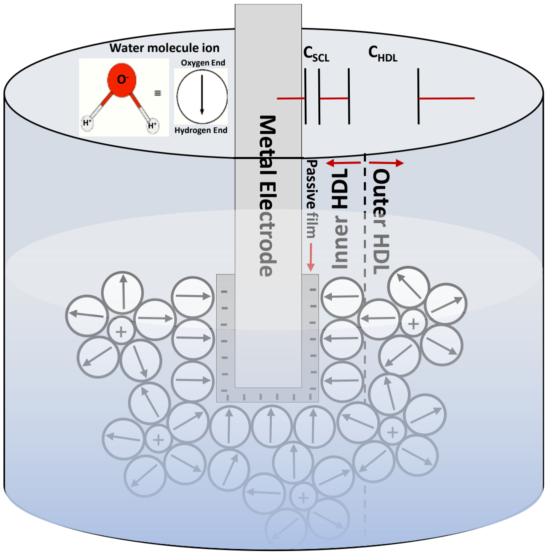

Figure 2-5. Helmholtz double layer (HDL) formed on passivated rebar in solution. Capacitors of the space charge layer (C_{SCL}) relative to the capacitance of the HDL (C_{HDL}) is also shown (not to scale).

2.4.3. Methods of studying the semiconductor passive film

Several methods have been employed to experimentally assess the semiconductor nature of passive film formed on steel [71]–[79], some of which are, electrochemical impedance spectroscopy (EIS), Mott-Schottky (M-S) analysis, photoelectrochemical spectroscopy (PECS), electrochemical scanning tunneling microscopy (ECSTM), and electrochemical tunneling spectroscopy (ECTS). The method employed in the current research is the M-S method.

2.4.3.1. Electrochemical impedance spectroscopy (EIS)

The basis for adopting the electrochemical impedance spectroscopy (EIS) technique for M-S analysis is that any behaviour or processes occurring at the semiconductor/electrolyte (S/E) interface can be modelled by an analogue electrical circuit - using sets of resistors, capacitors and inductors in parallel or series. The EIS employs a small amplitude alternating potential signal at different frequencies and measures the resulting impedance. For testing rebar in solution, mortar or concrete, the ohmic drop (V_Ω) across the solution, the capacitance of the passive film and resistance to polarization (Rp) of the rebar can be obtained by applying small oscillating AC potential to the working electrode in an electrochemical cell.

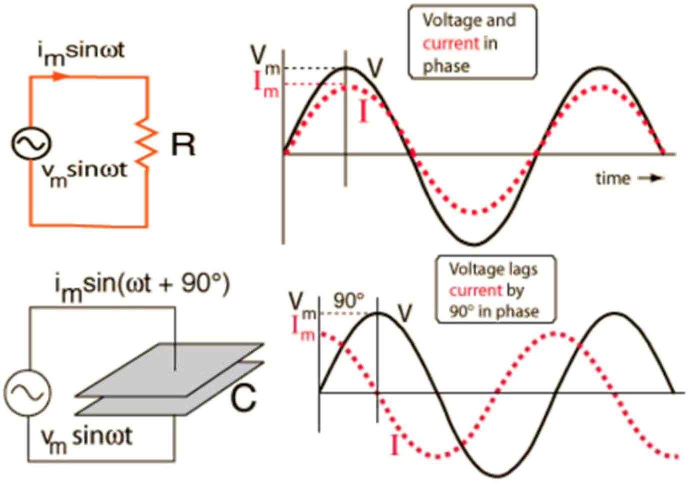

Figure 2-6. The figures on the left are circuit elements with resistor (top) and capacitor (bottom). The figures on the right are plots of applied potential (V) to the resistor and capacitor and the induced current response (I) versus time (t) in a circuit element [80].

In direct current (D.C.) circuits, the Ohm's law is given as Equation 2-4, while the relationship between the time-dependent applied potential and the time-dependent current response in AC condition is given by Equation 2-5 [80]. Direct current is essentially an alternating current at zero frequency [80]. When an AC potential is applied to a circuit system with a resistor, the corresponding current response will have the same frequency with no 'phase shift', as shown in the upper figures in Figure 2-6 [80]. In contrast, when an AC potential is applied to a circuit containing a capacitor, a phase shift (ϕ) exists between the applied AC potential and the induced current, as shown in the lower figures in Figure 2-6. This phase shift is represented by an imaginary component in the overall impedance in the system, Equation 2-6 [80]. The system's capacitance (C) can then be obtained from the imaginary impedance (Z") using the relationship in Equations 2-7 and 2-8.

$$R = \frac{V}{I}$$

Equation 2-4. R = actual resistor, V = potential, I = direct current

$$Z(\omega) = \frac{V(t)}{I(t)}$$

Equation 2-5. Z = impedance, V(t) = potential, I(t) = alternating current. $V(t) = V_0 \sin(\omega t)$ and $I(t) = I_0 \sin(\omega t+\phi)$, where V_0 = potential, ω = angular frequency (2πf), f = frequency, t = time, I_0 = current, ϕ = phase shift

$$Z(\omega) = Z'(\omega) + Z''(\omega)$$

Equation 2-6. Z = impedance, Z' = real impedance, Z" = imaginary impedance

$$C = -\frac{1}{2\pi f Z''}$$

Equation 2-7. Equation for capacitance in series.

$$C = \frac{Z''}{2\pi f |Z|^2}$$

Equation 2-8. Equation for capacitance in parallel.

Data from EIS test can be represented in a Nyquist plot or Bode plots, as shown in Figure 2-7. Both plots reveal different aspect of the impedance equation shown in Equation 2-8. The Nyquist plot shows the imaginary impedance versus real impedance at each frequency. The Bode plot shows two plots with a common abscissa, the impedance and phase shift vs frequency. It should be noted that Figure 2-7 only shows Nyquist and Bode plots for a single capacitor and resistor without mass transfer issue occurring at the steel surface typically represented by a Warburg impedance component in the circuit [81]. Other factors affecting the impedance of a system can be represented by another circuit component consisting of capacitors, resistors and inductors. For a passivated steel tested in solution, the resistance of the electrolyte is represented by the ohmic resistance (R_Ω), the resistance to charge transfer across the semiconductor/electrolyte interface is represented by the polarization resistance (R_P) and C_{dl} is the double layer capacitance [81].

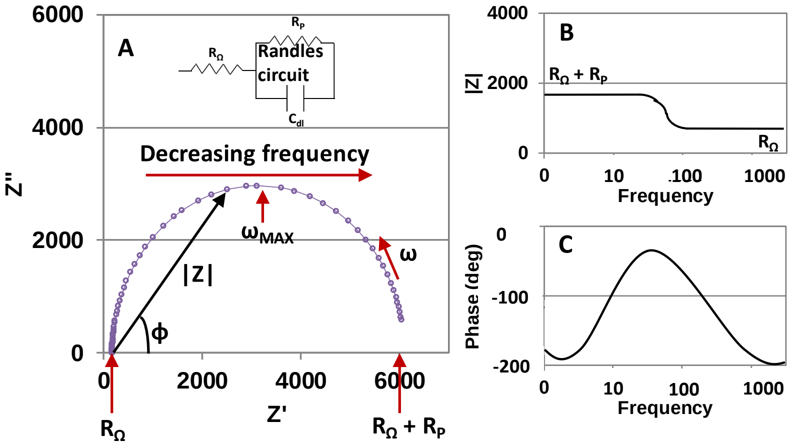

Figure 2-7. The Nyquist plot (A) and Bode plots (B and C) for the simple Randle circuit (A insert). R_Ω = ohmic resistance, R_P = polarization resistance, C_{dl} = double layer capacitance (same as C_H).

The EIS technique is typically used to provide information about a steel/concrete system. Some of the studies that have employed EIS were used to study: (i) the effectiveness of cathodic protection of reinforced concrete [82]; (ii) the precipitation of $Ca(OH)_2$ on a steel in reinforced mortar [83]; (iii) the freezing of water in cement paste [84]; (iv) the hardening process of cement paste [85]; (v) the long-term effectiveness of concrete inhibitors for steel in reinforced concrete [86]–[90]; (vi) the chloride permeability of high performance concrete (HPC) [91]; (vii) the chloride diffusivity in concrete [92]; and (viii) monitor the microstructural changes of the cement paste during rapid chloride permeability test [93]. The major reason for the common use of the EIS technique is because it does not perturb the system significantly, unlike other electrochemical techniques that employ direct current. As shown in Figure 2-8, there is a leak in both the SCL and HDL that result in an electrochemical reaction when DC is applied to an electrode, whereas the capacitors are only being charged and discharged with no leakage or electrochemical reaction on application of an AC.

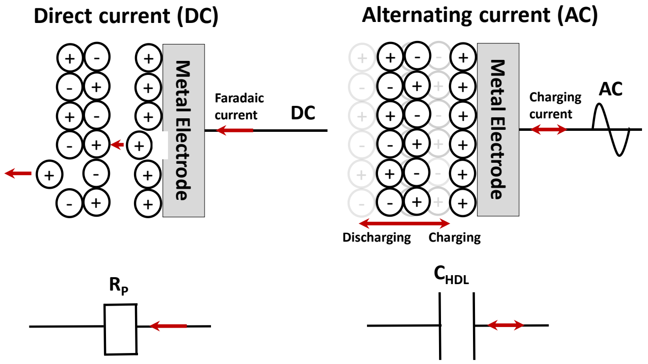

Figure 2-8. Behavior at metal/electrolyte interface on application of DC and AC.

2.4.3.2. Mott-Schottky technique

The Mott-Schottky (M-S) technique, commonly employed to assess the semiconductor nature of passive film [70], involves the application of EIS at different applied potential levels from the cathodic to anodic regions to obtain impedance and capacitance values of the passive film. The capacitance values obtained are of both the SCL and the HDL since they are in series with each other at the S/E interface, as shown by Equation 2-9. Harrington et al. [94] obtained a C_H value of 22 µF cm^2 for iron in synthetic pore solution using a surface enhanced Raman spectroscopy technique. The C_H is typically about 2-3 orders of magnitude greater than the space charge capacitance (C_{SC}) [34]. Therefore, the HDL component ($1/C_H$) in Equation 2-9 becomes insignificant and can be omitted to allow Equation 2-10 be used to obtain an M-S plot, a plot of the inverse of square capacitance (i.e. the C_{SC}) versus the applied potential, as shown in Figure 2-9.

$$1/C^2 = (1/C_{sc}^2 + 1/C_H^2)$$

Equation 2-9. Where C is the total capacitance, C_H is the capacitance of the HDL, C_{SC} is the capacitance of the SCL obtained from the relation $C_{SC} = 1/(-Z''2\pi f)$ [37], where Z” is imaginary part of the impedance (discussed later) and f is the frequency.

$$\frac{1}{C_{sc}^2} = \pm\frac{2}{\epsilon\epsilon_0 eN}\left(E - E_{FB} - \frac{kT}{e}\right)$$

Equation 2-10. Where C_{SC} = capacitance of SCL, N = defect density, E_{FB} is flatband potential, ε = relative permittivity of semiconductor, ε_0 = permittivity of free space, T is temperature, e = charge of electron.

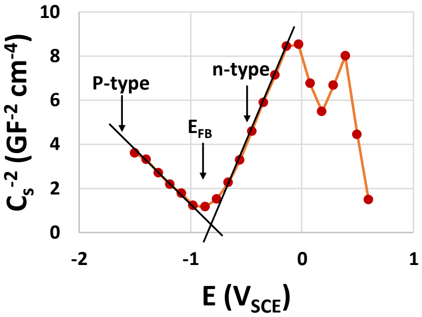

Figure 2-9. An example of a M-S plot of 316LN stainless steel alloy showing a p-type and an n-type semiconductor.

From the M-S plot, many properties of the passive film can be deduced. A positive and negative slope from the $1/C^2$ vs E plot is indicative of an n- and p-type semiconductor, respectively. As shown in Figure 2-9, some passive films, such as those on stainless steel alloys, can exhibit both semiconductor type. The dopant density (N) (density of defects in the SCL) can be obtained by rearranging Equation 2-10 or from the slope of the linear region in M-S plots. It should be noted that the M-S equation applies only to the linear regions of the M-S plot. For an n-type semiconductor, the dopant or defect density is referred to as the donor density (N_D), while for a p-type semiconductor, it is called acceptor density (N_A). The flatband potential (E_{FB}) can be obtained from the M-S plot by extending the linear regions of the plot to the x-axis (i.e. E value at $1/C^2 = 0$) as shown in Figure 2-9.

In the derivation of the M-S equation, shown in the work of Dean and Stimming [95]–[97], some major assumptions were made:

- The first assumption is that the semiconductor being evaluated is pure and intrinsic. This enables the system to produce a perfectly linear M-S plot (i.e. $1/C^2$ vs E plot) as predicted by Equation 2-10.
- The second assumption is that the capacitance (C) of the system consists only of capacitance of the SCL (C_{SC}) and of the HDL (C_H) in series.
- The third assumption is that, other than being potential dependent, the capacitance can also be frequency dependent due to: (i) the non-uniform nature of donor/acceptor defects in the oxide; (ii) possible contribution of surface states capacitance; (iii) dielectric relaxation phenomena; and (iv) the amorphous nature of the passive film [98]. Ahn and Kwon [99] and Sikora et al. [100] suggest that this frequency dependence can be addressed by finding a range of frequencies for which capacitance is unaffected by frequency change, observed to be 1 kHz.

The M-S technique has been used by several authors and has shown to be a repeatable and reliable method for analysing the electronic properties of passive films formed on zinc [101], titanium [102], tungsten [100], zirconium [103], iron/steel [104]–[106], stainless steel [75], [98], [107].

Staircase potentio-electrochemical impedance spectroscopy (SPEIS)

The SPEIS technique was used in the present work to study the semiconductor nature of passive film. The technique consists of a staircase potential sweep which allows users to divide the interested range of potential values into potential steps and carry out an EIS measurement (with desired frequency range) at each step. The choice of the selected potential range is such that the capacitance of the passive film can be observed/measured as the passive film on the bar is formed (i.e. as the potential is increased in the anodic direction). The detailed diagram is shown in Figure 2-10. This technique is peculiar to the BioLogic potentiostat and has been employed for testing across several field such as batteries, implants, electronics, steel reinforced structures, etc. [108].

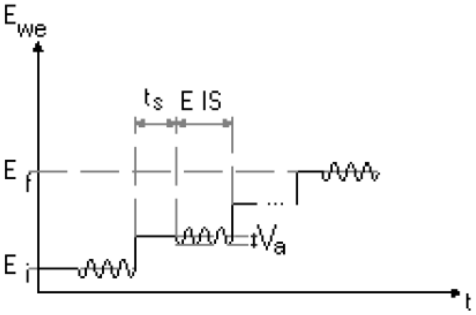

Figure 2-10. SPEIS description diagram. [108].

2.5. Other electrochemical evaluation methods

The ingress of chlorides in concrete and the initiation of active corrosion on bars are highly non-uniform, and because the on-set of corrosion in reinforced structures is not visible, some non-destructive testing methods have been used to assess the corrosion conditions of rebar. The least expensive and most commonly used method in the field is the Half-Cell Potential (or corrosion potential) measurement which gives the probability of corrosion but no information on the rate or spatial extent of corrosion. In interpreting the measured potentials, ASTM C876 [109] recommended a guideline for assessing the probability of corrosion of uncoated carbon steel, Figure 2-11 (left). Ogunsanya and Hansson [110] also recommended similar guideline for interpreting measured potentials of galvanized rebar, Figure 2-11 (right). It is clear that guideline employed to interpret measured potentials from this technique have the shortcoming of being dependent on the type of reinforcement. Consequently, other electrochemical measurements are typically employed in the laboratory to determine the corrosion rates of different reinforcing alloys. Some of the techniques employed in this work are linear polarization resistance (LPR), cyclic or potentiodynamic polarization (CP) and potentiostatic polarization.

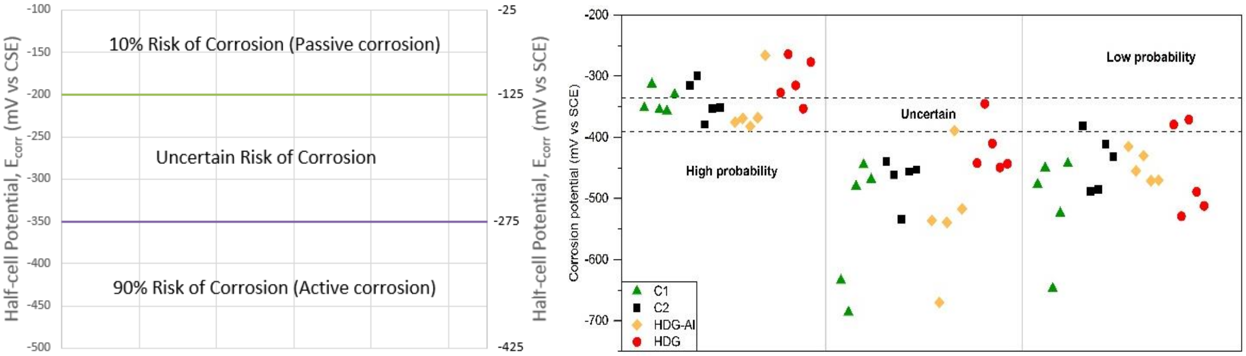

Figure 2-11. Half-cell potential guideline for carbon steel [109] (left) and galvanized steel [110] (right). Note the difference in scale.

The basis for most DC electrochemical measurement is the polarization measurement plot shown in Figure 2-12. This plot shows the relationship between applied potential and measured current, or vice versa, in the region of corrosion potential is approximately linear and the slope is defined as the "polarization resistance" (R_P) of the metal. Polarisation resistance (R_P) is the resistance of a specimen to oxidation on application of an external potential and corrosion rate of a bar can be calculated from it using Equation 2-16.

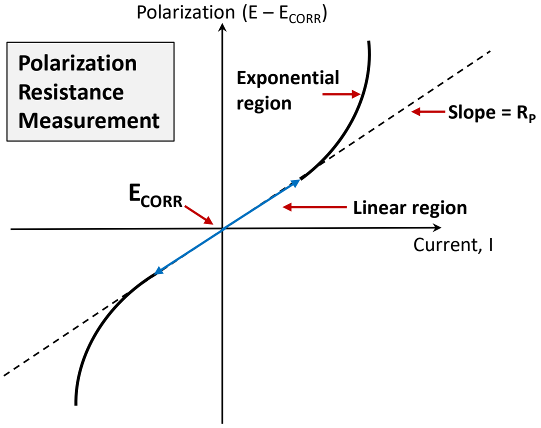

Figure 2-12. Polarization resistance curve.

$$\text{icorr} = \frac{\beta}{\text{Rp}}$$

Equation 2-11. i_{CORR} is the corrosion rate, Rp is the polarization resistance (= $(\Delta E/\Delta I)_{E=Ecorr}$) , ΔE and ΔI are change in potential from E_{CORR} and change in current from 0, E_{CORR} and I_{CORR} are corrosion potential and corrosion current, β is the Stern-Geary's constant from β= [βa.βc]/[2.3(βa+βc)], βa and βc are anodic and cathodic Tafel constant/slopes [111].

2.5.1. Potentiostatic linear and non-linear polarization resistance

Linear polarization resistance (LPR) measurements are performed by applying a potential in the range of ±10 – 20 mV about the corrosion potential, either as a constant pulse (potentiostatic) or a potential sweep (potentiodynamic) and measuring the current response, Figure 2-13. Alternatively, a current pulse (galvanostatic) or a current sweep (galvanodynamic) can be applied, and potential response is measured. In potentiostatic LPR technique, a constant ±10 – 20 mV potential is applied between the working electrode and reference electrode for a certain period of time that allows the current to reach steady state (typically 2-5 minutes for steel in concrete) and the current response is measured. The technique is popular in evaluation of corrosion rate of rebar and its advantage over other technique is that it is non-destructive and quick (results is typically obtained in few minutes). This technique was employed in Chapters 4 and 5. In potentiostatic non-linear polarization resistance technique, a constant ±200 – 400 mV potential (outside the linear region in Figure 2-12) is applied between the working electrode and reference electrode for a longer time (typically in days) and the current response is measured. This non-linear technique is not common because it is destructive. It is used in the current research to rapidly rank the corrosion resistance of different alloys in a very aggressive chloride environment [112], [113] as described in Chapter 8.

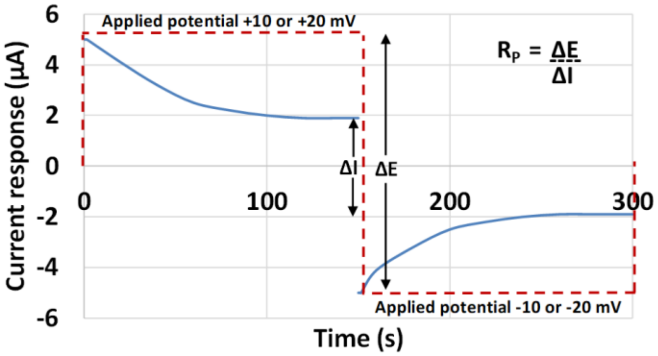

Figure 2-13. Potentiostatic linear polarization resistance curve.

2.5.2. Cyclic potentiodynamic or galvanodynamic non-linear polarization resistance

The non-linear potentiodynamic polarization resistance measurements are typically performed by applying a potential sweep at a specific scan rate from the corrosion potential of the working electrode in the anodic or cathodic direction and measuring the current response. The scan in the anodic region, as shown in Figure 2-14, reveal the passivity region of the specimen up to the region where there is a breakdown in passive film either by dielectric breakdown that occurs in the transpassive region, or by the onset of pitting at a lower potential. In cyclic polarization, the potential is reversed from below the transpassive region in the cathodic direction to observe any hysteresis loop which indicates a lower or higher potential and current values. This technique was employed in Chapters 6 and 7.

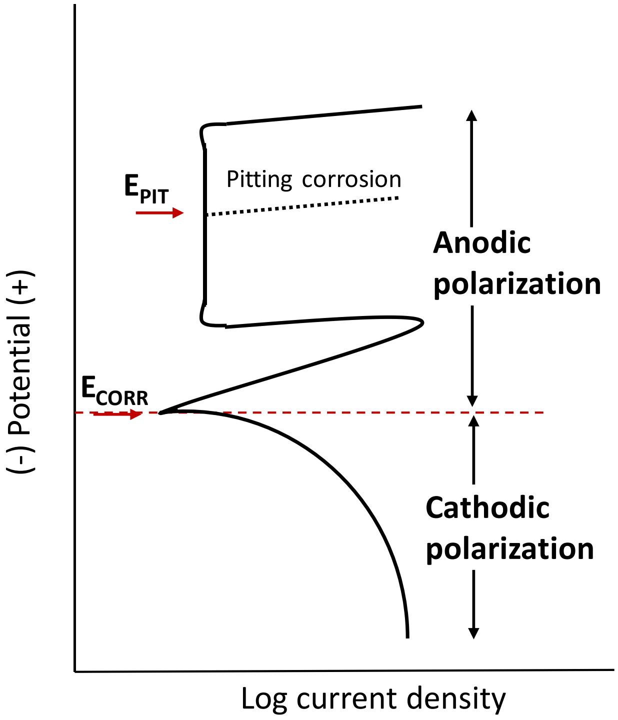

Figure 2-14. Potentiodynamic polarization resistance curve.

3. Analysis of pore solution of different cements with and without admixed chlorides[1]

3.1. Overview

The pore solution expressed from 28-day cement pastes was analyzed, as part of a wider research program investigating the corrosion behavior of stainless-steel reinforcing bars in concrete, using inductively coupled plasma and ion chromatography techniques. The pastes were prepared with: different water to cementitious materials (binder) ratios (w/cm); portland cement with and without supplementary cementitious materials, and with admixed sodium chloride in the range typical of the threshold values for stainless steel reinforcement. The major anion and cation concentrations are given, showing the influence of admixed chloride on the amount of chloride retained in solution and of sulfate released into the pore solution. The results are discussed in terms of the initial compositions of the cementitious materials and their effect on chloride binding.

3.2. Background

The cement paste component of hardened concrete is porous and, under normal conditions, the pores are partially, or completely, filled with a highly concentrated ionic solution. It is the composition (and availability) of this solution that determines whether any embedded metal will be passively or actively corroding. Analysis of the solution expressed from hardened cement pastes [5] has indicated that the pH ranges from ~12.6 – 13.8 with the dominant species being potassium hydroxide (KOH) [114]–[116]. The solution is buffered to the lowest level of this range by the presence of large amounts of portlandite ($Ca(OH)_2$) in the cement paste.

Nondestructive monitoring of the corrosion behaviour of reinforcing bars (rebar) in concrete is difficult for a number of reasons. First, the location and extent of corrosion cannot be seen or readily determined. Second, the content of chlorides in the pore solution or the level of carbonation in the cement paste adjacent to the rebar can be neither controlled nor measured. Consequently, in order to determine the relative corrosion resistance of different reinforcing materials, the chloride concentration necessary to initiate active corrosion or the influence of different salts on corrosion, researchers often resort to testing the rebar in simulated concrete pore solution. Most of these studies have used either saturated $Ca(OH)_2$) with pH ≈12.60 e.g. [62], [64], [117], a mixture of KOH and NaOH, such as that specified by ASTM A955 [118] or some with all three hydroxides, e.g. [19], [59], [119]. The actual pore solution analysis e.g. [2], [116], however, also shows some sulfate in solution and some researchers have included $CaSO_4$ in the simulated solution [20], [22], [120].

ASTM C1152 and C1218 [121], [122] recommend acid-soluble and water-soluble chloride analysis of the hardened concrete, respectively, but it is often difficult to “translate” those data to the amount of chlorides in the pore solution, because of variability in testing conditions. To address this predicament,

---

[1] The contents of this chapter have been accepted for publication in ACI Materials Journal and adapted with permission: C.B. Van Niejenhuis, I.G. Ogunsanya, C.M. Hansson. “Analysis of pore solution of different cements with and without admixed chlorides”, submitted to *ACI Materials Journal*, M-2018-320.R3.

pore solution was expressed from ordinary portland cement pastes with a water/cementitious (binder) materials ratio (w/cm) of 0.5 and different amounts of admixed chlorides, in levels considered to be critical for corrosion resistant rebar, such as stainless steel. The results were published in 2014 [123]. Feedback from this publication indicated the data were too limited because they involved only one cementitious mixture and only one w/cm, although both the presence of supplementary cementitious materials (SCMs) and the w/cm ratio are known to influence the pore solution composition at the lower chloride levels [6]. Subsequently, Vollpracht et al. [124] provided an excellent review of the literature on the influence SCM's on the composition of C-S-H and the alkalinity of the pore solution.

The goal of the current project was to extend the earlier work to cement pastes with different w/cm and with different SCMs. In addition, a complete chemical analysis of both cations and anions was obtained.

3.3. Research Significance

In order to study the effects of many parameters, such as concrete mixture design or chloride content within a reasonable timescale, many researchers make use of tests in simulated pore solutions rather than concrete. However, the relationship between the amount of chloride in concrete as, for example, in concrete tested the field, and the concentration in the pore solution of that concrete has not been well documented. This research is aimed at filling that gap in the knowledge, particularly in the range of chloride levels typical of the threshold concentrations for stainless steel rebar. Ideally, the composition of the pore solution in concrete in close vicinity of embedded rebar should be determined. Unfortunately, this is not feasible because there is insufficient cementitious material to be able to express and analyse the pore solution. Moreover, the chloride content of concrete exposed to saline conditions is highly inhomogeneous, both through the depth of the concrete cover and along the length of the interface between the concrete and the rebar [125], [126]. Due to these limitations, pore solution expression tests were conducted.

3.4. Experimental procedure

Cement pastes were cast using ordinary portland cement (OPC – Canadian General Use (GU) Cement [127]): (i) without any SCMs; (ii) with 25% replacement by ground granulated blast furnace slag (GU-BFS); (iii) with 25% replacement by Type CH fly ash (GU-FA) and (iv) interground with 7% replacement of silica fume (GU-SF). Analyses of each of the components, provided by the suppliers, are given in Table 3-1.

Table 3-1. Cement and supplementary cementitious materials composition, weight % as provided by the supplier.

Component	Portland cement (GU)	Silica Fume Cement (GU-SF)	Ground Granulated Blast furnace slag	Type CH Fly Ash
LOI	2.04	1.98	1.60	1.25
SiO_2	18.94	25.71	38.66	40.23
Al_2O_3	5.16	4.89	8.9	19.19
Fe_2O_3	2.31	2.32	0.52	8.25
CaO	62.76	56.39	38.53	21.87
MgO	2.31	2.17	11.32	3.99
SO_3	4.03	4.08	2.75	1.70
Total Alkali	0.98	0.97	0.77	1.91

For each cementitious mixture, pastes were cast with w/cm ratios of 0.40, 0.45, 0.50, and 0.55. For the 0.40 and 0.50 w/cm mixes, chlorides, added as reagent grade sodium chloride (NaCl), were dissolved in the distilled mixing water at concentrations of 0%, 2.5%, 5.0% and 7.5% by mass of the cementitious materials. For the 0.45 and 0.55 w/cm mixes, pastes were cast without chlorides and with 5.0 % Cl^- as NaCl. The pastes were mixed for three minutes, allowed to breath for three minutes, then remixed for a further three minutes. Then, each slurry was poured into four cylinders measuring 50 mm [1.97 in.] Ø × 100 mm [3.94 in.], compacted, sealed, and slowly rolled for 24 hours, to avoid bleeding. The cylinders were then removed from the roller but kept sealed in the moulds and held in laboratory conditions for another 27 days.

Thereafter, the hardened pastes were demoulded and inserted into the pore solution expression chamber. An 8-mm [0.32 in.] thick PTFE disk was inserted on top of the specimen to ensure the chamber was sealed, followed by an 8-mm [0.32 in.] thick nylon disk. The piston was then inserted into the expression chamber and a syringe was pressed into the outlet at the bottom of the unit to receive the expressed solution.

Pressure was applied slowly at increments of 50kN [11,250lbs.] up to ~1000kN [225,000 lbs]. Each load increment was held for approximately 2-5 minutes or until no more solutions was expressed into the syringe. The syringe was fitted with a 0.45µm filter, to prevent the inclusion of small solid particles. Solutions, typically in the amounts of 2-10 ml [0.06 – 0.34 fl oz], were obtained but, in cases in which less than 2 ml of pore solution was obtained, the solutions from two cylinders of the same mixture were combined into one syringe. The syringes were then sealed to ensure that CO_2 did not react with the $Ca(OH)_2$. The syringes were stored in the dark at ambient temperature until they were sent for analysis. The chemical compositions of three replicate samples were then determined using ion chromatography (IC) for the anions and inductively coupled plasma (ICP) analysis for the cations. For those cations in the mmols/L range of concentration, ICP -MS was used, while ICP-OES was for the lower concentration (µmols/l range) cations.

The evaporable water (W_{ep}) content of the pastes with the 0.40 w/cm ratio was determined by grinding hardened samples of the pastes, at 28 days, and weighing the samples (W_W), drying for 24 hours at 105°C, and re-weighing (W_D). Expressed as a percentage of the wet hardened paste, the evaporable water is $W_{ep} = (W_W - W_D)/W_W \times 100\%$. In order to express the evaporable water (W_e) in the same units as the admixed chlorides (% by mass of dry cement) Wep is then multiplied by (1+w/cm) in Equation 3-1.

$$W_e = \left(\frac{W_w - W_D}{W_W}\right) \cdot (1 + w/cm) \cdot 100\%$$

Equation 3-1. Relationship between evaporable water and w/cm of cement paste.

3.5. Experimental results

The complete data analysis are available upon request from the authors, but it is impossible to discuss the variation in composition of each of the elements. Consequently, only the major components of cementitious systems, given in Table 3-1, are included in Table 3-2 and considered in the Discussion.

It did not prove logistically possible to determine accurate and reproducible pH values for all of the three replicates of each of the forty-eight different paste mixes because of the limited amount of expressed solution. Diluting the solution to provide the necessary volume would have altered the equilibrium between the ions and, hence, the pH. Those that were measured varied from 13.1 to 13.6. It had been hoped that the pH values might be estimated by subtracting the molar anion content (chlorides + sulfates) from the total molar cation content. However, the excessively high chloride contents meant that a small inconsistency (< ±1%) in the chloride measurements results in a very large change in the pH calculations. Consequently, it was not possible to determine a correlation between chloride "saturation level" and pH.

The average values of the major components of the pore solution from replicate specimens of all mixture proportions are given in Table 3-2. Figure 3-1 shows the chloride content in the expressed pore solution versus the admixed chloride content for 0.40 and 0.50 w/cm mixes. Similarly, the sulfate contents of the pore solutions are plotted in Figure 3-2.

To illustrate the influence of w/cm ratio, all the pore solution chloride and sulfate data for 5.0% admixed chloride in the four cement mixes are shown in Figure 3-3.

Table 3-2. Major components of the expressed pore solution, mmol/L.

	w/cm	**Admixed Chloride**	**Cl**	**SO_4**	**S**	**Na**	**K**	**Ca**	**Al**	**Si**	**Fe**	**Mg**
GU	0.40	0.0	2	61	61	164	789	1.28	0.15	0.57	0.08	1.65
		2.5	2622	334	349	2036	946	0.63	0.19	0.78	0.01	1.65
		5.0	4827	572	657	4530	932	0.37	0.02	0.39	0.01	1.65
		7.5	4948	712	825	4859	821	0.64	0.01	0.23	0.01	1.65
	0.45	0.0	2	33	33	167	752	0.81	0.20	0.40	0.13	0.06
		5.0	4425	405	423	4509	896	0.31	0.07	0.43	0.01	0.72
	0.50	0.0	1	15	16	137	574	1.14	0.14	0.28	0.02	0.70
		2.5	2009	135	135	2434	744	0.83	0.04	0.55	0.08	0.70
		5.0	3934	279	291	3928	777	0.49	0.05	0.39	0.01	1.38
		7.5	5156	486	507	5255	711	0.42	0.03	0.30	0.20	1.38
	0.55	0.0	1	12	11	129	530	1.34	0.16	0.26	0.09	0.73
		5.0	3417	180	188	3431	670	0.58	0.05	0.39	0.01	1.38
GU-BFS	**w/cm**	**Admixed Chloride**	**Cl**	**SO_4**	**S**	**Na**	**K**	**Ca**	**Al**	**Si**	**Fe**	**Mg**
	0.40	0.0	3	13	37	125	478	1.52	0.09	0.27	0.23	1.65
		2.5	2225	157	285	2157	649	0.83	0.03	0.38	0.11	1.65
		5.0	4851	417	566	4048	683	0.45	0.01	0.41	0.07	1.65
		7.5	5309	622	712	4822	638	0.73	0.01	0.22	0.08	1.11
	0.45	0.0	2	10	25	126	477	0.46	0.18	0.32	0.17	0.69
		5.0	3728	235	350	3787	593	0.59	0.03	0.29	0.09	0.69
	0.50	0.0	2	5	13	111	403	1.68	0.08	0.18	0.09	0.02
		2.5	1830	120	211	1935	549	0.22	0.23	1.37	0.31	0.03
		5.0	3453	252	432	3587	543	0.74	0.02	0.28	0.32	1.85
		7.5	5132	353	555	5162	519	0.49	0.03	0.27	0.06	0.73
	0.55	0.0	1	4	11	100	358	0.98	0.10	0.17	0.05	0.71
		5.0	3065	159	299	3180	489	0.72	0.02	0.30	0.02	1.37

	w/cm	Admixed Chloride	Cl	SO_4	S	Na	K	Ca	Al	Si	Fe	Mg
GU-FA	0.40	0.0	2	22	24	185	585	1.08	0.28	0.44	0.16	1.65
		2.5	2153	247	273	2247	715	0.69	0.06	0.75	0.02	1.65
		5.0	4716	554	584	4219	767	0.39	0.03	0.58	0.02	1.65
		7.5	5163	798	785	4811	692	0.58	0.03	0.29	0.03	1.65
	0.45	0.0	1	12	13	179	564	1.22	0.34	0.45	0.16	0.70
		5.0	3872	415	412	3955	654	1.29	0.12	0.51	0.07	0.69
	0.50	0.0	1	6	6	165	485	1.27	0.22	0.29	0.02	0.02
		2.5	1608	119	120	1685	516	1.18	0.12	0.51	0.35	0.02
		5.0	3388	293	290	3473	580	1.06	0.12	0.55	0.09	1.66
		7.5	4752	514	539	5152	551	1.68	0.04	0.25	0.03	0.90
	0.55	0.0	1	3	4	141	415	0.95	0.21	0.25	0.08	0.75
		5.0	3044	226	230	3098	514	1.03	0.08	0.44	0.14	0.69
GU-SF	w/cm	Admixed Chloride	Cl	SO_4	S	Na	K	Ca	Al	Si	Fe	Mg
	0.40	0.0	4	38	41	94	341	1.00	0.17	0.46	7.03	1.65
		2.5	2742	262	263	2135	709	2.45	0.05	0.22	2.75	1.65
		5.0	5018	501	512	4024	758	2.38	0.01	0.14	0.49	1.65
		7.5	5772	545	554	4411	690	1.93	0.01	0.11	0.26	1.65
	0.45	0.0	3	20	19	86	316	0.06	0.24	0.51	1.47	0.71
		5.0	3953	391	425	4079	675	2.21	0.02	0.27	0.07	0.69
	0.50	0.0	3	9	10	75	268	1.08	0.17	0.34	0.80	0.70
		2.5	1687	108	113	1644	511	1.38	0.06	0.43	0.37	1.38
		5.0	3606	278	291	3439	583	1.93	0.03	0.30	0.08	0.71
		7.5	4815	464	485	4922	538	2.92	0.02	0.16	0.04	0.02
	0.55	0.0	3	7	7	73	258	0.72	0.18	0.27	0.65	0.02
		5.0	3110	206	216	3041	520	1.79	0.04	0.30	0.13	0.01

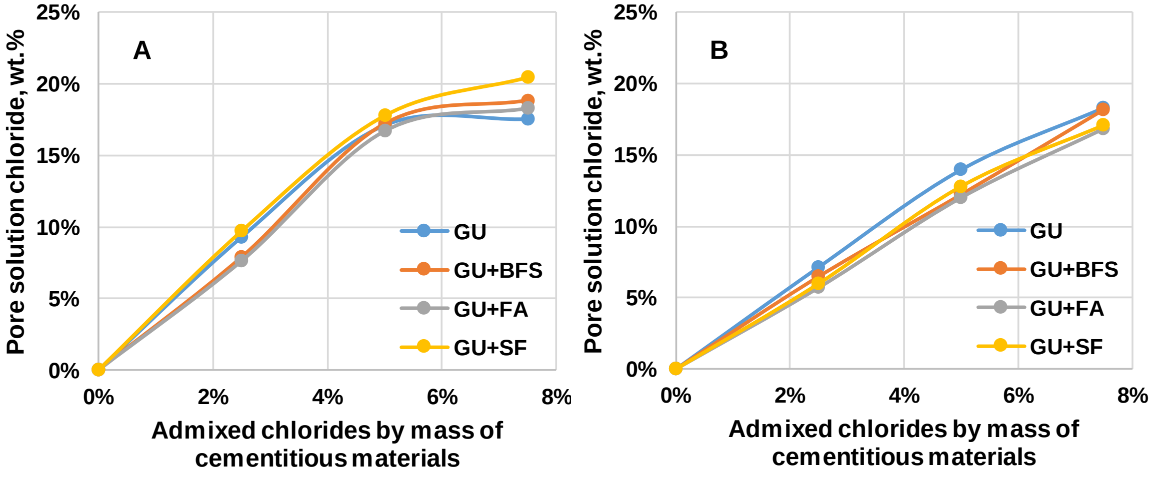

Figure 3-1. Chloride content (wt.%) of the expressed pore solution as a function of the admixed chloride content, (A) for mixes with w/cm ratio of 0.40 and (B) for mixes with w/cm 0.50.

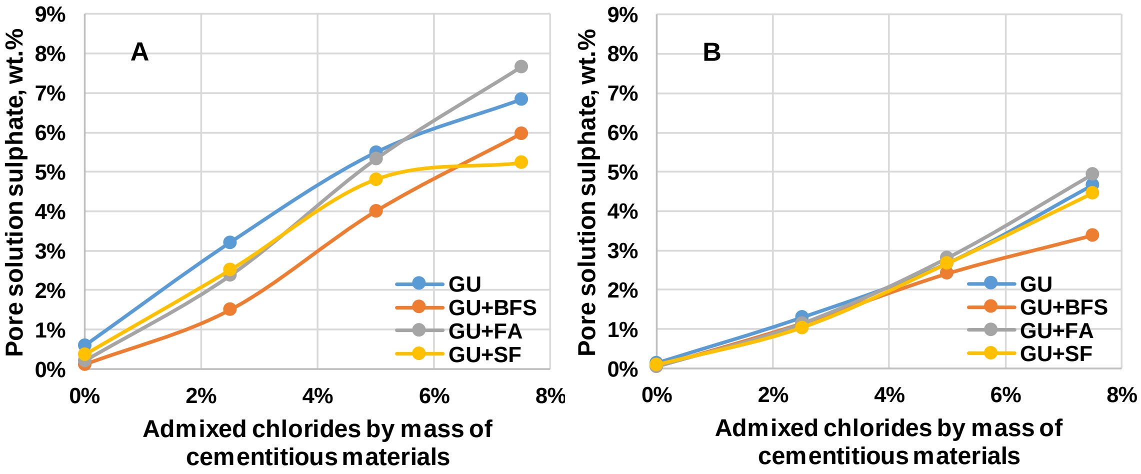

Figure 3-2. Sulfate content (wt.%) of expressed pore solution as a function of the admixed chloride content, (A) for mixes with w/cm ratio of 0.40 and (B) for mixes with w/cm 0.50.

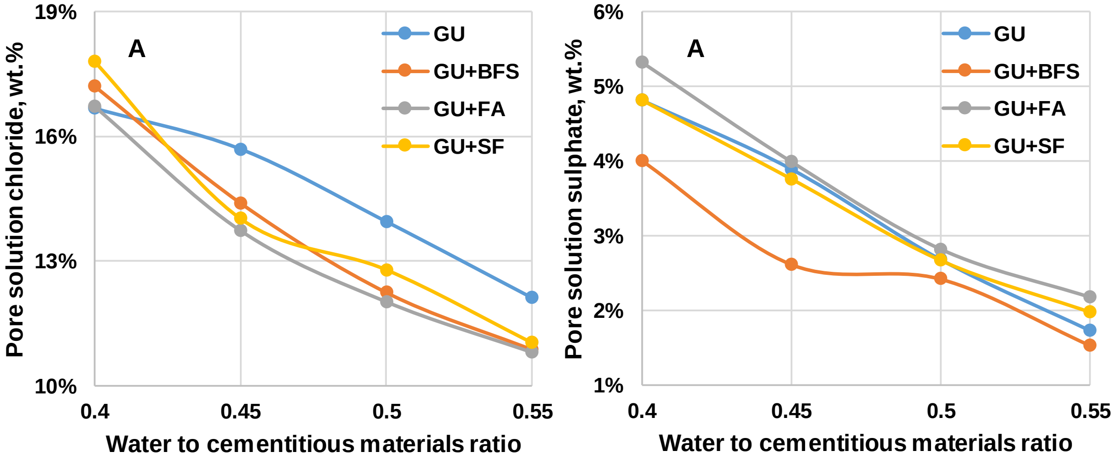

Figure 3-3. The influence of w/cm ratio on (A) the chloride and (B) sulfate contents (wt.%) of the pore solution expressed from pastes containing 5.0% admixed chlorides by weight of dry cementitious material.

3.6. Discussion

Figures 3-1 and 3-2 show that chloride and sulfate contents of the pore solution increased approximately linearly with admixed chloride content for the pastes with 0.50 w/cm.

In the pastes with 0.40 w/cm, on the other hand, the curves for pore solution chloride content began to level off at the high admixed chloride levels. This indicates that the dissolved chloride is approaching its saturation limit in pore solution. However, that limit increased from ~17.5% for the GU paste to ~21% for the GU-SF paste. This increase is likely to be related to the decreased pH level of the pastes with SCM's, similar to the findings of Vollpracht et al. [124]. However, as indicated above, it did not prove possible to determine accurate and reproducible pH values. Moreover, it did not prove feasible to determine the theoretical values of the pH thermodynamically for these high chloride contents using program such as Gibbs Energy Minimization Software (GEMS) Thermodynamic Modelling [128], [129].

This is because of the very large reservoir of solid $Ca(OH)_2$ in the paste which buffers the solution, but is not taken into account in the thermodynamic calculations.

It is important to mention, in this context, that NaCl was used rather than $CaCl_2$ or $MgCl_2$, for a number of reasons: (i) NaCl is the major component of seawater and, by far, the most extensively used de-icing agent; (ii) Admixed NaCl is also used in the proposed modification of EN 480 for a "Rapid Screening Test" for stainless steel rebar. This test is now incorporated into the British Standard BS 6744-16; (iii) NaCl is also the required salt for ASTM G109 and ASTM A955; and (iv) as a number of studies have observed that there is less chloride binding from NaCl than from other salts [130], [131]. However, it has also been shown that admixed NaCl increases the pH of the pore solution, while $CaCl_2$ decreases the pH [132]. Thus, the present data should not be extrapolated to systems in which salts other than NaCl are used.

Similarly, the sulfate pore solution contents in the 0.40 w/cm pastes levelled off at the high admixed chloride contents but, for these anions, the "ranking" was the reverse of that of the chlorides, with the GU paste having the highest pore solution sulfate content (~2.7%) and the GU-SF the lowest at ~1.75%. This difference cannot be attributed to any significant difference in the original sulfate content of the cements or to their aluminum content, as Table 3-1 indicates these are very similar in the two cements.

An alternative explanation for the different "ranking" could be the amount of chlorides bound in the form of Friedel's or Kuzel's salts, which is dependent on the aluminate phases [133]. Since chemical binding of chlorides involves substitution of other anions, particularly sulfates, from the aluminate phases, the highest chloride content might be expected to be accompanied by the lowest sulfate content in the pore solution. According to Table 3-1, the highest aluminate content is in the GU-FA paste which would, thus, be expected to have the highest level of bound chlorides and, in turn, the lowest level of chlorides in the pore solution, which was demonstrated by 3 of the 4 data points in Figure 3-3. Similarly, the GU-FA paste would have been expected to have the highest sulfate in the pore solution, as observed in Figure 3-3.

Although it is recognized that not all water evaporated at 105°C comprises the total amount of "evaporable" water, it is generally considered as a reasonable measure, [134]. Therefore, the amount of bound chlorides, and their influence on the amount of sulfates released into the pore solution, were calculated using the measured evaporable water content of the pastes with 0.40 w/cm ratio and the concentration of chlorides and sulfates in the expressed pore solution to give the total amount of these ions in solution. The procedure is shown for chlorides in Equations 2-3 and the same procedure was used to calculate the dissolved sulfates. These values were then subtracted from the amounts in the original pastes to give an estimate of the amount of bound chlorides and sulfates. These data are shown in Tables 3-3 and 3-4, respectively. If the presence of sulfates in the pore solutions is solely due to their replacement in the aluminate phases by chlorides, there should be a direct correlation between the molar amount of bound chlorides and the molar amount of dissolved sulfates. The molar contents of bound chlorides (calculated as described above) and of the dissolved sulfates are given in Table 3-5 and plotted in Figure 3-4. It should also be noted that the GU-SF mix had the lowest level of evaporable water, as expected, because of its more rapid hydration rate, while the GU-BFS and GU-FA had more evaporable water than the GU because of their slower hydration rate.

Table 3-3. Amounts of dissolved and bound or trapped chlorides in the pastes with 0.40 w/cm ratio.

Binder	Admixed Cl^- wt% of dry binder	Evaporable Water % of dry cement	Cl wt % in pore solution	Total dissolved Cl wt.% of dry binder	Bound/trapped Cl, wt.% of dry binder
	Cl_{add}	W_e	Cl_{diss}	Cl_{free}	Cl_{bound}
GU	0.0	19.1%	0.01	0.00	0.00
	2.5	18.8%	9.29	1.78	0.72
	5.0	17.4%	16.66	3.18	1.82
	7.5	19.0%	17.54	3.35	4.15
GU-BFS	0.0	19.5%	0.00	0.00	0.00
	2.5	20.1%	7.85	1.54	0.96
	5.0	19.1%	17.20	3.35	1.65
	7.5	19.4%	18.82	3.67	3.83
GU-FA	0.0	19.8%	0.00	0.00	0.00
	2.5	19.8%	7.63	1.51	0.99
	5.0	19.5%	16.72	3.31	1.69
	7.5	18.3%	18.31	3.62	3.88
GU-SF	0.0	18.2%	0.00	0.00	0.00
	2.5	18.2%	9.72	1.77	0.73
	5.0	18.2%	17.79	3.24	1.76
	7.5	18.0%	20.46	3.72	3.78

$$Cl_{free} = Cl_{diss} \cdot W_e$$

Equation 3-2. Relationship between free and dissolved chloride.

$$Cl_{bound} = Cl_{add} - Cl_{free}$$

Equation 3-3. Relationship between bound chloride and free chloride.

Table 3-4. Amounts of dissolved and bound or trapped sulfates in the pastes with 0.40 w/cm ratio.

Binder	Admixed Cl^- wt.% of dry binder	SO_4 - wt.% of dry binder	SO_4 wt% in pore solution	Total dissolved SO_4, wt.% of dry binder	Bound SO_4, wt.% of dry binder
W_e	Cl_{add}	$SO_{4\text{-cement}}$	$SO_{4\text{-diss}}$	$SO_{4\text{-free}}$	$SO_{4\text{-bound}}$
GU	0.0	4.84	0.59	0.12	4.72
	2.5	4.84	3.21	0.60	4.24
	5.0	4.84	4.01	0.77	4.07
	7.5	4.84	6.84	1.31	3.53
GU-BFS	0.0	4.45	0.13	0.03	4.42
	2.5	4.45	1.51	0.29	4.16
	5.0	4.45	4.01	0.78	3.67
	7.5	4.45	5.97	1.16	3.29
GU-FA	0.0	4.14	0.21	0.04	4.10
	2.5	4.14	2.38	0.47	3.67
	5.0	4.14	5.33	1.06	3.08
	7.5	4.14	7.66	1.52	2.62
GU-SF	0.0	4.90	0.37	0.07	4.83
	2.5	4.90	2.51	0.46	4.44
	5.0	4.90	4.81	0.88	4.02
	7.5	4.90	5.23	0.95	3.95

Table 3-5. Molar masses of bound chlorides and dissolved sulfates.

Binder	Admixed Cl wt.% of dry binder	Bound/trapped Cl mmol per 100 g dry binder	Dissolved SO_4 mmol per 100 g dry binder
GU	0.0	0	1.27
	2.5	20	6.25
	5.0	51	7.98
	7.5	117	13.61
GU-BSF	0.0	0	0.26
	2.5	27	3.07
	5.0	46	8.15
	7.5	108	12.13
GU-FA	0.0	0	0.43
	2.5	28	4.91
	5.0	48	10.99
	7.5	109	15.80
GU-SF	0.0	0	0.70
	2.5	21	4.76
	5.0	50	9.12
	7.5	106	9.92

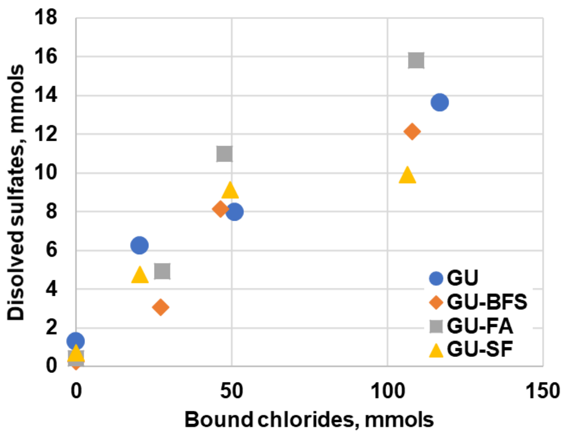

Figure 3-4. Molar masses of bound chlorides and dissolved sulfates per 100g binder.

While it is clear that there is not a direct 1:1 relation, there is a definite trend of increased dissolved sulfates with increased binding of the chlorides, with the GU-FA pastes exhibiting the highest sulfate content and GU-SF paste the lowest. It has been shown that chloride binding can also occur by adsorption on the aluminate phases without replacement of any anion, as well as exchange with hydroxyl ions [135] and in the C-S-H [136] which could explain the greater amount of bound chlorides than free sulfates in Figure 3-4. The “beneficial effect” of sulfates has also been observed in chloride threshold tests, both for carbon steel and stainless steel, in various synthetic pore solutions using the composition of the expressed pore solution [137], [138]. These tests have demonstrated that adding sulfates in proportion to the chlorides measured in the current project, results in a higher chloride threshold level, i.e. greater corrosion resistance, indicating the potential advantage of fly ash blended cements.

In a previous publication [112], it was observed that the corrosion resistance of stainless steel rebar embedded in GU concrete with 3% admixed chloride was significantly greater than those embedded in GU-BFS concrete of the same proportions. It was hypothesized that the chloride binding was less in the GU-BFS than in the GU, thereby leaving more chloride in solution in the GU-BFS. However, the current data, in Figure 3-1, indicate the chloride concentration in the GU pore solution is ~20% higher than that in the GU-BFS at 2.5% admixed Cl^-. The sulfate levels follow a similar trend. However, Table 3-2 shows that at 2.5% admixed chloride, there is more excess sulfur in the GU-BFS (128 mols) than in the GU (15 mols). This is in qualitative agreement with the reports of Vollpracht et al. [124]. Scott and Alexander [114] showed that excess sulfur, present as sulfide in the BFS mix, compromises the formation of the passive layer on the rebar, reducing its resistance to chloride attack.

In view of the fact that the chloride content of the expressed pore solution in the previous study [123] was determined by titration and, in the current study, by ion chromatography and that different batches of GU cement were used, the correspondence in data, shown in Figure 3-5, is considered to be very good.

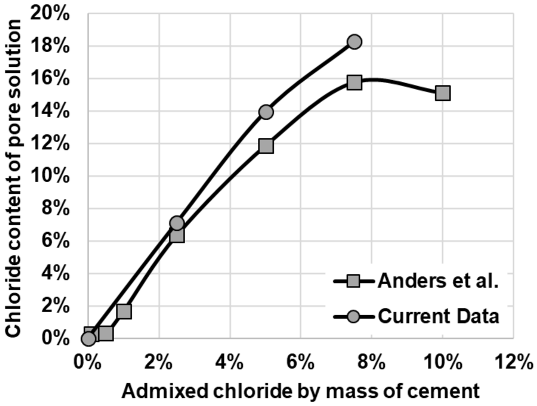

Figure 3-5. A comparison of the current data for pastes with 0.5 % w/cm ratio with those of Anders et al. [123] for similar pastes.

3.7. Summary and conclusions

The decrease in ionic concentration of the expressed pore solution with increased w/cm ratio of the pastes is, as expected, due to the dilution effect of the additional water.

The data indicate that a saturation limit of chlorides in the pore solution is reached, or approached, in the pastes with 0.40 w/cm ratio at an admixed chloride level of 7.5% Cl^- by mass of cementitious materials. The maximum pore solution chloride concentration was observed to be ~17.5 wt.% for GU, 18.3 wt.% for GU-FA, 18.8 wt.% for GU-BFS and 20.5 wt.% for GU-SF.

While the increase in pore solution chlorides with increased admixed chlorides was, obviously, expected, the high, and increasing, levels of sulfates had not been predicted. The maximum levels in the 0.40 w/cm ratio pastes were 5.2 wt.% in the GU-SF, 5.9 wt.% in the GU-FA, 6.8 wt.% in the GU and 7.7 wt.% in the GU-BFS.

Although it is known that the inclusion of SCMs retards the ingress of chlorides into concrete, an additional specific benefit of fly ash in highly chloride-contaminated concrete is its higher dissolved sulfate content and lower dissolved chloride content, than in other cement mixes.

Most determinations of critical chloride concentrations, $C_{crit,}$ for active corrosion initiation have been conducted on carbon steel in ordinary portland cement paste, mortar or concrete. This work has shown that the values may differ if SCMs are incorporated in the mix. For example, sulfate contents are significantly higher in the GU solution than in the GU-BFS, whereas the “free” sulfur (probably sulfide) is higher in the GU-BFS.

4. Influence of chloride and sulphate anions on the electronic and electrochemical properties of passive films formed on steel reinforcing bars[2]

4.1. Overview

Reinforced concrete structures are suffering from the application of de-icing salts, particularly due to premature reinforcement corrosion. To understand and, thereby, identify solutions to this problem, a study has been con- ducted of the chloride- and sulphate-induced instability of the semiconductor passive films formed on carbon and 2304 stainless steel alloys in a simulated concrete pore solution environment. Steels' vulnerability to corrosion when depassivation occurs, typically in the presence of chloride and/or low pH, makes it essential to understand the nature of their passive films in the effort to mitigate the effect of corrosion. The influence of major alloying elements in five different reinforcing bars and testing on different surface roughness was investigated in the first part of the study. In this second part, linear polarization resistance and potentiodynamic cyclic polarization tech- niques and Mott-Schottky (M-S) analysis were used to investigate the influence of varying ionic concentrations and, thus, pH of simulated concrete pore solutions on passive films formed on duplex 2304 stainless steel and carbon steel reinforcing bars. It was found that chloride ions increased the defect densities of passive films, most significantly in the lower pH solution, while sulphates decreased the densities. This is attributed to the formation of stable solid sulphides of Fe and Ni (as FeS, FeS_2, NiS, Ni_3S_2) in the outer Fe-rich layer of the passive films as predicted by ThermoCalc© calculations.

4.2. Background

Both carbon steels and stainless steels form stable passive films in concrete, largely because of the high pH solution in the pores of the cement paste component of the concrete. Unfortunately, these films can be destroyed by chlorides, for example, from anti-icing agents or sea water, causing active corrosion of the reinforcing bar (rebar). Studying the corrosion of rebar in concrete requires long term testing so, for expediency, many researchers use a simulated pore solution instead. The solutions used have included saturated calcium hydroxide, $Ca(OH)_2$, (pH ~ 12.6) [12]–[18]; hydroxides of sodium and potassium, NaOH+KOH (pH ~13.8) [118], and combination of all three hydroxides, $Ca(OH)_2$+NaOH+KOH, (pH ~13.5) [19], [20]. However, the solution expressed from hardened cement paste was found to be different from these simulated pore solutions previously used [11]. The major difference is that sodium chloride from the added salts reacts with the ettringite phase of the cement paste, binding the chloride in the formation of Friedel salt and releasing sulphate ions into the pore solution.

The properties of passive films on steel in lower pH solutions have been shown to be those of an extrinsic semiconductor [97], [105], [107], [139]–[142]. As a result, there has been increasing effort to relate the electronic behaviour of the semiconducting passive films formed in concrete to the steel's corrosion resistance using the Mott-Schottky (M-S) analysis [143], [144]. The first part of this study has

---

[2] The contents of this chapter have been adapted from Elsevier: I.G. Ogunsanya, C.M. Hansson. "Influence of chloride and sulphate anions on the electronic and electrochemical properties of passive films formed on steel reinforcing bars" *Materialia*, 8 (2019) 100491.
DOI: https://doi.org/10.1016/j.mtla.2019.100491

reported the corrosion behaviour and M-S analysis of several stainless steel reinforcing alloys [145]. The objective of the present second part, was to investigate the influence of varying the ionic concentration and the addition of sulphates in simulated concrete pore solutions, on the corrosion resistance and passive film characteristics of carbon steel and 2304 duplex stainless steel. The methods used were linear polarization resistance, cyclic polarization and M-S analysis. In order to relate the results to the corrosion behaviour of rebar in the field, these bars were tested in their as-received condition to determine the properties of the exposed in-service surface, rather than polished cross-sections.

Most previous M-S analyses have been carried out in an acidic, neutral or slightly alkaline environment – an environment significantly different from that in concrete, for which the pH is typically > 13 [2]. The M-S analysis uses electrochemical impedance spectroscopy at different applied potentials to obtain the capacitance of the space charge layer of the semiconducting passive films formed on steel. From Equation 4-1, the overall capacitance, C, represents the potential difference across the metal/electrolyte interface and is the sum of the space charge capacitance in the film, C_{SC}, and the Helmholtz double layer capacitance, C_H, in the solution [97]. However, since the Helmholtz double layer capacitance is typically about 2-3 orders of magnitude greater than the space charge capacitance, the $1/C_H$ component becomes insignificant and is, generally, omitted in studies of passive films [68]. Consequently, Equation 4-2 is used to obtain the M-S plot which presents the inverse of the square of the capacitance of the passive film versus the applied potential versus the applied potential.

$$1/C^2 = (1/C_{sc}^2 + 1/C_H^2)$$

Equation 4-1. Equation for calculating capacitance across a film/electrolyte interface

$$1/C_{sc}^2 = \pm(2/\varepsilon\varepsilon_0 eNA^2)(E - E_{FB} - kT/e)$$

Equation 4-2. Mott-Schottky equation for calculating capacitance of SCL.

Where C is the apparent capacitance; C_H and C_{SC} are defined above and $C_{SC} = 1/(-Z''2\pi f)$ [108], where Z" = imaginary part of the impedance, f = frequency; A is the exposed specimen area; N is the charge carrier density (N_D or N_A is the donor or acceptor density given by the slope (m) of the linear portion of the $1/C^2$ vs. E plot using the relation $N = 2/\epsilon\epsilon_0 em$ [107], [140], [141]); E_{FB} is the flatband potential, the potential at which the semiconducting passive film is in equilibrium with its environment [69]; ε = relative permittivity of the semiconductor or dielectric constant; ε_0 = permittivity of free space (8.85×10^{-13} F/mm); k = Boltzmann constant (1.38×10^{-23} J/K); T = temperature (K) and e = charge of the electron (1.602×10^{-19} C).

The M-S plot can illustrate whether the semiconducting nature of the passive film is p- or n-type and associated defect density associated with either type [65], [101]. Furthermore, the film thickness, d, in nm, can also be calculated [100], [103], [146]–[150] using the capacitance values.

$$d = (\varepsilon\varepsilon_0 A/C)$$

Equation 4-3. Relationship between film thickness and capacitance

The permittivity values used are ε = 10 for carbon steel [104], [151], [152] and 15.6 for stainless steel [141], C is capacitance (F) of the material calculated at different portion (e.g. flatband potential (E_{FB}) and corrosion potential (E_{CORR})) of the M-S plots.

4.3. Materials and methods

Specimen preparation

Ribbed carbon steel and 2304 stainless steel, Canadian 15M (US No.4) reinforcing bars of 16 mm nominal diameter were cut to 125 mm lengths, drilled at one end and soldered with a solid copper wire for electrical connection. Lacquer was applied to both ends to limit the exposed length to 76 mm, giving an exposed surface area of 3581 mm^2. Afterwards, the bars were cleaned with alcohol to remove oil and grease from handling and then rinsed with distilled water. The chemical compositions of both rebar grades are presented in Table 4-1.

Table 4-1. Composition of the bars from the mill certificate provided by the manufacturer.

Rebar grade (ASTM)	**Denoted in text as**	**Composition (wt.%)**								
		Cr	**Ni**	**Mo**	**Mn**	**Si**	**Cu**	**C**	**N**	**P**
UNS S32304	2304	22.40	3.92	0.20	1.80	0.60	0.30	0.02	0.14	0.01
400W	Carbon steel	0.10	0.06	0.01	1.31	0.18	0.26	0.21	0.01	0.01

Simulated concrete pore solutions

Three different “simulated concrete pore solutions”, the compositions of which are given in Table 4-2, were employed. They were: i) saturated calcium hydroxide (CH), as used by many researchers [12]–[18]; (ii) a KOH+NaOH+$Ca(OH)_2$ mix (PS) and (iii) the same tri-hydroxide mix but with $CaSO_4.2H_2O$ (PS+S). The compositions of the last two solutions correspond to those obtained from pore solution expression of a hardened cement paste of 75% OPC+25% ground granulated blast furnace slag paste with a 0.40 w/cm ratio with different amounts of admixed NaCl [11]. The expressed pore solution was found to contain sulphate ions in concentrations increasing with increasing chlorides, hence the incremental sulphate additions to the PS+S solution. Although some authors [2], [20]–[22] have incorporated sulphate in their test solutions, it was added only in the base solution and not increased with increasing chlorides content. Chlorides were added to the solutions in the concentration ranges that have been reported to cause corrosion initiation on carbon steel rebar [137] and on stainless rebar [19], [62]–[64] and the corresponding sulphate amount was added to the solution iii as per Table 4-3.

Table 4-2. Testing solutions.

Testing solution (denotations)	**Composition (Molar)**				**pH**
	$Ca(OH)_2$	KOH	NaOH	$CaSO_4.2H_2O$	
Calcium hydroxide (CH)	Saturated				~12.5
Pore solution (PS)	0.0014	0.48	0.13		~13.6
Pore solution plus sulphate (PS+S)	0.0014	0.48	0.13	0.014	~13.5

Table 4-3. Chloride and sulphate additions to testing solution in Table 4-2.

	Chloride (Sulphate) contents				
For 2304 stainless steel (wt.%)	0% (0.13%)	6% (1.32%)	12% (2.33%)	18% (4.61%)	21% (6.55%)
NaCl in all three solutions (M)	0	1.74	3.49	5.23	6.10
$CaSO_4.2H_2O$ in PS+S only (M)	0.014	0.141	0.250	0.521	0.915
For carbon steel (wt.%)	0% (0.13%)	0.6% (0.49%)	1.2% (0.68%)	1.8% (0.81%)	2.4% (0.89)
NaCl in all three solutions (M)	0	0.17	0.35	0.52	0.70
$CaSO_4.2H_2O$ in PS+S only (M)	0.014	0.053	0.074	0.088	0.097

Experimental setup

Three replicate specimens of each steel grade were tested in three-probe electrochemical cells with the specimens as the working electrodes (WE), a saturated calomel reference electrode (RE) and a mixed metal oxide-coated titanium mesh as counter electrode (CE), as shown in Figure 4-1. Each set of three bars was placed in different cells containing the three different testing solutions shown in Table 4-2 for two weeks to allow them form a stable passive film and their corrosion potentials, E_{corr} were monitored during this period. Afterwards, linear polarization resistance (LPR) and M-S tests were performed on the passivated bars. Chlorides were then added incrementally as NaCl into each of the solutions weekly in 6% increments for the 2304 stainless steel grade and 0.6% increments for carbon steel by mass of pore solution to a maximum of 21% and 2.4%, respectively. This maximum amount corresponds to the pore solutions of hardened cement pastes containing ~10.5% and 0.75% by mass of cementitious material according to [11], [123]. Calcium sulphate dihydrate was also added incrementally as per Table 4-3 to the PS+S solution corresponding to sulphates measured in the expressed pore solution [11].

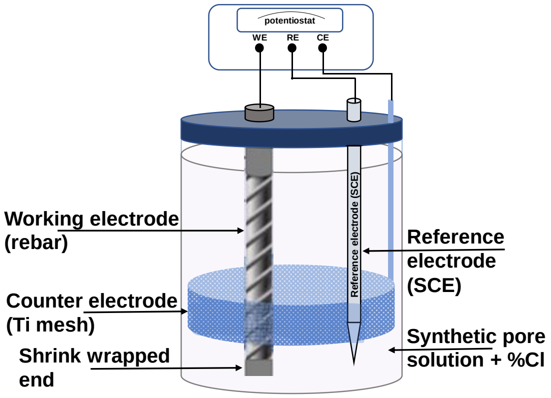

Figure 4-1. Test set-up for electrochemical and M-S analysis [137].

Experimental methods

A potentiostatic linear polarization resistance (LPR) [111] and staircase potential electrochemical impedance spectroscopy (SPEIS) [108] were performed using a BioLogic potentiostat, Model VSP, at every chloride level to determine the corrosion potential, E_{CORR}, the approximate corrosion current density, i_{CORR}, and the M-S behaviour, respectively. These tests were performed as follows: one week after each chloride (and sulphate) addition, an LPR was performed and 24 h later, the SPEIS test was conducted. After a further 24 h, the next increment of chloride (and sulphate) was added and the corrosion potentials of the bars were monitored for a week to ensure they had attained steady state before the next set of tests.

For the LPR test, ±10 mV potential was applied for 30 seconds and the steady state current was measured at the end of this period. The polarization resistance, R_P, the ratio of the applied potential to the measured current, was then converted to corrosion current with 26 mV as the Stern-Geary constant. The SPEIS technique is a function in the BioLogic potentiostat that allows users to divide the interested range of potential values for testing into potential steps and carry out an impedance measurement at each step. For the SPEIS technique, EIS was performed at 10 mV AC amplitude at frequencies from 100 – 1 kHz at 20 potentiostatic steps from -1.5 to +0.6 V_{SCE}. The M-S curves presented in this paper were plotted for data obtained at 1 kHz, to allow comparison with other results in the literature. It was also observed that the capacitance of the film at this frequency is nearly constant [20].

Using different specimens, taken from the same 1.2 m length of both grades of rebar, potentiodynamic cyclic polarization (CP) curves were obtained over the same potential range as the M-S tests in chloride-free CH, PS and PS+S solutions.

4.4. Results

Figure 4-2 shows the corrosion potentials (E_{CORR}) and current densities (i_{CORR}) of the specimens in the three test solutions with increasing chlorides and sulphates, where applicable. The i_{CORR} of all specimens increased gradually with increasing chlorides and sulphates, while their corresponding E_{CORR} values became gradually more negative, suggesting that the ionic and electronic resistances of the passive film were reduced by the chloride ions. In both rebar grades, the i_{CORR} levels were highest for specimens in the CH solution and lowest for the PS+S solution, although all values remained between 1 and 20 mA/m^2, equivalent to corrosion rates between approximately 1 and 20 µm/year. In Ref [153], the average passive current densities of sulphate-free specimens were shown to be an order of magnitude lower than those from specimens tested in sulphate-containing solution without chlorides, although some data sets overlapped. These data [153] can only be compared with those obtained in the present work for specimens tested in solution before increasing sulphates and chlorides. From Figure 4-2, the difference in current densities between PS and PS+S at 0% Cl- in solution is insignificant. The major distinction was observed at higher sulphates and chlorides. Therefore, it is apparent that passive current densities do not show the beneficial effect of sulphates, especially when added in small concentrations.

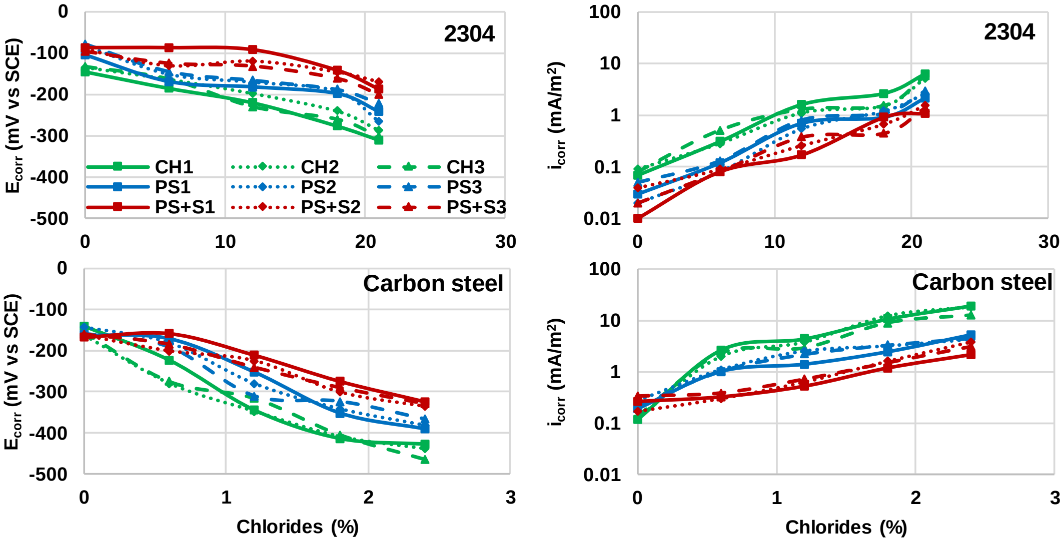

Figure 4-2. Corrosion potentials and current densities obtained from three replicates of bars in their respective testing solution with increasing chlorides and sulphates (only in PS+S).

Figure 4-3 shows the linear regions in the M-S plots of 2304 stainless steel and carbon steel for which the defect densities and film thicknesses of the passive film on the bars were calculated. The film thicknesses were obtained at flatband potentials (~ -0.8 V for 2304 and ~ -0.6 V for carbon steel), corrosion potentials (~ -0.2 V), the onset of the transpassive region (~ -0.35 V) and the end of the transpassive potential (- 0.6 V).

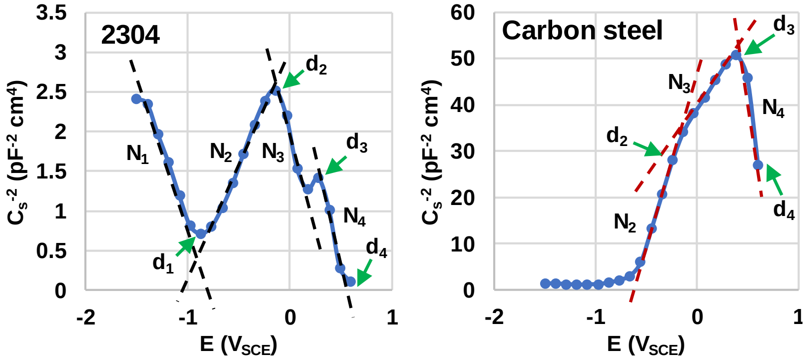

Figure 4-3. M-S plots of the 2304 stainless steel and carbon steel in CH solution without chlorides showing linear regions and capacitance values chosen to calculate defect densities and film thicknesses.

The M-S plots in Figure 4-3 show the influence of increasing chlorides and sulphates on one of three replicates of each steel grade tested in the three solutions. The negative slope observed in the M-S curves of the 2304 bars from -1.5 V_{SCE} to the flat band potential, represents the p-type semiconductor Cr-oxide inner passive layer. This is in agreement with data presented in first part of this work [145] and those of other authors [75], [107], [139]–[141], [154]–[160].

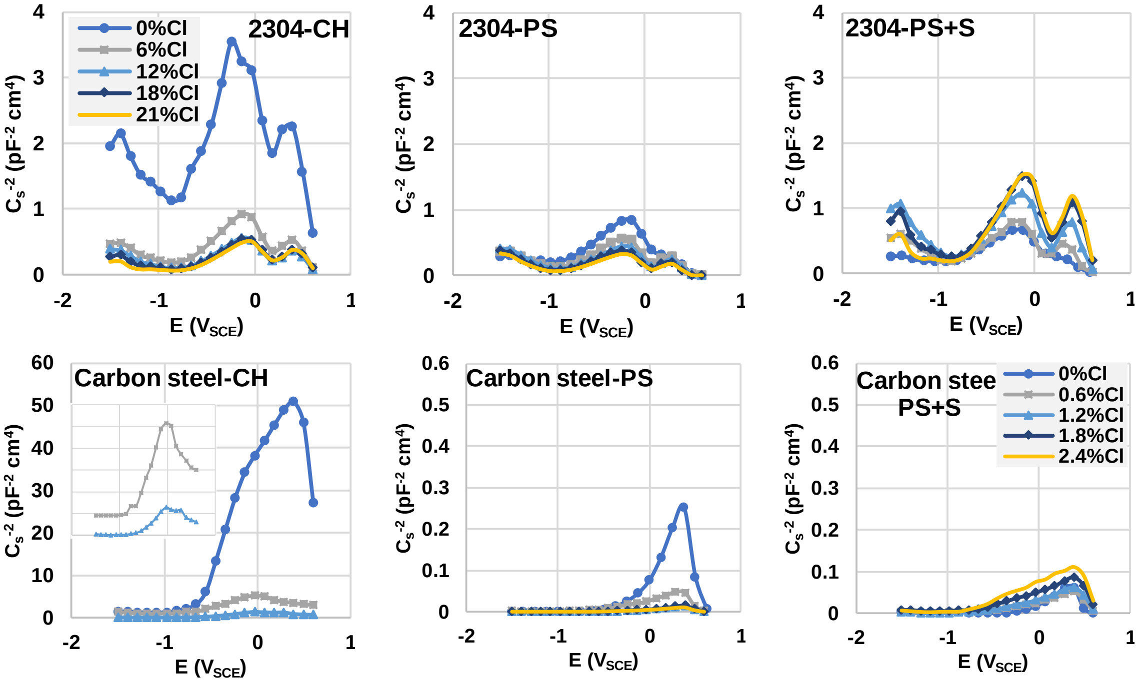

Figure 4-4. M-S plots of 2304 stainless steel and carbon steel bars in the CH, PS and PS+S solutions with increasing chloride and, for the PS+S, increasing sulphates corresponding to those in Table 4-3. Note, for the carbon steel bars: i) the $1/C^2$ axes in the PS and PS+S solution are two order of magnitude lower than those tested in the CH solution and (ii) the different peaks for 0.6 and 1.2% Cl in CH solution are magnified in the insert figure.

In CH and PS solutions, the space charge capacitance (C) of the films increases (shown in the figures as decreasing $1/C^2$) with increasing chlorides. Since there is a direct relation between C and the defect density (N) and, an inverse relationship between C and film thickness (d), these plots indicate a decrease in film thickness and an increase in passive film defect density with increasing chloride in solution. This increasing instability in the passive film structure with increasing chloride concentrations in solution agrees with the E_{CORR} and i_{CORR} data presented in Figure 4-2. The increasing capacitance values with chlorides in the CH and PS solutions was also observed by Williamson and Isgor [20] in solutions with similar pH and composition.

In chloride-free (0% Cl-) solutions, the space charge capacitance of both steel grades tested in the CH solution are significantly lower (higher $1/C^2$ values) than those tested in the PS solution, suggesting that the films formed in the chloride-free CH solution are less protective. This behavior was more significant in the M-S plots of the carbon steel than of the 2304 bars. The carbon steel bars tested in the CH solution showed two orders of magnitude higher $1/C^2$ values than those in the PS solution.

After the addition of 6% or 0.6% Cl- to the testing solutions of 2304 or carbon steel bars, respectively, there is a significant increase in capacitance of the passive films from their initial values at 0% Cl-. This effect was, again, more pronounced for bars tested in CH solution than for those tested in PS solution, indicating there is a greater instability in the films formed at lower pH when exposed to chlorides. This is consistent with the higher i_{CORR} and more negative E_{CORR} shown in Figure 4-2 for bars tested in CH solution than those in PS solution. This observation also agrees with previous findings [13], [137], [161] that chloride threshold, or corrosion resistance, is higher for films formed in higher pH solutions. The difference in capacitance between the first addition of chlorides and the subsequent, higher, levels is less than that observed between 0% Cl- and 6% Cl- for 2304 or 0.6% Cl- for carbon steel.

Another interesting observation that supports the finding that more defective films are formed in the lower pH CH solution, is the different shape of M-S plots obtained on carbon steel bars tested in this solution without and with chlorides. At 0% Cl-, the maximum $1/C^2$ peak leading to the transpassive region was observed at ~ +0.35 V_{SCE} after two linear regions representing the inner shallow (N_2) donor corresponding to the Fe^{2+} oxide layer and the deep (N_3) donor corresponding the outer Fe^{3+} oxide layer [20]. In contrast, at 0.6 and 1.2% Cl-, the maximum $1/C^2$ peak was observed after the first linear region (N_2) at ~ -0.10 V_{SCE}. This indicates that the outer Fe^{3+} oxide layer, previously reported [73] as the more porous oxide layer, was dissolved once chlorides were introduced. The inner layer was eventually dissolved after 1.8% Cl- addition in CH solution and so no M-S data are reported beyond 1.2% Cl-. This dissolved outer layer was not observed in films formed in higher pH, PS, solution.

In PS+S solution, the capacitance of films formed on both 2304 and carbon steel bars decreases with increasing chlorides and sulphates, which is contrary to observations in the CH and PS solutions. The M-S plots of both rebar grades tested in the chloride-free PS and PS+S solutions were similar, with slightly higher capacitance found for bars in PS+S. Thus, the initial 0.014 M sulphates in the PS+S solution did not have any apparent impact on the capacitance of the passive films, in agreement with the observation of Williamson and Isgor for carbon steel formed in similar solutions [20]. Unlike the carbon steel bars tested in CH solution with 0.6% Cl-, the outer layer of films formed in PS+S solution became more stable and less porous on sulphate additions, evidenced by the similar and aligning N_2 and N_3 slopes. This indicate that both a higher pH and sulphate are beneficial to the stability of passive films, particularly outer layer.

4.5. Discussions

Tables 4-4 and 4-5 summarize the electronic and electrochemical properties of one of three replicates of the 2304 and carbon steel bars tested in the CH, PS and PS+S solutions. The data for other replicates is presented in Appendix A1-A6. These tables provide the corrosion potentials (E_{CORR}) and current densities (i_{CORR}) from LPR measurements; the flatband potentials (E_{FB}), defect densities (N_1, N_2, N_3, N_4) and film thicknesses (d_1, d_2, d_3, d_4) at regions identified in Figure 4-3. The carbon steel specimens in CH solution showed significant corrosion before the M-S test at 1.8% Cl- addition and, therefore, only LPR tests were performed at the higher chloride contents. Also, only defect density of the shallow donor (N_2) was recorded at 0.6% and 1.2% Cl- contents in CH solution because of the absence of a deep donor (N_3) and the transition into the transpassive region as shown earlier in Figure 4-4.

No references were found reporting the electronic properties of 2304 stainless steel, but the N, E_{FB} and d values shown in Table 4-4 are in similar range to those reported for 304L, 316LN and 2205 stainless steel alloys [107], [139]–[141], [75], [154]–[160]. Similarly, the N, E_{FB} and d values shown in Table 4-5 are in similar range to those reported for carbon steel [8], [12], [151], [152], [162]–[164] in the literature despite the different test solution concentrations and, typically, lower pH. Furthermore, the flatband potentials presented in Tables 4-4 and 4-5 for 0% Cl- became more positive by 0.059 V per unit pH of the solution, which is expected as per Nernst equation [65].

Table 4-4. Corrosion and film semiconductor data for one of three replicates of 2304 bars tested in all three testing solutions, with the N_x and d_x values defined in Figure 4-4. Other replicates are presented in the Appendix

Chloride addition		**Electronic properties**										
		i_{CORR} (mA/m^2)	E_{CORR} (mV$_{SCE}$)	E_{FB} (mV$_{SCE}$)	N_1 (10^{21} cm^{-3})	N_2 (10^{21} cm^{-3})	N_3 (10^{21} cm^{-3})	N_4 (10^{21} cm^{-3})	d_1 (nm)	d_2 (nm)	d_3 (nm)	d_4 (nm)
CH	**0**	0.08	-133	-1330	2.42	1.49	0.79	1.09	0.83	1.09	0.88	0.63
	6	0.51	-163	-963	10.49	4.76	2.20	2.46	0.36	0.54	0.41	0.24
	12	1.30	-230	-900	12.16	7.08	3.72	3.38	0.29	0.44	0.34	0.22
	18	1.53	-260	-840	14.38	8.14	4.39	3.87	0.24	0.40	0.31	0.19
	21	5.80	-302	-800	14.88	8.89	4.87	4.05	0.21	0.37	0.29	0.18
PS	**0**	0.05	-79	-990	8.83	7.44	3.89	8.74	0.20	0.27	0.18	0.04
	6	0.13	-145	-970	11.64	9.66	4.67	9.40	0.16	0.22	0.17	0.03
	12	0.80	-166	-960	10.59	12.00	5.37	9.65	0.15	0.20	0.17	0.02
	18	1.07	-188	-960	11.41	13.21	6.29	11.21	0.14	0.18	0.13	0.01
	21	2.90	-221	-920	13.41	15.24	7.18	13.63	0.12	0.17	0.13	0.01
PS +S	**0**	0.02	-96	-1120	12.14	6.00	4.38	2.35	0.22	0.29	0.25	0.06
	6	0.08	-125	-1020	7.79	5.56	3.53	2.99	0.22	0.30	0.31	0.05
	12	0.38	-132	-990	4.36	4.65	3.63	2.79	0.23	0.33	0.37	0.06
	18	0.45	-162	-930	4.09	4.47	2.80	2.53	0.27	0.36	0.23	0.05
	21	1.40	-201	-910	3.66	3.78	2.29	1.47	0.24	0.37	0.51	0.10

Table 4-5. Corrosion and film semiconductor data for one of three replicates of carbon steel bars tested in all three testing solutions, with the N_x and d_x values defined in Figure 4-4. Other replicates are presented in the Appendix

Chloride addition		**Electronic properties**										
		i_{CORR} (mA/m^2)	E_{CORR} (mV$_{SCE}$)	E_{FB} (mV$_{SCE}$)	N_1 (10^{21} cm^{-3})	N_2 (10^{21} cm^{-3})	N_3 (10^{21} cm^{-3})	N_4 (10^{21} cm^{-3})	d_1 (nm)	d_2 (nm)	d_3 (nm)	d_4 (nm)
CH	**0**	0.40	-155	-620		0.36	0.59	0.08		0.49	1.54	1.16
	0.6	2.30	-275	-701		12.78				0.37	0.64	0.56
	1.2	2.90	-316	-740		39.41				0.07	0.17	0.15
	1.8	8.90	-405									
	2.4	12.5	-465									
PS	**0**	0.22	-159	-613		25	13	5		0.11	0.20	0.139
	0.6	1.03	-192	-624		295	132	41		0.02	0.05	0.017
	1.2	2.20	-311	-658		535	246	99		0.01	0.03	0.010
	1.8	3.30	-324	-676		711	321	112		0.01	0.03	0.006
	2.4	4.50	-367	-684		736	327	124		0.01	0.03	0.009
PS +S	**0**	0.33	-161	-734		35	17	21		0.04	0.08	0.06
	0.6	0.38	-185	-580		116	53	18		0.06	0.10	0.04
	1.2	0.71	-241	-650		107	52	15		0.08	0.12	0.06
	1.8	1.50	-290	-666		76	51	15		0.12	0.15	0.14
	2.4	3.10	-329	-697		157	87	6		0.17	0.19	0.20

Figure 4-5 shows the defect densities (N_1, N_2, N_3) of the three replicates bars tested in the different solutions. It can be seen that the defect densities of bars tested in CH and PS solutions increased with chlorides, and their film thicknesses presented in Tables 4-4 and 4-5 decreased with increasing chlorides, suggesting that there is increasing instability of the passive films with chlorides. This agrees with the increasing i_{CORR} and more negative E_{CORR} values with chlorides shown in Figure 4-2. Other authors [165], [166] have also observed increasing defect densities with increasing chlorides. Furthermore, the defect densities, N_2 and N_3, of the bars tested in the PS solution are shown to be higher than those from the CH solution. However, this cannot be interpreted as more protective films forming in CH solution because, as shown in Figure 4-4, the space charge capacitance of the initial films (at 0% Cl-) formed in CH solution are significantly lower than those formed in PS solution. In other words, defect densities shown in Figure 4-5 are with reference to the bars' initial space charge capacitance layers. As earlier mentioned, M-S data indicate that the outer layer (N_3) of film formed on carbon steel tested in CH solution dissolved once chlorides were added to the solution, and the defect density of the inner layer (N_2) increased until the layer eventually dissolved at 1.8% Cl-.

In contrast to the observations in CH and PS solutions, the defect densities of carbon steel and 2304 bars tested in PS+S solutions either remained almost constant or significantly decreased with sulphates additions. Similarly, the bars' passive film thicknesses presented in Tables A1 – A6 in the Appendix either remained the same or slightly increased with sulphate addition, suggesting that sulphate additions to the testing solution counteracted the detrimental effect of chloride ions. The beneficial effects of sulphates on pitting resistance has been previously documented for austenitic stainless steel in neutral chloride solutions [167], and more recently for carbon steel and austenitic and duplex stainless steels in alkaline solution [137], [138]. The findings in the present work documenting the influence of sulphate on passive film resistance to chlorides support these recent reports [137], [138] on improved pitting resistance with sulphates for the high pH levels found in concrete.

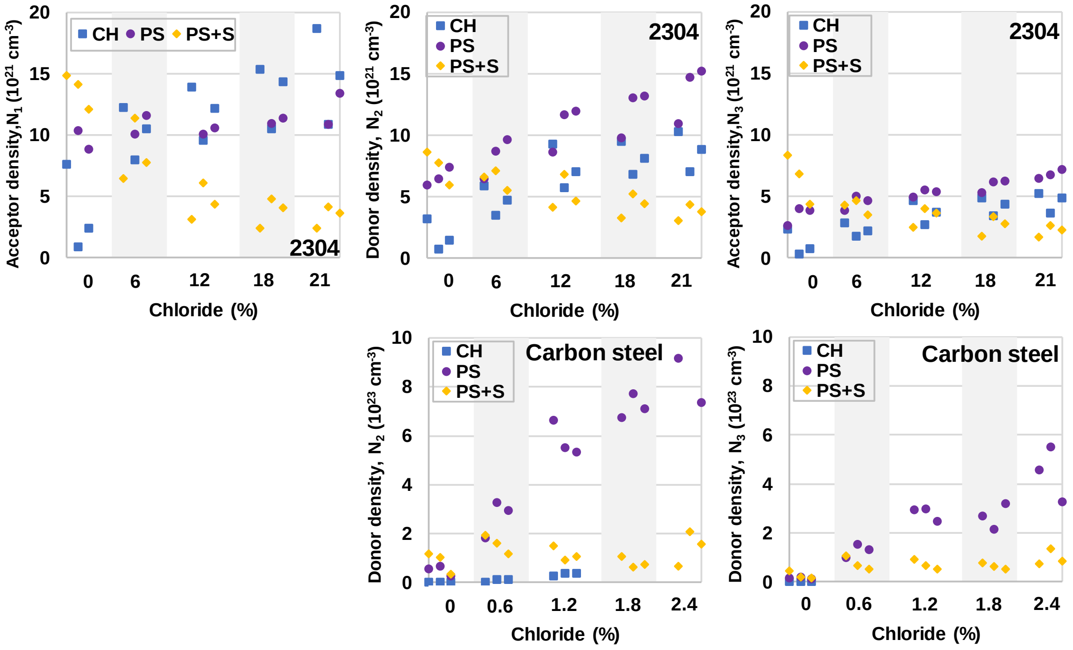

Figure 4-5. Change in acceptor and donor densities with chloride and sulphate addition in the CH, PS and PS+S testing solutions.

A general observation of the defect densities shown in Figure 4-5 and Table 4-4 is that N_1 values are higher than both N_2 and N_3 for the 2304 bars tested in CH and PS solution. The reason for the higher defects observed in the inner layer of the film than those of the outer layer was explained in Part I of this work using the models of Hakiki et al. [107], [139]–[141] and Marcus et al. [168]. The model presented explained that there is an outward ionic transport of Fe^{2+} from the inner layer of the passive film and a corresponding inward diffusion of Cl- (instead of O^{2-}) through oxygen vacancies in the passive film. Similar model can be used to explain the general decrease in defect densities with sulphates or greater decrease in N_1 values than both N_2 and N_3 values obtained from bars tested in the PS+S solution. Basically, the SO_4^{2-} is expected to diffuse inward, competing with Cl- to occupy the oxygen vacancies in the film, to combine with the outward ionic transport such as Fe^{2+} and Ni^+ to form stable sulphides of Fe and Ni (as FeS, FeS_2, NiS, Ni_3S_2) discussed later.

Figure 4-6 shows M-S and cyclic polarization (CP) curves obtained in chloride-free CH, PS and PS+S solution to correlate the electronic and electrochemical data of the 2304 stainless steel and carbon steel. The different regions in both M-S and CP plots are labelled according to information provided by Hakiki et al. [107], [139]–[141] and Beverskog & Puigdomenech [169] who presented M-S plots and E/pH diagrams of an Fe-Cr-Ni system, respectively. In addition, the regions are also labelled based on the stable phases in the E/pH diagrams, determined using ThermoCalc® and shown in Figures 4-7 and 4-8, of an Fe and Fe-Cr-Ni system in NaCl and $CaSO_4$ solution, representing the carbon and stainless steel bars tested in PS+S solutions, respectively.

A general observation in Figure 4-6 is that the flatband potential 2304 M-S plots corresponds approximately to the H^+/H_2 equilibrium potential, which agrees with many authors [20], [75] that when the applied potential is at flatband, the fermi level, which is the electrochemical potential of the electrode, is equal to the redox potential of the electrolyte. The highest peak in the M-S plots corresponds to the bars' corrosion potentials. The slight shift in corrosion potentials between M-S and CP plots is attributed to the difference in scan rate employed for both tests.

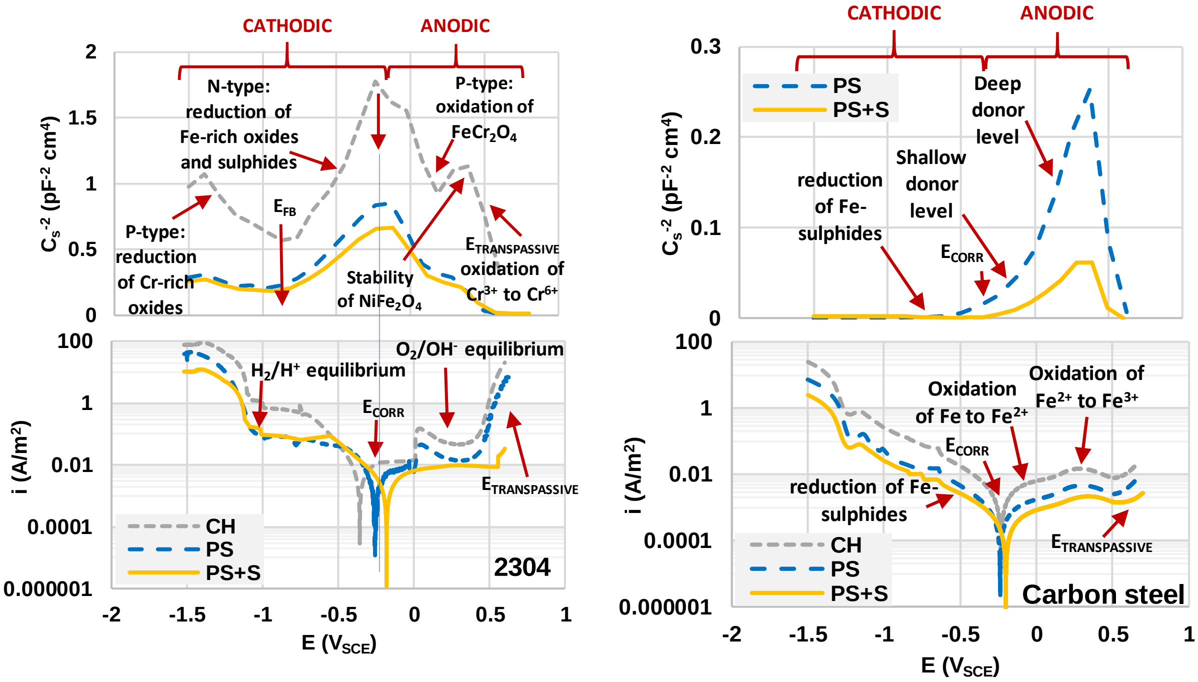

Figure 4-6. M-S and CP curves for 2304 and carbon steel bars performed in the same potential range (-1.5 - +0.6 V_{SCE}) in chloride-free solution. Note that the M-S plots of the CH specimens were not presented because of their significant difference in the order of magnitude of the $1/C^2$ axis as previously shown in Figure 4-4.

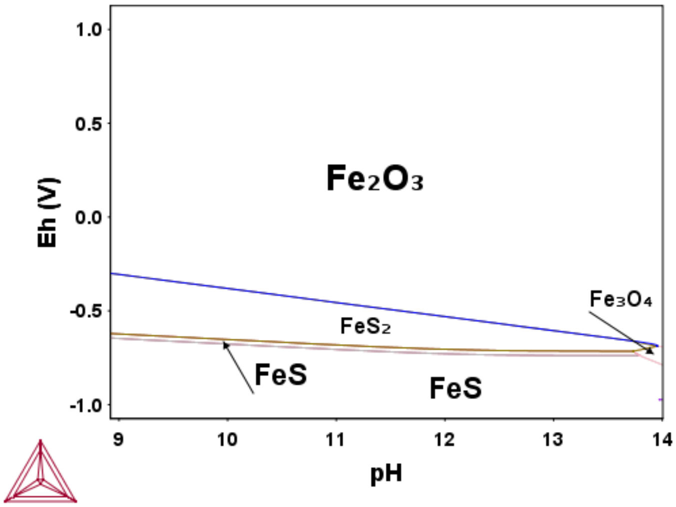

Figure 4-7. Electrochemical vs pH diagram for 0.001 M Fe in 1M NaCl + $CaSO_4$ showing equilibrium formation of Fe and Ni sulphides in passive films formed on carbon steels.

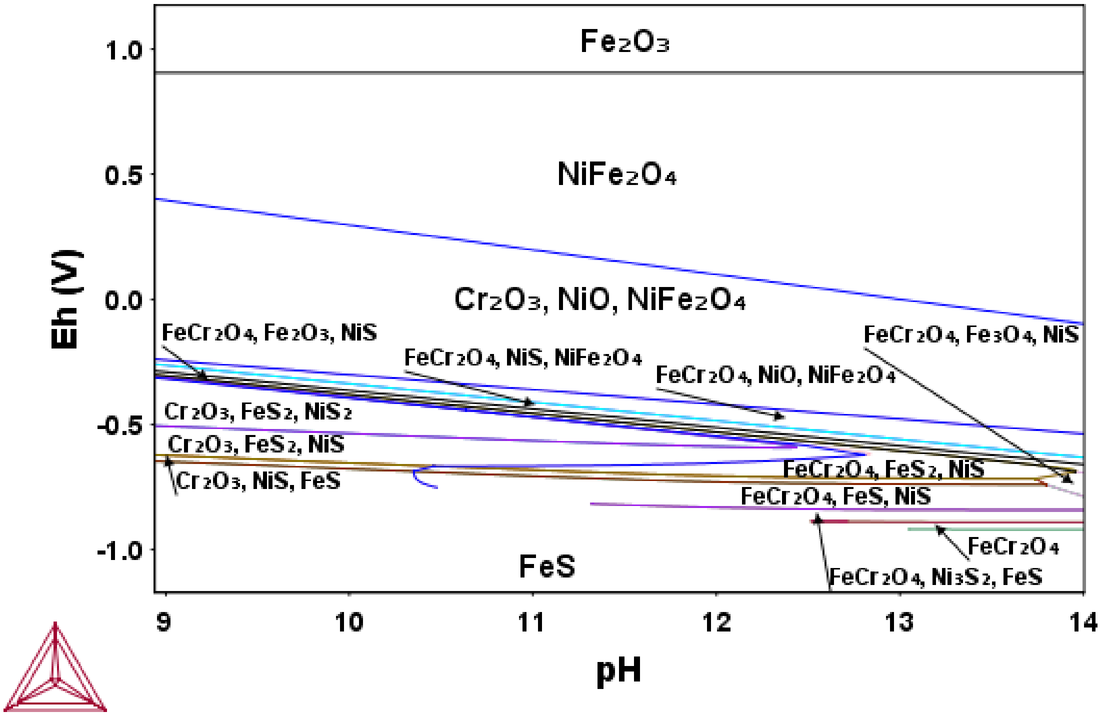

Figure 4-8. Electrochemical vs pH diagram for 0.001 M Fe + Cr + Ni in 1M NaCl + $CaSO_4$ showing equilibrium formation of Fe and Ni sulphides in the passive films formed on stainless steels.

In the M-S plot of 2304 stainless steel, the p-type inner Cr-rich oxide films becomes more unstable as the bar is scanned from -1.50 V_{SCE} to the flatband potential. As the potential scan continues in the anodic direction up to the corrosion potential, the n-type outer Fe-rich oxide and sulphides of Fe and Ni (as FeS, FeS_2, NiS, Ni_3S_2) for bars tested in sulphate-containing solution also become unstable. Beyond the corrosion potential of the bar, the spinel $FeCr_2O_4$ is oxidized to (Fe)CrO_4^{2-} until a more stable $NiFe_2O_4$ spinel is formed. In the transpassive region, these stable species are dissolved, to become CrO_4^{2-} and

FeO_4^{2-}. In the CP plots, the corrosion current densities (i_{CORR}) of the 2304 bars decreased with increasing pH (CH > PS) and sulphate (PS > PS+S), and their corresponding corrosion potentials (E_{CORR}) became more positive. This observation is consistent with E_{CORR} and i_{CORR} data from the LPR test, confirming better corrosion properties and electronic properties are obtained with increasing pH and sulphate in solution. An interesting observation in the CP plots of the 2304 bars is the decreasing intensity of $(Fe)CrO_4^{2-}$ oxidation with increasing pH (from CH to PS) and sulphate (from PS to PS+S), which is more pronounced in the PS+S curve. it appears that sulphate extended the stability of $NiFe_2O_4$ and delayed the transpassive region by forming NiS, Ni_3S_2 solid species.

In the M-S plot of carbon steel, no slope is observed (i.e. no p-type Cr-rich oxides) on increasing the potential from -1.50 V_{SCE} to the corrosion potential of the bar. However, as shown in Figure 4-7, there is a possibility of forming sulphides of Fe (as FeS, FeS_2) as stable solid species in this region for bars tested in PS+S solution, supporting the better corrosion properties found on these bars. On further increase beyond corrosion potentials to the peak at ~0.3 V_{SCE}, there oxidation of Fe to Fe^{2+} followed by the oxidation of Fe^{2+} to Fe^{3+}. As potential is increased beyond this peak, the region of transpassivity oxidation to FeO_4^{2-} is observed. In the CP plot, when the carbon steel is scanned beyond its corrosion potential, the oxidation peaks of both Fe to Fe^{2+} and Fe^{2+} to Fe^{3+} is also observed. The higher intensity of the second peak (oxidation of Fe^{2+} to Fe^{3+}) compared to the first (oxidation of Fe to Fe^{2+}) is consistent with previous observation [20] that inner Fe^{2+} oxide is more dense, coherent and more protective than the outer Fe^{3+} oxide. This also agrees with the complete dissolution of the deep donor (N_3) before the shallow donor (N_2) for bars tested in CH solution. Similar to what was observed in the 2304 bars, these oxidation peaks in the CP of carbon steel decreased with increasing pH and sulphate, which supports earlier discussions that films exposed to chlorides can be improved by sulphates.

4.6. Summary and conclusions

While it is well known that chloride additions to concrete pore solutions are detrimental to electrochemical properties of passive films, this project has demonstrated how they impact both electronic and electrochemical properties in relation to the corrosion behaviour of carbon steel and 2304 stainless steel rebar. The reduced thickness and more defective passive films on both grades of steel in the CH and PS solutions were reflected in the more negative corrosion potentials and increased corrosion current densities of the bars. These effects were more pronounced in the lower pH, CH, solution than in the PS solution, both in chloride-free and chloride-containing solutions. The films formed on carbon steel bars in the CH solution were more porous than those formed in other testing solutions, as shown by both the M-S and LPR results. The additions of ≥0.6% chlorides resulted in complete dissolution of the outer Fe^{3+} oxide layer on carbon steel, but the inner Fe^{2+} layer remained intact in CH solutions containing up to 1.8% chlorides.

When sulphate was incorporated into the testing solution together with chlorides, the passive film of both types of bars exhibited lower defect densities and thicker films, than those formed in the corresponding solutions without sulphates. This effect was reflected in the lower corrosion current densities and more positive corrosion than those tested in the sulphate-free solutions. The beneficial effect of the sulphate additions is attributed to the incorporation of solid sulphides of Fe and Ni (as FeS, FeS_2, NiS, Ni_3S_2) in the passive films as supported by the equilibrium stability of these species in the potential-pH diagram.

5. Detection of the critical chloride threshold of carbon steel rebar in synthetic concrete pore solutions[3]

5.1. Overview

Knowledge of the critical chloride content in concrete required to initiate corrosion of reinforcing steel is economically beneficial for the assessment and maintenance of existing structures. Also, many building codes now specify a service life of 75 – 100 years for highway bridges and the critical chloride content is an essential input parameter in the models used in design of structures. There have been numerous studies aimed at determining this parameter but there is no consensus because of the many factors influencing the corrosion. The current standard methods, e.g. ASTM G109, require many weeks or months of testing and are not appropriate for testing large numbers of specimens in different conditions. This project has demonstrated that a fairly rapid potentiodynamic polarization technique can be applied to carbon steel reinforcing bars in synthetic concrete pore solution to determine the critical value. The importance of selecting the appropriate synthetic concrete pore solution for this application is demonstrated by the different critical values obtained for different solutions.

5.2. Background

Chloride-induced corrosion of reinforcing steel bars (rebar) is one of the most common causes of deterioration of reinforced structure because of marine exposure and the increasing use of de-icing and anti-icing brines employed on reinforced structures (bridges, parking lots, etc.) during the harsh winter season experienced in many countries. Chlorides diffuse through the pores of concrete structures to the reinforcement and, in sufficient quantity, they initiate active corrosion on the rebar that was initially passivated due to the high pH solution in the pores of the concrete. The amount of chlorides the steel can withstand before the initiation of active corrosion is generally referred to as the chloride threshold level or critical chloride level, C_{CRIT}. The knowledge of the threshold is economically beneficial for the assessment and maintenance of existing structures, so that remediation steps can be taken prior to the deterioration of structure. Also, most building codes now specify a service live of 75 – 100 years for highway bridges and the C_{CRIT} is a critical input parameter in the models used in design of structures to be exposed to chloride environments.

A great amount of effort has been expended to determine the C_{CRIT} of a reinforcement, but the values obtained vary significantly. As described by Tang et al. [170], this can be attributed to many factors. The first is the external environment: outdoor, with its variable temperature, relative humidity and precipitation, or constant laboratory conditions. The second is the test environment: simulated pore solution, mortar or concrete. The chloride threshold of bars in concrete or mortar will be influenced by cement type, any supplementary cementitious materials and/or chemical admixtures, the total cementitious content of the mix, the water-to-cementitious ratio and the age of the mortar or concrete.

---

[3] The contents of this chapter have been adapted with no required permission (an open access publication: I.G. Ogunsanya, C.M. Hansson. “Detection of the critical chloride threshold of carbon steel rebar in synthetic concrete pore solutions” *RILEM technical letters*, 3 (2018) 75-83.
DOI: http://dx.doi.org/10.21809/rilemtechlett.2018.70

The third is the surface condition of the bars and the fourth is the measurement technique. For example, previous studies have employed corrosion potential monitoring, potentiostatic polarization, macrocell corrosion tests, and microcell corrosion tests. Many of these studies have been reviewed in references [60], [171], [172]. The decision on the methodology employed is often influenced by the time available to obtain results, but any accelerated technique has an effect on the result [4].

An additional factor is the method of introduction of the chloride. Some investigations have employed admixed chlorides in the concrete [173]–[176], while others have allowed chloride diffusion from outside of the concrete [177]–[179]. Although the former method takes less time, both methods can still take weeks to obtain results unless accelerated by other means. To reduce the time to obtain results and allow more control in testing, synthetic pore solutions have been widely employed as the test medium. Laboratory reagents are used to simulate the pore solutions inside of concrete and chlorides are added incrementally over time until active corrosion is observed electrochemically and/or visually. This way the chloride content at the surface of the bars is accurately known and the bars can be observed for immediate initiation of active corrosion. The disadvantage is that the same chloride concentrations exists over the whole bar, unlike the highly inhomogeneous concentrations existing in concrete structures.

In this paper, a method of determining the chloride threshold concentration was adapted from that of Williams et al. [180] who carried out tests on magnesium alloys in acid solution. It should be noted that these authors found the method to be successful for commercially pure magnesium but was less so for some magnesium alloys. This method, discussed in more detail in the next section, involves using anodic potentiodynamic polarization scans to determine the corrosion potential (E_{CORR}) and pitting potentials (E_{PIT}) of same grade of bars in chloride solutions. The E_{CORR} and E_{PIT} values are then plotted on the same graph against the increasing chloride concentration and both curves are extrapolated until they intersect. This intersection point represents the chloride concentration needed to initiate active corrosion on that particular grade of steel at its corrosion potential without any application of an anodic stimulus. It is important to mention that some authors have employed a similar method but plotting only the pitting potentials against chloride concentration without extrapolation [181], [182]. The goal in those papers was not to determine the C_{CRIT} of the bars, but to provide a relative comparison between different bars. The overall objective of the current work is to demonstrate this relatively rapid method of determining the threshold can be used for reinforcing bars in simulated concrete pore solution.

Many authors have tested rebar in saturated calcium hydroxide pH ~ 12.6 and some have used a synthetic pore solution based on KOH, NaOH and $Ca(OH)_2$ with pH ~ 13.6. Clearly, however, the pore solution composition must be representative of that in the specific concrete mix of interest. A recent study of the influence of the water/cementitious materials (w/cm) ratio and supplementary cementitious materials (SCM) content on the pore solution composition [11] has shown that, with increasing admixed chloride, there is an increased sulphate content in the pore solution. Yet only few authors have incorporated sulphate in their synthetic pore solution testing [2], [20]–[22], and only at the beginning of their test without further additions with increasing chlorides. Therefore, the second objective of the current work was to employ the anodic potentiodynamic polarization method to determine the chloride threshold of reinforcing bars rebar in different “pore solutions”.

5.3. Experimental methods

Carbon steel reinforcing bars (rebar), with composition shown in Table 5-1 were cut to 127 mm (5.0 in) in length, drilled on one end, soldered with a solid copper wire and lacquer was applied to both ends to allow an exposed length of 76 mm (3.0 in) The specimens were cleaned with alcohol to remove contaminations from handling. The specimens were then placed in their respective testing solutions in a three-probe electrochemical cell shown in Figure 5-1. The reference electrode was a saturated calomel electrode (SCE) and the cylindrical counter electrode was a mixed metal oxide coated titanium mesh.

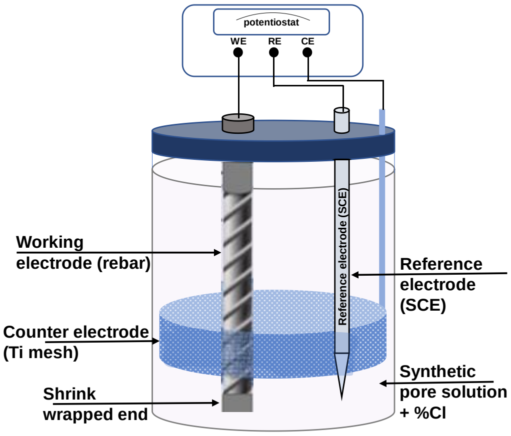

Figure 5-1. Three-probe electrochemical cell with a mixed metal-oxide titanium mesh counter electrode and a saturated calomel reference electrode (SCE).

Three testing solutions were employed in total as presented in Table 5-2. One solution (designated as PS+S) was based on the composition of the expressed solutions from a specific 75%Portland cement/25% ground granulated blast furnace slag mixture with a w/cm of 0.40 and different NaCl additions. The second solution (designated as PS) was based on the same solution but omitted the sulphates and the third solution was saturated $Ca(OH)_2$ solution (designated as CH). The percentages shown in Table 5-2 correspond to the amount of analytical reagent grade compound added to deionized water to make 100 mL of solution. Excess solid $Ca(OH)_2$ was present at all times in all solutions during testing. Each solution was stirred to ensure complete dissolution of all the salts and pH measurements were taken afterwards.

In the work of [11], increasing sulphates were found with increasing chlorides in the pore solutions expressed from cement pastes with increasing admixed chlorides after 28 days as shown in Figure 5-2. The equivalent amount of sulphate added at each chloride addition is shown Table 5-3.

Table 5-1. The mill certificate composition of tested carbon steel rebar

	Composition (wt. %)												
Constituent	C	Mn	P	S	Si	Cu	Ni	Cr	Mo	V	N	Sn	Fe
Amount	0.210	1.310	0.008	0.018	0.180	0.260	0.060	0.090	0.013	0.050	0.010	0.021	balance

Table 5-2. Testing solutions.

Testing solution (denotations)	**Composition (%)**				**pH**
	$Ca(OH)_2$	KOH	NaOH	$CaSO_4.2H_2O$	
Calcium hydroxide (CH)	Saturated				~12.5
Pore solution (PS)	0.01	2.68	0.51		~13.6
Pore solution plus sulphate (PS+S)	0.01	2.68	0.51	0.23	~13.5

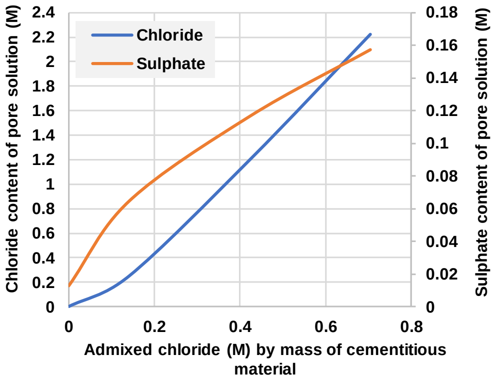

Figure 5-2. The chloride and sulphate contents of the pore solution expressed from 75% Portland cement/25% slag pastes 0.4 w/cm ratio and the admixed chlorides, as NaCl, in the 28 days old paste. Adapted from [11].

Table 5-3. Chlorides and sulphate additions to testing solutions.

Chloride and sulphate content as molar ion in solution and as mass % of compound in solution								
In CH solution								
M Cl- **(NaCl, %)**	0.028 (0.17)	0.056 (0.34)	0.085 (0.51)	0.113 (0.68)	0.141 (0.85)	0.310 (1.87)	0.338 (2.04)	0.366 (2.21)
In PS solutions								
M Cl- **(NaCl, %)**	0.451 (2.72)	0.507 (3.06)	0.563 (3.40)	0.620 (3.74)				
In PS + S Solution								
M Cl- **(NaCl, %)**	0.451 (2.72)	0.507 (3.06)	0.535 (3.23)	0.563 (3.40)	0.620 (3.74)			
M SO_4^{2-} **($CaSO_4.2H_2O$, %)**	0.080 (1.44)	0.084 (1.52)	0.086 (1.56)	0.089 (1.59)	0.091 (1.63)			

The bars were allowed to passivate in their respective testing solutions for two weeks before any chloride and sulphate was added and before any testing was carried out. After the bars have reached full passivation (determined by a non-varying corrosion potential), chlorides and sulphates (in the PS+S solution) were added as NaCl and $CaSO_4.2H_2O$ and the solutions were stirred for one minute with a magnetic stirrer to completely dissolve the solutes. After the corrosion potential of the steel bars stabilized, indicating equilibrium had been reached, an anodic potentiodynamic polarization test was performed on each bar in its respective solution with a scan rate of 0.01 mV/s as suggested by [4] using the BioLogic potentiostat Model VSP. Each bar was scanned from its corrosion potential in the anodic direction to 0.5 V_{SCE} (or to the current limit of 5 mA) and, if the bar did not display any pitting potential, reversed in the cathodic direction to observe any hysteresis loop. The values of the corrosion potential, E_{CORR}, pitting potential, E_{PIT}, were noted. The E_{CORR} and E_{PIT} values from each polarization curve were then plotted against the chloride content of the solution.

5.4. Results

Figure 3 shows examples of the corrosion potentials of the bars allowed to passivate in their different testing solutions without chlorides. It can be seen that the E_{CORR} values were relatively similar after 200 hrs, indicating that the bars had reached equilibrium with the testing solution. After the addition of chlorides, a longer wait time before the application of anodic polarization was attempted but, due to the inhomogeneity of the mill scale on the rebar, the potential values of some bars in the solutions with higher chloride contents, became more negative after ~30 mins and then remained approximately constant thereafter. This suggests initiation of pitting corrosion and repassivation on some regions on those bars. When anodic polarization was applied to these bars, some showed curves with defined pitting potentials, while others exhibited general corrosion behaviour. Therefore, for consistency, 30 minutes “wait time” was chosen for all bars in solution at all chloride concentrations.

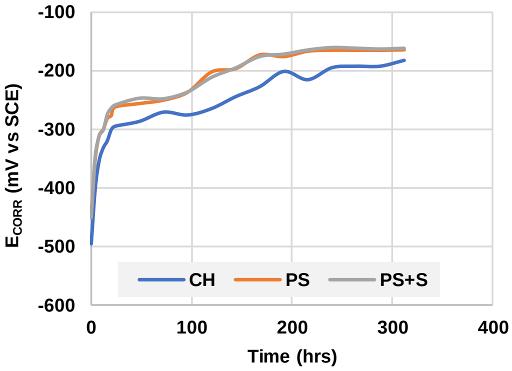

Figure 5-3. Corrosion potentials of bars in solution over the course of passivation.

An important point to mention is the success rate of obtaining pitting potentials from the anodic scans of these carbon steel bars. Although plots with data point of three replicates of bars tested in each solution are presented in the figures below, about five specimens were tested to obtain each data point. Some results were discarded because the tested bars showed crevice corrosion underneath the lacquer in addition to exhibiting pitting corrosion in the exposed area, as shown in Figure 5-4. As also evident in Figure 5-4, there was generally good bonding between the bar and the lacquer, although crevice corrosion did occur in some cases. A few other potentiodynamic scans exhibited the behaviour of general corrosion with no clear onset of pitting and, examination of their pre-test photographs revealed a mill scale that was characterised with several pits along the length of the specimen, Figure 5-5. Again, such results were discarded. In general, as observed by [180], the success rate of obtaining C_{CRIT} results using the potentiodynamic scans is dependent on the type and/or surface condition of the material.

Particularly in this work, it was mostly due to the nature of the mill scale (a complex iron oxide layer) that forms on these bars during the hot rolling process of their steel fabrication which affects the behaviour of the steel in solution. The variation in mill scale between manufacturers, the inhomogeneity along the length of a specimen to be tested, the non-uniformity in thickness and microstructure, and the influence of these factors on electrochemical test results in the presence of chlorides is well documented in the work of Ghods et al. [183].

Before and after pitting corrosion

Bars discarded due to crevice corrosion

Figure 5-4. An example of before and after testing for pitting potential is shown at the top of the figure. The after tested bar showed clear pitting corrosion underneath the side rib with no crevice corrosion underneath the lacquer. Bars at the bottom, tested for similar purpose but showed crevice corrosion, albeit pitting corrosion in some case, were discarded.

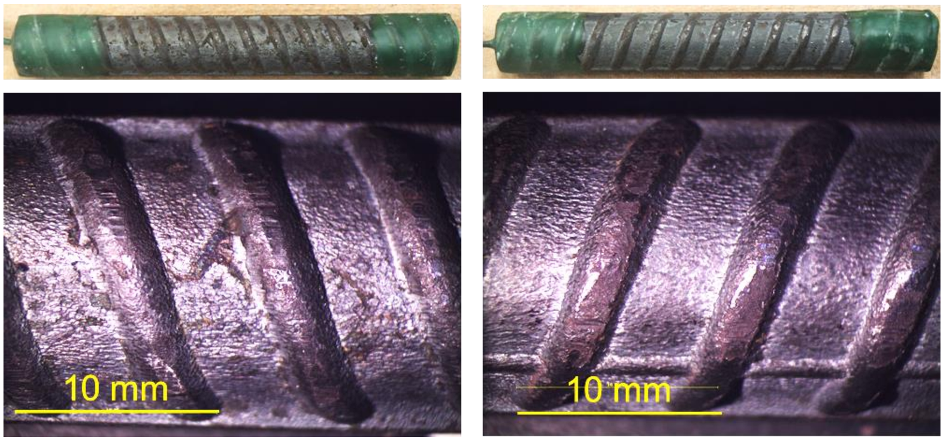

Figure 5-5. An example of as-received bars prepared for testing (top photos) and their micrographs showing the condition of their mill scales (bottom photos). The bar on the left shows a rough mill scale with several pits than those on the right, which in turn resulted in general corrosion when tested.

The initial tests in the PS and PS+S solutions were in the same chloride range as those in the CH solution, that is, from 0.014 to 0.423 M by mass of solution in 0.014 M increments. However, all of the curves indicated passive behaviour, with the return sweep at lower current densities than exhibited in the forward sweep, as shown for the PS solution with 0.423 M Cl in Figure 5-6. In contrast, it was difficult to obtain a defined pitting onset from the polarization curves obtained from specimens in PS solution with chloride contents greater than 0.62 M by mass of solution because of the high rate of corrosion.

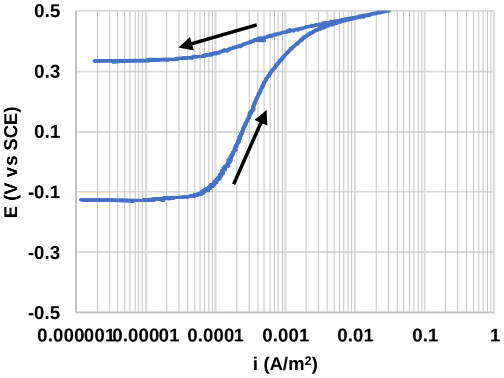

Figure 5-6. Polarization curves of specimens in PS solution with 1.5% Cl- by mass of solution showing no pitting potentials.

Figures 5-7 – 5-9 shows the polarization curves obtained from specimens tested in the CH, PS and PS+S solutions with chlorides respectively. The potential value before the sharp increase in current is known as the breakdown or pitting potential (E_{PIT}). A general observation is the more negative E_{CORR} values and decreasing passivity range with increasing chlorides, as found in other work [161], [181], [182], [184]. A decreasing E_{CORR} value of carbon steel rebar has been observed in both tests carried out in chloride-contaminated pore solution [161], [181], and in cracked concrete exposed to chlorides [110], [184], [185]. This behaviour is mainly influenced by the surface finish of the bar, particularly the mill scale. At the higher chloride levels, the passive current density increased gradually up to the pitting potential in Figures 5-7 – 5-9.

The polarization curves from bars in the PS and PS+S solutions are similar, but the presence of sulphates results in more anodic E_{PIT} values. The passive current densities of bars in these solutions are similar and lower than those in the CH solution, which is consistent with past findings [13], [186]. A current density value with the order of magnitude of 10^{-3} A/m^2 is typically considered passive [187].

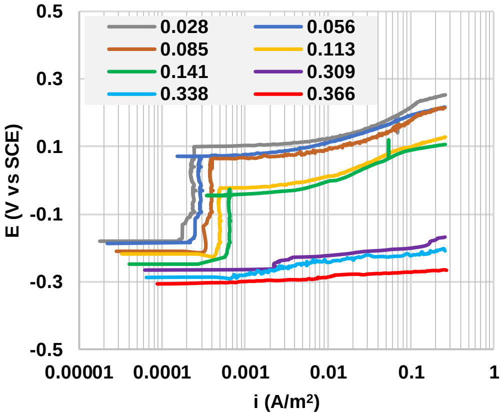

Figure 5-7. Polarization curves of specimens in CH solution with chlorides from 0.028 to 0.366 M by mass of solution showing pitting corrosion.

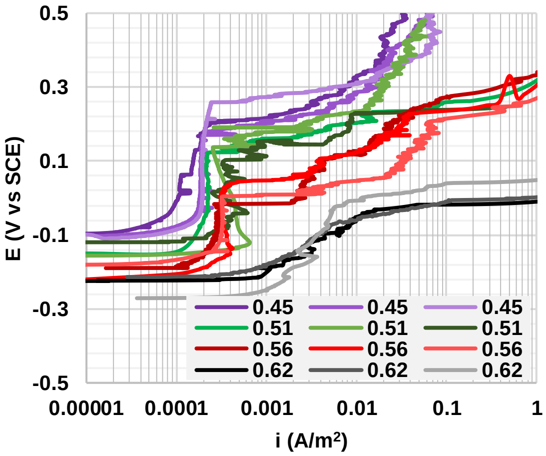

Figure 5-8. Polarization curves of specimens in PS solution with chlorides from 0.45 to 0.62 M by mass of solution showing pitting corrosion.

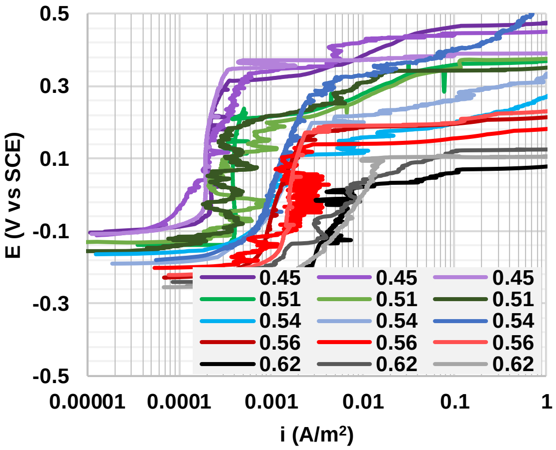

Figure 5-9. Polarization curves of specimens in PS+S solution with chlorides from 0.45 to 0.62 M by mass of solution showing pitting corrosion.

5.5. Discussion

Figures 5-10 to 5-12 show the potential versus chloride plots that summarize the passivity and pitting behaviour and, allows prediction of the chloride thresholds of carbon steel rebar in the CH, PS and PS+S solutions, respectively. Each figure shows the data for the corrosion potentials (E_{CORR}) and pitting potentials (E_{PIT}) obtained from the polarization curves above, as a function of the chloride content of the solution. Trendlines for the E_{CORR} and E_{PIT} data are extrapolated to their intersection point which, as described above, represents the chloride content of the solution at which corrosion is initiated without the application of an external stimulus, that is the chloride threshold value, C_{CRIT}.

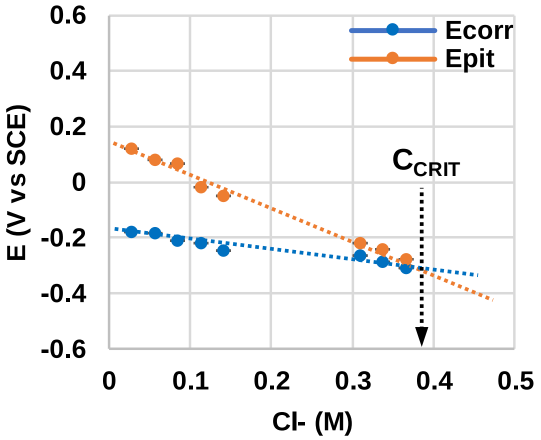

Figure 5-10. E_{CORR} and E_{PIT} versus chlorides extrapolated to predict the chloride threshold of carbon steel in CH solution. Note the difference in scale from Figures 5-10 and 5-11.

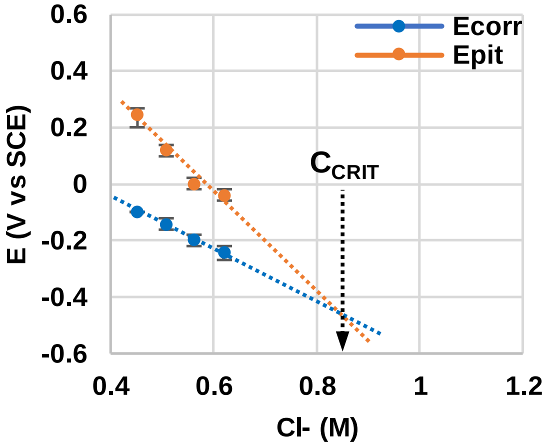

Figure 5-11. The average and maximum and minimum of three replicates of E_{CORR} and E_{PIT} versus chlorides extrapolated to predict the chloride threshold of carbon steel in PS solution.

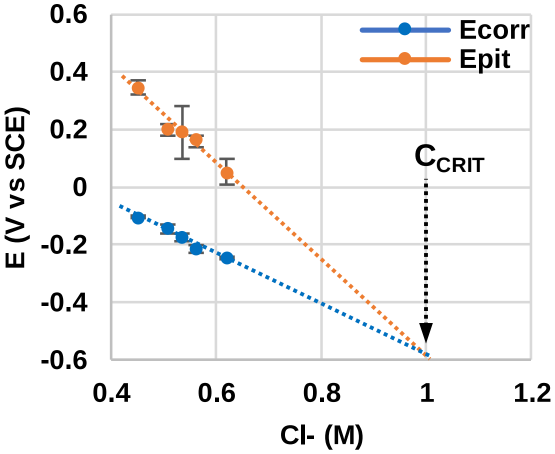

Figure 5-12. The average and maximum and minimum of three replicates of E_{CORR} and E_{PIT} versus chlorides extrapolated to predict the chloride threshold of carbon steel in PS+S solution.

The critical chloride threshold obtained for bars in the CH, PS and PS+S solutions were found to be approximately 0.38 M, 0.85 M and 1 M by mass of testing solution respectively. Using the data for the expressed pore solutions shown in Figure 5-2, these values translate to approximately 0.17 M, 0.34 M and 0.37 M Cl- by mass of cementitious material in cement or concrete. The C_{CRIT} values of bars in CH and PS solutions fall within the range (0.07 – 0.56 M by mass of cementitious) of those observed by [13], [175], [176], [188]–[193] using different methodology. No comparison for C_{CRIT} value could be made for bars in the PS+S solution because there does not appear to be any literature using similar solutions. However, Leckie and Uhlig [167] showed in their work in the 60's that sulphate increment in acid solution improved the pitting resistance of stainless steel bar.

The pH of the solutions was determined only at the start of the tests and it is clear that the concept of a constant Cl^-/OH ratio does not hold for these solutions, based on the initial pH values. This observation is in agreement with the results of a parallel study of expressed pore solution from cement pastes with admixed NaCl for which the pH varied with chloride content between 13.2 and 13.5 and molar ratios of Cl/OH in solution varied from 0.077 to 1.44.

To confirm that the C_{CRIT} values obtained in this work can initiate active corrosion on the carbon steel rebar tested in all three solutions, a test was carried out to monitor the corrosion potentials of bars in solution before and after the addition of chlorides and sulphates.

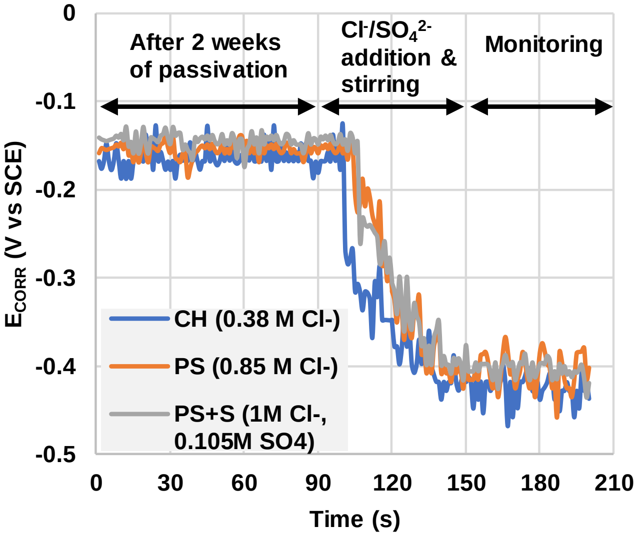

Figure 5-13. Corrosion potentials of bars in each of the three solutions containing the "critical chloride concentration" for each.

Similar to other bars being tested, these bars were passivated for 2 weeks in their respective containers and then placed on a stirrer. Each cell was hooked up to a potentiostat to monitor the E_{CORR} values for 90 seconds before the addition of salt. After 90 seconds, salts were added and, each solution was stirred using a magnetic stirrer for a minute. The E_{CORR} values were then monitored to observe any subsequent changes and the data are shown in Figure 5-13.

It is important to emphasize that the PS and PS+S solutions employed in this work were prepared based on composition of expressed solution from a particular cementitious mixture type (75%Portland cement/25% ground granulated blast furnace slag mixture with a w/cm of 0.40) at 0% admixed chloride. This same base mixture was prepared for each chloride (and sulphate) level.

On the question of applicability of these results to chlorides penetrating into concrete from the environment, it is generally accepted that it is the highly concentrated ionic solution in the pores of the concrete, not the solid phases, which is responsible for the passivation of the steel in the non-contaminated concrete, and for the corrosion once the concrete is contaminated. Ideally, therefore, one should determine the composition of the pore solution in the close vicinity of the rebar. Unfortunately, this is not feasible because there is insufficient cementitious material to be able to express and analyse the pore solution. Moreover, as discussed in detail by Tang et. al [170], the chloride content in concrete exposed to saline conditions is highly inhomogeneous, both through the depth of the concrete cover and along the length of the interface between the concrete and the rebar. Determining the critical chloride concentration of structures in service is fraught with even more difficulties including: selection of the most appropriate locations for sampling; the lack of knowledge of the corrosion initiation time and, hence the chloride concentration at that time and the inclusion of possible carbonation effects [194].

The sulphates in cement paste are known to be concentrated in the aluminate phases, ettringite and monosulphate and, therefore, it may be assumed that these phases are the source of the sulphates found in the pore solution [195]. Friedel and Kuzel [196] salts are major solid phases formed during chloride binding and their formation process requires ion exchange of the sulphates in the aluminate phases into the pore solution [197]. The formation of these salts has been found to occur for both admixed and ingressed chlorides [36]. Therefore, this work considers the PS+S solution close to the scenario found in field concrete and, therefore, it is deemed important to determine the effect of the sulphate release on the corrosion resistance of the embedded rebar.

5.6. Potential applications and developments

The test procedure is currently being applied to five different stainless steel rebar grades in a synthetic pore solution of the same composition as the PS+S used in the current tests, in order to assess their relative resistance to chloride attack. It is also being used to evaluate the relative effects of different chloride salts, namely $CaCl_2$, $MgCl_2$ in comparison to the commonly used NaCl. Future developments of the test method will focus on the critical chloride levels of steel in mortar. Rebar will be cast in cylindrical mortar specimens with a small cover and, after curing, will be exposed to chlorides for different time periods prior to the cyclic potentiostatic polarization. Details of the procedure require “trial and error” determination. If successful, this procedure will lend itself to assessment of the effect of mortar mixture design, rebar surface finish, environmental conditions etc. A comparison of the results of these tests with those presented here will also clarify the relevance of testing corrosion in synthetic pore solution.

5.7. Summary and conclusions

- The potentiodynamic polarization scan method of determining chloride threshold level was successful in determining the C_{CRIT} of carbon steel rebar in three different synthetic pore solutions. Obtaining results through this method is shown to be dependent on the surface condition of the carbon steel rebar. On average, five specimens were tested before three replicates in each data point in Figures 5-11 and 5-12 were obtained. Furthermore, at chloride concentrations close to the C_{CRIT} value of the bar in solution, it was difficult to obtain a polarization curve with defined pitting onset.

- The threshold level determined by this method increased from 0.38 M in the CH solution to 1 M in the synthetic pore solution containing sulphates. Using the data in Figure 5-2 obtained from expressed pore solution at 28 days of slag cementitious mix with admixed chloride, the latter value would be equivalent to 0.37 M by mass of cementitious materials in cement paste, mortar or concrete with the same cementitious mix.
- Corrosion potential monitoring test confirms that the C_{CRIT} values obtained in this work for each of the three solutions is sufficient to initiate active corrosion on the carbon steel rebar tested.
- The addition of sulphate to pore solution at levels corresponding to those measured in expressed pore solution increased the C_{CRIT} of bars from 0.85 M to 1.00 M Cl^- by mass of pore solution. This is approximately 18% and equivalent to 0.03 M by mass of cementitious material.
- Sulphate increments, which were shown to improve the pitting resistance in acid solution in a past research [167], are also shown here to have positive impact on the C_{CRIT} value obtained from the extrapolation of E_{CORR} and E_{PIT} obtained from the potentiodynamic polarization curves of bars tested in alkaline solution.
- As mentioned above, there are numerous factors influencing the critical chloride concentration for rebar in concrete, including environmental conditions, rebar surface state, concrete mixture design and chloride cation type. However, by replicating the pore solution composition of the specific concrete of interest, and using the applicable chloride salt, this potentiodynamic scan method can be used to determine the influence of the last two factors.

6. The semiconductor properties of passive films and corrosion behavior of stainless steel reinforcing bars in simulated concrete pore solution[4]

6.1. Overview

The vulnerability of concrete reinforcing steels to corrosion when depassivation occurs, typically in the presence of chloride, makes it important to understand the nature of the steels' passive films. In Part I of the study, electrochemical techniques and Mott–Schottky analysis were used to investigate these films formed on five different grades of stainless steel and carbon steel reinforcing bars exposed to simulated concrete pore solution. The influence of the steel composition and surface finish on Mott–Schottky plots and the electronic properties are discussed in relation to the steels' corrosion resistance. A p-type semiconductor behavior was observed in the stainless steel alloys in the cathodic potential regions and an n-type in the anodic potential regions. The n-type behavior is similar to that observed in the carbon steel. The electronic and electrochemical properties of the austenitic grades were superior to the duplex grades. The molybdenum-containing grades, 316LN and 2205, did not show the expected superior properties compared to molybdenum-free grades, 304L and 2304. Also, the replacement of nickel by manganese in the 24100 alloy was not found to be detrimental. The as-received bars showed electronic and electrochemical properties that are more realistic to field conditions than those of the polished cross-sections.

6.2. Background

The passive films formed on steel have been well studied in the literature using several techniques [71]–[79] such as in-situ Raman spectroscopy (RS), x-ray photoelectron spectroscopy (XPS), electron energy loss spectroscopy (EELS), electrochemical tunneling spectroscopy (ECT), electrochemical quartz crystal microbalance (EQCM), ellipsometry. Studies at the atomic structure level have described these films as extrinsic semiconductors [97], [105], [107], [139]–[142]. Thus, it is expected that understanding the films' electronic behaviour can provide insight into the corrosion resistance of the steel. The Mott-Schottky (M-S) analysis [144], [198], which uses electrochemical impedance spectroscopy (EIS) to measure the film capacitance, has been used extensively to understand the electronic behaviour of the films formed on carbon steel [8], [12], [20], [151], [152], [162]–[164], the traditional austenitic 316LN and 304L grades of stainless steel [75], [107], [139]–[141], [154]–[157], and more recently, 2205 duplex stainless steel grade [158]–[160]. The potential difference across the semiconductor/electrolyte interface is the sum of those across the space charge layer of the semiconductor and the Helmholtz double layer in the electrolyte [97]. A series capacitor model is generally used to describe the capacitors present at the metal/electrolyte interface. However, the Helmholtz double layer capacitance is typically about 2-3 orders of magnitude greater than the space charge capacitance. Therefore, in the relationship

---

[4] The contents of this chapter have been adapted with permission from Elsevier: I.G. Ogunsanya, C.M. Hansson. "The semiconductor properties of passive films and corrosion behavior of stainless steel reinforcing bars in simulated concrete pore solution" *Materialia*, 6 (2019) 100321.
DOI: https://doi.org/10.1016/j.mtla.2019.100321

applied to M-S analysis, Equation 6-1, the Helmholtz double layer component ($1/C_H$) becomes insignificant is normally omitted in studies of passive films [68].

The most commonly reported result from the M-S analysis is a plot of the inverse of the square of the capacitance of the passive film versus the applied potential, commonly called the M-S plot. In addition to providing information on the capacitance of the film, the M-S analysis can reveal whether the semiconductor is p- or n-type and the defect density, N, of the film. Most studies have shown the passive film on iron-based alloys to be predominantly n-type, represented by Equation 6-2 [65], [101]. This M-S equation shows relationship between the capacitance of the space charge layer in the semiconducting passive film and applied electrode potential, E.

$$1/C^2 = (1/C_{sc}^2 + 1/C_H^2)$$

Equation 6-1. Capacitance across a metal/electrode interface.

$$1/C_{sc}^2 = \pm(2/\varepsilon\varepsilon_0 e N_A A^2)(E - E_{FB} - kT/e)$$

Equation 6-2. Capacitance of the SCL.

In this equation, C is the apparent capacitance, C_H is the capacitance of the Helmholtz double layer, C_{SC} is the capacitance of the space charge layer (i.e. interfacial capacitance) obtained from the relation $C = 1/(-Z''2\pi f)$ [108], where Z” is imaginary part of the impedance and f is the frequency. A is the specimen area and ε and ε_0 are relative permittivities or (dielectric constants) of the semiconductor and of free space ($8.85\text{x}10^{-13}$ F/mm), respectively. E_{FB} is the flatband potential, the potential at which the semiconducting passive film is in equilibrium with its environment [69]. k = Boltzmann constant ($1.38\text{x}10^{-23}$ J/K); T = temperature (K) and e = charge of the electron ($1.602\text{x}10^{-19}$ C). N is the charge carrier density (N_D or N_A is the donor or acceptor density given by the slope (m) of the linear portion of the $1/C^2$ vs. E plot using the relation $N = 2/\epsilon.\epsilon_0.e.m$ [107], [140], [141]).

In addition, the film thickness, d, in nm, can be calculated [100], [103], [146]–[150] using the capacitance from the above analysis.

$$d = (\varepsilon\varepsilon_0 A/C)$$

Equation 6-3. Relationship between film thickness and capacitance.

Where $\varepsilon = 10$ for carbon steel [104], [151], [152] and 15.6 for stainless steel [141], C is capacitance of the material calculated at different parts of the M-S plots (e.g. flatband potential (E_{FB}) and corrosion potential (E_{CORR})).

In most studies of the properties of the passive film, the physical meaning of the defect density, N, and flatband potential, E_{FB}, has not been well related to the corrosion behaviour of the material. Those studies correlating electronic properties of passive film with corrosion behaviour were either in non-ferrous materials [199], in very different solutions from that of this study [74], or in carbon steel [20] which is not main focus of this work. More recently, Cheng and co-workers [158]–[160] also related electronic properties of passive film to corrosion behaviour to observe the influence of ferrite and austenite phases in duplex stainless steel grades. Consequently, the overall goal of the present study has been to relate all the information obtained from the M-S analysis to the corrosion behaviour of the stainless steels determined by conventional electrochemical techniques. Moreover, most previous M-S tests on ferrous alloys have been performed on polished cross-sections. These studies have concentrated on carbon steel [8], [12], [20], [151], [152], [162]–[164], or 316LN and 304L stainless steel alloys [75], [107], [139]–[141], with a few recent studies on 2205 [154]–[160]. The environments used were acidic, neutral or slightly alkaline, whereas the pore solution in concrete is highly alkaline with a pH greater than 13 [2].

The objectives of the present research were to analyze the semiconducting properties of the passive film formed on three austenitic and two duplex stainless steel grades of reinforcing bars (rebar) in the environments (pH and ionic concentrations) found in chloride-free and chloride-contaminated concrete and to relate these properties to the bars' corrosion behaviour in simulated concrete pore solution. The chloride levels investigated in this study were in the range found to initiate corrosion on stainless rebar in concrete [19]. The influence of surface condition on the semiconductor parameters was assessed by testing the polished cross-section as well as "as-received" bars. Measurements were also made on carbon steel rebar (also known as "black steel rebar") for comparison purposes.

6.3. Materials and methods

For application as concrete reinforcement, the surface of stainless reinforcing bars is sand blasted and acid-pickled after their hot rolling and heat treatment to remove the mill-scale and any chromium-depleted layer, respectively. The bars are heavily deformed with circumferential and longitudinal ribs and, consequently, it is anticipated that their surface films and corrosion behaviour would be highly non-uniform. Investigating the bars in this condition was aimed at determining the corrosion behaviour as it would occur in service.

The M-S tests and corrosion tests were carried out in "simulated concrete pore solution": a $KOH+NaOH+Ca(OH)_2$ mix corresponding to that obtained by pore solution expression from a 75% Portland cement+25% slag paste with a 0.40 water/cementitious materials ratio [11]. Chlorides were added to the solutions in the concentration range that has been reported to cause corrosion initiation on stainless rebar [19], [62]–[64]. The grades and chemical compositions of the steels are presented in Table 6-1.

Specimen preparation

All bars were ribbed obtained from a commercial supplier. The 304L bars had a 20 mm nominal diameter while all the other bars were 15 mm nominal diameter. For the specimens designated as 'as-received' bars, 125 mm lengths of each grade were prepared as follows. A hole was drilled at one end and a solid copper wire was soldered for an electrical connection. Lacquer was applied to both ends to cover the soldered connection and limit the exposed length to 76 mm, giving an exposed surface area of 3581 mm^2 (4780 mm^2 for the 304L). The bars were then cleaned with alcohol to remove oil and grease from handling and rinsed with distilled water. For the cross-section specimens, solid copper wires were soldered to 12.5 mm lengths of the bars which were then mounted in a silica fume mortar (2 parts sand, 1 part silica fume cement and 0.5 parts water). The exposed cross-sectional area was 177 mm^2 (314 mm^2 for the 304L). The specimens were then ground with increasing grit size up to 1200 and polished down to 1 µm with a diamond polish to achieve a consistent surface finish.

Table 6-1. Grades and composition of the bars from the mill certificate provided by the manufacturer.

Class	Rebar grade	In text as	Composition (wt.%)							
			Cr	Ni	Mo	Mn	Si	Cu	C	N
Austenitic	UNS S31653	316LN	17.60	9.50	2.01	1.10	0.70	0.40	0.03	0.14
	UNS S30403	304L	17.90	8.20	0.50	1.30	0.60	0.60	0.03	0.13
	UNS S24100	24100	17.10	0.90	0.19	12.12	0.70	0.14	0.04	0.34
Duplex	UNS S32205	2205	22.70	4.60	3.03	1.40	0.60	0.20	0.02	0.14
	UNS S32304	2304	22.40	3.92	0.20	1.80	0.60	0.30	0.02	0.14
Carbon steel	400W	Carbon	0.10	0.06	0.01	1.31	0.18	0.26	0.21	0.01

Experimental setup

For each type of specimen (as-received and cross-section), three replicate specimens from each grade were placed in cells with testing solution, shown in Table 6-2, for two weeks to allow them to reach equilibrium before any testing. The open circuit potentials, or corrosion potentials, E_{corr}, were monitored over this period. After initial testing, described below, chlorides were added as NaCl into each of the solutions weekly in 6% increments for the stainless steel grades and 0.6% increments for carbon steel by mass of pore solution. The maximum chloride contents were 21% and 2.4%, corresponding to pore solution contents in concrete with approximately 10.5% and 0.75% Cl^- by mass of cementitious material according to [11], [137].

Table 6-2. Testing solutions.

Composition (Molar)			pH
$Ca(OH)_2$	KOH	NaOH	
0.0014	0.48	0.13	~13.6

Table 6-3. Chlorides addition to testing solution.

	Chloride increment				
For stainless steel (wt.%)	0	6	12	18	21
NaCl (M)	0	1.74	3.49	5.23	6.10
For carbon steel (wt.%)	0	0.6	1.2	1.8	2.4
NaCl (M)	0	0.17	0.35	0.52	0.70

The specimens were tested in a three-electrode electrochemical cell with the steel specimens as the working electrodes (WE), a saturated calomel reference electrode (RE) and a mixed metal oxide-coated titanium mesh as counter electrode (CE), as shown in Figure 6-1.

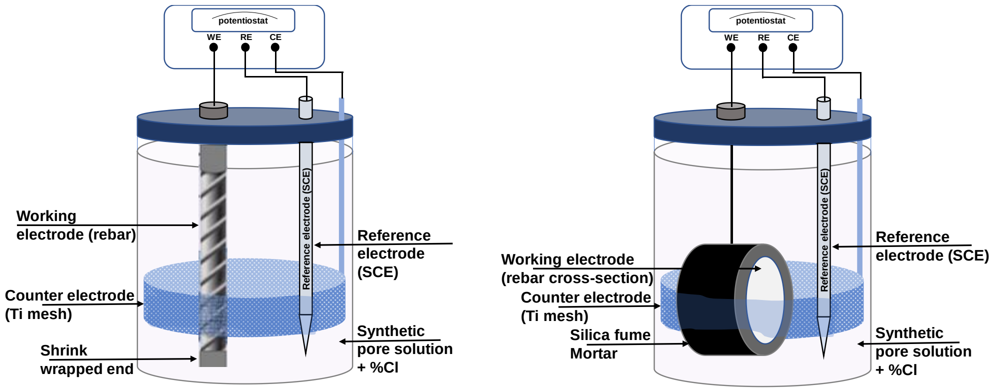

Figure 6-1. Test set-up for corrosion testing and M-S analysis on as-received bars (left) and rebar cross-sections (right) [137].

Experimental methods

Using a BioLogic potentiostat, Model VSP, a potentiostatic linear polarization resistance (LPR) [111] and staircase potential electrochemical impedance spectroscopy (SPEIS) [108] were performed at every chloride level to determine the corrosion potential and current and the M-S behaviour, respectively. The potentiostatic LPR test consisted of the application of ±10 mV for 30 seconds and measurement of the steady state current at the end of the 30 s. The ratio of the applied potential to the measured current represent the Polarization resistance, R_P which was converted to corrosion current with the commonly used value of 26 mV as the Stern-Geary constant. This constant values was measured for stainless steel rebar [200] to range from 20 to 28 mV. The SPEIS technique consists of a staircase potential sweep in which an impedance measurement (with desired frequency range) is conducted at each of a series of potential steps. The SPEIS was performed at 10 mV AC amplitude at frequencies from 100 – 1 kHz. The M-S plots presented in this paper were at 1 kHz, the maximum frequency at which the capacitance of the film was observed to be relatively unchanged [20]. 1kHz and a potential range of -1.5 – 0.6 V_{SCE} were also chosen to allow comparison with other results in the literature [107], [141].

One week after each chloride addition, an LPR was performed to detect the corrosion behaviour of the bar and, after a further 24 hours, the SPEIS test was conducted. After another 24 hours, chloride was increased in the solution and the film was allowed to attain equilibrium for a week before the next set of tests.

Using different specimens, taken from the same 1.2 m length of rebar, potentiodynamic cyclic polarization curves were obtained over the same potential range as the M-S tests in chloride-free and 6% chloride-containing solution.

6.4. Results

An initial test was conducted to determine if it is possible to conduct multiple potential sweeps on the same sample without any adverse effect. This first part of the test was performed on two separate “as-received” 2205 samples passivated in individual cells with chloride-free solution for two weeks. After passivation, NaCl was added to one of the cells at a concentration of 18% Cl^- and, after one week, the M-S tests were performed on both samples (Curve A – 0% Cl-, Curve B – 18% Cl^- in Figure 6-2). An M-S test was also performed on a passivated sample in solution without chlorides, Curve C, and again after 18% Cl^- addition, Curve D in Figure 6-2, which shows the M-S plots from these samples.

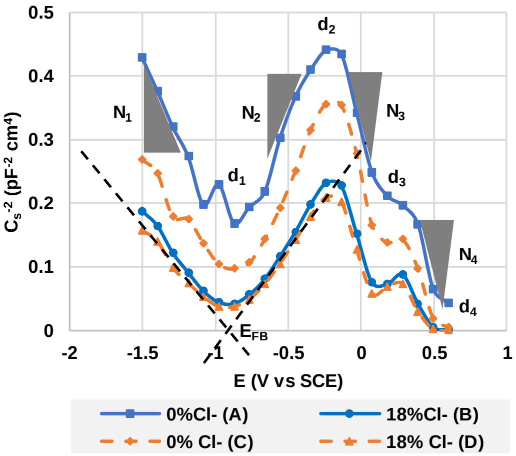

Figure 6-2. M-S plot conducted on 2205 samples in pore solution (PS) with and without chlorides. Curve A and B were obtained from two different bars tested in solution without and with chlorides respectively. Curve C and D were obtained from the same sample tested in solution before and after chlorides were added.

The curves with 0% Cl^- (Curves A and C) showed some variation which is attributed to the heterogenous surface of the bars. On the other hand, those plots for samples exposed to 18% Cl^- (Curves B and D) are very similar, suggesting that the influence of chlorides is greater than that of the surface inhomogeneities. The electronic properties of the passive films from this test, identified in Figure 6-2 and given in Table 6-4, are very similar, suggesting that multiple potential sweeps can be conducted on a specimen. These data cannot be compared directly with those presented later in the paper because of the different exposed area of the 2205 bars employed in this preliminary test.

For corrosion measurements, the corrosion potential of three replicates of each steel grade was first monitored over a two-week period. Figure 6-3 shows the E_{CORR} values of one of the three replicates of each grade. The E_{CORR} of all samples remained unchanged from day 8 to day 15, indicating that they reached steady state during that period.

Table 6-4. Electronic properties of curves identified in Figure 6-2. Linear regions and peaks where the defect densities (N_1 to N_4) and film thicknesses (d_1 to d_4) were calculated using Equations 6-2 and 6-3

M-S plots	**Electronic properties**								
	Acceptor density, N_1 (10^{21} cm^{-3}) -1.5 to -1	Donor density, N_2 (10^{21} cm^{-3}) -0.7 to -0.2	Acceptor density, N_3 (10^{21} cm^{-3}) -0.15 to 0.1	Acceptor density, N_4 (10^{21} cm^{-3}) 0.3 to 0.6	Flatband potential E_{FB} (V_{SCE})	Film at FB (-0.9 V) d_1 (nm)	Film at E_{CORR} (-0.2 V) d_2 (nm)	Film at 0.1 V d_3 (nm)	Film at 0.6 V d_4 (nm)
Curve A	6.21	5.30	2.85	4.27	-1.22	0.46	0.55	0.41	0.17
Curve B	8.79	7.30	3.49	6.72	-0.93	0.28	0.39	0.23	0.03
Curve C	8.06	5.10	2.83	4.27	-1.20	0.36	0.49	0.34	0.06
Curve D	10.51	8.00	3.70	7.26	-0.93	0.27	0.37	0.20	0.01

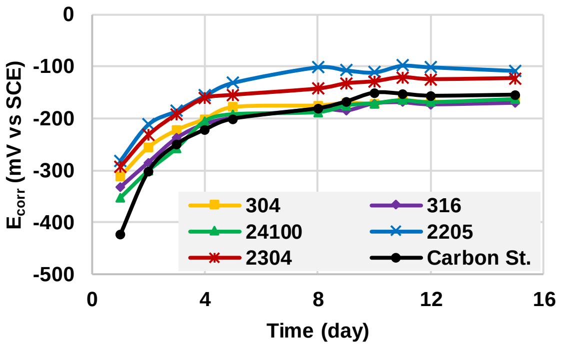

Figure 6-3. E_{CORR} values of bars in solution allowed to equilibrate for 2 weeks before any testing.

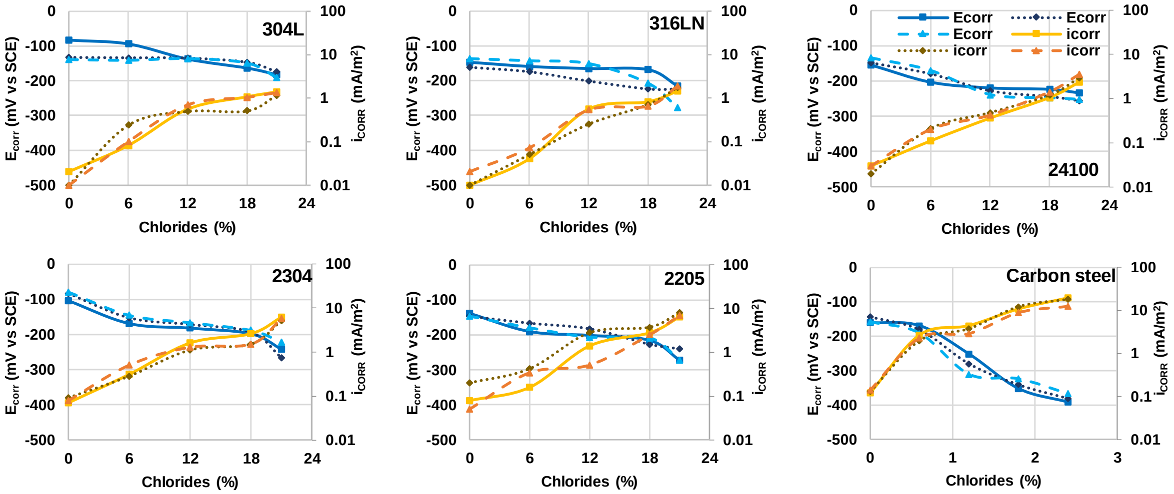

Figure 6-4. Corrosion potentials and current densities obtained for three replicates of each grade of “as-received” rebar in pore solution with increasing chlorides.

The corrosion potentials (E_{CORR}) and current densities (i_{CORR}) of the as-received bars in the pore solution with increasing chlorides are presented in Figure 6-4. The i_{CORR} values of all bars increased gradually with increasing chlorides, while their corresponding E_{CORR} values became gradually more negative. This behaviour indicates that the ionic and electronic resistances of the passive film was reduced by the chloride ions. The i_{CORR} values of the stainless steel and carbon steel in solution with 21% and 2.4% chlorides, respectively, were between 1 - 10 mA/m^2 equivalent to corrosion rates of between 1 - 10 µm/year. However, these values are the average over the whole exposed area of the bar, and it is highly likely that there are small areas of much higher corrosion rates causing the more negative potentials. Consequently, it is not possible to determine a critical chloride concentration for corrosion initiation from these data.

The M-S plots in Figure 6-5 show the influence of increasing chlorides on one of three replicates of each steel grade tested in their as-received conditions. A general observation for all the stainless steel bars in chloride-free solutions, is the negative slope of the curves from -1.5 V_{SCE} to their flat band potential, a feature not observed in the curves for carbon steel. Furthermore, on scanning the bars in solution in the anodic direction, both the stainless steels and carbon steel displayed a positive slope n-type semiconductor passive film up to their corrosion potentials (~ -0.15 V_{SCE}). At higher anodic potentials, the carbon steel showed a second positive slope n-type semiconductor at potentials between -0.15 and 0.3 V_{SCE}, while the stainless steel bars displayed a negative slope p-type semiconducting passive film at the same potential range. Both negative slopes are attributed to the presence of alloying elements, particularly chromium These findings are in agreement with others' observations [75], [107], [139]–[141], [154]–[160].

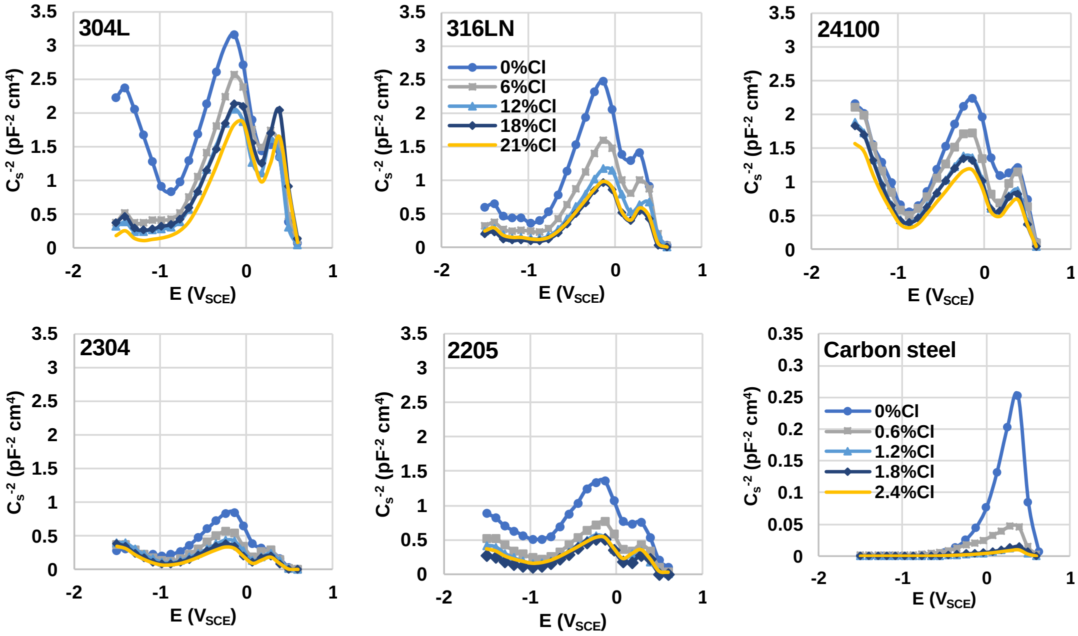

Figure 6-5. M-S plot of the austenitic and duplex steels tested in the pore solutions with increasing chloride. Note the order of magnitude lower 1/C^2 value for carbon steel.

The space charge capacitance, C, increases (shown in Figure 5 as decreasing $1/C^2$) with increasing chlorides. Since there is a direct relation between C and defect density, N, and, an inverse relationship with film thickness, d, these plots indicate an increase in defect density and decrease in film thickness with increasing chlorides in solution. This trend indicates that the passive film structure is increasingly unstable with increasing chloride concentrations, which agrees with the E_{CORR} and i_{CORR} data in Figure 6-4. The difference in capacitance between specimens in chloride-free solution and in solutions containing 6% Cl- (0.6% Cl-) is much greater than that between 6% Cl- (0.6% Cl-) and higher chloride levels. The increasing C values with chlorides is similar to those observed by [20] in similar solution pH and composition.

Figures 6-6A and 6-6B present the M-S plots obtained from three replicates of polished cross-sections of the 2205 bars tested in the solutions without chlorides and with 21% Cl-, respectively. Figures 6-6C and 6-6D are those obtained from testing the as-received bars in similar solutions, respectively and are presented here for easy comparison. Since there is good reproducibility in the M-S behaviour of the polished surfaces, the electronic properties obtained from only one sample of each stainless steel alloy are presented in Table 6-6. A general observation is that the *shape* of the M-S curves is not affected by the surface finish of the bars, but the *scale* of the $1/C^2$ axis is shown to be different. Another observation from Figure 6-6 is that the M-S plots of the as-received bars are not as reproducible as those of the polished surfaces, but the effect of chlorides on both surface conditions is similar.

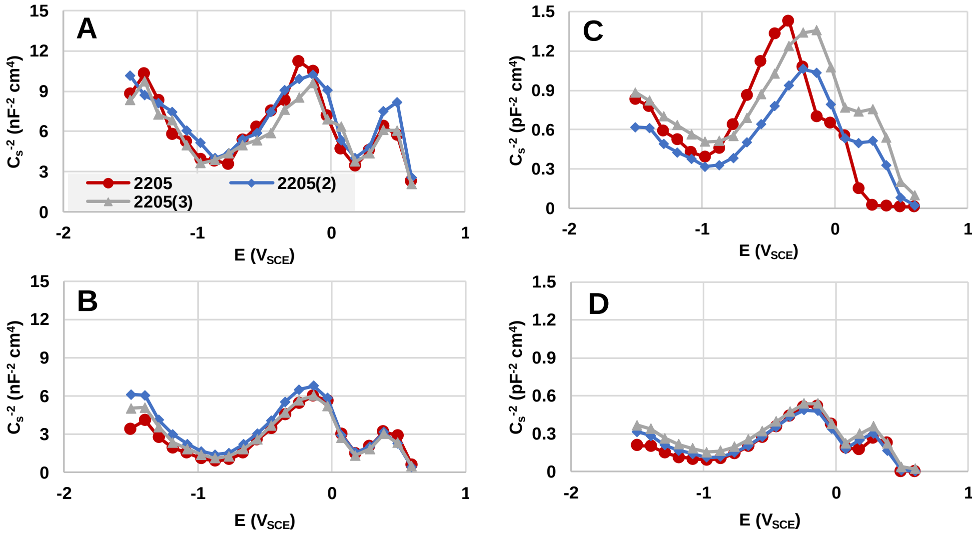

Figure 6-6. M-S plots of three replicates of the 2205 stainless steel polished cross-sections (A and B) and as-received bars (C and D) bar tested in pore solution with 0% (A and C) and 21% (B and D) chlorides. Their electronic properties are shown in Tables 6-5 and 6-6.

6.5. Discussions

The SPEIS test cycles the specimen through a large range of potential and the concern is that this could irrevocably change the environment around the steel. However, repeated tests demonstrated that the environment "recovered" after one week giving reproducible results. Feng et al. [155] also repeated potential sweep on the same specimens and found no outliers in their result. Williamson and Isgor [20] found only slight differences in electronic properties obtained from repeated potential sweep on the same specimen and those from single potential sweep applied on a specimen. It is worth noting that in their test, potentials were applied at different passivation times (from 0.5 hours to 10 days) and not at different chloride additions as employed in this paper. In the current project, bars were allowed to reach steady state before any application of potential sweeps, both initially and after each chloride addition.

Table 6-5 summarize the electronic and electrochemical properties of one of three replicates of each grade of the as-received steels tested in pore solution. Table 6-6 presents the corresponding data for the polished cross-sections of the stainless steel bars. The complete data is shown in the appendix (Appendix B-1 – B-6). These tables provide the corrosion current density (i_{CORR}) and corrosion potentials (E_{CORR}) from LPR measurements; the flatband potential (E_{FB}), defect densities (N_1, N_2, N_3, N_4) and film thicknesses (d_1, d_2, d_3, d_4) at capacitance values corresponding to those shown in Figure 6-2.

These data are discussed below in terms of the influence of increasing chlorides in the pore solution, the rebar composition and the surface finish. A comparison of the defect densities, flatband potential, and film thicknesses, shown in Table 6-5 with those from the literature shows that they are similar to those reported for 304L, 316LN and 2205 stainless steel alloys [75], [107], [139]–[141], [154]–[160] and carbon steel [8], [12], [151], [152], [162]–[164], despite their different test solution concentration and pH. No references were found for the electronic properties of the 24100 and 2304 grades.

In chloride-free pore solution, the i_{CORR} values presented in Table 6-6 for the polished cross-sections of the bars were an order of magnitude lower than those tested in the as-received conditions, shown in Table 6-5. However, after the addition of chlorides, the potentials and current densities in the two sets of specimens were similar. As indicated in Figure 6-2, the first negative slope in the M-S plots was used to calculate the N_1 values (the p-type, Cr-rich layer), while the next positive and negative slopes were used to calculate the values of N_2 (the n-type, Fe-rich layer) and N_3 (the p-type outer spinel layer) respectively.

Influence of increasing chlorides in the testing solution on electronic properties

Figure 6-7 shows that the defect densities (N_1 and N_2) increased with increasing chloride concentration, while film thicknesses (d_1 and d_2) decreased. This is in agreement with the decreasing (more negative) E_{CORR} and increasing i_{CORR} values with chlorides shown in Figure 6-4. It is reasonable that a passive film attacked by chlorides has a higher density of defects, indicating the non-stoichiometry of the space charge layer of the passive film. A high defect density is closely associated with a high probability of passivity breakdown since defects are potential sites for corrosion initiation. The austenitic grades had consistently lower defect densities and higher film thicknesses at all chloride levels than the duplex grades. This is consistent with the austenitic grades exhibiting the slightly lower average corrosion current densities than those of the duplex grades. Furthermore, the defect densities of the austenitic grades increase only slightly with increase in chlorides, whereas those of the duplex grades significantly increased in the presence of chlorides.

Table 6-5. Corrosion data and film semiconductor data of one of three replicates of as-received stainless steel bars tested in pore solution, with the N_x and d_x values defined in Figure 6-2. Only 0 and 21% Cl- is shown in the table, other concentrations are presented in the Appendix.

Chloride addition		**Electronic properties**										
		i_{CORR} (mA/m^2)	E_{CORR} (mV$_{SCE}$)	E_{FB} (mV$_{SCE}$)	N_1 (10^{21} cm^{-3})	N_2 (10^{21} cm^{-3})	N_3 (10^{21} cm^{-3})	N_4 (10^{21} cm^{-3})	d_1 (nm)	d_2 (nm)	d_3 (nm)	d_4 (nm)
304L	0%	0.01	-133	-1030	1.08	1.27	0.84	0.90	0.49	0.67	0.66	0.22
	21%	1.17	-175	-910	6.16	2.96	1.66	1.53	0.36	0.42	0.48	0.42
316LN	0%	0.01	-161	-1010	5.69	2.62	1.56	1.78	0.34	0.45	0.42	0.13
	21%	1.74	-224	-955	8.44	5.19	3.59	4.02	0.22	0.32	0.28	0.04
24100	0%	0.02	-149	-1111	1.98	2.42	1.83	1.34	0.35	0.47	0.55	0.17
	21%	2.91	-256	-1040	2.56	4.66	3.08	2.15	0.26	0.34	0.42	0.10
2304	0%	0.02	-83	-1070	10.40	6.44	3.99	7.51	0.22	0.29	0.20	0.04
	21%	2.63	-266	-970	10.91	14.75	6.76	9.60	0.13	0.18	0.15	0.01
2205	0%	0.02	-147	-1120	9.25	5.35	2.96	4.00	0.25	0.32	0.28	0.83
	21%	3.98	-240	-880	15.35	11.12	4.93	7.07	0.17	0.22	0.20	0.16
Carbon	0%	0.28	-143	-637		67	20	9.00		0.06	0.11	0.083
	2.4%	4.2	-381	-680		1379	551	194		0.00	0.02	0.002

Table 6-6. Corrosion data and film semiconductor data for polished cross-sections of all stainless steel bars tested in pore solution, with the N_x and d_x values defined in Figure 6-2.

Chloride addition		**Electronic properties**										
		i_{CORR} (mA/m^2)	E_{CORR} (mV$_{SCE}$)	E_{FB} (mV$_{SCE}$)	N_1 (10^{21} cm^{-3})	N_2 (10^{21} cm^{-3})	N_3 (10^{21} cm^{-3})	N_4 (10^{21} cm^{-3})	d_1 (nm)	d_2 (nm)	d_3 (nm)	d_4 (nm)
304L	0%	0.02	-164	-950	2.15	2.03	0.98	0.71	0.58	0.77	0.69	0.48
	21%	1.01	-202	-910	3.21	2.22	1.19	1.16	0.53	0.70	0.61	0.44
316LN	0%	0.02	-169	-1220	2.76	2.71	1.89	0.99	0.60	0.78	0.76	0.41
	21%	0.98	-200	-1180	4.75	2.93	2.13	1.95	0.54	0.72	0.70	0.38
24100	0%	0.02	-177	-1140	3.38	2.40	1.36	0.78	0.58	0.63	0.64	0.39
	21%	1.20	-210	-1100	4.11	3.52	2.73	2.51	0.53	0.60	0.58	0.38
2304	0%	0.05	-185	-1070	4.49	3.92	2.87	1.69	0.58	0.58	0.60	0.41
	21%	1.64	-231	-1010	7.65	4.31	3.65	2.99	0.53	0.53	0.52	0.39
2205	0%	0.04	-187	-1060	4.63	4.10	3.01	2.23	0.44	0.57	0.54	0.33
	21%	1.72	-242	-1010	7.70	4.53	3.43	3.09	0.43	0.53	0.51	0.32

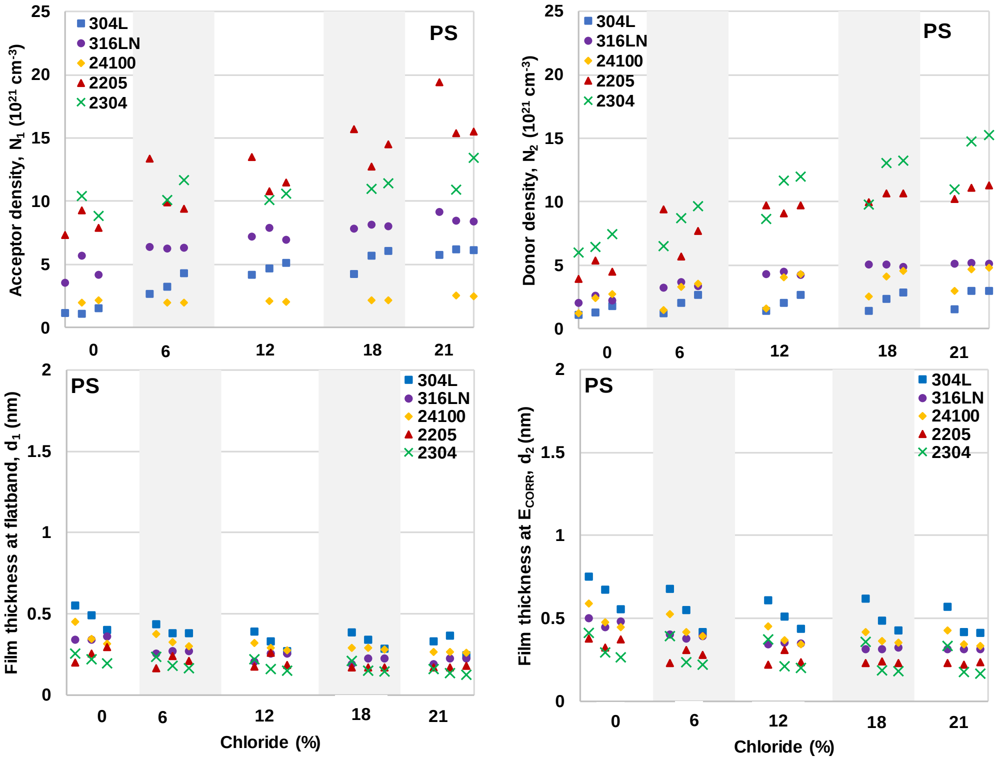

Figure 6-7. Change in acceptor and donor densities and film thicknesses at flatband and corrosion potentials for the stainless steel rebar with increasing chloride content in pore solutions.

Influence of alloying elements on electronic properties

Influence of chromium (Cr) in stainless steel bars on the electronic properties of the films.

As shown in Figure 6-5 and Table 6-5, the influence of chromium was found both in the cathodic and anodic regions of the M-S plots and the defect densities associated with both regions. At very low cathodic potentials, the negative slope (indicative of a p-type semiconductor) not found in the carbon steel, reveals the inner Cr-rich oxide layer of the passive film. At more positive potentials, the plots of the carbon steel bars reveal a shallow (N_2) and deep (N_3) donor level, both characteristics of an n-type semiconductor, corresponding to Fe oxides in the space charge layer of the passive film. In the stainless bars, a positive sloped linear region, indicative of the outer Fe oxide in the passive film, was observed and, unlike the Cr-free carbon steel, a second acceptor level of the outer Fe-rich oxide layer exhibited a p-type semiconductor attributed to a Fe-Cr spinel. These findings agree with those of other authors who have tested Fe-Cr system [156], [157]. Tables 6-5 and 6-6 show that the defect densities, N_1 to N_4, and film thicknesses, d_1 to d_4, of the tested stainless steel bars are 1-2 orders of magnitude lower and higher, respectively, than those of the carbon steel bars with and without chlorides. This indicates that, although carbon steel does readily passivate at this high pH, the presence of Cr in the stainless steels promotes a more coherent, dense and thicker passive film.

Influence of nickel (Ni) in 304L and its replacement with manganese (Mn) in 24100 on the electronic properties of the films.

Due to the high cost of nickel (Ni) in the traditional 304L alloy, manganese (Mn) is used as an alternative austenite-promoting element in the production of the less costly 24100 grade. The effect can be assessed by comparing the electronic properties of both grades. Figure 6-7 show that the N_1 and N_2 values of the 24100 bars in pore solution with chlorides were lower and higher, respectively, than those of the 304L bars. The lower N_2 (also N_3 and N_4 shown in Table 6-5) values of the 304L bars in the presence of chlorides suggest that the Ni-Fe oxides formed in the outer layer of the passive film of the 304L bars are denser and more coherent, and thus, offers more protection, than the possible Fe-Mn spinel formed in the passive films of the 24100 bars. From the lower and relatively constant N_1 values of the 24100, it is clear that the Mn stabilizes the inner Cr-rich oxide layers in the presence of chlorides. Some authors [141], [201] have also observed the influence of Ni only in the Fe-rich outer layer of the passive films.

Influence of molybdenum (Mo) in the austenitic and duplex stainless steel grades on the electronic properties of the films

The influence of molybdenum (Mo) on the electronic properties can be considered by comparing the pairs of the austenitic 304L and 316LN grades and the duplex 2205 and 2304 grades. The differences in two of the four defect densities (N_1, N_2) and film thicknesses (d_1, d_2) of both pairs of steels in solutions with and without chlorides can be graphically seen in Figure 6-7. The defect densities and film thicknesses of the Mo-containing bars, for both pairs of alloys are higher and lower, respectively, than those of their Mo-free counterparts.

In [107], [139]–[141], the difference in semiconducting properties of traditional 304L and 316LN alloys was observed in the linear region of the M-S plot in potential range corresponding to those between potentials of -0.15 – +0.1 V, region for which defect densities N_3 were calculated, in this work. The authors found slightly lower defect densities for the 304L grade which is consistent with the data presented in the present work. No reference was found for which the electronic properties of both 2205 and 2304 steel grade had been assessed in the same work. The lower defect densities and higher film thicknesses of the 304L and 2304 bars than the 316LN and 2205 bars shown in Figure 6-7 and Table 6-5 are consistent with their electrochemical properties in Figure 6-4.

Molybdenum is known to have a beneficial influence on the pitting resistance of stainless steels in acidic and neutral chloride solutions [202]. However, the corrosion potentials and corrosion current densities shown in Figure 6-4 do not show any improvement in corrosion resistance of 316LN over that or 304L, nor of 2205 over 2304. These results are in agreement with the findings of Mesquita et al. [203]–[205] who have shown that the beneficial effect of Mo in austenitic stainless alloys decreased with increasing pH from 0.6 to 7 to 10, at which level, its effect was negligible. For the duplex alloys, on the other hand, Mesquita et al. [203]–[205] and Cheng et al. [158]–[160] showed that the Mo and Cr were partitioned preferentially in the ferrite phase and that the positive influence of Mo diminished only slightly with increasing pH in 2205. Moreover, these authors found the ferrite and austenite acted synergistically in the 2205 to provide corrosion protection by promoting the formation of a denser and more homogeneous passive film. This provides an explanation for the superior corrosion resistance of 2205 grade compared with both 2304 and 316LN observed in previous work [185]. However, in the present work, 2205 did not perform as well as expected. Therefore, some of the untested bars of the 2205 specimens were sectioned, polished and observed by optical microscopy. It was found that the surface of these bars was heavily pitted on a micro-scale, as shown in Figure 6-8. It is believed that this is a result of the pickling process mentioned earlier and that it has allowed an increased level of corrosion to occur in the current tests. This surface pitting explains why there is more scatter in the corrosion current densities, shown in Figure 6-4, of the 2205 bars than of other rebar grades.

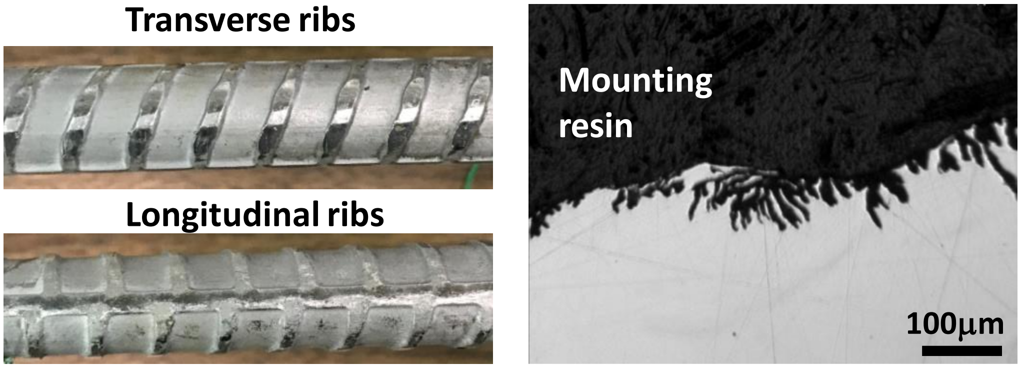

Figure 6-8. Sample of the 2205 stainless steel rebar showing the transverse and longitudinal ribs (left) and the image of the cross section showing micropits on the longitudinal rib (right)

In order to correlate the electronic and electrochemical corrosion data, the M-S curves and corresponding cyclic polarization (CP) curves for 304L and 316LN and for the 2304 and 2205 bars tested 0% and 6% Cl^- solutions are shown in Figures 6-9 and 6-10 respectively.

The information provided by Hakiki et al. [107], [139]–[141] and Beverskog & Puigdomenech [206]–[208] are considered in interpreting these graphs, which have been labelled to reflect the state of the passive film in the different regions of the M-S and cyclic polarization plots. The flatband potential of the M-S plots of the stainless steel bars presented in Figures 6-9 and 6-10 corresponds approximately to the H^+/H_2 equilibrium potential. The highest peak in the M-S plots corresponds to the corrosion potentials and, the onset of the transpassive region corresponds to the O_2/OH^- equilibrium potential on the E/pH diagram at the pH of the pore solution. The slight shift in potentials between the M-S and the CP plots is attributed to the difference in scan rates of the two tests.

The plots shown in Figures 6-9 and 6-10 indicate that, on raising the potential in the anodic direction from -1.50 V_{SCE}, the p-type semiconducting Cr-rich oxide films become more unstable and, at potentials more positive than the flatband potential, the M-S curve is dominated by an n-type Fe_2O_3 and/or the spinel $FeCr_2O_4$ films. At potential more positive than the corrosion potential of the material, there is an oxidation of the spinel $FeCr_2O_4$ to $(Fe)CrO_4^{2-}$ until the stable $NiFe_2O_4$ spinel is formed. At even more positive potentials, there is transpassive oxidation back to CrO_4^{2-} and FeO_4^{2-} [209]. The last potential range (~ +0.3 – +0.6 VSCE) on the M-S plots for which the N_4 defect densities were calculated is interpreted to be the transpassive region as per their CP plots. Williamson and Isgor [20], used the inversion layer theory of Morrison [36] to explain this characteristic transition in carbon steel rebar to a p-type behaviour. They interpreted the transition as being due to exhaustion of the two distinct donor layers within the band gap (N_2 and N_3 values in the present study), thus requiring transfer of charge from the valence band and further conduction by holes, i.e. p-type conduction. Nevertheless, for both stainless steel and carbon steel in the present study, this p-type behaviour results in the M-S curve approaching zero corresponding to the sharp increase in current density of the cyclic polarization curve, i.e. equivalent to transpassive behaviour. The interpretation made in the present study regarding oxide species formed at the different potentials agrees well with the E/pH diagrams in [206]–[208] and observations from M-S analysis by other authors [75], [107], [139]–[141], [154]–[160].

With respect to the influence of Mo, the corrosion current densities of the Mo-free 304L bars are lower than those of the Mo-containing 316LN grades and, as discussed, the expected superior behaviour of the Mo-containing 316LN was not observed. At 6% chloride additions, the corrosion potentials of the 316LN bars became more negative; a behaviour not observed in the 304L bars. These findings support other authors' observation [158]–[160], [203]–[205],[210] that the influence of Mo in austenitic phase diminishes with pH. On the other hand, both the corrosion current densities of the Mo-containing 2205 grades and the intensity of the peak attributed to the $FeCr_2O_4$ oxidation are lower than those of the Mo-free 2304 grades. However, after the addition of chlorides, the $FeCr_2O_4$ oxidation peak was higher in the 2205 bars due to the heavy pitting observed around the bars. These findings are also consistent with those from other authors [158]–[160], [203]–[205],[210] who observed Mo to be beneficial in the ferritic phases of the duplex alloys. The overall observation in Figures 6-9 and 6-10 is consistent with previous data presented on corrosion potential, corrosion current density, defect densities and film thicknesses.

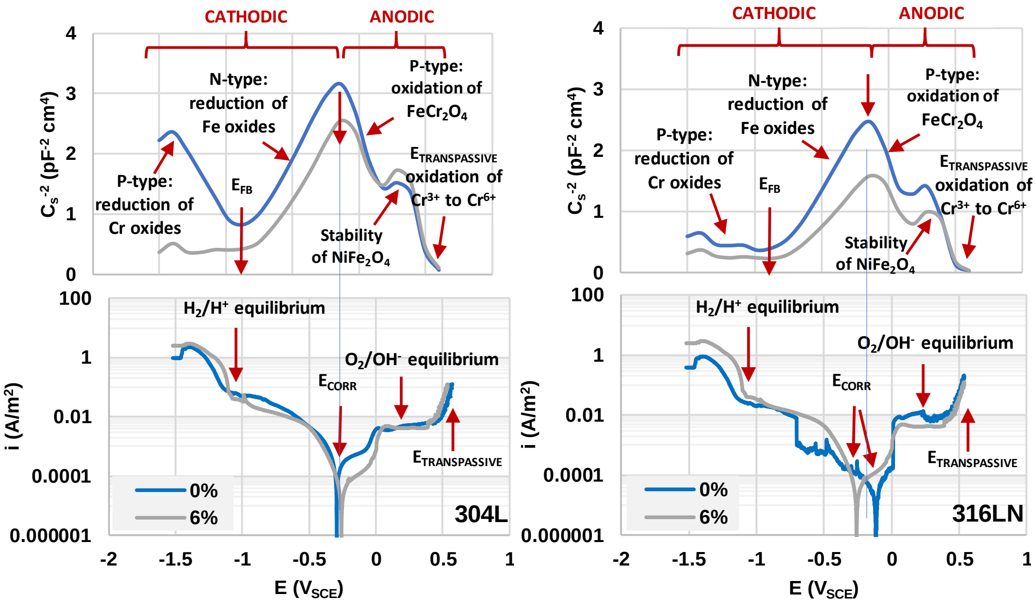

Figure 6-9. M-S and cyclic polarization curves for 304L and 316LN stainless steel bars in solution without and with 6% chlorides. Test were carried out with similar potential range. Note that the plots are shifted slightly to align the corrosion potentials, to account for the different scan rates and specimens employed for the two tests.

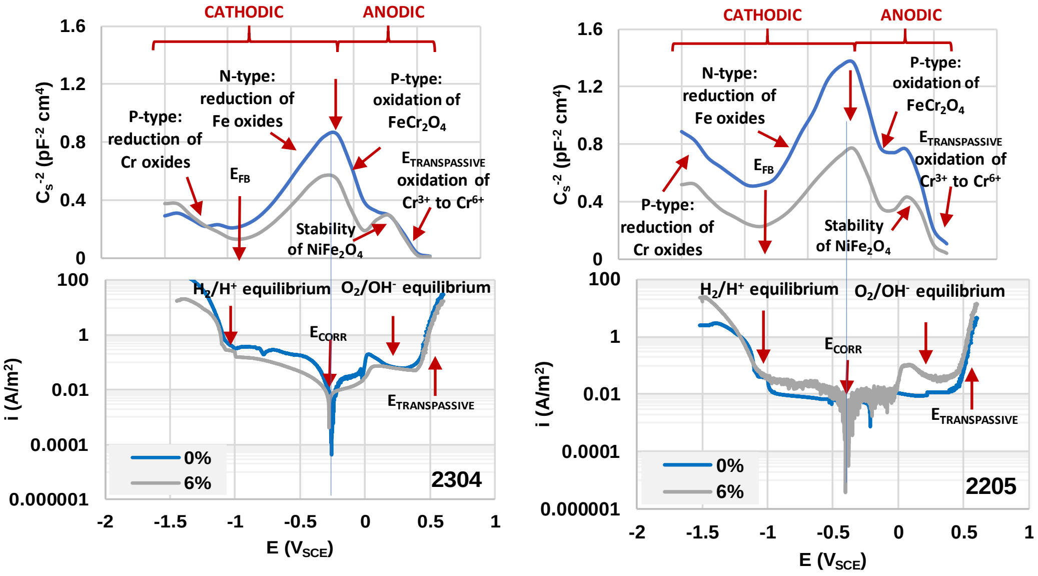

Figure 6-10. M-S and cyclic polarization curves for 2304 and 2205 stainless steel bars in solution without and with 6% chlorides. Test were carried out with similar potential range. Note that the plots are shifted slightly to align the corrosion potentials, to account for the different scan rates and specimens employed for the two tests.

Breakdown of passive film by chlorides

An interesting observation in the CP and M-S plots of the 304L bars shown in Figure 6-9 is that there is little effect of 6% Cl- on the polarization curve, while there is a significant drop in the slope attributed to the Cr-rich component of the film in the cathodic region of the M-S plot. This can also be observed in the defect densities presented in Tables 6-5 and 6-6 for both as-received and polished cross-section where the N_1 values are generally higher than the N_2 and N_3 values. This is surprising in view of the fact the N_1 represents the defects in the inner layer of the film and there appears to be little effect on the outer Fe-rich layer. A possible explanation to this observation can be explained considering the film breakdown.

Most models of chloride-induced corrosion of reinforcing steels include an incubation period in which both the corrosion potential, E_{corr}, and passive corrosion current density, $i_{corr,}$ are approximately constant. When sufficient chloride is present at the steel surface to breakdown the passive film and initiate active corrosion (the so-called threshold value), the models predict a sharp increase in i_{corr} accompanied by a shift in E_{corr} to more negative values. In practice, this is not what happens. As illustrated in Figure 6-4 for both carbon steel and stainless steel rebar, there is a gradual increase in i_{corr} and decrease in E_{corr} with increasing chloride content of the solution, requiring a very different model of the process. The model of Marcus et al. [168], shown schematically in Figure 6-11, can provide a basis for such a model.

Marcus and colleagues propose that there is a sharp potential difference, ΔE, at the interface between the metal and the passive film and another at the interface between the film and the solution, with a gradual potential gradient across the film. Increasing the defects in the film by, for example, diffusion of chloride ions, allows for reduced electronic and ionic resistance and thinning of the film. Such a process would result in a greater leakage current and a more negative potential difference. This model can be coupled with that of Hakiki et al. [140] shown in Figure 6-12 in which Cl^- diffuses through the oxygen vacancies of the Fe-rich layer and reacts with the Fe^{2+} ions diffusing outwards through the Cr-rich layer. This would explain the significant effect of 6% chloride on the inner Cr-rich layer of 304L with little effect on the Fe-rich layer, observed by M-S analysis and little effect on the measured cyclic polarization curves Figure 6-9.

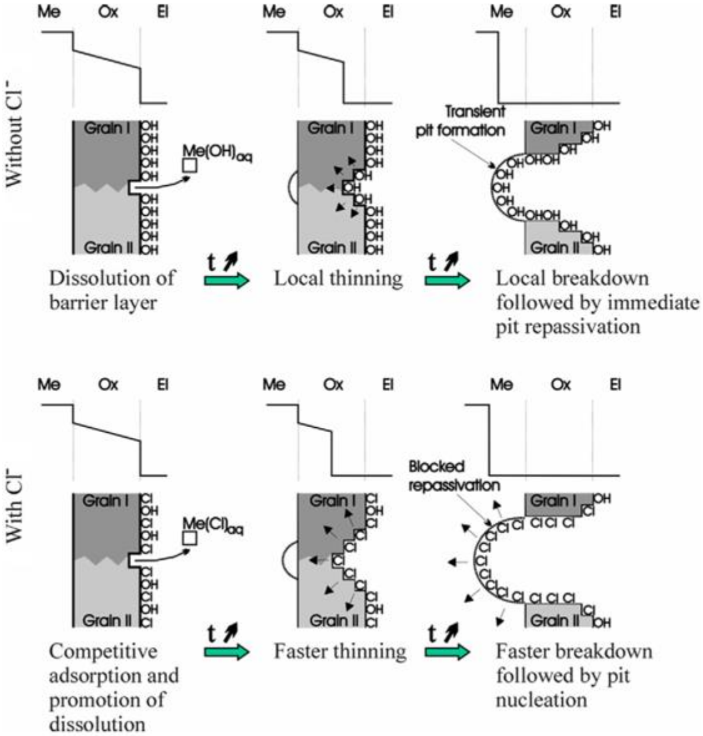

Figure 6-11. Mechanism of local breakdown of passivity driven by the potential drop at the oxide/electrolyte interface of an inter-granular boundary of the barrier layer. The effect of chlorides is shown [168].

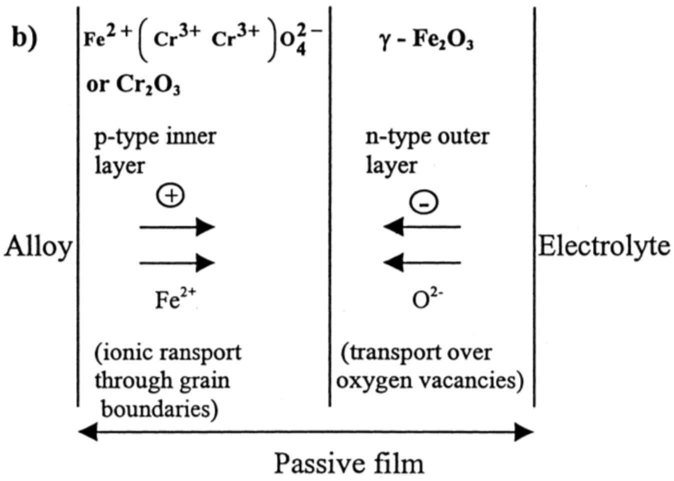

Figure 6-12. Schematic representation of the diffusion processes through the individual layers of passive films [140].

Influence of surface finish on electronic properties

From Tables 6-5 and 6-6, the defect densities obtained from the polished cross-section specimens are slightly lower than those from the as-received austenitic stainless steel grades and, significantly lower than those from the as-received duplex grades, suggesting that the passive films formed on the polished cross-sections were more protective in the presence of chlorides. Apart from the larger surface area available for chlorides to attack in the as-received bars, the surface roughness of the bars (an example for which is shown in Figure 6-8) being attacked by chlorides contributes to the higher defect density values. This is also supported by the slightly more negative E_{CORR} and higher i_{CORR} values at 21% chlorides shown in Table 6-6 than those in Table 6-5. The corrosion resistant properties of a polished rebar has been previously reported [13], [211], [212] to be higher than as-received rebar. Feng and co-workers [213], [214] also showed increasing defect densities with increasing degree of deformation of the substrate, agreeing with the lower defect densities observed for the polished specimens than for the as-received specimens tested in this work.

Similar to the trend found in the as-received bars, the defect densities from the polished cross-sections of the duplex stainless steel alloys are also higher than those of the austenitic grades. Similar results, in most cases, obtained in both polished cross-sections and the as-received bars suggest that the relative performance of bars to be compared can be tested in their as-received conditions, without polishing their cross-sections. However, in other cases, the impact of chlorides on the duplex stainless steel cross-sections was underestimated, emphasising the importance of replicating test conditions found in the field.

6.6. Summary and conclusions

- The positive impact of the chromium in the stainless steel bars is attributed to the significantly lower defect densities, by 1 – 2 orders of magnitude, of their passive film than that of the carbon steel bars.
- Molybdenum, which is the major difference in composition between austenitic 304L and 316LN and the duplex 2205 and 2304, did not show the anticipated positive impact on the electrochemical and electronic properties of the 316LN and 2205 alloys in all testing solutions with and without chlorides.
- On comparing the data for the 304L and 24100 bars to evaluate the influence of replacing Ni with Mn, manganese was found to reduce the defect density of the inner Cr-rich oxide layer while nickel decreased that of the outer Fe-rich oxides. In general, the electronic properties and electrochemical behaviour of the Ni-containing 304L bars were not significantly superior than those of the Mn-containing 24100 bars.
- The roughness, on both macro- and micro-scale, of the as-received surface of the bars did not influence the shape of the M-S plots, but their passive films had a higher defect density than those of the polished surface. Consequently, M-S analysis can be performed on as-received bars, although great amount of scatter may be obtained.
- Increasing additions of chlorides to the solution made the passive films on all tested bars more defective and reduced their thicknesses, resulting in a gradual increase in the passive current densities accompanied by a more negative corrosion potential.

- For the stainless steels, the M-S analysis indicates that the chlorides affect the Cr-rich inner layer of the passive film more than the Fe-rich outer layer.
- The electronic properties of the passive films on the three austenitic stainless steel grades tested did not vary significantly with chlorides, whereas those of the duplex grades changed significantly in the presence of chlorides. This observation is consistent with the higher corrosion rate and more negative corrosion potential values of the duplex stainless steel grades.

7. The critical chloride threshold of austenitic and duplex stainless steel reinforcing bars[5]

7.1. Overview

Values of the critical chloride threshold concentration for initiation of reinforcing bar (rebar) corrosion are essential input parameters for service life predictions for reinforced concrete structures. For highway infrastructure, the specified service life is currently 75 to 120 years depending on the jurisdiction. Different techniques have been employed to determine these threshold concentrations because of the many factors influencing the corrosion initiation. The current standard methods, e.g. ASTM G109, require weeks or months of testing and are often not logistically feasible for testing large numbers of specimens in different conditions in a reasonable time frame.

The work presented here employed a fairly rapid potentiodynamic polarization technique to determine the critical chloride threshold value of different grades of stainless steel reinforcing bars in synthetic concrete pore solution corresponding to a specific concrete mixture design. This method was successfully employed in identifying the influence of alloying composition, testing solution and rebar surface finish on their critical chloride threshold value. The threshold values of Ni-containing stainless steel grades were higher than Mn-containing grade, and Mo only improved the pitting resistance of the duplex grades, but not the austenitic grades. The chloride threshold values of tested bars with processing flaw was lower by 13%. The inclusion of sulphate as measured in pore solution expressed from cement pastes in the pore solution was found to increase the threshold values of these rebar grades by 4 – 8%.

7.2. Background

Despite its high initial cost, stainless steel is one of the most viable options for ensuring the durability of reinforced concrete in environments prone to chloride attack (such as marine areas and structures exposed to de-icing salts). The first recorded successful use of stainless steel as concrete reinforcement is to the 2100-metre-long pier built between 1937 – 1941 in the Port of Progreso, Mexico [28]. In the first 75 years of its service life, the stainless steel reinforced pier showed little corrosion, per a visual inspection and chloride penetration analysis [29]. In comparison, a newer carbon steel reinforced pier built in the early 1970's already deteriorated by 1999 [215].

In today's market, two classes of stainless steel alloys are commonly used for construction, the single-phase austenitic grades and the duplex grades containing both ferrite and austenite phases. Within these two categories, the composition and, hence, price, can vary, largely on the basis of the nickel (Ni) and molybdenum (Mo) contents [216]. For example, the 316LN and 2205 grades are the most expensive stainless steel grades but, solely on the basis of today's material component costs, 316LN is ~19% more expensive than 2205, because it contains approximately twice the amount of Ni. Similarly, the 304L and 2304 grades, are ~32% and ~38% less costly than their Mo-containing counterparts, 316LN and 2205,

---

[5] The contents of this chapter have been submitted and adapted with permission from ASM International & TMS: I.G. Ogunsanya, C.M. Hansson. "The critical chloride threshold of austenitic and duplex stainless steel reinforcing bars" submitted to *Metallurgical and Materials Transactions*, E-TP-19-1282-A, 2019.

respectively. The least costly grade of stainless steel rebar is the austenitic 24100 grade because of the replacement of Ni with manganese (Mn). Although most published literature on stainless steel rebar has focused on the traditional austenitic rebar grades (304L, 316LN) [62], [107], [140], [141], [182], [217]–[219], some work has also shown positive corrosion performances of the duplex and the leaner grades. Some authors found the corrosion performance of Mo-free duplex 2304 to be similar to Mo-containing duplex 2205 [220], and both grades to be better than [203], [204], [221], [222] the traditional austenitic grades.

Life-cycle cost modelling is often used to show that the use of stainless steel rebar in highly aggressive environment is economically beneficial on the long term and to select between the different grades. Since critical chloride threshold value is an important input parameter in these models, it is essential to assess the contributions of the expensive Ni and Mo elements in stainless steels towards their critical chloride threshold values. The chloride threshold level or critical chloride level (C_{CRIT}) may be defined as the concentration of chloride at the steel surface necessary to break down its passive film and initiate active corrosion. The major advantage of stainless steel is its ability to withstand significantly higher chloride threshold than carbon steel. To determine this value for any rebar, different experimental systems have been employed [170], including but not limited to [58]–[60], [171]–[179]:

- Rebar environment: concrete; mortar; synthetic pore solution
- Specimen exposure: laboratory atmosphere (approximately constant temperature and relative humidity); outdoor exposure (variable temperature, relative humidity and precipitation).
- Chloride addition: admixed during mixing; ingressed from the environment through the mortar or concrete.
- Measurement techniques: potential mapping; linear polarization resistance; cyclic polarization; electrochemical impedance spectroscopy; potentiostatic tests and galvanostatic tests.

Results from one experimental system can vary significantly from those obtained using another system, making comparison difficult. For example, a C_{CRIT} test conducted on steel in concrete will vary with water-to-cementitious materials ratio; supplementary cementitious materials; curing time; concrete age; type of chloride; rebar surface condition, etc. [61]. The decision on the methodology employed is often influenced by the time intended to obtain results. To fast track the time to obtain results and properly account for the time to corrosion initiation on the rebar, most investigations have moved from testing in concrete or mortar to testing in synthetic pore solution. Laboratory reagents are used to simulate the pH and ionic environment inside of concrete and chlorides are added incrementally over time until active corrosion is observed visually and/or electrochemically. The chloride amount employed to initiate active corrosion must then be translated from percent Cl^- by mass of solution to percent Cl- by mass of cementitious materials or concrete to provide useful interpretation in the field and useful input parameter for life-cycle models. Many laboratories have incorporated different pH and ionic compositions in testing solutions to simulate the environment in concrete, but no test was found to incorporate the recently observed [11] increasing sulphates in cement pore solution of a chloride-contaminated cement paste. The authors recently reported the influence of these increasing sulphate to be beneficial to carbon steel rebar C_{CRIT} value [137]. Its influence on stainless steel is yet to be reported.

The goal of this project was to determine the influence of alloying elements such as Mo, Ni, Mn, and testing solutions on C_{CRIT} value of five different grades of stainless steel using a fairly rapid potentiodynamic polarization technique adapted from the authors' earlier work on carbon steel rebar [137]. The impact on C_{CRIT} value of processing flaws or artefact developed during production of these bars was also determined.

7.3. Experimental methods

Stainless steel reinforcing bars, with composition shown in Table 7-1, were first visually examined and photographed to be compared later after testing. The bars were cut to 127 mm (5.0 in) in length, drilled on one end, soldered with a solid copper wire and lacquer was applied to both ends to allow an exposed length of 76 mm (3.0 in). The specimens were cleaned with alcohol and rinsed in distilled water to remove contaminations from handling. The specimens were then placed in their respective testing solutions with a saturated calomel reference electrode (SCE) and a mixed metal oxide coated titanium mesh as counter electrode, as shown in Figure 7-1. The cells were all covered to minimize the possibility of carbonation.

Table 7-1. The mill certificate composition of stainless steel bars. NR = not reported.

Class	**Rebar grade (ASTM)**	**Denoted in text as**	**Composition (wt.%)**							
			Cr	**Ni**	**Mo**	**Mn**	**Si**	**Cu**	**C**	**N**
Austenitic	UNS S31653	316LN	17.60	9.70	2.00	1.10	0.60	NR	0.02	0.14
	UNS S30403	304L	17.90	8.25	NR	1.20	0.40	NR	0.02	0.13
	UNS S24100	24100	17.20	0.70	0.19	12.12	0.50	0.10	0.04	0.31
Duplex	UNS S32205	2205	22.71	4.91	3.03	1.46	0.59	0.30	0.02	0.14
	UNS S32304	2304	22.40	4.05	0.19	1.61	0.43	0.30	0.02	0.14

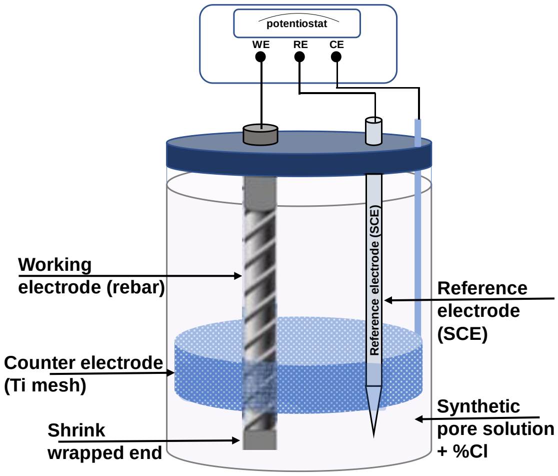

Figure 7-1. Three-probe electrochemical cell with a mixed metal-oxide titanium mesh counter electrode and a saturated calomel reference electrode (SCE) [137].

Three testing solutions were employed as presented in Table 7-2. The first was saturated $Ca(OH)_2$ solution (designated as CH). The second solution (designated as PS) was based on the hydroxide contents of the expressed solutions from a specific 75% Portland cement+25% ground granulated blast furnace slag mixture (OPC+25%GGBFS) with a w/cm of 0.40 and different NaCl additions. The third solution (designated as PS+S) was based on the same solution as PS but included the sulphates measured in the expressed pore solution [11]. The sulphate addition shown in Table 7-3 and PS+S solution shown in Table 7-2 are based on values obtained in [11] shown in Figure 7-2.

Table 7-2. Testing solutions.

Testing solution (denotations)	**Composition (M)**				**pH**
	$Ca(OH)_2$	KOH	NaOH	$CaSO_4.2H_2O$	
Calcium hydroxide (CH)	Saturated				~12.5
Pore solution (PS)	0.0014	0.48	0.13		~13.6
Pore solution plus sulphate (PS+S)	0.0014	0.48	0.13	0.002	~13.5

Table 7-3. Chlorides and sulphate additions to testing solutions.

Chloride and sulphate content as mass % of solution and as molar content of the compounds						
In CH and PS solutions						
Cl-, M **(NaCl, wt.%)**	0.85 (5.03)	1.69 (10.08)	2.54 (15.13)	3.38 (20.12)	4.23 (25.11)	5.07 (30.19)
In PS+S Solution						
Cl-, M **(NaCl, wt.%)**	0.85 (5.03)	1.69 (10.08)	2.54 (15.13)	3.38 (20.12)	4.23 (25.11)	5.07 (30.19)
SO_4^{2-}, M **($CaSO_4.2H_2O$, wt.%)**	0.01 (1.73)	0.14 (2.42)	0.18 (3.28)	0.24 (4.36)	0.35 (6.34)	0.48 (9.01)

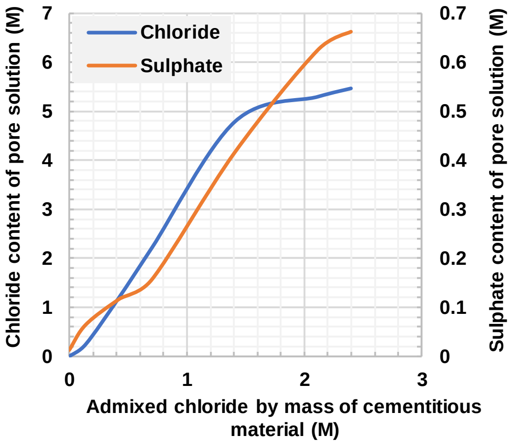

Figure 7-2. The chloride and sulphate contents of the pore solution expressed from 75% Portland cement/25% slag pastes, 0.4 w/cm ratio and the admixed sodium chlorides in the paste. The figure is adapted from [11].

The specimens were allowed to passivate in their respective testing solutions for two weeks before any chloride and sulphate was added and before any testing was carried out. After passivation, chlorides, and sulphates in the PS+S solution, were added as NaCl and $CaSO_4.2H_2O$ and the solutions were stirred between 5 - 15 minutes with a magnetic stirrer to completely dissolve the solutes. The corrosion potentials of the bars were monitored until they stabilized, indicating equilibrium had been reached (approximately 2 hours). An anodic potentiodynamic polarization test was performed on each bar in its respective solution with scan rates between 0.005 - 0.01 mV/s as suggested by [4] using the BioLogic potentiostat Model VSP. The slower scan rate was required in some cases, particularly the 2205 bars, to allow pitting to occur. Each bar in solution was scanned from its corrosion potential in the anodic direction to 0.5 V_{SCE} or to the current limit of 5 mA in cases where the bars showed some pitting corrosion. The values of the corrosion potential, $E_{CORR,}$ pitting potential, E_{PIT}, from each polarization curve were plotted against the chloride content of the solution.

7.4. Results

Figure 7-3 shows averages of three replicates of the corrosion potentials of each of the stainless steel grades during the two weeks in the PS solution without chlorides. The E_{CORR} values were relatively stable after 120 hours, indicating that the bars were in equilibrium with the testing solution before the addition of salts and application of potential scans. Bars in other solutions showed similar behavior to those in the PS solution presented in Figure 7-3.

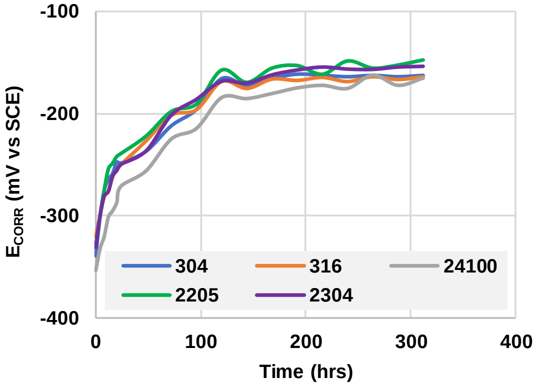

Figure 7-3. Average corrosion potentials of three replicate of bars in PS solution over the course of passivation.

Figure 7-4 shows the polarization curves obtained from five different stainless steel bars tested in the CH, PS and PS+S solutions with chlorides. A general observation from the curves obtained from bars tested in all types of solutions is the relatively constant corrosion potential (E_{CORR}) values with increasing chlorides, which is contrary to the decreasing (more negative) E_{CORR} observed by [137] on carbon steel rebar. Unlike carbon steel rebar, the mill scale on the stainless steel rebar and any underlying Cr-depleted layer had been removed and the bars were passivated during the pickling process. The relatively constant E_{CORR} values at each chloride level, following their equilibrium potential shown in Figure 7-3, suggests that the bars' film remained protective in the chloride-contaminated solution before anodic polarization. The adherent nature, stability and rapid repassivation of stainless steels' passive films in the presence of high chloride concentrations compared to the non-uniform and porous iron oxide mill scale found on carbon steel rebar has been reported by many [107], [140], [141], [145].

The polarization curves from bars tested in the PS and PS+S solutions are similar and typically showed lower passive current densities than those in the CH solution, which is consistent with past findings [13], [186].

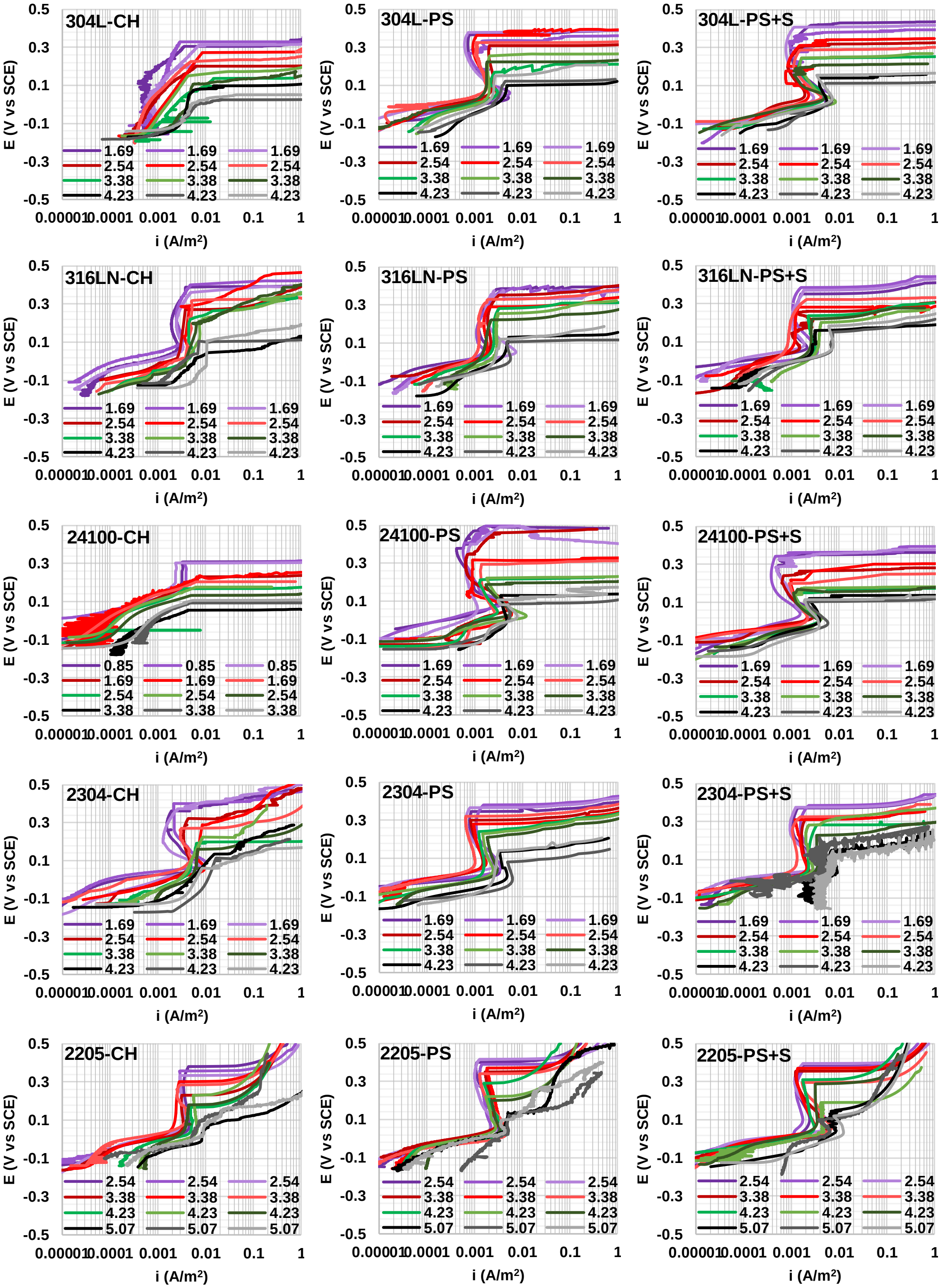

Figure 7-4. Polarization curves of 304L, 316LN, 24100, 2304 and 2205 specimens in CH, PS and PS+S solutions with 0.85 - 5.07 M Cl- exhibiting pitting corrosion.

Figure 7-5 shows some examples of the different stainless steel grades that showed pitting corrosion. None of the bars displayed general corrosion as was previously observed in carbon steel [137]. As illustrated in in Figure 7-6, none of the bars exhibited crevice corrosion under the lacquer.

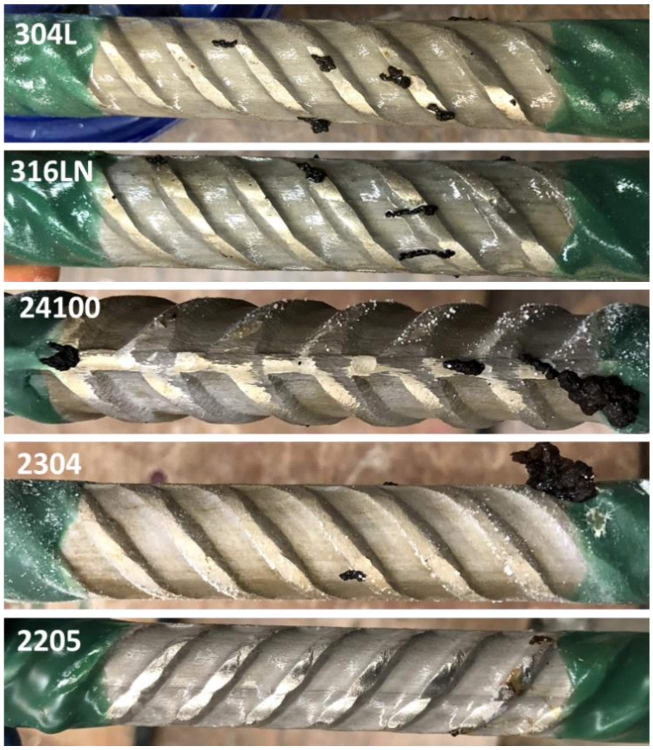

Figure 7-5. Examples of tested 304L, 316LN, 24100, 2304 and 2205 bars showing signs of pitting corrosions. It should be noted that the left side of the figure is the top of the bar placed in solution and so crevice corrosion was not observed on the 24100 and 2304 because their corrosion products flowed downward.

Figure 7-6. The 24100 rebar shown in Figure 7-5 with the area underneath the lacquer exposed to show the absence of crevice corrosion.

Each potential versus chloride plot shown in Figure 7-7 summarises the passivity and pitting corrosion behavior obtained from the potentiodynamic polarization tests to allow prediction of the C_{CRIT} values of stainless steel rebar grades tested in the CH, PS and PS+S solutions. In each plot, the trendlines for both corrosion potentials (E_{CORR}) and pitting potentials (E_{PIT}) are extrapolated to their intersection point and then traced down to the chloride axis. The resulting value, chloride threshold value, C_{CRIT}, represents the chloride amount at which corrosion is initiated on the bars without the application of an external stimulus. A general observation in Figure 7-7 is that the C_{CRIT} values of each rebar grade follows PS+S > PS > CH.

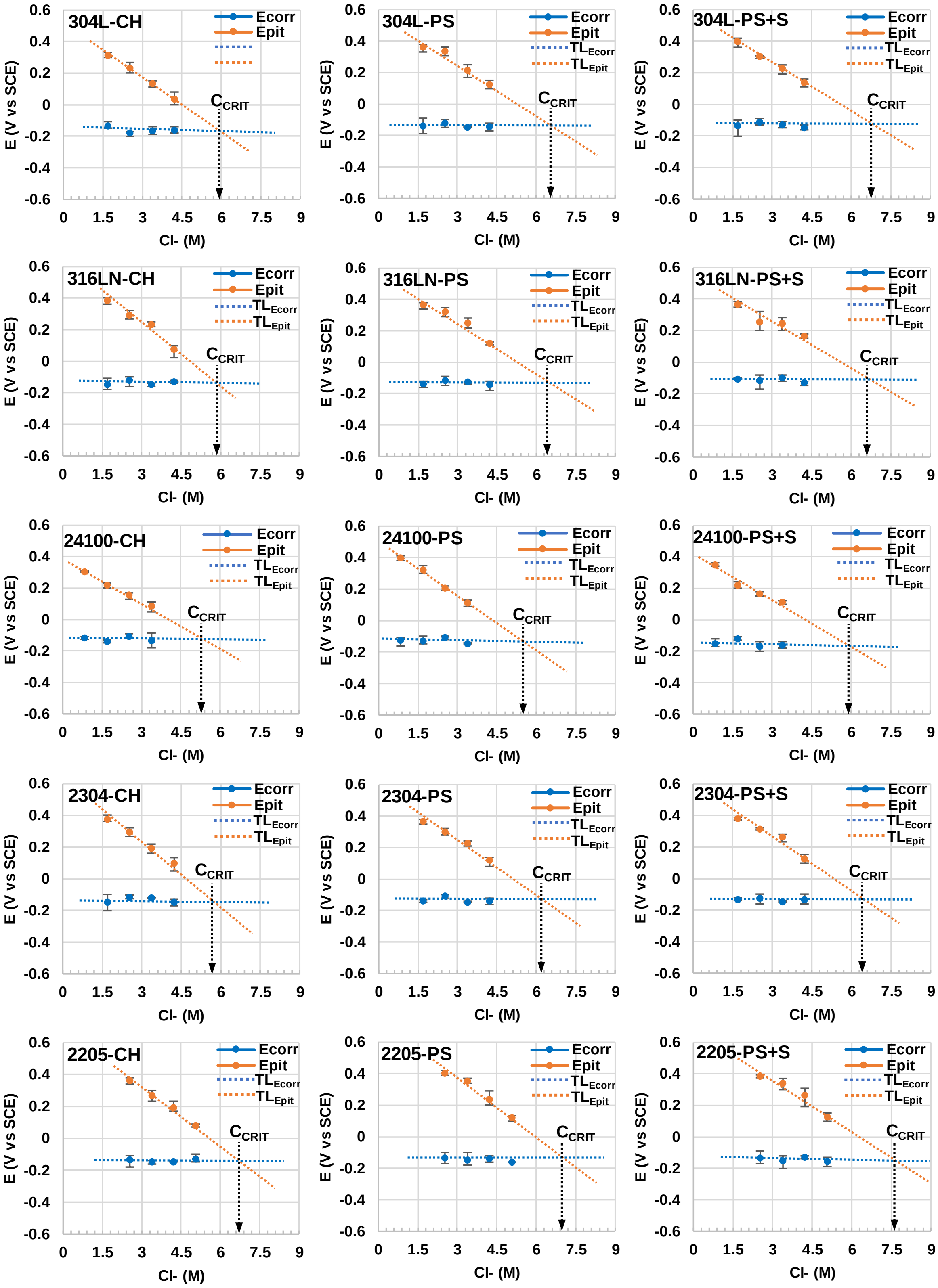

Figure 7-7. E_{CORR}, E_{PIT} and their trendlines (TL) versus chlorides extrapolated to predict the chloride threshold of 304L, 316LN, 24100, 2304 and 2205 stainless steel bars tested in CH, PS and PS+S solutions.

7.5. Discussions

An interesting observation in Figure 7-4 is the large amount of chloride employed before pitting corrosion was observed in the different rebar grades. Pitting was initiated in the austenitic 24100 bars in solution with 0.85 M Cl^-, whereas the 2205 did not begin to corrode until a chloride concentration of 2.54 M. The 304L, 316LN and 2304 grades all showed signs of active corrosion in all three testing solutions with 1.69 M Cl-. These values are similar to those obtained by Bertolini and Gastaldi for both 304L and 2304 grades with 5% (1.41 M) Cl- in saturated $Ca(OH)_2$ solution. However, these authors did not observe pitting in 316LN in solution with up to 8% (2.25 M) Cl- in this solution [117]. The pitting potentials from their work were also slightly higher than those observed in the present work, which may be due to their faster scan rate, 0.3 mV/s.

The C_{CRIT} value of the low-Ni/high-Mn austenitic grade, 24100, ranked the lowest. Although the influence of Mn on pitting resistance in acidic environments has been previously reported to be either positive [223], [224] or negative [225], it did not show any positive influence in the present work carried out in the high alkaline environment of concrete. In reference [145], Mn was found to reduce the defect density of inner layer of passive film formed on 24100 grade, while Ni was found to reduce the defect density of the outer layer of passive film formed on 304L grade. The significantly higher C_{CRIT} values of the Ni-containing 304L bars obtained in the present work suggest better overall pitting resistance of this grade than the Mn-containing 24100 rebar grade, justifying the preference for the Ni-containing alloys. The slightly higher C_{CRIT} value of the 304L grade than that of the 316LN supports recent observation of Mesquita et al. [203], [204] that the previously reported beneficial effect of Mo in austenitic stainless steels decreases with increasing pH of the environment and is negligible at the pH levels employed here. In contrast, Mo showed a positive influence in the duplex alloy with 2205 bars having a higher C_{CRIT} value than 2304 bars. Similar beneficial effect of Mo in duplex stainless steel grades has been reported for specimens tested in increasing pH up to pH 10 [203], [204] and at pH greater than 13 [226]. These observations suggest that Mo-free 304L grade can be used in place of Mo-containing 316LN grade to save cost.

Other than the methods of testing discussed earlier, another reason for the variations in relative corrosion resistance of different rebar grades reported in the literature [13], [19], [61], [62], [64], [117], [161] is the surface finish of the tested bars. The authors of the present work have observed a dark line parallel to the longitudinal rib of bars of different grades from different manufacturers and varying degrees of surface roughness, both of which influence their corrosion behavior [185], [226]. Consequently, the chloride threshold values of a 2304 bar, with compositions in Table 4, exhibiting such dark line shown in Figure 7-8 was determined and compared with the 2304 bar shown earlier in Figure 7-5. From Figure 7-8, it is evident that these sites were preferentially corroded compared to the random corroded areas shown in Figure 7-5. The potential values of the former are plotted in Figure 7-9 and show an estimated threshold value of 5.63M compared with 6.48M for the bars without the dark line. The 2304 grade shown in Figure 7-5 possessed C_{CRIT} values only slightly lower than those of the austenitic grades, making it a strong lower cost candidate for reinforcement in aggressive environment. The 13% lower C_{CRIT} value shown for 2304 bars with processing artefacts in Figure 7-8, indicate that the threshold limit of this grade can be even lower than that obtained for 24100 grade, which ranked the lowest, in PS+S solution. Similar observation was found in [226] where some 2304 bars without initial micropits present in the as-received conditions, developed during pickling of the bars in acid, performed better than 2205 bars with severe micropits. This does not only emphasize the detrimental effect of processing flaws on rebar, which has been discussed in details in [226], but also shows that this method of obtaining the critical chloride threshold can differentiate the pitting resistance of bars with different surface roughness. This technique also allows comparison of pitting resistance of several rebar grades and their C_{CRIT} values to be determined from a single test in a shorter period than current ASTM A955 or ASTM G109 standards which takes ~96 weeks, reducing the variation that comes from comparing rebar from different tests.

Table 7-4. The mill certificate composition of 2304 stainless steel bars with processing artefacts.

Class	Rebar grade (ASTM)	Denoted in text as	Composition (wt.%)							
			Cr	Ni	Mo	Mn	Si	Cu	C	N
Duplex	UNS S32304	2304	22.45	4.05	0.21	1.65	0.43	0.31	0.02	0.14

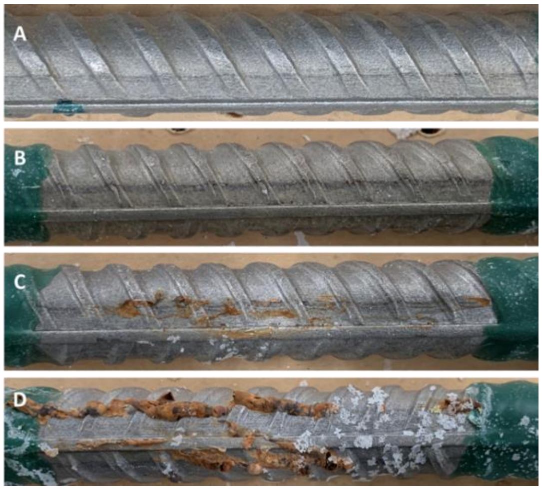

Figure 7-8. Example of 2304 bars with preferential corrosion along the processing artefact parallel to the longitudinal rib. Untested bar (A) and bars tested in PS+S solution with 1.69 M Cl- (B), 3.38 M Cl- (C) and 4.23 M Cl- (D).

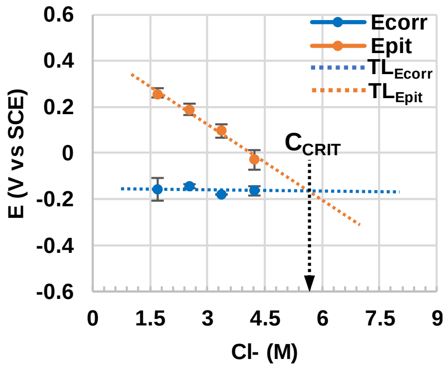

Figure 7-9. Plot of E_{CORR}, E_{PIT} and their trendlines (TL) versus chlorides extrapolated to predict the chloride threshold of 2304 bars with surface artefact tested in the PS+S solution.

Figure 10 summarizes C_{CRIT} values obtained for all the alloys (excluding those with the surface artefact) in all three testing solutions. After varying the trendlines extrapolated to predict the C_{CRIT} values, a minimum and maximum value was obtained and added to Figure 7-10. This figure shows the C_{CRIT} of all bars increased with pH from CH to PS solution and with sulphate from PS to PS+S solution. A similar trend was observed for carbon steel [137]. The beneficial effect of sulphate increments in testing solutions, which was not incorporated in many testing solutions until recently [137], [227], is apparent in this figure. Sulphates increased C_{CRIT} values of all grades by 4 – 8%, which is in similar range of increase observed when pH was increased from 12.6 to 13.6 (i.e. between CH and PS solution). It was recently reported that testing carbon and 2304 stainless steels in sulphate-containing solutions results in the formation of Fe and Ni sulphides in their passive films, offering additional protection against corrosion [227]. These data show that assessment in lower pH and sulphate-free solutions underestimates the pitting corrosion resistance and threshold values of reinforcing bars. However, it should be noted that the C_{CRIT} values obtained in the present work are only representative of values in a sound, non-cracked concrete for which the pH and ionic concentrations around the reinforced bars is similar to those in this work. Unfortunately, most field concretes contain structural or shrinkage cracks and studies [185], [228] have shown that even stainless steel rebar can corrode locally at the intersection of structural cracks when the concrete is exposed to the highly concentrated brines currently used as anti-icing agents in Ontario. In other words, the lower pH at concrete crack intersections decreases C_{CRIT} values of embedded rebar from PS+S to CH or even lower.

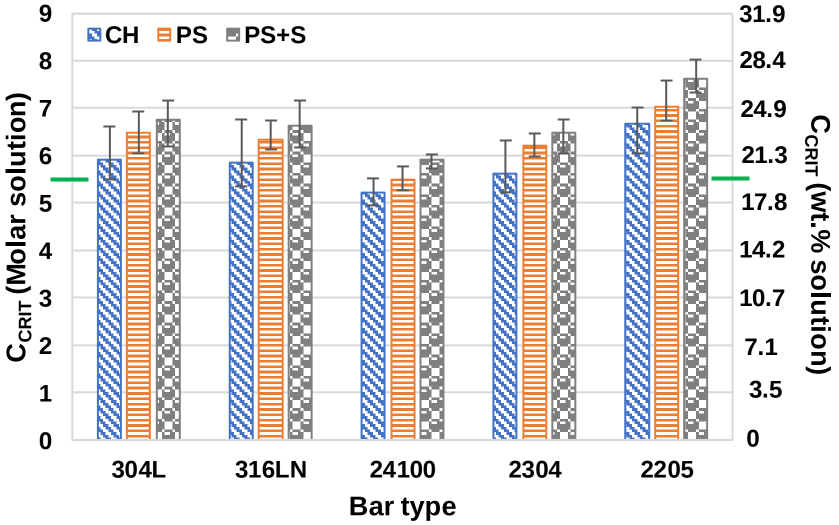

Figure 7-10. Summary of average C_{CRIT} values and variations observed for each rebar grade tested in solution. The green line shows maximum chloride in pore solution found in Figure 7-2.

Using Figure 7-2 to convert the C_{CRIT} values presented in Figure 7-10 to their equivalent concentrations by mass of cementitious materials shows that it was only possible for 24100 bars tested in CH and PS solutions. Conversion of higher C_{CRIT} values obtained in solution to obtain equivalent chloride by mass of cementitious materials was not possible because the saturation limit of chlorides and sulphates in the cement pore solution, shown by the almost constant peak of the curve, was reached in Figure 7-2. This saturation limit, obtained from OPC+25%GGBFS cement pastes with admixed NaCl, is approximately 5.49 M Cl- (equivalent to 2.35 M Cl- by mass of cementitious materials) as shown by the green line in the vertical axis of Figure 7-10. The implication of this saturation limit is that chloride threshold of these grades of austenitic and duplex stainless steel rebar in concrete cannot be reached without decrease in surrounding pH, typically through carbonation of the concrete.

Table 7-5. Comparison of average, minimum and maximum chloride threshold values by mass of solution from the present work with values reported in literature for similar pH solution.

Testing solution	**C_{CRIT}, (M) solution**				
	304L	**316LN**	**24100**	**2304**	**2205**
CH	5.92	5.85	5.21	5.63	6.67
(Max)	(6.61)	(6.76)	(5.52)	(6.32)	(7.02)
(Min)	(5.49)	(5.35)	(4.95)	(5.22)	(6.04)
PS	6.48	6.34	5.49	6.20	7.04
(Max)	(6.92)	(6.73)	(5.77)	(6.46)	(7.59)
(Min)	(6.04)	(6.12)	(5.27)	(5.99)	(6.74)
PS+S	6.76	6.62	5.92	6.48	7.61
(Max)	(7.17)	(7.15)	(6.03)	(6.76)	(8.01)
(Min)	(6.20)	(6.17)	(5.73)	(6.04)	(7.32)
(Max)	(4.23)	(4.23)	-	(> 2.82)	(> 4.23)
(Min)	(0.8)	(0.8)		(1.3)	-
REFERENCE	[19], [59], [62], [117], [119], [229], [230], [231]	[19], [59], [62], [64], [117], [229], [230], [231]		[62], [117], [232]	[59]

Table 7-5 compares the C_{CRIT} values obtained in this work with the minimum and maximum values found in literature obtained using other testing methodology. No data was found reporting the threshold values for 24100 stainless steel rebar grade, indicating the importance of this work. Data from available literature shows that the maximum chloride content at the rebar level in a concrete highway structure is 0.22% Cl^- (0.06 M Cl-) by mass of concrete, or approximately 1.0% Cl- (0.28 M Cl-) by mass of cementitious material [233]. From Figure 7-2, this would result in a pore solution chloride concentration of approximately 0.4 M. The C_{CRIT} values of all rebar grades exceed this by more than an order of magnitude, indicating that the cheaper austenitic 24100 and duplex 2304 grades of stainless steel will excel in many aggressive conditions.

7.6. Summary and conclusions

- The potentiodynamic polarization scan method of determining chloride threshold level was successful in determining the influence of alloying elements on C_{CRIT} values of five different stainless steel rebar grades tested in three different synthetic pore solutions. This method was also appropriate to differentiate bars with different surface conditions.
- The critical chloride threshold values obtained by this method for all grades of stainless steel bars increased with increase in pH in testing solution and, with addition of sulphate at levels corresponding to those measured from the expressed pore solution of OPC+25%GGBFS cement paste

at 28 days. These results showed that testing rebar in lower pH and sulphate-free solutions greatly underestimates their pitting resistance and chloride threshold value.

- The C_{CRIT} ranking of the tested bars in all types of solution was in the order of 2205 > 304L > 316LN > 2304 > 24100 > 2304 (with processing artefacts). It is clear that the poor surface control can significantly reduce the corrosion. The Ni-containing stainless steel grades showed higher C_{CRIT} values than the low-Ni/high-Mn. The observed pitting behavior and C_{CRIT} values confirm previous findings that molybdenum does not have any beneficial effect on the corrosion resistance of austenitic stainless steels rebar in highly alkaline concrete environment but does provide increased resistance in the duplex alloys. Nevertheless, the cheaper Mo-free duplex 2304 grade showed similar values to the traditional austenitic grades, which makes it a strong candidate for reinforcement.
- The significantly higher C_{CRIT} values of all rebar grades than the observed saturation limit of dissolved chlorides in cement pore solution and chloride contents currently reported in the field suggest that the least costly stainless steel grade tested in this work, 24100, can withstand most aggressive conditions found in the field.

8. Reproducibility of the corrosion resistance of UNS S32205* and UNS S32304+ stainless steel reinforcing bars[6]

8.1. Overview

One strategy to address the 75-year service life requirement of a number of highway bridge design codes is the use of more corrosion-resistant reinforcement. Over the last few decades, many stainless steel grades have become available for reinforcing concrete. Of these, two duplex alloys, UNS S32205 and UNS S32304, have become the preferred choices for major highway structures in North America. The purpose of the present study was to investigate the consistency, or variability, of the corrosion performance of bars of these grades from different steel manufacturers. Metallography, chemical analysis, corrosion resistance and corrosion product evaluation were used to evaluate the bars. It was found that micropits exist to varying degree in the as-received conditions of these bars and that was the most dominant factor in determining the corrosion performance of the bars.

8.2. Background

Unlike carbon steel (black steel) reinforcing bars, the mill scale on stainless steel alloys formed during hot rolling and annealing is first removed through abrasive blasting and then pickling in a mixture of nitric and hydrofluoric acid [234]–[236]. These procedures can result in some defects on the bars, such as the dark line shown parallel to the longitudinal rib in Figure 8-1A which was observed to play an important role in corrosion initiation [185]. This dark line contains several micropits, as evident in the micrograph shown in Figure 8-1B, which aided corrosion initiation. Bertolini and Gastaldi [117] found similar defects and re-pickled the bars in the laboratory to remove them before electrochemical testing. While this extra pickling process may be appropriate for testing the bars in the laboratory, it is unrealistic as it will not be applied in the field. It is clear that these defective regions can be sites for preferential corrosion and, the variation in surface conditions can affect chloride threshold values or corrosion performances in general [13], [19], [61], [62], [64], [117], [161].

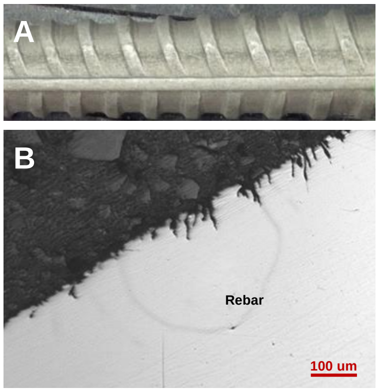

Figure 8-1. A - As-received pickled sample of UNS S30453 showing a processing feature typical of bars from one supplier, B - Cross-section of the rebar showing pits in the dark line.

---

[6] The contents of this chapter have been adapted with permission from NACE: I.G. Ogunsanya, C.M. Hansson. "Reproducibility of the corrosion resistance of UNS S32205 and UNS S32304 stainless steel reinforcing bars" *Corrosion*, 6 (2019) 100-321.
DOI: https://doi.org/10.5006/3360 (* UNS S32205 = 2205, + UNS S32304 = 2304)

The limiting factor for most recommended tests for evaluating the corrosion behaviour of steel in concrete is the time necessary to obtain the results. Stainless steel rebar is expected to provide service life between 75 – 100 years [237] and some grades have a good track record of service; an example is the Progresso Bridge in Mexico reinforced with UNS S30403 in 1941. In order to satisfy the authorities' wish to use less costly grades, accelerated tests are typically used to rank these grades in comparison with the traditional ones of UNS S30453 and UNS S31653. Some of these tests have been performed in concrete; (i) with cast-in chloride [117], [238]; (ii) ponded with chloride solution [117], [185], [228]; (iii) with induced artificial crack and submerged in chloride-filled tubs [118], [185], [228] to replicate field conditions and shorten time to obtain results. The current standard method of assessing the corrosion behaviour of newer grades of rebar is the ASTM A955 which takes between 4 – 22 months of testing and does not allow for testing large numbers of specimens in different conditions. To allow more rapid testing and monitoring the behaviour of the steel during the test, other researchers have performed tests in simulated concrete pore solution [13], [19], [62], [64], [117], [137], [138], [145], [161], [227]. However, some drawbacks associated with pore solution testing include, but are not limited to [239]: (i) the difficulty in translation of chloride content of the solution to the equivalent mass of cement or concrete; (ii) absence of the steel/concrete interface effects where porosity and change in pH due to hydration or carbonation occur over time [126], [240] and (iii) the uniform chloride concentrations existing over the whole bar surface in solution, unlike the highly inhomogeneous concentrations existing in concrete structures.

Previous work has shown that duplex stainless steel rebar grades have similar or superior corrosion resistance to traditional austenitic rebar grades [117], [138], [220]–[222]. Therefore, duplex UNS S32205 and UNS S32304 grades have been selected in this work. The variability of composition, microstructure and surface condition of both rebar grades received from the three different suppliers at three 6-month intervals were investigated to determine the effects of these factors on corrosion behaviour. The electrochemical method of screening the stainless steel bars in this work is based on modifications by [112], [113] to a proposed European test, EN-480-14:2006, by Schonning and Randstrom [241]. This test is now included in the British Standard BS 6744-16. This test gives comparative corrosion resistance only and does not provide any information on corrosion rates expected in service.

8.3. Materials and methods

Evaluation procedure

Three batches (Batch 1, 2 and 3) of UNS S32205 and UNS S32304 stainless steel samples produced at different time intervals by different manufacturers (A, B, C) were obtained from three rebar distributers. The mill certificate compositions provided by these producers are shown in Table 8-1. The evaluation procedure between batches and between all three manufacturers is as follows:

(i) The bars were evaluated visually, photographed and 3D scanned using Keyence VR-5000 wide-area system to identify any observable processing artifacts. The 3D scanning equipment projects white LED beams on the sample at a known angle and uses the horizontal displacement of the light pattern to triangulate differences in surface height;

(ii) It is suspected that some regions on the bars may be unintentionally quenched more slowly than others due to the processing methods employed. Consequently, hardness and microhardness values were obtained on the longitudinal and side ribs, the areas between two side ribs, areas of any observable flaws or discoloration, such as that in Figure 8-1A, and polished cross-sections of the bars using Rockwell and Vickers hardness tester;

(iii) Compositions of the bars were determined by x-ray fluorescence (XRF) and optical emission spectroscopy (OES) analysis on different parts of the rebar from each supplier. This is important because a high carbon content, although within specification, coupled with inadequate quenching from the annealing temperature, can lead to sensitization of steel;

(iv) Metallography of the cross-section and longitudinal section of the bars was conducted using both optical microscopy (OM) and scanning electron microscope (SEM), to observe any pitting due to the pickling process, such as that illustrated in Figure 8-1B, and any variations in microstructure due to differences in hot rolling and/or annealing processes between the manufacturers;

(v) A potentiostatic rapid screening test, recently included in the British Standard BS 6744-16 and, more recently, modified by [113] to fit the Canadian climate, was used to rank the corrosion resistance of the bars;

(vi) After electrochemical assessment, the specimens were autopsied and the extent/character of any corrosion were analyzed and documented using procedure (i) above. Any differences in corrosion behaviour were analyzed in light of the any difference in composition, microstructure or surface roughness and/or flaw.

Table 8-1. Chemical composition of both UNS S32205 and UNS S32304 bars from mill certificates.

Bar / Producer / Batch			**Alloying elements wt.% (ASTM A276 specification** [242]**)**							
			Cr (22 - 23)	**Ni (4.5 - 6.5)**	**Mo (3 - 3.5)**	**Mn (< 2)**	**Si (< 1)**	**Cu (NR)**	**C (< 0.03)**	**N (0.14 - 0.2)**
UNS S32205	A	1	21.40	4.70	2.60	1.70	0.40	0.20	0.02	0.19
		2	21.40	4.70	2.60	1.70	0.40	0.20	0.02	0.18
		3	21.32	4.64	2.57	1.80	0.42	0.27	0.02	0.17
	B	1	22.17	4.62	3.21	1.58	0.28	NR	0.02	0.17
		2	22.12	4.70	3.20	1.61	0.30	NR	0.02	0.16
		3	22.17	4.62	3.21	1.58	0.42	NR	0.02	0.19
	C	1	22.85	5.18	3.23	1.49	0.47	NR	0.03	0.16
		2	22.76	5.01	3.17	1.42	0.49	NR	0.02	0.20
		3	22.82	5.13	3.22	1.46	0.48	NR	0.02	0.17
			22 - 24	**3.5 - 5.5**	**0.1 - 0.6**	**< 2**	**< 1**	**0.05 - 0.6**	**< 0.03**	**0.05 - 0.2**
UNS S32304	A	1	22.70	3.60	0.30	1.70	0.40	0.27	0.02	0.16
		2	22.70	3.60	0.30	1.70	0.44	0.26	0.02	0.16
		3	22.91	3.62	0.28	1.71	0.40	0.34	0.02	0.17
	B	1	22.59	4.01	0.20	1.64	0.40	0.27	0.02	0.20
		2	22.51	3.98	0.19	1.67	0.44	0.26	0.02	0.20
		3	22.72	4.15	0.23	1.62	0.29	0.28	0.02	0.16
	C	1	23.50	4.28	0.34	1.35	0.53	NR	0.02	0.10
		2	23.46	4.35	0.37	1.26	0.63	NR	0.02	0.10
		3	23.61	4.31	0.36	1.32	0.55	NR	0.02	0.10

Rapid screening test

1. *Specimen preparation*

All bars were ribbed with nominal diameter of 16 mm (US #5; Canadian 15M). The bars were cut to 126 mm lengths, drilled in one end and soldered with a solid copper wire to create an electrical connection. Double coats of electroplating stop-off lacquer were then applied on both ends of each bar and finally sealed with plastic shrink-fit tubing, leaving an exposed length of 76 mm. The specimens were cast in concrete with mixture design shown in Table 8-2 for a general use (GU) Portland cement with 25% ground granulated blast furnace slag (GGBFS) replacement (compositions shown in Table 8-3) and 0.4 water-to-cementitious (w/cm) ratio. 7.5% chloride, as NaCl, by mass of cementitious materials was dissolved in the mixing water of the concrete. The average compressive strength at 28 days of all concrete cast was in the range between 37 - 40 MPa.

Table 8-2. Concrete Mixture Design

Constituent	**Cast mixture design**
	Amount (m^3)
Gravel (14mm)	1045 kg
Sand	705 kg
GU Cement	297 kg
Slag	98 kg
Air Extrainer	237 mL
Superplasticizer	900 mL
Water	158 L
w/c	0.40

Table 8-3. Cement and supplementary cementitious materials composition as provided by the supplier.

Composition	**Cementitious materials (wt.%)**	
	Portland Cement (GU)	**Ground Granulated Blast Furnace Slag (GGBFS)**
LOI	2.04	1.60
SiO_2	18.94	38.66
Al_2O_3	5.16	8.9
Fe_2O_3	2.31	0.52
CaO	62.76	38.53
MgO	2.31	11.32
SO_3	4.03	2.75
Total Alkali	0.98	0.77

For consistency purpose, one bar of UNS S32304 and UNS S32205 grades from each manufacturer was cast in the same concrete batch and tested at one time. This step was then repeated until seven and nine replicates of each types of UNS S32304 and UNS S32205 grades, respectively, were cast. After casting, all concrete specimens were cured in their respective moulds and covered with plastic wrap for 24 hours.

2. Experimental setup

After curing, concrete specimens were demoulded, submerged in calcium hydroxide with a saturated calomel reference electrode (SCE) and a mixed metal oxide coated titanium mesh as counter electrode, as shown in Figure 8-2. The corrosion potentials (E_{CORR}) of the embedded bars were monitored for 24 hours. Afterwards, either +300 mV_{SCE} or +400 mV_{SCE} polarization potentials were applied to all specimens for another 96 hours. Six replicates of each of the UNS S32304 and UNS S32205 bars were first tested using +300 mV_{SCE} polarization potential. After most of the UNS S32205 bars exhibited resistance at this applied polarization, one additional UNS S32304 and three more replicates of the UNS S32205 were tested at +400 mV_{SCE}. The decision to employ 7.5% admixed Cl- by mass of cementitious materials and polarization potentials between +300 and +400 mV_{SCE} was based on the findings of Loudfoot [113] after modifications to the European test. According to the recommended pass/fail criterion, a bar has failed this test if the current density is > 25 x 10^{-3} A/m^2 for more than two hours.

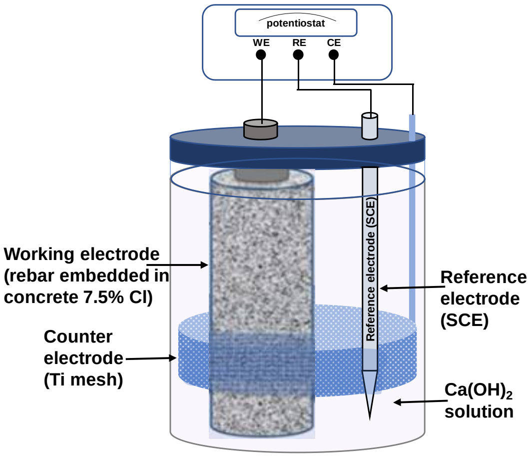

Figure 8-2. Steel reinforced concrete submerged in saturated $Ca(OH)_2$ along with titanium mesh counter electrode and saturated calomel reference electrode.

8.4. Results

Material properties

The surface condition of the bars was documented for any obvious defect or flaws as described above. An example of the scan of the first batch of the UNS S32205 and UNS S32304 grades prior to corrosion testing is shown in Figure 8-3. These images are representative of all batches of both stainless steel grades from each manufacturer. The A bars have varying bright and dark parts along their length and sometimes with dark lines near the longitudinal rib, similar to that shown in Figure 8-1. The B bars appeared the brightest and free of any obvious defects. Note that light reflections resulting from the scan are shown on the ribs of these bars and should not be mistaken for defects. The C bars generally appeared the most matt and free from any apparent defects, although there were few stains or discolouring on the UNS S32304 bars.

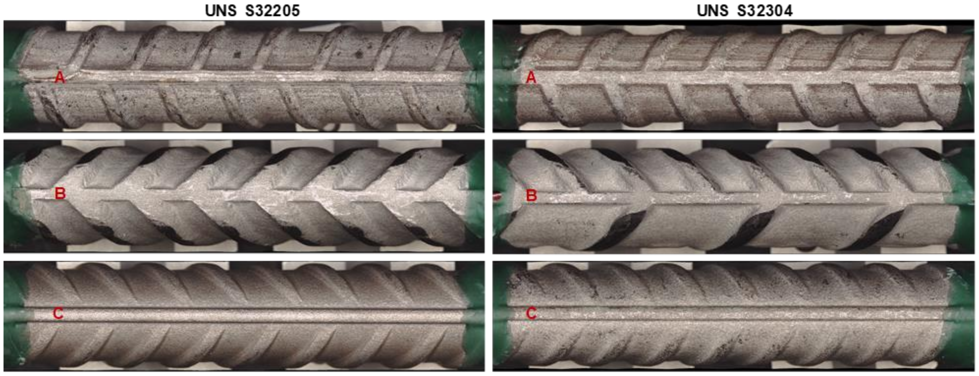

Figure 8-3. Bars from the first batch from Manufacturers A, B and C.

Table 8-4. Chemical composition of UNS S32205 and UNS S32304 bars from x-ray fluorescence (XRF) and optical emission spectroscopy (OES).

Bar / Producer / Batch			**Alloying elements wt.% (ASTM A276 specification** [242]**)**							
			Cr (22 - 23)	**Ni (4.5 - 6.5)**	**Mo (3 - 3.5)**	**Mn (< 2)**	**Si (< 1)**	**Cu (NR)**	**C (< 0.03)**	**N (0.14 - 0.2)**
UNS S32205	A	1	**21.00**	**4.34**	**2.50**	1.70	0.60	0.20	0.024	-
		2	**20.80**	**4.32**	**2.40**	1.80	0.70	0.20	0.025	-
		3	**20.90**	**4.20**	**2.50**	1.80	0.60	0.30	0.027	-
	B	1	**21.50**	**4.30**	3.05	1.60	0.50	0.30	0.018	-
		2	**21.40**	**4.32**	3.03	1.66	0.90	0.25	0.018	-
		3	**21.40**	**4.40**	3.10	1.60	0.80	0.30	0.019	-
	C	1	22.30	4.50	3.10	1.60	0.40	0.20	0.020	-
		2	22.10	4.51	3.00	1.70	0.90	0.20	0.016	-
		3	22.90	4.50	3.10	1.20	0.60	0.30	0.020	-
			22 - 24	**3.5 - 5.5**	**0.1 - 0.6**	**< 2**	**< 1**	**0.05 - 0.6**	**< 0.03**	**0.05 - 0.2**
UNS S32304	A	1	22.70	**3.20**	0.30	1.80	0.50	0.30	0.022	-
		2	22.60	**3.10**	0.30	1.80	0.50	0.27	0.022	-
		3	22.80	**3.20**	0.30	1.80	0.60	0.30	0.026	-
	B	1	**21.70**	3.72	0.20	1.70	0.60	0.30	0.018	-
		2	**21.77**	3.70	0.19	1.74	0.62	0.27	0.019	-
		3	22.10	3.90	0.20	1.70	0.60	0.30	0.025	-
	C	1	23.30	3.98	0.34	1.17	0.83	0.38	0.030	-
		2	22.80	3.70	0.20	1.70	0.60	0.30	0.023	-
		3	22.60	4.00	0.40	1.30	0.90	0.60	0.023	-

Compositions from XRF analysis of the as-received bars are shown in Table 8-4. These values are slightly lower than compositions from the mill certificate shown earlier in Table 8-1. The Cr, Ni and Mo compositions in all three batches of UNS S32205 C bars shown in Table 8-4 are below the ASTM A276, whereas the mill certificates indicated only Cr and Mo are below specification. The Cr and Ni content in all three batches of UNS S32205 B bars shown in Table 8-4 are below ASTM A276 specification, whereas the mill certificates indicated they met the specification. The mill compositions of both UNS S32304 A and B bars show they meet ASTM A276 specification, whereas their Ni and Cr, respectively, shown in

Table 8-4 are below specification. Only C bars are within specification in both Tables 8-1 and 8-4. The impact of the elements below ASTM A276 specification is expected to be seen on the bars' corrosion behaviour.

The hardness values of the longitudinal rib, side rib, areas between side ribs and apparent processing defects on all three batches of bars from all manufacturers were all between 21 – 33 HRC and, the microhardness values of bars' cross-sections were between 235 – 307 Vickers. The data range for each rebar, consisting of 20 data points obtained on each of the different regions on the bars, slightly overlap with no clear trend on the differences in regions on the same bars, between batches and between manufacturers.

Micrographs of the cross-sections of the bars at the edge of the longitudinal rib, side rib and areas between side ribs were taken for all the bars. However, only micrographs obtained from the longitudinal ribs are shown in Figures 8-4 and 8-5 for UNS S32205 and UNS S32304 grades, respectively, because they represent the worst cases of observed roughness. A general observation is the presence of micropits on some of these bars, which is consistent between batches of both grades from the same manufacturer and increased in severity as B > A > C. The C bars showed severe micropits that are consistent along the length of the longitudinal ribs of both grades, except the first batch of the UNS S32205 bars. The depth of the micropits on UNS S32205 bars (~ 90 µm) from this manufacturer are shallower than those on the UNS S32304 bars (~160 µm). The A bars also showed micropits which are consistent between batches of both grades, but at a significantly shallower depth (~20 µm) than those found on C bars. The B bars showed few broader "micropits" that are present on only a few bars. The influence of these micropits on the bars' corrosion behaviour is discussed below.

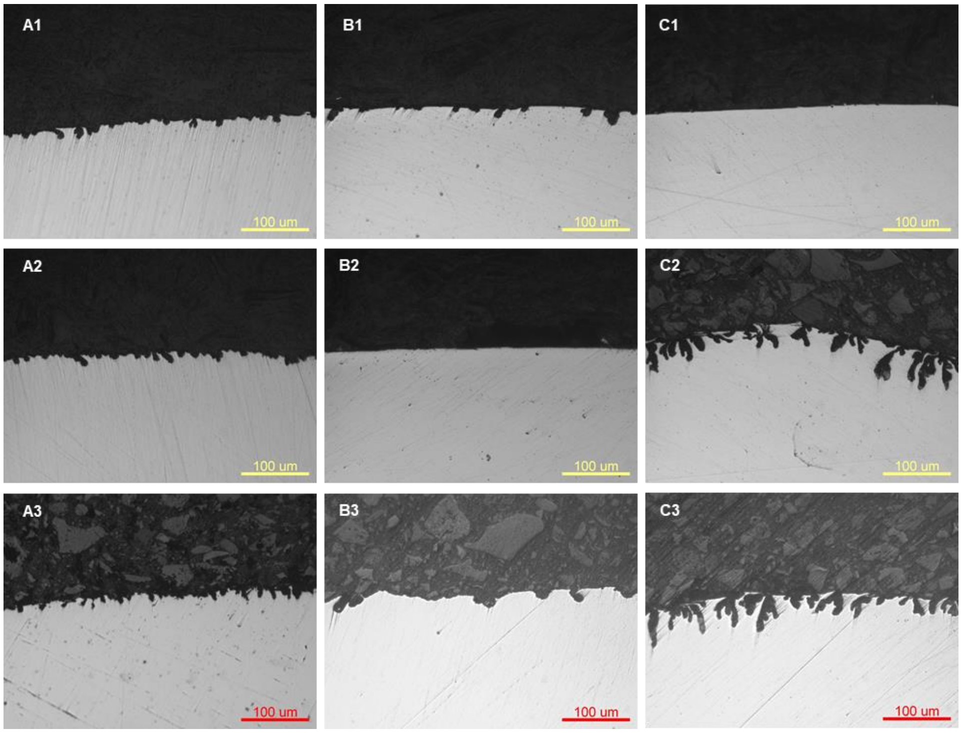

Figure 8-4. Micrograph of cross-sections of the UNS S32205 stainless steel bars showing micropits that may not easily be seen on the bar surface. The labels represent the manufacturers and the batch.

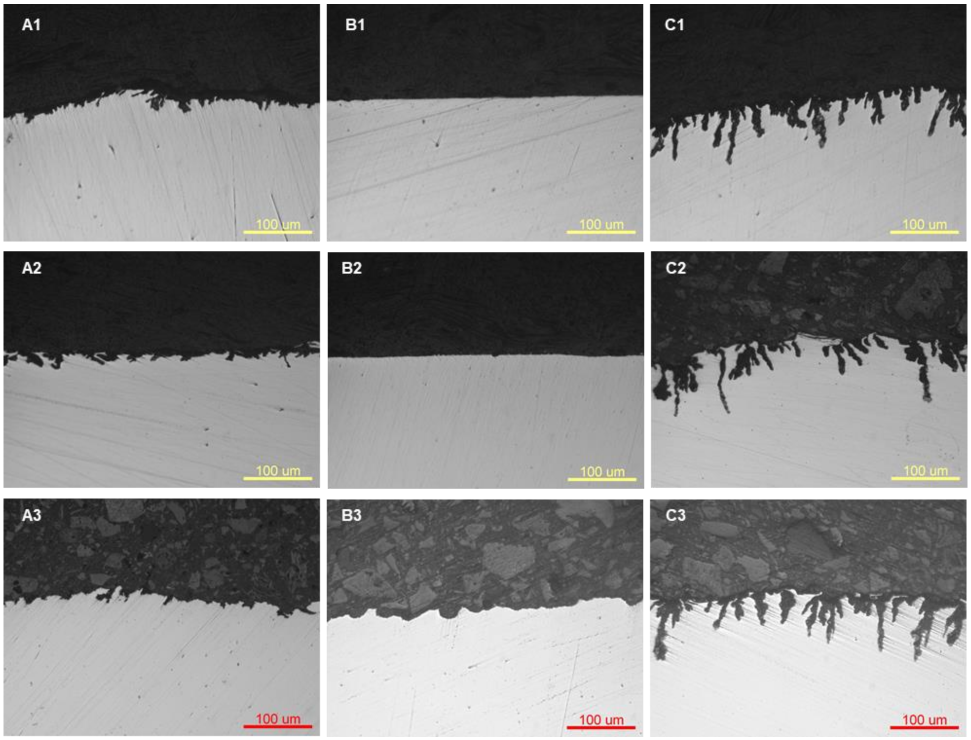

Figure 8-5. Micrograph of cross-sections of the UNSS32304 stainless steel bars showing micropits that may not easily be seen on the bar surface. The labels represent the manufacturers and the batches.

Figure 8-6 and 8-7 shows the microstructure of the longitudinal section of the three batches of UNS S32205 and UNS S32304 bars, respectively, from all manufacturers. These micrographs show similar elongated grains with rolling direction and a relatively homogeneous distribution of the austenite (light) and ferrite (dark) phases. Image analysis, using imageJ® software, was carried out to determine the phase percentage of austenite and ferrite phases on a minimum of 20 images each collected on the longitudinal and transverse cross-sections. The average austenite amount, shown in Figure 8-8, are mostly lower than 50% with few exceptions. The austenite phase is also generally higher in the UNS S32205 bars than the UNS S32304 bars. Since austenite is intrinsically more corrosion resistant than ferrite [204], the higher percentage of the austenite phase present in the UNS S32205 bars suggests superior corrosion resistance. This is supported by the preferential dissolution of the ferrite phase (dark phase) in the longitudinal rib of the untested UNS S32304 alloy found with micropits in Figures 8-4 and 8-5, as shown in Figure 8-9. The decreasing amount of austenite phase from batch 1 to 3 in the UNS S32304 A bars also suggests decreasing corrosion resistance.

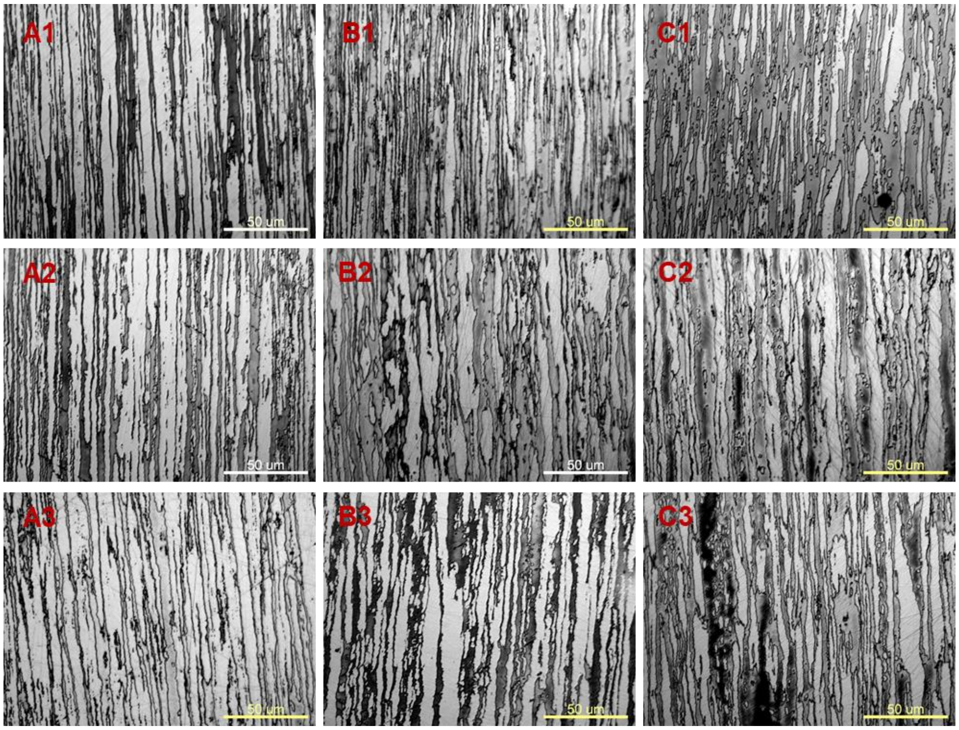

Figure 8-6. Micrograph of longitudinal sections of the UNS S32205 stainless steel bars showing austenite and ferrite phases. The alphabets (A, B, C) from left to right indicate the manufacturer, the numbers (1, 2, 3) from top to bottom indicate the batches.

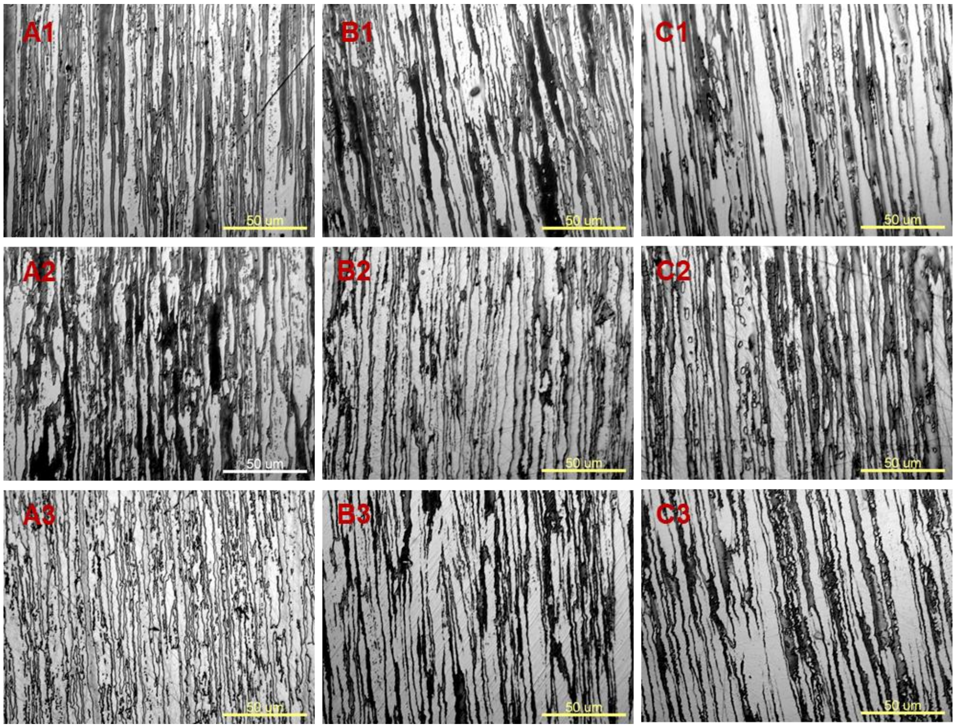

Figure 8-7. Micrograph of longitudinal sections of the UNS S32304 stainless steel bars showing austenite and ferrite phases. The alphabets (A, B, C) from left to right indicate the manufacturer, the numbers (1, 2, 3) from top to bottom indicate the batches.

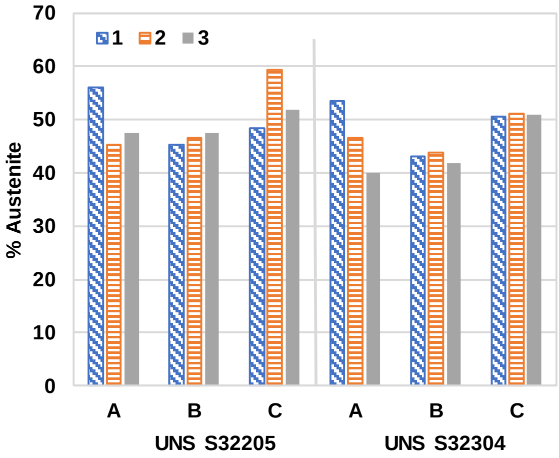

Figure 8-8. Average value, volume percent, of austenite phase present in the three batches of both UNS S32205 and UNS S32304 stainless steel grades.

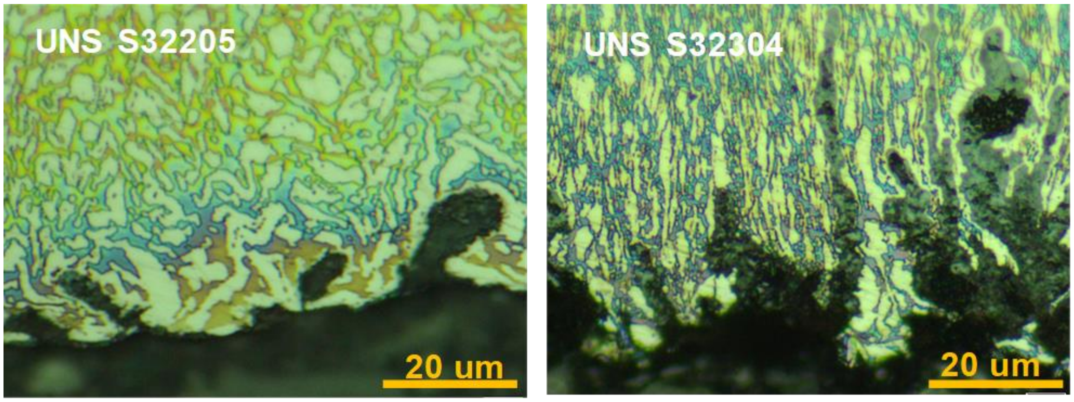

Figure 8-9. Micrograph of longitudinal rib of the third batch of as-received UNS S32205 and UNS S32304 C bars showing dissolved ferrite and/or austenite phases. Yellow and red arrows show islands of austenite (light phase) and regions of dissolved ferrite (dark phase) from acid pickling, respectively. Note that the cloudy dark green color where the red arrow point is polishing solution and not ferrite phase.

Table 8-5 shows the average values of alloying compositions obtained from x-ray energy dispersive spectroscopy (EDX) analysis of several regions of the austenite and ferrite phases in the UNS S32205 and UNS S32304 bars. It can be seen the Cr and Mo content in the ferritic phases are higher than in the austenite and are reported to be ferrite stabilizers [34], [35], while Ni and Mn content are higher in the austenitic phases as expected austenite stabilizers [34], [35]. Some authors [203]–[205], [158]–[160] also found preferential partitioning of Mo in the ferritic phase and showed it to improve pitting resistance of this phase in duplex stainless steel alloys tested in high pH. The higher Mo content in the UNS S32205 bars shown in Table 8-4 than the UNS S32304 bars and the non-preferential dissolution of the ferrite phase in the as-received UNS S32205 bars, as was found in the UNS S32304 bars, shown in Figure 8-9 suggests better pitting resistance of the former alloy. The Mo content is highest in both rebar grades from Manufacturer C, again, suggesting superior corrosion resistance.

Table 8-5. Average chemical composition from an EDX analysis of the austenite and ferrite phases in the first batch of both UNS S2205 and UNS S32304 bars.

Bar / Producer		**Phase**	**Alloying elements wt.% (ASTM A276 specification [242])**					
			Cr (22 - 23)	**Ni (4.5 - 6.5)**	**Mo (3 - 3.5)**	**Mn (< 2)**	**Si (< 1)**	**Cu (NR)**
UNS S32205	A	Austenite	20.83	5.48	2.75	2.15	0.45	1.01
		Ferrite	22.97	4.55	3.23	1.52	0.50	0.42
	B	Austenite	22.03	5.49	2.73	1.64	0.46	0.71
		Ferrite	23.35	4.14	3.55	1.77	0.50	0.42
	C	Austenite	21.83	5.53	2.79	1.80	0.26	0.70
		Ferrite	24.85	3.49	3.71	1.91	0.43	0.42
			22 - 24	**3.5 - 5.5**	**0.1 - 0.6**	**< 2**	**< 1**	**0.05 - 0.6**
UNS S32304	A	Austenite	22.51	4.32	0.42	1.77	0.47	0.57
		Ferrite	24.91	3.03	0.48	1.73	0.46	0.52
	B	Austenite	22.23	4.62	0.39	2.08	0.53	0.77
		Ferrite	24.95	3.57	0.67	1.66	0.68	0.54
	C	Austenite	21.75	5.20	0.43	1.56	0.50	0.85
		Ferrite	25.12	3.80	1.15	1.27	0.68	0.41

Corrosion behaviour

The corrosion potentials of all the reinforced concrete specimens 24 hours after casting (i.e. upon immersion in $Ca(OH)_2$) and 48 hours after casting (i.e. 24 hours after immersion in $Ca(OH)_2$) are shown in Figure 8-10 which presents only the first batch, other batches are presented in the Appendix C-1 – C-4.

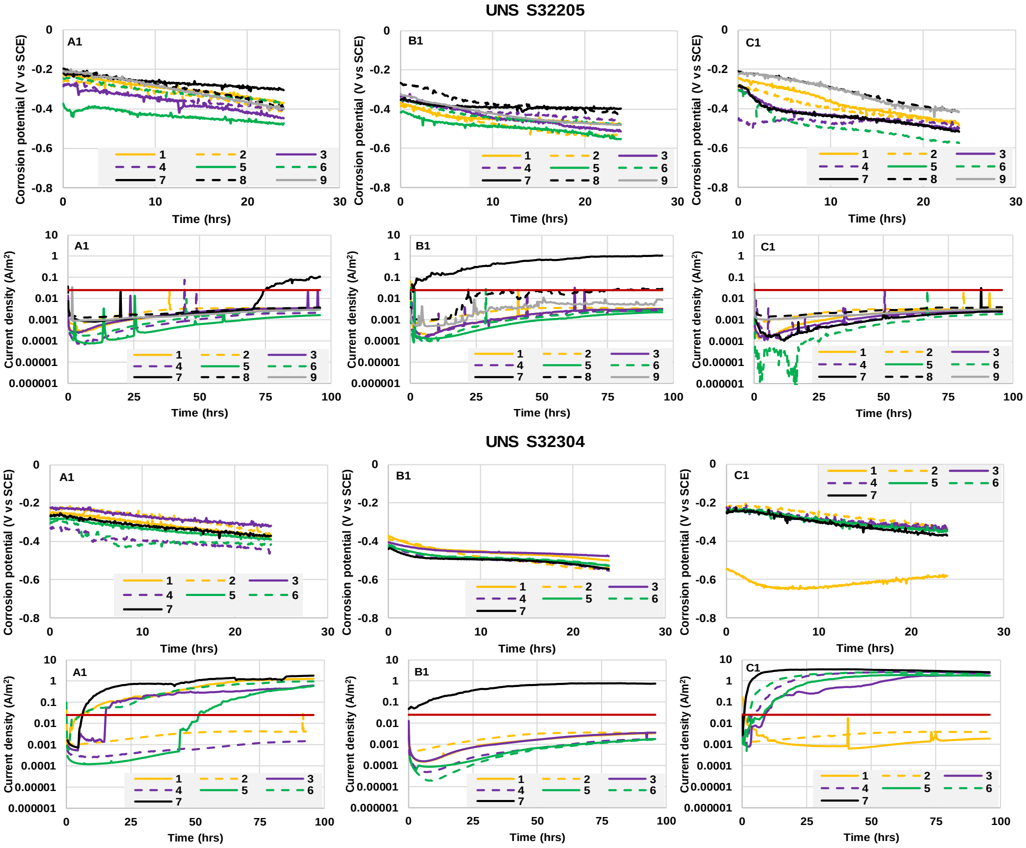

Figure 8-10. The corrosion potentials and current densities of the first of three batches of UNS S32205 and UNS S32304 bars from all manufacturers (A, B, C).

A general observation is the negative trend of potentials over the 24 hour period. The two rebar grades exhibited similar potential values on immersion, with the UNS S32304 grade showing slightly more positive average potential after 24 hrs. There is also consistency in the corrosion potentials between batches of the same rebar grade despite the significant differences in initial micropits. The B bars, with the least amount of micropits exhibited the most negative potentials, while C bars, with the most micropits, showed the most positive potentials.

Figure 8-10 shows the current response of the first batch (other batches are presented in the Appendix) of UNS S32205 bars to anodic potentiostatic polarization. A polarization potential of +300 mV_{SCE} was applied to Samples 1 – 6 and the additional specimens (Samples 7 - 9) were tested at a polarization potential of +400 mV_{SCE}. Of the nine replicates tested at +400 mV_{SCE} (Samples 7 - 9), failures included five A bars (one from the 1st and two each from second and third batches), three B bars (two from the first and one from the second batch) and four C bars (two each from the 2nd and 3rd batches). No sample from the first batch of the UNS S32205 C bars failed, which is consistent with the absence of micropits in the as-received conditions of these bars.

Figure 8-10 also shows the current response of the first batch (other batches are presented in the Appendix) of UNS S32304 bars to anodic potentiostatic polarization. The polarization potential of +300 mV_{SCE} was generally sufficient to rank the corrosion behaviour of these bars. Four or five of the six UNS S32304 A and C bars from each batch exceeded the pass/fail limit at the applied +300 mV_{SCE} potential, whereas only a single B bar (from Batch 2) failed the test. One additional bar from each batch was then tested at a potential of +400 mV_{SCE}. All three of the A and C bars and two of the B bars tested at +400 mV_{SCE} failed the test. Although the number of failed A and C bars are similar, the active current densities of the UNS S32304 C bars are slightly higher than the A bars, which is consistent with the extent of micropits found in their as-received bars.

Autopsy

The concrete cylinders were autopsied at the end of testing and all bars were examined for corrosion. The failed samples exhibited similar corrosion character but to varying extents corresponding with the amount and severity of micropits observed prior to testing. The bars with the least and most corroded area and corrosion product were B and C bars, respectively. Similarly, the most corroded area and greatest amount of corrosion product was found on the longitudinal ribs. Figures 8-11 and 8-12 are 3D scans of the whole and selected portion on the longitudinal rib of tested bars from Batch 1, respectively. These bars are the same as those shown in Figure 8-3 in their as-received conditions. It can be seen that the UNS S32304 C bars suffered severe pitting corrosion on the longitudinal- and side- ribs, which were regions with the most micropits. The UNS S32304 A bars showed lesser pit and/or pitted areas compared with Bar C, but similar to bars C corrosion pits, consistent with the tiny micropits found in the as-received bars. The UNS S32304 B bars mostly showed surface discoloring with absence of corrosion products. The corroded area, surface discoloring and roughness of the UNS S32205 bars were significantly lesser than the UNS S32304 grades, which is consistent with the extent of micropits and lower current densities shown earlier. The UNS S32205 A bars were the roughest after testing, while the B and C bars only showed discoloring. It should be reminded that this UNS S32205 C bar is from the first batch with no micropits as illustrated in Figure 8-3 and for which all the bars passed the corrosion test.

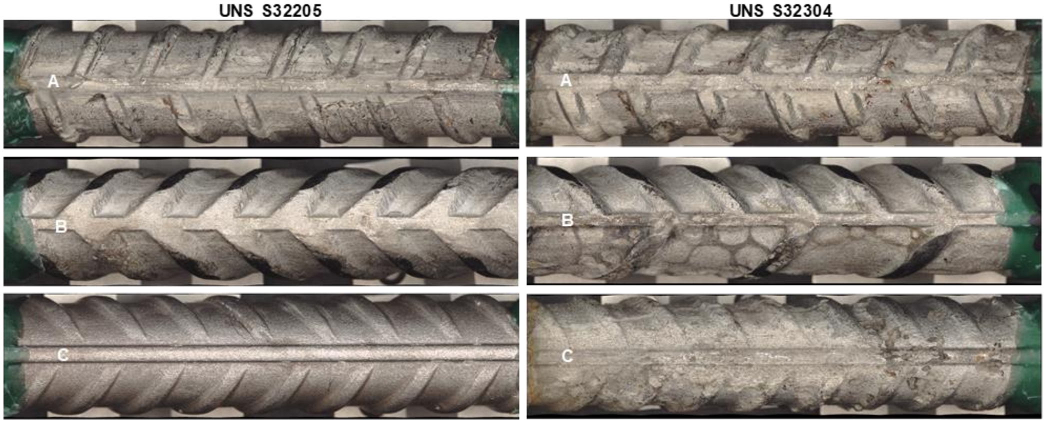

Figure 8-11. Corroded UNS S32205 and UNS S32304 bars after pickling the samples to remove corrosion products. These bars are the same as those shown in Figure 8-3.

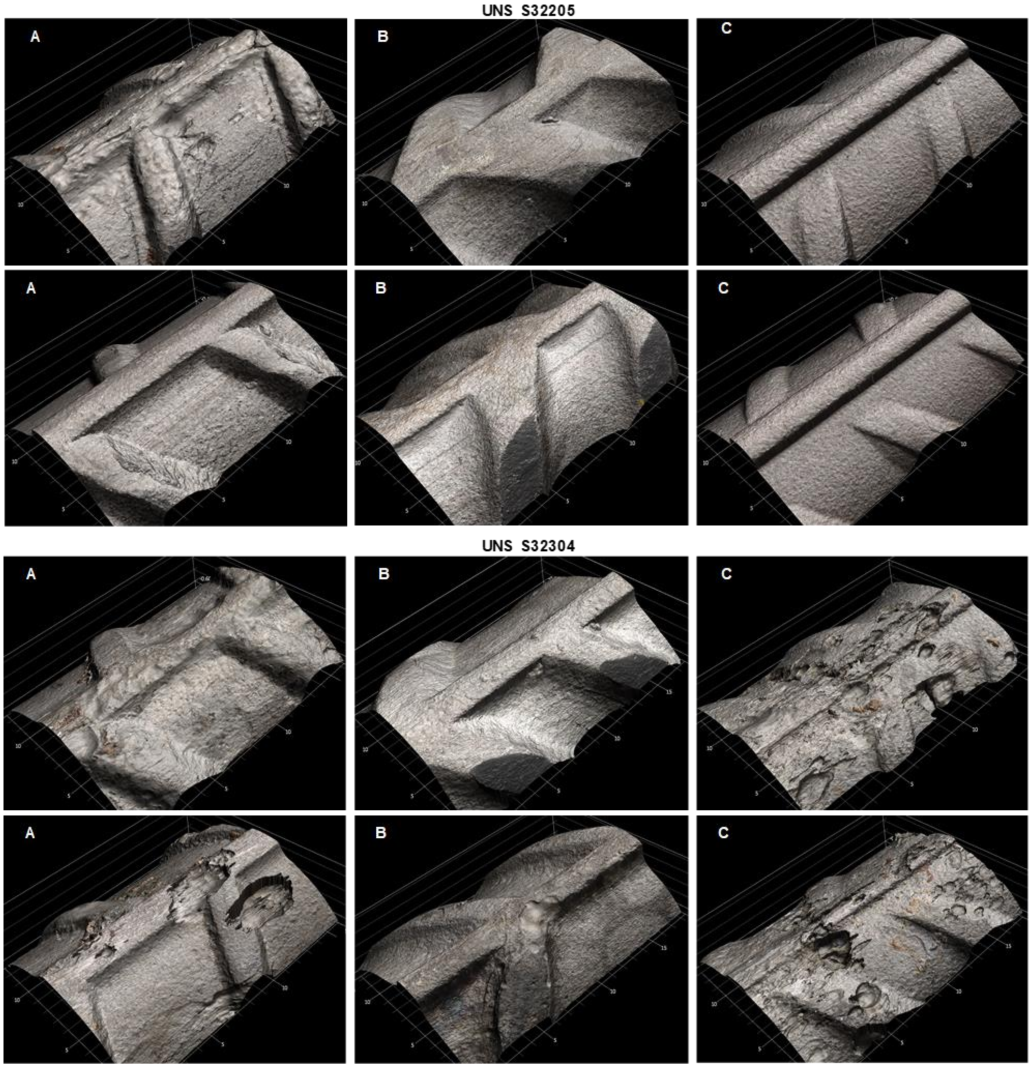

Figure 8-12. 3D scan of selected areas of the longitudinal rib of the corroded bars shown in Figure 8-11. The top and bottom images on each rebar are both sides of the longitudinal rib on the same bar.

To quantify the impact of corrosion, the average volume loss of both sides of the longitudinal rib shown in Figure 8-12 are presented in Figure 8-13. These values were obtained by determining the depth loss from comparing the scans of the as-received bars shown in Figure 8-3 with the tested bars shown in Figure 8-11. Figure 8-13 shows that B bars with the least micropits on the as-received bars showed the least volume loss at 0.2 – 1.2% in both grades. The C bars with the deepest micropits in the as-received condition (UNS S32304) showed up to 10% loss of its longitudinal rib, while 0.5 – 0.7% is lost in the absence of micropits (UNS S32205). Although the micropits of A bars are significantly shallower than the corresponding C bars, they lost between 1.8 – 4% of their longitudinal rib.

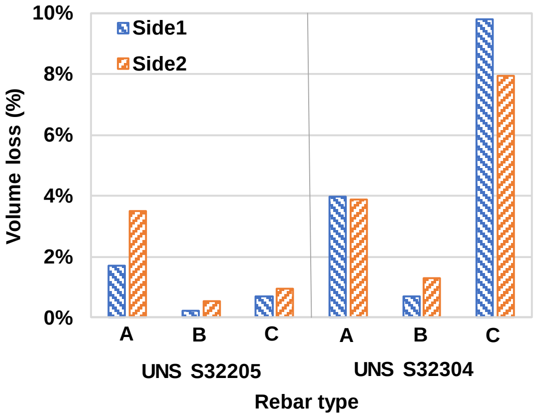

Figure 8-13. Volume loss percent on both sides (Side1 = S1, Side2 = S2) of the longitudinal rib of the first batch of UNS S32205 and UNS S32304 bars from all manufacturers determined by a non-contact 3D measurement system.

To further characterize the extent of corrosion suffered by these bars and the affected phases in the duplex alloys, metallographic examination of the longitudinal rib of the first batch of UNS S32205 and UNS S32304 C bars shown in Figure 8-11 was carried out and the micrographs are shown in Figure 8-14. The micrographs of UNS S32205 showed many tiny micropits that were not originally present in the bar but resulted after corrosion testing, whereas the UNS S32304 micrograph showed complete loss of some section of this rib, that was initially heavily pitted. This emphasizes the importance of finishing and quality control of these bars to improve on their corrosion performance. The micrographs in the middle and right of Figure 8-14 shows preferential corrosion of the ferrite phase in the UNS S32304 alloy and the resistance and/or dissolution of both austenite (light) and ferrite (dark) phases to corrosion in the UNS S32205 alloy. The preferential corrosion of ferrite phase in the Mo-free UNS S32304 alloy and the resistance of this phase to corrosion in the Mo-containing UNS S32205 alloy is consistent with results shown in Figure 8-9 and recent findings by other authors [203]–[205], [158]–[160] that Mo enhances the pitting resistance of the ferrite phase in a duplex alloy tested in alkaline environment. Unlike the pits produced.

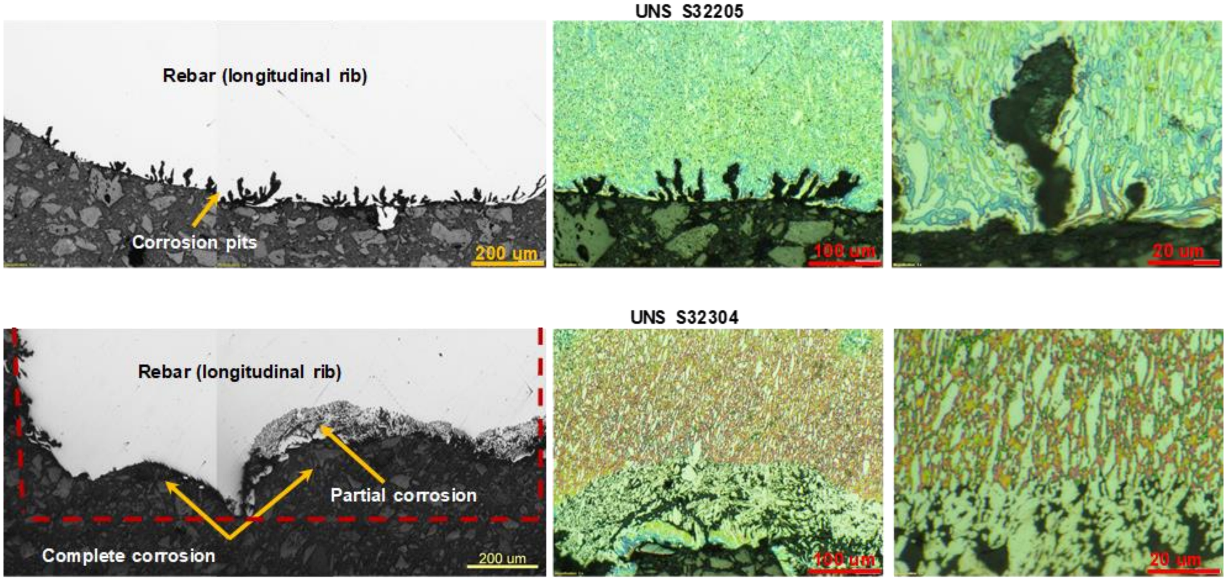

Figure 8-14. Micrograph of tested UNS S32205 and UNS S32304 C bars shown in Figure 8-11. Left – unetched micrograph of the longitudinal ribs showing partial and severe corrosion. Middle and Right – low and high magnification micrograph of some regions with corroded phases in the rib. The dark and bright phases are the ferrite and austenite phases, respectively.

8.5. Discussions

Tables 8-6 and 8-7 summarize observations from the procedures employed to screen and rank the bars. Visual observation and LED scanning of both UNS S32205 and UNS S32304 grades showed similar appearance and surface condition between batches from the same manufacturers. The B bars were the shiniest with no apparent surface flaw, while the A and C bars were both matt and a darker colour with no macroscopic defects on most regions on the bars, except a dark line parallel to the longitudinal rib of A bars. Microscopic examination of the rebar edges supports the visual observation and LED scanning that B bars showed the least flaws, while it showed the surfaces of A and C bars to be pitted, giving rise to the matt appearance. The C bars had the heaviest micropits. Only the C bars met the ASTM A276 composition specification for both rebar grades and, thus, ranked the best in this category, whereas, at least one of the major alloying elements expected to aid corrosion resistance in the A bars was below the minimum ASTM A276 specification. The hardness values of the different regions on these bars did not reveal any information that suggests the faster cooling/quenching of some regions or batches than others; the range of values overlap between different regions on a bar, batches and manufacturers. The C bars had the highest austenite content and the most Mo element in the ferritic phase reported to improve the corrosion resistant of the phase.

Furthermore, bars C possessed the most positive average corrosion potentials 48 h after cast in chloride contaminated concrete, while bars B possessed the most negative potentials, suggesting lower and higher probability of active corrosion, respectively, yet, the number of failed bars is highest for bars C and lowest for bars B. The more negative average corrosion potentials and greater variability found on bars B is surprising in view that, not only are these bars with significantly less micropits, the number of failed bars and the amount of visual corrosion products were lesser than bars from other manufacturers.

Since the measured potentials are a mixed potential of the anodic (corroding) and cathodic (non-corroding) sites on the bars, it was expected that these bars should posses the most positive potentials. The reason for this behaviour is yet to be understood but it is hypothesised that these potentials are in respect with the phases being attacked during corrosion of the bars which is subject to further investigation. Bars A and C showed similar number of failed bars in both tested grades (5 – 6 failed in tested 27 for UNS S32205 and 15 – 16 failed in tested 21 for UNS S32304), following the presence of micropits found on these bars. This emphasizes the detrimental impact of the observed micropits whether present in shallower (20 µm) or deeper (160 µm) depth as found in bars A and C respectively, although the current densities and rebar volume loss of the latter was higher. An interesting observation is the similar number of failed samples between the UNS S32205 and UNS S32304 bars B, which, unlike bars from other manufacturers, were mostly observed on application of +400 mV_{SCE} polarization potential. Although the active current densities of the UNS S32304 (0.8 – 3 A/m^2) were mostly higher than the UNS S32205 (0.03 – 1 A/m^2), this observation indicate similar corrosion resistance of both grade in the absence of micropits.

In general, the present work has shown that the most determining factor in the corrosion resistance of these duplex stainless steel alloys is the pickling-induced micropits in their as-received bars. This is supported by the worse corrosion performances found in bars C with the most micropits despite ranking the best in other categories shown in Tables 8-6 and 8-7. The absence of failed bars from the first batch of UNS S32205 bars C with no micropits observed in their as-received conditions and the lesser failed bars in both grades of bars B with the least micropits further supports these findings. Furthermore, the preferential corrosion around the ribs where most of these micropits were found and the volume loss of the longitudinal rib according to the severity of the observed micropits also supports these findings. Although the beneficial effect of Mo in enhancing corrosion resistance of duplex UNS S32205 alloy was observed, the similar number of failed UNS S32205 and UNS S32304 bars B indicate that its influence is secondary to surface conditions of the bars.

The mechanism of pitting has been long studied by many researchers and reviewed in [149], [243], [244]. The many mechanistic models of pitting can be summarized in two main groups. For the first group, it is proposed that there is a competition for anionic sites in the passive film where chlorides are exchanged with hydroxide ions causing local thinning or dissolution. A second group proposed a mechanical breakdown of passive films by chloride ions, resulting from their penetration through defective sites or low energy areas (such as grain boundaries in the passive film). The occurrence of one model to the other will be determined predominantly by the nature (stoichiometry, defect density, composition etc.) of each passive film. Therefore, any or combinations of these models is a possible consequence of the micropits found on the as-received bars resulting from the manufacturer's pickling process. When the heavily pitted bars are placed in concrete, it is expected that the subsequently formed passive films developed on these surfaces will be highly non-uniform, making it easier for chloride penetration through the film and growth of these existing pits. Other than the surface area effect, another possible reason for the increased corrosion rate of the initially pitted bars in concrete is that the acid pickling leaves a predominantly austenitic surface layer, Figure 8-9, which is not as stable at high pH. Another factor could be the trapping of the salt-laden mixing water solution in the pits during casting of the concrete and while the rest of the mixing water becomes increasingly alkaline during setting and hardening of the cement, the solution in the pits does not. This would mean that the initial pits may not have the same detrimental effect in concrete in which the chlorides penetrate from outside the concrete. These possibilities will be further investigated. Nevertheless, it is therefore recommended that a more quantitative specification regarding finishing of rebar should be provided to assist manufacturers with the reproducibility of bars. Although the impact of alloying compositions below specification and significant variation in hardness were not observed in isolation, manufacturers must either improve quality control to meet ASTM A276 standard to avoid variation in corrosion performance in the absence of micropits or provide a study to show sufficient corrosion protection can be obtained by compositions below this standard. It is expected that, other than these pickling-induced pits and dark lines parallel to the longitudinal ribs, other forms of processing flaw will result in similar variation in corrosion performances, emphasizing the need for a more quantitative guideline for production. Nevertheless, the stainless steel grades tested in the present work, with and without heavy micropits, is expected to provide sufficient and greater protection in critical corrosion affected areas than conventional carbon or galvanized steels. Of course, increased protection will be obtained from bars with no micropits.

Table 8-6. Ranking summary of the UNS S32205 bars from all manufacturers. ND = not determined.

Criteria	Manufacturer	**Summary**			**Rank**
		Batch 1	**Batch 2**	**Batch 3**	
Depth of micropits on as-received bars	A	20 µm	20 µm	20 µm	2
	B	20 µm	-	20 µm	1
	C	-	70 µm	100 µm	**3**
XRF composition below ASTM A276	A	Cr, Ni, Mo	Cr, Ni, Mo	Cr, Ni, Mo	3
	B	Cr, Ni	Cr, Ni	Cr, Ni	2
	C	-	-	-	**1**
Microhardness, Vickers	A	263 - 279	270 - 281	266 - 290	-
	B	247 - 276	267 - 296	235 – 287	-
	C	251 - 285	255 - 288	252 - 276	-
Austenite phase	A	55%	45%	47.5%	2
	B	45%	46%	47%	3
	C	48.5%	59%	52%	**1**
Mo in ferrite phase (wt.%)	A	3.23	ND	ND	3
	B	3.55	ND	ND	2
	C	3.71	ND	ND	**1**
Ave. corrosion potentials at 48h (mV)	A	-411	-439	-399	2
	B	-501	-511	-503	3
	C	-485	-395	-351	**1**
Failed bars (9 tested bars / batch)	A	1	2	2	2
	B	2	1	0	1
	C	0	4	2	**3**
Current densities (A/m^2)	A	0.1	0.3 – 1	0.1 – 1	2
	B	0.03 – 1	0.3	No failed	1
	C	No failed	0.03 - 2	0.2 - 2	**3**
Volume loss on long. Rib (%)	A	1.6 – 3.5	ND	ND	3
	B	0.2 – 0.5	ND	ND	1
	C	0.6 – 0.8	ND	ND	**2**

Table 8-7. Ranking summary of the UNS S32304 bars from all manufacturers. ND = not determined.

Criteria	Manufacturer	Summary of failed bars			Rank
		Batch 1	**Batch 2**	**Batch 3**	
Depth of micropits on as-received bars	A	20 µm	20 µm	20 µm	2
	B	-	-	20 µm	1
	C	130 µm	160 µm	150 µm	**3**
XRF composition below ASTM A276	A	Ni	Ni	Ni	2
	B	Cr	Cr	-	2
	C	-	-	-	**1**
Microhardness, Vickers	A	250 – 274	260 – 285	257 – 269	-
	B	259 – 261	285 – 307	248 – 265	-
	C	251 - 269	283 - 301	235 - 255	-
Austenite phase	A	53%	47%	40%	2
	B	43%	44%	42%	3
	C	50%	51%	51%	**1**
Mo in ferrite phase (wt.%)	A	0.48	ND	ND	3
	B	0.67	ND	ND	2
	C	1.15	ND	ND	**1**
Corrosion potentials at 48h (mV)	A	-391	-388	-378	2
	B	-511	-487	-461	3
	C	-385	-375	-341	**1**
Failed bars (7 tested bars / batch)	A	5	5	6	3
	B	1	2	0	1
	C	5	5	5	**3**
Current densities (A/m^2)	A	0.8 – 2	0.8 – 4	0.8 - 2	2
	B	1	0.8 - 3	No failed	1
	C	2 – 3	2 – 7	2 – 3	**3**
Volume loss on long. Rib (%)	A	3.8 – 3.9	ND	ND	2
	B	0.6 – 1.2	ND	ND	1
	C	7.9 – 9.8	ND	ND	**3**

8.6. Summary and conclusions

- The evaluation procedures employed in this work were efficient in screening the different batches of UNS S32205 and UNS S32304 bars obtained from different manufacturers in a significantly shorter period than the existing ASTM A955 which takes 4-22 months.
- Bars were screened based on the influence of variation in elemental compositions, microstructure and phases present in the bars and surface condition on their corrosion performance under anodic potentiostatic polarization. Unfortunately, it was not possible to isolate some of these factors to determine the influence of each because of their interrelation. Nevertheless, it was found that the severity of pickling-induced pitting on the as-received bars overwhelmed other factors in determining their corrosion performances.
- Bars from manufacturer C, whose compositions are the only ones to conform to ASTM A276 specification and possess the highest proportion of corrosion resistant austenitic phase and the highest Mo content in the ferritic phase, exhibited the most positive corrosion potentials and the worst corrosion performance. On the contrary, bars B with the least observable pitting on their as-received surfaces possessed superior corrosion resistance despite some of the alloy

constituents being below ASTM A276 specification, lowest proportion of austenitic phase and the most negative corrosion potentials.

- Metallographic examination suggested that the different manufacturers employ different processing techniques in the production of their bars, leading to different surface conditions. The depth of micropits observed on the bars indicates over-pickling by Manufacturer C and, to a lesser extent, by Manufacturer A as the A bars showed shallow but extensive micropits, which eventually resulted in similar number of failed bars as the C bars.
- The findings from the present work indicate that Mo-free UNS S32304 stainless steel grade has good corrosion resistance. The positive impact of Mo on corrosion resistance of UNS S32205 alloy in this alkaline concrete environment, which was also recently reported in the literature, loses its benefit in bars with an over-pickled surface. This is supported by the similar corrosion performance found in the two grades from Manufacturer B and the superior corrosion performance of the Mo-free UNS S32304 from Manufacturer B than the Mo-containing UNS S32205 from other manufacturers.

9. Summary, Conclusion and Recommendation

9.1. Comprehensive summary

The Canadian bridge design code specifies the service life of highway bridges to be 75-100 years. Since long term tests of this lifetime are not realistic, laboratory short term tests are typically used to predict the long-term corrosion behavior of steel reinforcements in these structures. The disadvantages of most accelerated tests have been discussed in [4]. Consequently, the overall goal of the project was to provide the scientific basis for determining whether the more economical grades of stainless steel rebar have a high probability of providing the required 100+ year service life under the severe environmental conditions experienced in Ontario.

To achieve this, the first step was to examine the environment these bars will experience in concrete. Pore solution analysis was used to determine the ionic concentration and pH of different chloride-contaminated concrete mixes, with emphasis on the high chloride concentrations employed in Ontario, Canada. The increasing sulphate with chloride observed in the cement pores of many of these mixes, the impact of which had not been previously investigated for rebar corrosion, facilitated a decision to report the variation in corrosion properties between one of these mixes (OPC+25%GGBFS and 0.4w/cm) and other common sulphate-free conservative simulated pore solutions, such as saturated $Ca(OH)_2$. Since corrosion resistance of steel rebar is dependent on the protection offered by the passive films formed on the bars' surface, it was important to determine the variation in passive film properties exposed to different chloride-contaminated concrete. The M-S, LPR and CP techniques were used to evaluate the influence of testing solutions containing deleterious species found in field concrete, alloying elements and surface roughness on passive film properties of carbon- and stainless steels by correlating films' electronic and electrochemical properties with their long-term product from equilibrium E/pH diagrams. The methodology employed was efficient to make prediction and correlation between film and rebar corrosion properties in the absence of sophisticated microscopy characterization equipment. It was then necessary to determine the implication of observed variation in passive film properties influenced by testing solution, alloying elements and surface roughness on bars' pitting characteristics and C_{CRIT} values. A rapid potentiodynamic polarization technique was developed to characterize these engineering properties for several traditional and newer stainless steel alloys. This technique proposes alternative to existing longer assessment methods, e.g. ASTM G109. Results obtained with this method are in the range of data reported using other methods, as discussed in Chapters 5 and 7. To further emphasize the need for consistency in corrosion properties, a screening procedure was employed to observe the influence of variability in rebar production leading to differences in flaws, composition, microstructure on the corrosion performance of batches of stainless steel alloys from difference manufacturers. This assessment further manifested the influence of surface roughness that was previously observed on passive films properties, pitting characteristics and C_{CRIT} values. Results from each influencing factor is further summarized below.

Testing solutions

Chlorides were unsurprisingly detrimental to electronic and electrochemical properties of passive films formed on both carbon and stainless steels, and especially more pronounced in films formed in lower pH $Ca(OH)_2$ solution because of their initial (i.e. before introduction of chlorides) less compact film structure. Chlorides generally increased film defects, reduced film thicknesses, decreased (more negative) corrosion potentials and increased current densities. However, this detrimental effect was suppressed when sulphate was introduced in the testing solution; the defect densities decreased, film thicknesses increased, corrosion potential were more positive, and current densities were lower. This additional protection is suggested to be due to the presence of stable solid sulphides of Fe and Ni (as FeS, FeS_2, NiS, Ni_3S_2) in these passive films as supported by the equilibrium stable species in the E/pH diagram. Passive film properties were better with increasing pH and sulphates in solution, and similar trends were also observed on the bar's pitting resistance and C_{CRIT} values. Higher pH (between CH/PS) and sulphates (between PS/PS+S) were found to increase the C_{CRIT} values of carbon steel by 123% and 18%, respectively, and stainless steel by 5-10% and 4-8%, respectively. This indicates that film properties and corrosion resistance of bars tested in lower pH or sulphate-free solutions are underestimated.

Alloying elements

Chromium was observed to lower, by 1-2 orders of magnitude, the defective nature of inner and outer oxide layers formed on stainless steel alloys and increase the C_{CRIT} values of all stainless steel grades by 6.5 – 8.3 than carbon steel. The previously reported positive influence of Mo was not observed on the passive film properties of both austenitic and duplex stainless steel alloys; the film properties of the Mo-free 304L and 2304 alloys similar to or slightly better than the Mo-containing 316LN and 2205 grades. The absence of Mo influence on film properties was unexpected for the duplex grades because recent studies showed that Mo preferentially precipitate in the ferritic phase and improve corrosion resistance of the duplex grades. The preferential corrosion of ferrite phase in Mo-free 2304 alloys and lack of thereof in the Mo-containing 2205 grade shown in Chapter 8 also support this finding. It was later found that the presence of heavy micropits in the longitudinal ribs of as-received 2205 bars negatively affected their film properties. When other micropits-free specimens were tested for C_{CRIT} analysis, the duplex Mo-containing 2205 alloys showed 17% higher C_{CRIT} values than Mo-free 2304 grade. Therefore, the absence of positive Mo impact on passive film and corrosion properties was only true for austenitic grades, as supported by the slightly higher C_{CRIT} values in the Mo-free 304L grade than Mo-containing 316LN grade. Ni replacement with Mn was beneficial in improving the stability of the inner oxide layer of passive films, while Ni improved the outer oxide layer. However, the protection offered by Ni in the outer layer of passive film increased the C_{CRIT} value of 304L grade by 13.5 – 18% than the 24100 grade. Nevertheless, the C_{CRIT} values of most stainless steel alloys were beyond the maximum solubility of chlorides observed in pore solution of the concrete mixes used in this research, indicating that it is impossible for them to corrode in these concretes, provided there is no cracks or major flaws.

Surface roughness

Film properties formed on polished rebar cross-sections were unsurprisingly superior to those formed on as-received surface, but the latter showed scatter expected from corrosion of rebar in field concrete. Particularly, the superior film properties of 2304 than the 2205 grade, influenced by heavy pitting found on the latter, emphasizing the need for consistent smooth surface finish, even on as-received bars, to reduce variation in corrosion properties. Furthermore, 2304 bars with processing artefacts (dark line near the longitudinal rib) also showed 13% lower C_{CRIT} values than same grade without such artefacts, further manifesting variation in corrosion properties influenced by surface roughness. Assessment on the effect of variation in composition, microstructure and processing flaw on the corrosion performance of batches of 2304 and 2205 alloys, showed that bars from Manufacturer C with compositions within the ASTM C276 specification, containing more corrosion resistant austenitic phase and more Mo content in their ferritic phase, showed the worse corrosion resistance. This was because these bars were heavily pitted in their as-received conditions, especially on the longitudinal rib with depth between 130 - 160 µm, 7-9% higher than other bars. The importance of quality surface finish was finally made apparent as it was the defining factor in these bars' corrosion resistance. It is also apparent that rebar manufacturers employ different finishing techniques that leads to significant variation in surface roughness in the bars.

9.2. Conclusions

This research showed there is significant variation in ionic concentration of the pore solutions in different concretes that should be accounted for in simulated solutions employed to test rebar corrosion resistance. One aspect of these variations was the increase in dissolved sulphate ions with increasing chlorides in pore solution which proved to be beneficial to the passive film properties of both carbon and stainless steels and, hence, the pitting resistance and chloride threshold values. The influence of sulphate attack on concrete was not studied in this work and these conclusions should not be extrapolated to effects of external sulphates.

These data demonstrate the corrosion performance of Mo-free austenitic 304L alloy is slightly better than that of 316LN alloy in the alkaline environments, in contrast to their relative corrosion resistance in acid or neutral solutions. However, Mo was beneficial to the corrosion performance of duplex 2205 alloy, except in the cases where the as-received bars showed poor surface finish from pickling. Thus, it is concluded that Mo-free 304L and 2304 alloys provide economical alternatives to 316LN and 2205 alloys for concrete reinforcement in highly corrosive environment. Although cheaper Mn alloying element that was a substitute for Ni in the 24100 alloy showed beneficial effect in improving their inner passive layer, the overall corrosion performance of the Ni-containing 304L alloy was significantly better, justifying the inclusion of Ni in stainless steel bars. Nevertheless, the cheaper Mn-containing 24100 alloy can be used in less severe corrosive environments since its C_{CRIT} value is at least 5 times greater than those of carbon steel rebar. Most service life predictions require the C_{CRIT} value as an input parameter, and these results show how different concrete mixes, rebar alloying elements and surface roughness and finish affect the C_{crit} value. More importantly, for the particular concrete mixture used in this research, the critical chloride threshold concentration, found by extrapolation of the experimental data, was greater than the solubility limit of chlorides in cement pores. This implies that chloride induced corrosion of these stainless alloys would not be possible in this concrete in the absence of cracks or major flaws.

9.3. Recommendations for future work

Although this work presents several significant findings, it also uncovered several research opportunities which can be further investigated. In this section, some research focus is recommended to further the understanding of variation of corrosion properties of steel rebar.

- Since the present work only employed one of the concrete mixes determined from Chapter 3, it is recommended that passive film analysis, critical chloride threshold test or corrosion resistance research should be conducted in other mixes to observe variation in rebar corrosion behavior.

- The findings from Chapter 3 facilitated a decision to investigate, with other colleague, the influence of other salt type (e.g. $MgCl_2$, $CaCl_2$) on ionic concentrations in the pores of OPC cement and resulting influence on corrosion behavior of embedded rebar. Ontario uses brine solution that contains NaCl, $CaCl_2$ and $MgCl_2$ at different concentrations. It is also recommended that these different salts should be employed on other cementitious type (FA, GGBFS, SF) to observe the possible similar increasing sulphate in pore solution. Pore solution expression of cement pastes with these salts penetrated from the surrounding (ingress chlorides) is also recommended for research to observe the variation in ionic concentrations in pore solution.
- It is recommended that the critical chloride threshold test be repeated on cement paste (cement and water), mortar (cement, sand and water) or concrete with cast-in (admixed) chlorides at different concentrations. The expected variation due to inhomogeneity of concrete which cannot be simulated in pore solution may then be observed.
- It is also recommended that the corrosion resistance test of batches of bars from different manufacturer should be performed on their “pre-rust” bars. These bars should be exposed outdoor to allow natural corrosion to initiate on them and then cast in mortar or cement paste with small cover to reduce the time to obtain results. The specimens should then be submerged in calcium hydroxide to prevent leaching of the paste or mortar and chlorides should be increased in solution over time. This will allow the influence of corrosion initiated on bars exposed to the environment on site because of delays in construction on corrosion resistance to be observed. This will be an interesting aspect of study because the synergistic effect on corrosion of possible micropits from processing and pre-rusting can be observed.

Research contributions to date

- L. Brock, I. G. Ogunsanya, H. Hamed, M. Vlasea, C. M. Hansson. "Performance characterization of fluid power based on the top 2 core and relevant skin recipes". To be submitted to Journal of Materials and Manufacturing, December 2019.
- I.G. Ogunsanya and C. M. Hansson, *Influence of chloride cations on the critical chloride threshold of carbon steel rebar in synthetic concrete pore solutions*, to be submitted to Corrosion, September 2019.
- M.J. Benoit, I.G. Ogunsanya, M. Emrich, S. Winkler, C. M. Hansson, *Internal corrosion of warm formed aluminum alloy automotive heat exchangers*, to be submitted to Materials and Corrosion, September 2019.
- I.G. Ogunsanya and C. M. Hansson, *Influence of clad composition on the corrosion resistance of stainless steel clad rebar in cracked concrete*, submitted to Materials and Corrosion, August 2019.
- C. B. Van Niejenhuis, I.G. Ogunsanya, and C.M. Hansson *Analysis of pore solution of different cements with and without chlorides*, currently under review at ACI Materials Journal, June 2018.
- I.G. Ogunsanya and C. M. Hansson, *Reproducibility of the corrosion resistance of UNS S32205 and UNS S32304 stainless steel reinforcing bars*, submitted to Corrosion, August 2019.
- I.G. Ogunsanya and C. M. Hansson, *Influence of Sulphate on the Electronic and Electrochemical Properties of Passive Films Formed on Steel Reinforcing Bars*, submitted to Materialia, MTLA-D-19-00423, July 2019.
- I.G. Ogunsanya and C. M. Hansson, *Detection of the critical chloride threshold of stainless steel rebar in synthetic concrete pore solutions*, currently under review at RILEM Technical Letters, July 2019.
- I.G. Ogunsanya and C. M. Hansson, *The semiconductor properties of passive films and corrosion behaviour of stainless steel reinforcing bars in simulated concrete pore solution*, Materialia 2019, 6 (100321).
- I.G. Ogunsanya and C. M. Hansson, *Detection of the critical chloride threshold of carbon steel rebar in synthetic concrete pore solutions*, RILEM Technical Letters, 2018 (3) 75-83.
- I.G. Ogunsanya and C. M. Hansson, *The Influence of Coating Thickness and Composition on the Corrosion Propagation Rates of Galvanized Rebar in Cracked Concrete*, Corrosion 2017, 74(1) 134-143.

Letter of copyright permission

The necessary copyright permissions have been obtained for using the published journals in Chapters 4, 6, and 8 from the publishers. Chapter 5 was published as an open access and does not require any permission. At the time of this writing, Chapter 3 and 7 has been submitted for publication and is yet to be reviewed, so no permissions are given.

Influence of chloride and sulphate anions on the electronic and electrochemical properties of passive films formed on steel reinforcing bars

Author: I.G. Ogunsanya,C.M. Hansson
Publication: Materialia
Publisher: Elsevier
Date: December 2019

© 2019 Published by Elsevier Ltd on behalf of Acta Materialia Inc.

Please note that, as the author of this Elsevier article, you retain the right to include it in a thesis or dissertation, provided it is not published commercially. Permission is not required, but please ensure that you reference the journal as the original source. For more information on this and on your other retained rights, please visit: https://www.elsevier.com/about/our-business/policies/copyright#Author-rights

© 2019 Copyright - All Rights Reserved | Copyright Clearance Center, Inc. | Privacy statement | Terms and Conditions
Comments? We would like to hear from you. E-mail us at customercare@copyright.com

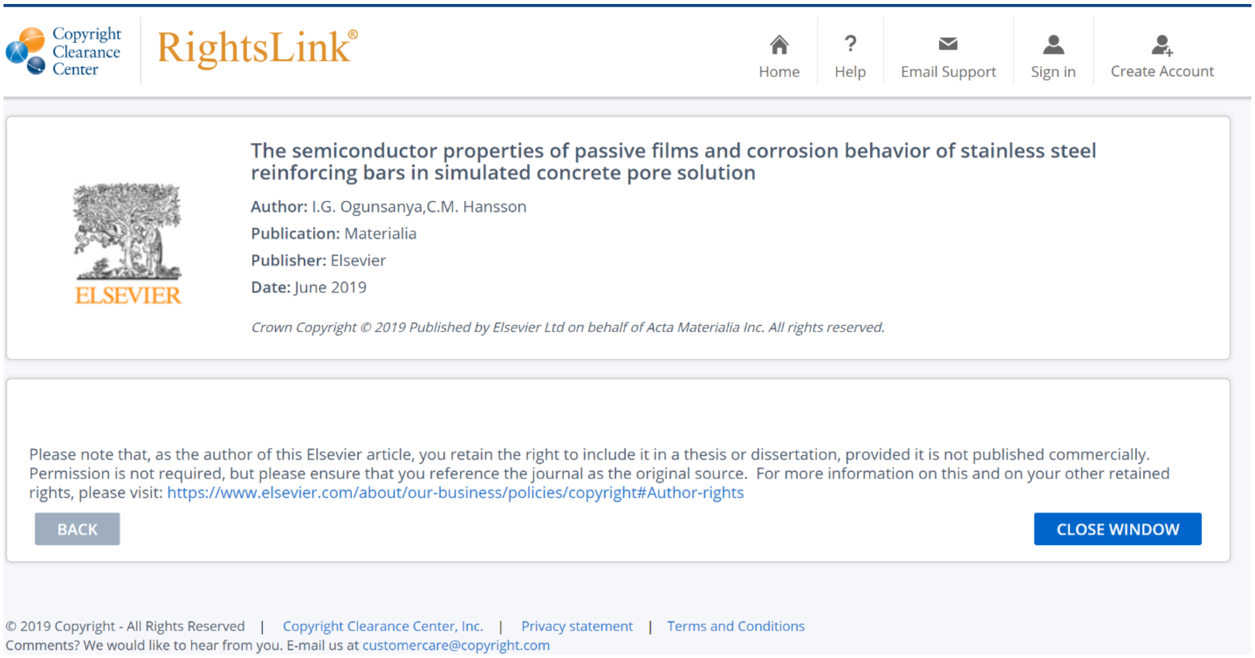

The semiconductor properties of passive films and corrosion behavior of stainless steel reinforcing bars in simulated concrete pore solution

Author: I.G. Ogunsanya,C.M. Hansson
Publication: Materialia
Publisher: Elsevier
Date: June 2019

Crown Copyright © 2019 Published by Elsevier Ltd on behalf of Acta Materialia Inc. All rights reserved.

Please note that, as the author of this Elsevier article, you retain the right to include it in a thesis or dissertation, provided it is not published commercially. Permission is not required, but please ensure that you reference the journal as the original source. For more information on this and on your other retained rights, please visit: https://www.elsevier.com/about/our-business/policies/copyright#Author-rights

© 2019 Copyright - All Rights Reserved | Copyright Clearance Center, Inc. | Privacy statement | Terms and Conditions
Comments? We would like to hear from you. E-mail us at customercare@copyright.com

References

[1] H. F. W. Taylor, *Cement Chemistry*. Thomas Telford Service Ltd, 1997.

[2] T. D. Marcotte and C. M. Hansson, “Corrosion products that form on steel within cement paste,” *Mater. Struct.*, vol. 40, no. 3, pp. 325–340, 2007.

[3] O. Gepraegs and C. Hansson, “A comparative evaluation for three commercial instruments for Field Measurements of Reinforcing Steel Corrosion Rates. in Electrochemical Techniques for Evaluating Corrosion Performance and Estimating Service-Life of Reinforced Concrete,” in *Journal of astm international*, 2004, pp. 1–16.

[4] A. Poursaee and C. M. Hansson, “Potential pitfalls in assessing chloride-induced corrosion of steel in concrete,” *Cem. Concr. Res.*, vol. 39, no. 5, pp. 391–400, 2009.

[5] R. S. Barneyback, S. Diamond, and W. Lafayette, “Expression and analysis of pore fluids from hardened cement pastes and mortar,” *Cem. Concr. Compos.*, vol. 11, no. 2, pp. 279–285, 1981.

[6] K. Byfors, C. M. Hansson, and J. Tritthart, “Pore solution expression as a method to determine the influence of mineral additives on chloride binding,” *Cem. Concr. Res.*, vol. 16, no. 5, pp. 760–770, 1986.

[7] CAN/CSA-S6-06, “Canadian Highway Bridge Design Code,” *CSA Stand.*, vol. 1, no. 1, 2011.

[8] Y. Zhang and A. Poursaee, “Study of the semi-conductive behavior of the passive film on carbon steel in simulated concrete pore solution under stress,” *Anti-Corrosion Methods Mater.*, vol. 62, no. 6, pp. 363–370, 2015.

[9] S. H. Kosmatka, B. Kerkhoff, and W. C. Panarese, *Design and Control Design and Control of Concrete Mixtures*, vol. EB001. 2003.

[10] R. H. Bogue, *The Chemistry of Portland Cement*. New York: Reinhold Corp, 1955.

[11] C. B. Van Niejenhuis, I. G. Ogunsanya, and C. M. Hansson, “Analysis of pore solution expressed from Portland cement pastes with and without supplementary cementitious materials and admixed chlorides,” *ACI Mater. J.*, vol. submitted, 2018.

[12] Y. Zhang and Q. Li, “Electrochemical study on semiconductive properties of the passive film on rebar in concrete,” *J. Zhejiang Univ. Sci. A*, vol. 7, no. 8, pp. 1447–1452, 2006.

[13] L. T. Mammoliti, L. C. Brown, C. M. Hansson, and B. B. Hope, “The influence of surface finish of reinforcing steel and pH of test solution on chloride threshold,” *Cem. Concr. Res.*, vol. 26, no. 4, pp. 545–550, 1996.

[14] E. Ramírez, J. A. González, and A. Bautista, “The protective efficiency of galvanizing against corrosion of steel in mortar and in Ca(oH)2 saturated solutions containing chlorides,” *Cem. Concr. Res.*, vol. 26, no. 10, pp. 1525–1536, 1996.

[15] J. A. Gonza, J. M. Miranda, E. Otero, and S. Feliu, “Effect of electrochemically reactive rust layers on the corrosion of steel in a Ca(OH)2 solution,” *Corros. Sci.*, vol. 49, pp. 436–448, 2007.

[16] J. A. Gonza, A. Cobo, M. N. Gonza, and E. Otero, “On the effectiveness of realkalisation as a rehabilitation method for corroded reinforced concrete structures,” vol. 103, pp. 97–103, 2000.

[17] G. Blanco, A. Bautista, and H. Takenouti, “EIS study of passivation of austenitic and duplex

stainless steels reinforcements in simulated pore solutions," *Cem. Concr. Compos.*, vol. 28, no. 3, pp. 212–219, 2006.

[18] J. Hou and D. D. L. Chung, "Effect of admixtures in concrete on the corrosion resistance of steel reinforced concrete," *Corros. Sci.*, vol. 42, pp. 1489–1507, 2000.

[19] S. Randstrom, M. Almen, R. Pettersson, and M. Adair, "Reproducibility of critical chloride threshold levels for stainless steel reinforcement," in *Structural Faults*, 2010.

[20] J. Williamson and O. B. Isgor, "The effect of simulated concrete pore solution composition and chlorides on the electronic properties of passive films on carbon steel rebar," *Corros. Sci.*, vol. 106, pp. 82–95, 2016.

[21] M. J. Hunt and C. M. Hansson, "The influence of cations in anti-icing brines on the corrosion of reinforcing steel in synthetic concrete pore solution," *Corrosion*, vol. 71, no. 6, pp. 749–757, 2015.

[22] Z. Q. Tan and C. M. Hansson, "Effect of surface condition on the initial corrosion of galvanized reinforcing steel embedded in concrete," *Corros. Sci.*, vol. 50, no. 9, pp. 2512–2522, 2008.

[23] R. D. Hooton, "Canadian use of ground granulated blast-furnace slag as a supplementary cementing material for enhanced performance of concrete," *Can. J. Civ. Eng.*, vol. 27, no. 4, pp. 754–760, 2000.

[24] B. Lothenbach, K. Scrivener, and R. D. Hooton, "Supplementary cementitious materials," *Cem. Concr. Res.*, vol. 41, no. 12, pp. 1244–1256, 2011.

[25] J. A. Larbi, A. L. A. Fraay, and J. M. J. M. Bijen, "The chemistry of the pore fluid of silica fumeblended cement systems," *Cem. Concr. Compos.*, vol. 20, no. 4, pp. 506–516, 1990.

[26] C. Arya, N. R. Buenfeld, and J. B. Newman, "Assessment of Simple Methods of Determining the Free Chloride Ion Content of Cement Paste.," *Cem. Concr. Res.*, vol. 17, no. 6, pp. 907–918, 1987.

[27] K. Basham, "Choices in Corrosion-Resistant Rebar: A Comparison of the Features, Performance, and Costs of Five Rebar Options," *Concr. Constr.*, 1999.

[28] J. T. Pérez-Quiroz, J. Terán, M. J. Herrera, M. Martínez, and J. Genescá, "Assessment of stainless steel reinforcement for concrete structures rehabilitation," *J. Constr. Steel Res.*, vol. 64, no. 11, pp. 1317–1324, 2008.

[29] M. Mistry, C. Koffler, and S. Wong, "LCA and LCC of the world's longest pier: a case study on nickel-containing stainless steel rebar," *Int. J. Life Cycle Assess.*, vol. 21, no. 11, pp. 1637–1644, 2016.

[30] D. A. Jones, *Principles and prevention of corrosion*. Macmillan, 1992.

[31] G. F. Li, Y. F. Kaneshima, and T. Shoji, "Effects of impurities on environmentally assisted crack growth of solution-annealed austenitic steels in primary water at 325??C," *Corrosion*, vol. 56, no. 5, pp. 460–469, 2000.

[32] J. O. Park, T. Suter, and H. Böhni, "Role of manganese sulfide inclusions on pit initiation of super austenitic stainless steels," *Corrosion*, vol. 59, no. 1, pp. 59–67, 2003.

[33] A. J. Sedriks, *Corrosion of Stainless Steels*. Wiley Interscience Publications, 1979.

[34] A. L. Schaeffler, "Selection of austenitic electrodes for welding dissimilar metals," *Weld. J.*, vol. 26, no. 10, pp. 601–620, 1947.

[35] M. Onozuka, T. Saida, S. Hirai, M. Kusuhashi, I. Sato, and T. Hatakeyama, "Low-activation Mn–Cr austenitic stainless steel with further reduced content of long-lived radioactive elements," *J. Nucl. Mater.*, vol. 255, no. 2–3, pp. 128–138, 1998.

[36] F. C. Hull, "Delta Ferrite and Martnesite Formation in Stainless Steels," *Weld. J.*, vol. 53, no. May, pp. 193–203, 1973.

[37] M. Kemp, A. van Bennekom, and F. P. A. Robinson, "Evaluation of the corrosion and mechanical properties of a range of experimental CrMn stainless steels," *Mater. Sci. Eng. A*, vol. 199, no. 2, pp. 183–194, 1995.

[38] J. Glownia, B. Kalandyk, and K. Hübner, "Delta ferrite predictions for cast duplex steels with high nitrogen content," *Mater. Charact.*, vol. 47, no. 2, pp. 149–155, 2001.

[39] A. L. Schaeffler, "Data sheet 680-B.," *Met. Prog.*, vol. 56, p. 680, 1949.

[40] C. J. Long and W. T. DeLong, "Ferrite content of austenitic stainless steel weld metal," *Weld. J.*, vol. 52, no. 7, p. 281, 1973.

[41] D. L. Olson, "Prediction of Austenitic Weld Metal Microstructure and Properties," *AWS 65th Annu. Meet.*, pp. 280–295, 1984.

[42] K. H. Lo, C. H. Shek, and J. K. L. Lai, "Recent developments in stainless steels," *Mater. Sci. Eng. R Reports*, vol. 65, no. 4–6, pp. 39–104, 2009.

[43] T. Takemoto, Y. Murata, and T. Tanaka, "Effects of Alloying Elements and Thermomechanical Treatments on Mechanical and Magnetic Properties of Cr-Ni Austenitic Stainless Steel.," *ISIJ Int.*, vol. 30, no. 8, pp. 608–614, 1990.

[44] K. Lorenz and G. Medawar, "On the corrosion behavior of austenitic chromium-nickel-molybdenum steels with and without the addition of nitrogen, with special consideration," *Thysseen Res.*, vol. 1, p. 97, 1969.

[45] J. Charles and S. Bernhardsson, "No Title," in *Proceedings of the Duplex Stainless Steels, vol. 1*, 1991, p. 185.

[46] R. F. A. Jargelius-Pettersson, "Application of the Pitting Resistance Equivalent Concept to Some Highly Alloyed Austenitic Stainless Steels," *Corrosion*, vol. 54, no. 2, pp. 162–168, 1998.

[47] N. Suutala and M. Kurkela, "Localized Corrosion Resistance of High Alloy Austenitic Stainless Steels and Welds," in *Proceedings of Stainless Steel*, 1984, no. 84, pp. 240–247.

[48] H. Ogawa, H. Omata, I. Itoh, and H. Okada, "Auger Electron Spectroscopic and Electrochemical Analysis of the Effect of Alloying Elements on the Passivation Behavior of Stainless Steels.," *Corrosion*, vol. 34, no. 2. pp. 52–60, 1978.

[49] K. Sugimoto and Y. Sawada, "Role of Alloyed Molybdenum in Austenitic Stainless Steels in the Inhibition of Pitting in Neutral Halide Solutions.," *Corrosion*, vol. 32, no. 9. pp. 347–352, 1976.

[50] R. F. A. Jargelius-Pettersson, "Electrochemical investigation of the influence of nitrogen alloying on pitting corrosion of austenitic stainless steels," *Corros. Sci.*, vol. 41, no. 8, pp. 1639–1664,

1999.

[51] C. O. A. Olsson, “The influence of nitrogen and molybdenum on passive films formed on the austenoferritic stainless steel 2205 studied by AES and XPS,” *Corros. Sci.*, vol. 37, no. 3, pp. 467–479, 1995.

[52] I. Olefjord and L. Wegrelius, “THE INFLUENCE OF NITROGEN ON THE PASSIVATION OF STAINLESS STEELS,” *Corros. Sci.*, vol. 38, no. 7, pp. 1203–1220, 1996.

[53] A. A. Hermas, K. Ogura, S. Takagi, and T. Adachi, “Effects of alloying additions on corrosion and passivation behaviors of type 304 stainless steel,” *Corrosion*, vol. 51, no. 1, pp. 3–10, 1995.

[54] P. Combrade and J.-P. Audouard, “Duplex Stainless Steels and Localized Corrosion Resistance,” in *Proceedings of Stainless Steel*, 1991, vol. 1, pp. 257–281.

[55] T. Sourisseau, E. Chauveau, and B. Baroux, “Mechanism of copper action on pitting phenomena observed on stainless steels in chloride media,” *Corros. Sci.*, vol. 47, no. 5, pp. 1097–1117, 2005.

[56] H. Ohashi, T. Adachi, and C. Maekita, “EFFECT OF COPPER ON LOCAL CORROSION OF AUSTENITIC STAINLESS STEEL,” *Tetsu-to-Hagane*, vol. 66, no. 11, p. S1309, 1980.

[57] A. A. Hermas and I. M. Hassab-Allah, “Evaluation of stress corrosion cracking susceptibility of nanocrystallized stainless steel 304L welded joint by small punch test,” *J. Mater. Sci.*, vol. 36, pp. 3415–3422, 2001.

[58] S. Goñi and C. Andrade, “Synthetic concrete pore solution chemistry and rebar corrosion rate in the presence of chlorides,” *Cem. Concr. Res.*, vol. 20, no. 4, pp. 525–539, 1990.

[59] M. Kouřil, P. Novák, and M. Bojko, “Threshold chloride concentration for stainless steels activation in concrete pore solutions,” *Cem. Concr. Res.*, vol. 40, no. 3, pp. 431–436, 2010.

[60] C. Alonso, C. Andrade, M. Castellote, and P. Castro, “Chloride threshold values to depassivate reinforcing bars embedded in a standardized OPC mortar,” *Cem. Concr. Res.*, vol. 30, no. 7, pp. 1047–1055, 2000.

[61] C. M. Hansson and B. Sorensen, “The Threshold Concentration of Chloride in Concrete for the Initiation of Reinforcement Corrosion,” in *Corrosion Rates of Steel in Concrete, Issue 1065*, 1990, pp. 3–17.

[62] L. Bertolini, F. Bolzoni, T. Pastore, and P. Pedeferri, “Behaviour of stainless steel in simulated concrete pore solution,” *Br. Corros. J.*, vol. 31, no. 3, pp. 218–222, 1996.

[63] L. Bertolini and M. Gastaldi, “Corrosion resistance of austenitic and low-nickel duplex stainless steel bars,” in *Corrosion from the nanoscale to the plant*, 2009.

[64] M. F. Hurley and J. R. Scully, “Threshold chloride concentrations of selected corrosion-resistant rebar materials compared to carbon steel,” *Corrosion*, vol. 62, no. 10, pp. 892–904, 2006.

[65] S. R. Morrison, *Electrochemistry at semiconductor and oxidized metal electrodes*. Springer, New York, USA, 1980.

[66] V. A. Myamlin and Y. V. Pleskov, “THE ELECTROCHEMISTRY OF SEMICONDUCTORS,” *Russ. Chem. Rev.*, vol. 32, no. 4, pp. 207–223, 1963.

[67] H. Tsuchiya and S. Fujimoto, “Semiconductor properties of passive films formed on sputter-

deposited Fe-18Cr alloy thin films with various additive elements," *Sci. Technol. Adv. Mater.*, vol. 5, no. 1–2, pp. 195–200, 2004.

[68] A. W. Bott and D. Ph, "Electrochemistry of Semiconductors," *Sol. Energy*, vol. 8, no. 4, p. 136, 1964.

[69] A. J. Nozik, "Annual review of physical chemistry," *Annu. Rev. Phys. Chem.*, vol. 29, pp. 189–222, 1978.

[70] Y. Xu and M. A. Schoonen, "American mineralogist," *Am. Mineral.*, vol. 85, pp. 543–556, 2000.

[71] P. Ghods, O. B. Isgor, J. R. Brown, F. Bensebaa, and D. Kingston, "XPS depth profiling study on the passive oxide film of carbon steel in saturated calcium hydroxide solution and the effect of chloride on the film properties," *Appl. Surf. Sci.*, vol. 257, no. 10, pp. 4669–4677, 2011.

[72] P. Ghods, O. Burkan Isgor, F. Bensebaa, and D. Kingston, "Angle-resolved XPS study of carbon steel passivity and chloride-induced depassivation in simulated concrete pore solution," *Corros. Sci.*, vol. 58, pp. 159–167, 2012.

[73] H. B. Gunay, P. Ghods, O. B. Isgor, G. J. C. Carpenter, and X. Wu, "Characterization of atomic structure of oxide films on carbon steel in simulated concrete pore solutions using EELS," *Appl. Surf. Sci.*, vol. 274, pp. 195–202, 2013.

[74] H. Schmuki, P., Bohni, "Metastable Pitting and Semiconductive Properties of Passive films," *J. Electrochem. Soc.*, vol. 139, no. 7, pp. 1908–1913, 1992.

[75] A. Simoes, M. Ferreira, B. Rondot, and M. Da Cunha Belo, "Study of passive films on AISI 304 Stainless steel by impedance measurement and photoelectrochemistry," *J. Electrochem. Soc.*, vol. 137, no. 1, pp. 82–87, 1990.

[76] A. Di Paola, F. Di Quarto, and C. Sunseri, "Photochemical characterization of passive films on stainless steels," *Corros. Sci.*, vol. 26, no. 11, pp. 935–948, 1986.

[77] I. Díez-Pérez, P. Gorostiza, and F. Sanz, "Direct Evidence of the Electronic Conduction of the Passive Film on Iron by EC-STM," *J. Electrochem. Soc.*, vol. 150, no. 7, p. B348, 2003.

[78] I. Dıez-Perez, A. G. Guell, F. Sanz, and P. Gorostiza, "Conductance Maps by Electrochemical Tunneling Spectroscopy To Fingerprint the Electrode Electronic Structure," *Anal. Chem.*, vol. 78, no. 20, pp. 7325–7329, 2006.

[79] M. D. Porter, T. B. Bright, D. L. Allara, and C. E. D. Chidsey, "Spontaneously organized molecular assemblies. 4. Structural characterization of n-alkyl thiol monolayers on gold by optical ellipsometry, infrared spectroscopy, and electrochemistry," *J. Am. Chem. Soc.*, vol. 109, no. 12, pp. 3559–3568, Jun. 1987.

[80] C. R. Nave, "HyperPhysics," Georgia State: http://hyperphysics.phy-astr.gsu.edu/hbase/hframe.html, 2016.

[81] Gamry instrument, "Common Equivalent Circuit Models Part 3," *Gamry Instruments*, vol. 3, pp. 1–13, 2017.

[82] F. Pruckner, J. Theiner, J. Eri, and E. G. Nauer, "In-situ monitoring of the efficiency of the cathodic protection of reinforced concrete by electrochemical impedance spectroscopy," *Electrochim. Acta*, vol. 41, no. 7/8, pp. 1233–1238, 1996.

[83] L. Lemoine, F. Wenger, and J. Galland, “Study of the Corrosion of Concrete Reinforcement by Electrochemical Impedance Measurement. in Corrosion Rates of Steel in Concrete,” *Astm Stp*, vol. 1065, 1990.

[84] S. Perron and J. . Beaudoin, “Freezing of water in portland cement paste – an ac impedance spectroscopy study,” *Cem. Concr. Compos.*, vol. 24, no. 5, pp. 467–475, 2002.

[85] C. Andrade, V. M. Blanco, a. Collazo, M. Keddam, X. R. Nóvoa, and H. Takenouti, “Cement paste hardening process studied by impedance spectroscopy,” *Electrochim. Acta*, vol. 44, no. 24, pp. 4313–4318, 1999.

[86] L. Dhouibi, E. Triki, and A. Raharinaivo, “The application of electrochemical impedance spectroscopy to determine the long-term effectiveness of corrosion inhibitors for steel in concrete,” *Cem. Concr. Compos.*, vol. 24, no. 1, pp. 35–43, 2002.

[87] C. Monticelli, A. Frignani, and G. Trabanelli, “Study on corrosion inhibitors for concrete application,” *Cem. Concr. Res.*, vol. 30, no. 4, pp. 635–642, 2000.

[88] G. Trabanelli, C. Monticelli, V. Grassi, and A. Frignani, “Electrochemical study on inhibitors of rebar corrosion in carbonated concrete,” *Cem. Concr. Res.*, vol. 35, no. 9, pp. 1804–1813, 2005.

[89] P. Gu, S. Elliott, R. Hristova, J. J. Beaudoin, R. Brosseau, and B. Baldock, “A study of corrosion inhibitor performance in chloride contaminated concrete by electrochemical impedance spectroscopy,” *ACI Mater. J.*, vol. 94, no. 5, pp. 385–395, 1997.

[90] B. B. Hope and A. K. C. Ip, “corrosion inhibitors for use in concrete,” *ACI Mater. J.*, vol. 86, no. 6, pp. 602–608, 1989.

[91] M. R. Hansen, M. L. Leming, P. Zia, and S. Ahmad, “Chloride permeability and AC impedance of high performance concrete,” *ACI - SP140-06*, vol. 140, pp. 121–146, 1993.

[92] M. Shi, Z. Chen, and J. Sun, “Determination of chloride diffusivity in concrete by AC impedance spectroscopy,” *Cem. Concr. Res.*, vol. 29, no. 7, pp. 1111–1115, 1999.

[93] C. Aldea, J. Shane, T. O. Mason, and S. P. Shah, “Assessment of microstructural changes during rapid chloride permeability test using impedance spectroscopy measurements,” *ACI - SP189-19*, vol. 189, pp. 333–350, 2000.

[94] S. P. Harrington, F. Wang, and T. M. Devine, “The structure and electronic properties of passive and prepassive films of iron in borate buffer,” *Electrochim. Acta*, vol. 55, no. 13, pp. 4092–4102, 2010.

[95] M. H. Dean and U. Stimming, “No Title,” *J. Phys. Chem.*, vol. 93, pp. 8053–8059, 1989.

[96] M. H. Dean and U. Stimming, “The electronic properties of disordered passive films,” *Corros. Sci.*, vol. 29, no. 2–3, pp. 199–211, 1989.

[97] M. H. Dean and U. Stimming, “Capacity of semiconductor electrodes with multiple bulk electronic states Part I. Model and calculations for discrete states,” *J. Electroanal. Chem.*, vol. 228, no. 1–2, pp. 135–151, 1987.

[98] A. Di Paola, “Semiconductor Properties of Passive Films on Stainless Steel,” *Electrochim. Acta*, vol. 34, no. 2, pp. 203–210, 1989.

[99] S. J. Ahn and H. S. Kwon, “Effects of solution temperature on electronic properties of passive film formed on Fe in pH 8.5 borate buffer solution,” *Electrochim. Acta*, vol. 49, no. 20, pp. 3347–3353, 2004.

[100] J. Sikora, E. Sikora, and D. D. MacDonald, “Electronic structure of the passive film on tungsten,” *Electrochim. Acta*, vol. 45, no. 12, pp. 1875–1883, 2000.

[101] J. F. Dewald, “The charge distribution at the zinc oxide-electrolyte interface,” *J. Phys. Chem. Solids*, vol. 14, pp. 155–161, 1960.

[102] J. Schultze, U. Stimming, and J. Weise, “Capacity and Photocurrent Measurements at Passive Titanium Electrodes,” *Berichte der Bunsengesellschaft fur Phys. chemie*, vol. 86, no. 4, pp. 276–282, 1982.

[103] A. Goossens, M. Vazquez, and D. D. Macdonald, “The nature of electronic states in anodic zirconium oxide films part 1: the potential distribution,” *Electrochim. Acta*, vol. 41, no. 1, pp. 35–45, 1996.

[104] U. Stimming and J. Schultze, “The capacity of passivated iron electrodes and the band structure of the passive layer,” *Berichte der Bunsengesellschaft für Phys. Chemie*, vol. 80, no. 12, pp. 1297–1302, 1976.

[105] U. Stimming and J. W. Schultze, “A semiconductor model of the passive layer on iron electrodes and its application to electrochemical reactions,” *Electrochim. Acta*, vol. 24, no. 8, pp. 859–869, 1979.

[106] K. Azumi, T. Ohtsuka, and N. Sato, “No Title,” *J. Electrochem. Soc.*, vol. 134, pp. 1352–1357, 1987.

[107] N. E. Hakiki, S. Boudin, B. Rondot, and M. Da Cunha Belo, “The electronic structure of passive films formed on stainless steels,” *Corros. Sci.*, vol. 37, no. 11, pp. 1809–1822, 1995.

[108] B. science Instrument, “EC-Lab Software : Techniques and Applications,” *BioLogic*, vol. 10.37, no. February, 2011.

[109] ASTM C876-09, “Standard Test Method for Half-Cell Potentials of Uncoated Reinforcing Steel in Concrete,” *ASTM Int.*, vol. 09, pp. 1–6, 2009.

[110] I. G. Ogunsanya and C. M. Hansson, “The influence of coating thickness and compostion on corrosion propagation rates of galvanized rebar in cracked concrete,” Waterloo, CJ-1612-OA-2370, 2016.

[111] M. Stern and A. L. Geary, “Electrochemical Polarization. I. A Theoretical Analysis of the Shape of Polarization Curves,” *J. Electrochem. Soc.*, vol. 104, no. 9, p. 559, 1957.

[112] C. B. Van Niejenhuis, T. W. Bandura, and C. M. Hansson, “Evaluation of the proposed European test procedure for ranking stainless steel rebar,” *Corrosion*, vol. 72, no. 6, pp. 834–842, 2016.

[113] P. G. Loudfoot, “The Adaptation of a Rapid Screening Test to Rank the Corrosion Behaviour of Stainless Steel Reinforcing Bars in Concrete,” University of Waterloo, 2018.

[114] A. Scott and M. G. Alexander, “Effect of supplementary cementitious materials (binder type) on the pore solution chemistry and the corrosion of steel in alkaline environments,” *Cem. Concr. Res.*, vol. 89, pp. 45–55, 2016.

[115] A. Hidalgo, G. De Vera, M. A. Climent, C. Andrade, and C. Alonso, “Measurements of Chloride Activity Coefficients in Real Portland Cement Paste Pore Solutions,” *J. Am. Ceram. Soc.*, vol. 12, pp. 3008–3012, 2001.

[116] B. Elsener, L. Zimmermann, and H. Böhni, “Non destructive determination of the free chloride content in cement based materials,” *Mater. Corros.*, vol. 54, no. 6, pp. 440–446, 2003.

[117] L. Bertolini and M. Gastaldi, “Corrosion resistance of low-nickel duplex stainless steel rebars,” *Mater. Corros.*, vol. 62, no. 2, pp. 120–129, 2011.

[118] ASTM A955/A955M-14, “Standard Specification for Deformed and Plain Stainless-Steel Bars for Concrete,” *Astm*, vol. i, pp. 1–13, 2015.

[119] D. B. McDonald, M. R. Sherman, D. W. Pfeifer, and Y. P. Virmani, “Stainless steel reinforcing as corrosion protection,” *Concrete International*, vol. 17, no. 5. pp. 65–70, 1995.

[120] M. J. Hunt and C. M. Hansson, “The Influence of the Cations in Anti-icing Brines on the Corrosion of Reinforcing Steel in Synthetic Concrete Pore Solution,” *Corrosion*, vol. 71, no. 6, pp. 749–757, 2015.

[121] ASTM C1152/C 1152M-04, “Standard Test Method for Acid-Soluble Chloride in Mortar and Concrete,” 2004.

[122] ASTM C1218, “Standard Test Method for Water-Soluble Chloride in Mortar and Concrete,” *ASTM Int.*, 2004.

[123] K. A. Anders, B. P. Bergsma, and C. M. Hansson, “Chloride concentration in the pore solution of Portland cement paste and Portland cement concrete,” *Cem. Concr. Res.*, vol. 63, pp. 35–37, 2014.

[124] A. Vollpracht, B. Lothenbach, R. Snellings, and J. Haufe, “The pore solution of blended cements: a review,” *Mater. Struct.*, vol. 49, no. 8, pp. 3341–3367, 2016.

[125] K. D. Stanish, R. D. Hooton, and M. D. . Thomas, “Testing the Chloride Penetration Resistance of Concrete : A Literature Review,” *FHWA Contract DTFH61-97-R-00022*, pp. 1–31, 1997.

[126] U. M. Angst *et al.*, “The effect of the steel – concrete interface on chloride- induced corrosion initiation in concrete : a critical review by RILEM TC 262-SCI,” *Mater. Struct.*, vol. 52:88, 2019.

[127] A. C. D. N. CSA, “Cementitious materials compendium,” *CSA A3000-13*, 2018.

[128] T. Wagner, D. A. Kulik, F. F. Hingerl, and S. V. Dmytrievava, “Gem-selektor geochemical modeling package: TSolMod library and data interface for multicomponent phase models,” *Can. Mineral.*, vol. 50, no. 5, pp. 1173–1195, 2012.

[129] D. A. Kulik *et al.*, “GEM-Selektor geochemical modeling package: Revised algorithm and GEMS3K numerical kernel for coupled simulation codes,” *Comput. Geosci.*, vol. 17, no. 1, pp. 1–24, 2013.

[130] C. Arya, N. R. Buenfeld, and J. B. Newman, “Factors influence chloride-binding in concrete,” *Cem. Concr. Res.*, vol. 20, pp. 291–300, 1990.

[131] A. Delagrave, J. Marchand, J. P. Ollivier, S. Julien, and K. Hazrati, “Chloride binding capacity of various hydrated cement paste systems,” *Adv. Cem. Based Mater.*, vol. 6, no. 1, pp. 28–35, 1997.

[132] C. M. Hansson, T. Frølund, and J. B. Markussen, “The effect of chloride cation type on the

corposion of steel in concrete by chloride salts," *Cem. Concr. Res.*, vol. 15, no. 1, pp. 65–73, 1985.

[133] I. Galan and F. P. Glasser, "Chloride in cement," *Adv. Cem. Res.*, vol. 27, no. 2, pp. 63–97, 2015.

[134] H. S. Wong and N. R. Buenfeld, "Determining the water-cement ratio, cement content, water content and degree of hydration of hardened cement paste: Method development and validation on paste samples," *Cem. Concr. Res.*, vol. 39, no. 10, pp. 957–965, 2009.

[135] A. k. Suryavanshi, J. D. Scantlebury, and S. B. Lyon, "Mechanism of Friedel's Salt Formation in Cements Rich in Tri-Calcium Aluminate," *Cem. Concr. Res.*, vol. 26, no. 5, pp. 717–727, 1996.

[136] K. De Weerdt, A. Colombo, L. Coppola, H. Justnes, and M. R. Geiker, "Impact of the associated cation on chloride binding of Portland cement paste," *Cem. Concr. Res.*, vol. 68, pp. 196–202, 2015.

[137] I. G. Ogunsanya and C. M. Hansson, "Detection of the critical chloride threshold of carbon steel rebar in synthetic concrete pore solutions," *RILEM Tech. Lett.*, vol. 3, pp. 75–83, 2018.

[138] I. G. Ogunsanya and C. M. Hansson, "The critical chloride threshold of austenitic and duplex stainless steel reinforcing bars," *Submitt. to Metall. Mater. Trans.*, vol. E-TP-19-12.

[139] M. F. Montemor, M. G. S. Ferreira, N. E. Hakiki, and M. Da Cunha Belo, "Chemical composition and electronic structure of the oxide films formed on 316L stainless steel and nickel based alloys in high temperature aqueous environments," *Corros. Sci.*, vol. 42, no. 9, pp. 1635–1650, 2000.

[140] N. E. Hakiki, M. F. Montemor, M. G. S. Ferreira, and M. da Cunha Belo, "Semiconducting properties of thermally grown oxide films on AISI 304 stainless steel," *Corros. Sci.*, vol. 42, no. 4, pp. 687–702, 2000.

[141] N. E. Hakiki, M. Da Cunha Belo, A. M. P. Simoẽs, and M. G. S. Ferreira, "Semiconducting properties of passive films formed on stainless steels: Influence of the alloying elements," *J. Electrochem. Soc.*, vol. 145, no. 11, pp. 3821–3829, 1998.

[142] N. Sato, "An overview on the passivity of metal," *Corros. Sci.*, vol. 31, pp. 1–19, 1990.

[143] N. Mott, "No Title," *R. Soc. London*, vol. 171, no. Series A, p. 27, 1939.

[144] W. Schottky, "Zur Halbleitertheorie der Sperrschicht- und Spitzengleichrichter," *Nat. Sci.*, vol. 26, no. 843, pp. 1432–1904, 1938.

[145] I. G. Ogunsanya and C. M. Hansson, "The semiconductor properties of passive films and corrosion behaviour of stainless steel reinforcing bars in simulated concrete pore solution," *Materialia*, vol. 6, no. February, p. 100321, 2019.

[146] D. D. Macdonald, "The Point Defect Model for the passive state," *J. Electrochem. Soc.*, vol. 139, no. 12, p. 3434, 1992.

[147] D. D. Macdonald, "On the Existence of Our Metals-Based Civilization," *J. Electrochem. Soc.*, vol. 153, no. 7, p. B213, 2006.

[148] E. Sikora and D. D. Macdonald, "Nature of the passive film on nickel," *Electrochim. Acta*, vol. 48, no. 1, pp. 69–77, 2002.

[149] D. D. Macdonald, "Passivity–the key to our metals-based civilization," *Pure Appl. Chem.*, vol. 71, no. 6, pp. 951–978, 1999.

[150] E. Cho, H. Kwon, and D. D. Macdonald, “Photoelectrochemical analysis on the passive film formed on Fe-20Cr in pH 8.5 buffer solution,” *Electrochim. Acta*, vol. 47, no. 10, pp. 1661–1668, 2002.

[151] M. Sánchez, J. Gregori, C. Alonso, J. J. García-Jareño, H. Takenouti, and F. Vicente, “Electrochemical impedance spectroscopy for studying passive layers on steel rebars immersed in alkaline solutions simulating concrete pores,” *Electrochim. Acta*, vol. 52, no. 27 SPEC. ISS., pp. 7634–7641, 2007.

[152] L. Hamadou, A. Kadri, and N. Benbrahim, “Characterisation of passive films formed on low carbon steel in borate buffer solution (pH 9.2) by electrochemical impedance spectroscopy,” *Appl. Surf. Sci.*, vol. 252, no. 5, pp. 1510–1519, 2005.

[153] P. Ghods, O. B. Isgor, G. Mcrae, and T. Miller, “The effect of concrete pore solution composition on the quality of passive oxide films on black steel reinforcement,” *Cem. Concr. Compos.*, vol. 31, no. 1, pp. 2–11, 2009.

[154] J. J. Kim and Y. M. Young, “Study on the passive film of type 316 stainless steel,” *Int. J. Electrochem. Sci.*, vol. 8, no. 10, pp. 11847–11859, 2013.

[155] Z. Feng, X. Cheng, C. Dong, L. Xu, and X. Li, “Effects of dissolved oxygen on electrochemical and semiconductor properties of 316L stainless steel,” *J. Nucl. Mater.*, vol. 407, no. 3, pp. 171–177, 2010.

[156] I. H. Toor, M. Ejaz, and H. S. Kwon, “Mott–Schottky analysis of passive films on Cu containing Fe–20Cr–xCu (x=50, 4) alloys,” *Corrison Eng. Sci. Technol.*, vol. 49, no. 5, pp. 1–6, 2014.

[157] I. Toor, “Mott-Schottky Analysis of Passive Films on Si Containing Stainless,” *J. Electrochem. Soc.*, vol. 158, no. 11, pp. 391–395, 2011.

[158] H. Luo, C. F. Dong, X. G. Li, and K. Xiao, “The electrochemical behaviour of 2205 duplex stainless steel in alkaline solutions with different pH in the presence of chloride,” *Electrochim. Acta*, vol. 64, pp. 211–220, 2012.

[159] H. Tian, X. Cheng, Y. Wang, C. Dong, and X. Li, “Effect of Mo on interaction between a/g phases of duplex stainless steel,” *Electrochim. Acta*, vol. 267, pp. 255–268, 2018.

[160] X. Cheng, Y. Wang, C. Dong, and X. Li, “The beneficial galvanic effect of the constituent phases in 2205 duplex stainless steel on the passive films formed in a 3.5% NaCl solution,” *Corros. Sci.*, vol. 134, pp. 122–130, 2018.

[161] A. Poursaee, “Corrosion of steel bars in saturated Ca(OH)2 and concrete pore solution,” *Concr. Res. Lett.*, vol. 1, no. 3, pp. 90–97, 2010.

[162] M. Sánchez, J. Gregori, M. C. Alonso, J. J. García-Jareño, and F. Vicente, “Anodic growth of passive layers on steel rebars in an alkaline medium simulating the concrete pores,” *Electrochim. Acta*, vol. 52, no. 1, pp. 47–53, 2006.

[163] Y. F. Cheng and J. L. Luo, “Passivity and pitting of carbon steel in chromate solutions,” *Electrochim. Acta*, vol. 44, no. 26, pp. 4795–4804, 1999.

[164] D. G. Li, Y. R. Feng, Z. Q. Bai, J. W. Zhu, and M. S. Zheng, “Influence of temperature, chloride ions and chromium element on the electronic property of passive film formed on carbon steel in

bicarbonate/carbonate buffer solution," *Electrochim. Acta*, vol. 52, no. 28, pp. 7877–7884, 2007.

[165] J. Kang, Y. Yang, X. Jiang, and H. Shao, "Semiconducting properties of passive films formed on electroplated Ni and Ni – Co alloys," *Corros. Sci.*, vol. 50, no. 12, pp. 3576–3580, 2008.

[166] A. A. Valeria and M. A. B. Christopher, "Characterisation of passive films formed on mild steels in bicarbonate solution by EIS," *Electrochim. Acta*, vol. 47, pp. 2081–2091, 2002.

[167] H. P. Leckie and H. H. Uhlig, "Environmental Factors Affecting the Critical Potential for Pitting in 18–8 Stainless Steel," *J. Electrochem. Soc.*, vol. 113, no. 12, p. 1262, 1966.

[168] P. Marcus, V. Maurice, and H. H. Strehblow, "Localized corrosion (pitting): A model of passivity breakdown including the role of the oxide layer nanostructure," *Corros. Sci.*, vol. 50, no. 9, pp. 2698–2704, 2008.

[169] B. Beverskog and I. Puigdomenech, "Pourbaix diagrams for the ternary system of iron-chromium-nickel," *Corrosion*, vol. 55, no. 11, pp. 1077–1087, 1999.

[170] L. Tang *et al.*, "Experiences from RILEM TC 235-CTC in recommending a test method for chloride threshold values in concrete," *RILEM Tech. Lett.*, vol. 3, p. 25, 2018.

[171] G. K. Glass and N. R. Buenfeld, "The presentation of the chloride threshold level for corrosion of steel in concrete," *Corrosion Science*, vol. 39, no. 5. pp. 1001–1013, 1997.

[172] U. Angst, B. Elsener, C. K. Larsen, and Ø. Vennesland, "Critical chloride content in reinforced concrete - A review," *Cem. Concr. Res.*, vol. 39, no. 12, pp. 1122–1138, 2009.

[173] B. B. Hope and A. K. C. Ip, "Chloride corrosion threshold in concrete," *ACI Mater. J.*, pp. 306–314, 1987.

[174] K. W. J. Treadaway, R. N. Cox, and B. L. Brown, "Durability of corrosion resisting steels in concrete," *Proc. Inst. Civ. Eng. Part 1*, vol. 86, pp. 305–331, 1989.

[175] W. Morris, A. Vico, and M. Vazquez, "Chloride induced corrosion of reinforcing steel evaluated by concrete resistivity measurements," *Electrochim. Acta*, vol. 49, pp. 4447–4453, 2004.

[176] W. Morris, A. Vico, M. Vazquez, and S. R. De Sanchez, "Corrosion of reinforcing steel evaluated by means of concrete resistivity measurements," *Corros. Sci.*, vol. 44, pp. 81–99, 2002.

[177] M. D. A. Thomas, "Field studies of fly ash concrete structures containing reactive aggregates," *Mag. Concr. Res.*, vol. 48, no. 177, pp. 265–279, 1996.

[178] M. D. A. Thomas and P. B. Bamforth, "Modelling chloride diffusion in concrete effect of fly ash and slag," *Cem. Concr. Res.*, vol. 29, no. 4, pp. 487–495, 1999.

[179] P. Sandberg, "Studies of chloride binding in concrete exposed in a marine environment," *Cem. Concr. Res.*, vol. 29, no. 4, pp. 473–477, 1999.

[180] G. Williams, H. A. L. Dafydd, and H. N. Mcmurray, "Chloride Ion Concentration Effects on Passivity Breakdown in Magnesium," *224th ECS Meet.*, vol. 73, no. i, p. 2013, 2017.

[181] P. Ghods, O. B. Isgor, G. A. McRae, and G. P. Gu, "Electrochemical investigation of chloride-induced depassivation of black steel rebar under simulated service conditions," *Corros. Sci.*, vol. 52, no. 5, pp. 1649–1659, 2010.

[182] B. Elsener, D. Addari, S. Coray, and A. Rossi, “Stainless steel reinforcing bars - Reason for their high pitting corrosion resistance,” *Mater. Corros.*, vol. 62, no. 2, pp. 111–119, 2011.

[183] P. Ghods, O. B. Isgor, G. A. McRae, J. Li, and G. P. Gu, “Microscopic investigation of mill scale and its proposed effect on the variability of chloride-induced depassivation of carbon steel rebar,” *Corros. Sci.*, vol. 53, no. 3, pp. 946–954, 2011.

[184] A. Poursaee, “Potentiostatic transient technique, a simple approach to estimate the corrosion current density and Stern-Geary constant of reinforcing steel in concrete,” *Cem. Concr. Res.*, vol. 40, no. 9, pp. 1451–1458, 2010.

[185] C. B. Van Niejenhuis, S. Walbridge, and C. M. Hansson, “The performance of austenitic and duplex stainless steels in cracked concrete exposed to concentrated chloride brine,” *J. Mater. Sci.*, vol. 51, no. 1, pp. 362–374, 2016.

[186] A. Poursaee, “Determining the appropriate scan rate to perform cyclic polarization test on the steel bars in concrete,” *Electrochim. Acta*, vol. 55, no. 3, pp. 1200–1206, 2010.

[187] N. Nakayama and A. Obuchi, “Inhibitory effects of 5-aminouracil on cathodic reactions of steels in saturated Ca(OH)2 solutions,” *Corros. Sci.*, vol. 45, pp. 2075–2092, 2003.

[188] B. Elsener, L. Zimmermann, D. Fluckiger, D. Burchler, and H. Bohni, “Chloride penetration - non destructive determination of the free chloride content in mortar and concrete,” in *Proc. RILEM Int. Workshop “Chloride penetration into concrete,”* 1997.

[189] P. Schiessl and M. Raupach, “Influence of concrete composition and microclimate on the critical chloride content in concrete,” in *Proc. 3rd Int. Symp. “Corrosion of Reinforcment in Concrete”, Elsevier Applied Science*, 1990, pp. 49–58.

[190] K. Pettersson, “Chloride threshold value and the corrosion rate in reinforced concrete,” in *Proc. of the Nordic Seminar, Lund*, 1995, pp. 257–266.

[191] K. Pettersson, “Corrosion threshold value and corrosion rate in reinforced concrete,” *CBI Rep. 292, Swedish Cem. Concr. Res. Inst.*, 1992.

[192] C. L. Page, P. Lambert, and P. R. W. Vassie, “Investigations of reinforcement corrosion. 1. The pore electrolyte phase in chloride-contaminated concrete,” *Mater. Struct.*, vol. 24, pp. 243–252, 1991.

[193] P. Lambert, C. L. Page, and P. R. W. Vassie, “Investigations of reinforcement corrosion. 2. Electrochemical monitoring of steel in chloride-contaminated concrete,” *Mater. Struct.*, vol. 24, pp. 351–358, 1991.

[194] U. M. Angst, C. Boschmann, M. Wagner, and B. Elsener, “Experimental Protocol to Determine the Chloride Threshold Value for Corrosion in Samples Taken from Reinforced Concrete Structures,” *J. Vis. Exp.*, no. 126, pp. 1–11, 2017.

[195] H. Zibara, “Binding of External Chlorides by Cement Pastes,” *Dep. Build. Mater. PhD thesis, Univ. Toronto, Canada*, pp. 1–320, 2001.

[196] A. K. Suryavanshi, J. D. Scantlebury, and S. B. Lyon, “The binding of chloride ions by sulphate resistant portland cement,” *Cem. Concr. Res.*, vol. 25, no. 3, pp. 581–592, 1995.

[197] Q. Yuan, C. Shi, G. De Schutter, K. Audenaert, and D. Deng, “Chloride binding of cement-based

materials subjected to external chloride environment - A review," *Constr. Build. Mater.*, vol. 23, no. 1, pp. 1–13, 2009.

[198] N. F. Mott, "The theory of crystal rectifiers," *R. Soc. London*, vol. 171, no. 944, pp. 153–165, 1939.

[199] H. Wu, Y. Wang, Q. Zhong, M. Sheng, H. Du, and Z. Li, "The semi-conductor property and corrosion resistance of passive film on electroplated Ni and Cu – Ni alloys," *J. Electroanal. Chem.*, vol. 663, no. 2, pp. 59–66, 2011.

[200] Kyle A. Anders, "The Effect of Surface and Loading Conditions on the Corrosion Performance of Stainless Steel Rebar," *MASc thesis Mech. Mechatronics Eng. Univ. Waterloo*, 2009.

[201] E. Hamada *et al.*, "Direct imaging of native passive film on stainless steel by aberration corrected STEM," *Corros. Sci.*, vol. 52, no. 12, pp. 3851–3854, 2010.

[202] W. A. Badawy and F. M. Al-Kharafi, "Corrosion and passivation behaviors of molybdenum in aqueous solutions of different pH," *Electrochim. Acta*, vol. 44, no. 4, pp. 693–702, 1998.

[203] T. J. Mesquita, E. Chauveau, M. Mantel, N. Kinsman, and R. P. Nogueira, "Influence of Mo alloying on reinforcement steels used as concrete pitting corrosion of stainless," *Metall. Mater.*, vol. 66, no. 2, pp. 173–178, 2013.

[204] T. J. Mesquita, E. Chauveau, M. Mantel, N. Kinsman, and R. P. Nogueira, "Anomalous corrosion resistance behavior of Mo-containing SS in alkaline media: The role of microstructure," *Mater. Chem. Phys.*, vol. 126, no. 3, pp. 602–606, 2011.

[205] T. J. Mesquita, E. Chauveau, M. Mantel, and R. P. Nogueira, "A XPS study of the Mo effect on passivation behaviors for highly controlled stainless steels in neutral and alkaline conditions," *Appl. Surf. Sci.*, vol. 270, pp. 90–97, 2013.

[206] B. Beverskog and I. Puigdomenech, "Revised Pourbaix diagrams for iron at 25-300°C," *Corros. Sci.*, vol. 38, no. 12, pp. 2121–2135, 1996.

[207] B. Beverskog and I. Puigdomenech, "Revised Pourbaix Diagrams for Cr at 25C-300C.pdf," *Corros. Sci.*, vol. 39, no. 1, pp. 43–57, 1997.

[208] B. Beverskog and I. Puigdomenech, "Revised pourbaix diagrams for nickel at 25-300°C," *Corros. Sci.*, vol. 39, no. 5, pp. 969–980, 1997.

[209] H. Luo, H. Su, C. Dong, and X. Li, "Passivation and electrochemical behavior of 316L stainless steel in chlorinated simulated concrete pore solution," *Appl. Surf. Sci.*, vol. 400, pp. 38–48, 2017.

[210] L. A. Shaik and S. K. Thamida, "Simulation of corrosion of a dual phase alloy steel based on its constituent phase polarization properties," *Materialia*, vol. 2, pp. 183–189, 2018.

[211] D. Boubitsas and L. Tang, "The influence of reinforcement steel surface condition on initiation of chloride induced corrosion," *Mater. Struct. Constr.*, vol. 48, no. 8, pp. 2641–2658, 2015.

[212] T. U. Mohammed and H. Hamada, "Corrosion of steel bars in concrete with various steel surface conditions," *ACI Mater. J.*, vol. 103, no. 4, pp. 233–242, 2006.

[213] X. Feng, X. Lu, Y. Zuo, and D. Chen, "The passive behaviour of 304 stainless steels in saturated calcium hydroxide solution under different deformation," *Corros. Sci.*, vol. 82, pp. 347–355, 2014.

[214] X. Feng, X. Lu, Y. Zuo, N. Zhuang, and D. Chen, "The effect of deformation on metastable pitting

of 304 stainless steel in chloride contaminated concrete pore solution," *Corros. Sci.*, vol. 103, pp. 223–229, 2016.

[215] A. Knudsen, O. Klinghoffer, and T. Skovsgaard, "Pier in Progreso, Mexico. Inspection Report," Arminox Stainless, Denmark, 1999.

[216] A. Bautista, G. Blanco, and F. Velasco, "Corrosion behaviour of low-nickel austenitic stainless steels reinforcements: A comparative study in simulated pore solutions," *Cem. Concr. Res.*, vol. 36, no. 10, pp. 1922–1930, 2006.

[217] G. N. Flint and R. N. Cox, "The resistance of stainless steel partly embedded in concrete to corrosion by seawater," *Mag Concr Res*, vol. 40, no. 142, pp. 13–27, 1988.

[218] L. Veleva, M. A. Alpuche-Aviles, M. K. Graves-Brook, and D. O. Wipf, "Comparative cyclic voltammetry and surface analysis of passive films grown on stainless steel 316 in concrete pore model solutions," *J. Electroanal. Chem.*, vol. 537, no. 1–2, pp. 85–93, 2002.

[219] C. M. Abreu, M. J. Cristóbal, R. Losada, X. R. Nóvoa, G. Pena, and M. C. Pérez, "High frequency impedance spectroscopy study of passive films formed on AISI 316 stainless steel in alkaline medium," *J. Electroanal. Chem.*, vol. 572, no. 2, pp. 335–345, 2004.

[220] L. Bertolini and P. Pedeferri, "Laborartory and field experience on the use of stainless steel to improve durability of reinforced concrete," *Corrosion Reviews*, vol. 20. p. 129, 2002.

[221] L. Bertolini, M. Gastaldi, P. Pedeferri, and E. Redaelli, "Factors influencing the corrosion resistance of austenitic and duplex stainless steel bars in chloride bearing concrete," in *15th International Corrosion Congress, paper 382*, 2002, p. paper 382.

[222] A. Bautista, G. Blanco, and F. Velasco, "Corrosion resistance in Ca(OH)2 solutions with chlorides of austenitic and duplex stainless steels rebars," in *VII National Materials Congress*, 2004.

[223] V. S. RAJA and A. RAMKUMAR, "Technical note Comparative study of intergranular corrosion behaviour of three high manganese austenitic stainless steels," *Br. Corros. J.*, vol. 31, no. 2, pp. 153–157, Jan. 1996.

[224] A. Di Schino and J. M. Kenny, "Effect of grain size on the corrosion resistance of a high nitrogen-low nickel austenitic stainless steel," *J. Mater. Sci. Lett.*, vol. 21, pp. 1969–1971, 2002.

[225] G. Rondelli, B. Vicentini, and A. Cigada, "Influence of nitrogen and manganese on localized corrosion behaviour of stainless steels in chloride environment," *Mater. Corros.*, vol. 46, no. 11, pp. 628–632, 1995.

[226] I. G. Ogunsanya, "Reproducibility of the corrosion resistance of stainless steel reinforcing bars - PRESENTATION," *Corrosion*, vol. online, no. https://doi.org/10.5006/3360, 2019.

[227] I. G. Ogunsanya and C. M. Hansson, "Influence of chloride and sulphate anions on the electronic and electrochemical properties of passive films formed on steel reinforcing bars," *Materialia*, vol. 8, no. September, p. 100491, 2019.

[228] I. G. Ogunsanya and C. M. Hansson, "The Influence of Coating Thickness and Composition on the Corrosion Propagation Rates of Galvanized Rebar in Cracked Concrete," *Corrosion*, vol. 74, no. 1, pp. 134–143, 2017.

[229] P. Pedeferri, L. Bertolini, F. Bolzoni, and T. Pastore, "Behavior of Stainless Steels in Concrete," in

Proceedings of the International Seminar: The State of the Art of the Repair and Rehabilitation of Reinforced Concrete Structures Eds. W.F. Silver-Araya, O.T. De Rincon, L.P. O'Neill, (Reston, VA: ASCE), 1998, p. 192.

[230] B. Sorensen, P. B. Jensen, and E. Maahn, "The Corrosion Properties of Stainless Steel Reinforcement," in *C.L. Page, K.W.J. Treadaway, P.B. Bamworth, eds. Corrosion of Reinforcement in Concrete, Wishaw, UK. Elsevier Applied Science*, 1990, pp. 601–610.

[231] M. C. García-Alonso *et al.*, "Corrosion behaviour of innovative stainless steels in mortar," *Cem. Concr. Res.*, vol. 37, no. 11, pp. 1562–1569, 2007.

[232] H. Mahmoud, M. Sanchez, and M. C. Alonso, "Ageing of the spontaneous passive state of 2304 duplex stainless steel in high-alkaline conditions with the presence of chloride," *J. Solid State Electrochem.*, vol. 19, no. 10, pp. 2961–2972, 2015.

[233] S. G. Balakumaran, R. E. Weyers, and M. . Brown, "Linear Cracking in Bridge Decks, Final Report VTRC 18-R13," *Virginia Dep. Transp. March*, 2018.

[234] L. F. Li, P. Caenen, and J. P. Celis, "Chemical pickling of 304 stainless steel in fluoride- And sulfate-containing acidic electrolytes," *J. Electrochem. Soc.*, vol. 152, no. 9, pp. 352–357, 2005.

[235] S. D. Cramer *et al.*, "Corrosion prevention and remediation strategies for reinforced concrete coastal bridges," *Cem. Concr. Compos.*, vol. 24, no. 1, pp. 101–117, 2002.

[236] ASSDA, "Pickling and Passivation - Brisbane, Australia," *Australian Stainless Steel Development Association*, 2008. [Online]. Available: http://www.assda.asn.au/index.php?option=com_content&task=view&id=78&Itemid=103.

[237] Canadian Standards Association (CSA), "Canadian highway bridge design code S6-14," *CSA*, 2014.

[238] A. Djerbi, S. Bonnet, A. Khelidj, and V. Baroghel-bouny, "Influence of traversing crack on chloride diffusion into concrete," *Cem. Concr. Res.*, vol. 38, no. 6, pp. 877–883, 2008.

[239] C. L. Page, "Initiation of chloride-induced corrosion of steel in concrete: role of the interfacial zone," *Mater. Corros.*, vol. 60, no. 8, pp. 586–592, Aug. 2009.

[240] U. M. Angst *et al.*, "The steel – concrete interface," *Mater. Struct.*, vol. 50:143, 2017.

[241] M. Schönning and S. Randström, "Adaptation of EN 480-14:2006 as a Test Method for Determining a Critical Chloride Threshold Level for Stainless Steel Rebar," in *EUROCORR*, 2011, p. paper no. 4903.

[242] A. A276/276M, "Standard Specification for Stainless Steel Bars and Shapes," *ASTM Int.*, pp. 1–8, 2017.

[243] G. S. Frankel, "Pitting corrosion of metals," *J. Electrochem. Soc.*, vol. 145, no. 6, p. 2186, 1998.

[244] Z. Szklarska-Smialowska, "Mechanism of pit nucleation by electrical breakdown of the passive film," *Corros. Sci.*, vol. 44, no. 5, pp. 1143–1149, 2002.

Appendix

A. Appendix information from the published journal in Chapter 4

Tables A-1 – A-6 present the electronic and electrochemical properties of three replicates of each grade of bars tested in the three different pore solution.

Table A-1. Corrosion and film semiconductor data for 2304 bars tested in CH solution, with the N_x and d_x values defined in Figure 4-4.

Chloride addition		**Electronic properties**										
		i_{CORR} (mA/m^2)	E_{CORR} (mV$_{SCE}$)	E_{FB} (mV$_{SCE}$)	N_1 (10^{21} cm^{-3})	N_2 (10^{21} cm^{-3})	N_3 (10^{21} cm^{-3})	N_4 (10^{21} cm^{-3})	d_1 (nm)	d_2 (nm)	d_3 (nm)	d_4 (nm)
0%	**1**	0.07	-145	-1003	7.62	3.20	2.35	1.59	0.68	0.89	0.74	0.39
	2	0.09	-135	-1310	0.89	0.74	0.32	0.39	1.17	1.34	1.21	1.00
	3	0.08	-133	-1330	2.42	1.49	0.79	1.09	0.83	1.09	0.88	0.63
6%	**1**	0.31	-185	-920	12.27	5.89	2.87	2.92	0.30	0.47	0.36	0.17
	2	0.28	-164	-975	7.99	3.51	1.76	1.66	0.42	0.63	0.48	0.25
	3	0.51	-163	-963	10.49	4.76	2.20	2.46	0.36	0.54	0.41	0.24
12%	**1**	1.60	-220	-880	13.89	9.28	4.63	3.94	0.22	0.37	0.30	0.14
	2	1.10	-198	-900	9.56	5.78	2.69	2.45	0.31	0.49	0.39	0.23
	3	1.30	-230	-900	12.16	7.08	3.72	3.38	0.29	0.44	0.34	0.22
18%	**1**	2.60	-276	-860	15.40	9.53	4.86	4.45	0.21	0.36	0.31	0.16
	2	1.50	-240	-860	10.53	6.84	3.41	2.94	0.27	0.44	0.35	0.22
	3	1.53	-260	-840	14.38	8.14	4.39	3.87	0.24	0.40	0.31	0.19
21%	**1**	6.17	-310	-840	18.68	10.27	5.27	5.19	0.19	0.34	0.30	0.16
	2	5.10	-286	-840	10.91	7.06	3.65	3.01	0.26	0.43	0.34	0.23
	3	5.80	-302	-800	14.88	8.89	4.87	4.05	0.21	0.37	0.29	0.18

Table A-2. Corrosion and film semiconductor data for 2304 bars tested in PS solution, with the N_x and d_x values defined in Figure 4-4. The first replicate was tested between -1 and 0.4 V_{SCE} and, as a result, did not show linear regions to calculate N_1 and N_4.

Chloride addition		**Electronic properties**										
		i_{CORR} (mA/m^2)	E_{CORR} (mV$_{SCE}$)	E_{FB} (mV$_{SCE}$)	N_1 (10^{21} cm^{-3})	N_2 (10^{21} cm^{-3})	N_3 (10^{21} cm^{-3})	N_4 (10^{21} cm^{-3})	d_1 (nm)	d_2 (nm)	d_3 (nm)	d_4 (nm)
0%	**1**	0.03	-104	-980		5.97	2.65		0.26	0.41	0.46	
	2	0.02	-83	-1070	10.40	6.44	3.99	7.51	0.22	0.29	0.20	0.04
	3	0.05	-79	-990	8.83	7.44	3.89	8.74	0.20	0.27	0.18	0.04
6%	**1**	0.12	-169	-860		6.49	3.87		0.24	0.39	0.38	
	2	0.08	-152	-997	10.11	8.73	5.05	7.66	0.18	0.23	0.19	0.03

	3	0.13	-145	-970	11.64	9.66	4.67	9.40	0.16	0.22	0.17	0.03
12%	**1**	0.70	-182	-850		8.63	4.98		0.22	0.37	0.37	
	2	0.55	-171	-990	10.08	11.65	5.51	8.37	0.16	0.21	0.18	0.02
	3	0.80	-166	-960	10.59	12.00	5.37	9.65	0.15	0.20	0.17	0.02
18%	**1**	0.91	-198	-861		9.80	5.29		0.21	0.36	0.35	
	2	1.20	-193	-992	10.98	13.08	6.17	8.66	0.15	0.19	0.15	0.01
	3	1.07	-188	-960	11.41	13.21	6.29	11.21	0.14	0.18	0.13	0.01
21%	**1**	2.14	-242	-840		10.95	6.47	1.22	0.16	0.33	0.29	0.06
	2	2.63	-266	-970	10.91	14.75	6.76	9.60	0.13	0.18	0.15	0.01
	3	2.90	-221	-920	13.41	15.24	7.18	13.63	0.12	0.17	0.13	0.01

Table A-3. Corrosion and film semiconductor data for 2304 bars tested in PS+S solution, with the N_x and d_x values defined in Figure 4-4.

Chloride addition		**Electronic properties**										
		i_{CORR} (mA/m^2)	E_{CORR} (mV$_{SCE}$)	E_{FB} (mV$_{SCE}$)	N_1 (10^{21} cm^{-3})	N_2 (10^{21} cm^{-3})	N_3 (10^{21} cm^{-3})	N_4 (10^{21} cm^{-3})	d_1 (nm)	d_2 (nm)	d_3 (nm)	d_4 (nm)
0%	**1**	0.01	-87	-1063	14.88	8.63	8.34	4.40	0.22	0.22	0.07	0.05
	2	0.04	-92	-1050	14.13	7.76	6.86	3.91	0.19	0.27	0.27	0.05
	3	0.02	-96	-1120	12.14	6.00	4.38	2.35	0.22	0.29	0.25	0.06
6%	**1**	0.08	-87	-979	6.48	6.64	4.32	3.08	0.20	0.28	0.30	0.07
	2	0.09	-131	-980	11.39	7.12	4.64	3.54	0.20	0.27	0.28	0.05
	3	0.08	-125	-1020	7.79	5.56	3.53	2.99	0.22	0.30	0.31	0.05
12%	**1**	0.17	-92	-940	3.14	4.18	2.52	2.07	0.23	0.35	0.44	0.12
	2	0.26	-120	-970	6.11	6.80	3.99	3.43	0.21	0.28	0.19	0.04
	3	0.38	-132	-990	4.36	4.65	3.63	2.79	0.23	0.33	0.37	0.06
18%	**1**	0.92	-142	-850	2.45	3.29	1.74	1.69	0.24	0.39	0.51	0.22
	2	0.67	-146	-950	4.79	5.22	3.37	2.89	0.22	0.31	0.34	0.06
	3	0.45	-162	-930	4.09	4.47	2.80	2.53	0.27	0.36	0.23	0.05
21%	**1**	1.09	-188	-820	2.41	3.10	1.71	1.52	0.23	0.39	0.54	0.23
	2	1.55	-170	-890	4.17	4.38	2.61	1.83	0.21	0.34	0.46	0.11
	3	1.40	-201	-910	3.66	3.78	2.29	1.47	0.24	0.37	0.51	0.10

Table A-4. Corrosion and film semiconductor data for carbon steel bars tested in CH solution, with the N_x and d_x values defined in Figure 4-4.

	Electronic properties

Chloride addition		i_{CORR} (mA/m^2)	E_{CORR} (mV$_{SCE}$)	E_{FB} (mV$_{SCE}$)	N_1	N_2 (10^{21} cm^{-3})	N_3 (10^{21} cm^{-3})	N_4 (10^{21} cm^{-3})	d_1	d_2 (nm)	d_3 (nm)	d_4 (nm)
0%	**1**	0.50	-140	-716		0.10	0.23	0.04		1.22	2.89	2.58
	2	0.30	-163	-648		0.16	0.27	0.05		0.76	2.24	1.95
	3	0.40	-155	-620		0.36	0.59	0.08		0.49	1.54	1.16
0.6%	**1**	2.67	-233	-770		11.02				0.69	1.09	0.86
	2	1.98	-280	-668		14.04				0.58	0.90	0.68
	3	2.30	-275	-701		12.78				0.37	0.64	0.56
1.2%	**1**	4.40	-345	-771		27.69				0.22	0.52	0.39
	2	3.74	-348	-720		36.65				0.16	0.35	0.27
	3	2.90	-316	-740		39.41				0.07	0.17	0.15
1.8%	**1**	10.7	-414									
	2	12.1	-409									
	3	8.9	-405									
2.4%	**1**	19.3	-428									
	2	17.9	-439									
	3	12.5	-465									

Table A-5. Corrosion and film semiconductor data for carbon steel bars tested in PS solution, with the N_x and d_x values defined in Figure 4-4.

Chloride addition		**Electronic properties**										
		i_{CORR} (mA/m^2)	E_{CORR} (mV$_{SCE}$)	E_{FB} (mV$_{SCE}$)	N_1	N_2 (10^{21} cm^{-3})	N_3 (10^{21} cm^{-3})	N_4 (10^{21} cm^{-3})	d_1	d_2 (nm)	d_3 (nm)	d_4 (nm)
0%	**1**	0.19	-161	-684		56	15	7		0.06	0.18	0.022
	2	0.28	-143	-637		67	20	9		0.06	0.11	0.083
	3	0.22	-159	-613		25	13	5		0.11	0.20	0.139
0.6%	**1**	1.01	-170	-710		183	98	34		0.04	0.07	0.025
	2	1.10	-181	-651		328	153	53		0.01	0.04	0.011
	3	1.03	-192	-624		295	132	41		0.02	0.05	0.017
1.2%	**1**	1.39	-252	-713		665	295	99		0.01	0.03	0.004
	2	2.50	-280	-707		551	299	89		0.02	0.04	0.009
	3	2.20	-311	-658		535	246	99		0.01	0.03	0.010
1.8%	**1**	2.4	-352	-701		675	268	103		0.01	0.03	0.006
	2	3.1	-341	-710		771	215	111		0.03	0.04	0.035
	3	3.3	-324	-676		711	321	112		0.01	0.03	0.006
2.4%	**1**	5.2	-391	-704		918	456	145		0.01	0.03	0.004
	2	4.2	-381	-680		1379	551	194		0.00	0.02	0.002

	3	4.5	-367	-684		736	327	124		0.01	0.03	0.009

Table A-6. Corrosion and film semiconductor data for carbon steel bars tested in PS+S solution, with the N_x and d_x values defined in Figure 4-4.

Chloride addition		**Electronic properties**										
		i_{CORR} (mA/m^2)	E_{CORR} (mV$_{SCE}$)	E_{FB} (mV$_{SCE}$)	N_1	N_2 (10^{21} cm^{-3})	N_3 (10^{21} cm^{-3})	N_4 (10^{21} cm^{-3})	d_1	d_2 (nm)	d_3 (nm)	d_4 (nm)
0%	**1**	0.26	-167	-631		118	45	28		0.05	0.05	0.00
	2	0.17	-163	-613		104	19	19		0.04	0.07	0.06
	3	0.33	-161	-734		35	17	21		0.04	0.08	0.06
0.6%	**1**	0.32	-158	-630		192	105	24		0.04	0.07	0.04
	2	0.30	-201	-650		161	68	26		0.04	0.08	0.03
	3	0.38	-185	-580		116	53	18		0.06	0.10	0.04
1.2%	**1**	0.52	-211	-660		150	94	21		0.04	0.08	0.05
	2	0.63	-225	-701		91	66	14		0.02	0.09	0.04
	3	0.71	-241	-650		107	52	15		0.08	0.12	0.06
1.8%	**1**	1.2	-275	-702		108	76	16		0.06	0.10	0.07
	2	1.6	-301	-680		65	62	12		0.12	0.15	0.14
	3	1.5	-290	-666		76	51	15		0.12	0.15	0.14
2.4%	**1**	2.2	-325	-801		67	76	12		0.08	0.12	0.09
	2	3.8	-336	-744		208	134	10		0.20	0.22	0.20
	3	3.1	-329	-697		157	87	6		0.17	0.19	0.20

B. Appendix information from the published journal in Chapter 6

Tables B-1 – B-6 present the electronic and electrochemical properties of three replicates of each grade of the as-received steels tested in pore solution.

Table B-7. Corrosion and film semiconductor data for as-received 304L bars tested in pore solution, with the N_x and d_x values defined in Figure 6-2.

Chloride addition		**Electronic properties**										
		i_{CORR} (mA/ m^2)	E_{CORR} (mV$_{SCE}$)	E_{FB} (mV$_{SCE}$)	N_1 (10^{21} cm^{-3})	N_2 (10^{21} cm^{-3})	N_3 (10^{21} cm^{-3})	N_4 (10^{21} cm^{-3})	d_1 (nm)	d_2 (nm)	d_3 (nm)	d_4 (nm)
0%	**1**	0.02	-83	-1020	1.13	1.10	0.65	0.65	0.55	0.75	0.76	0.18
	2	0.01	-133	-1030	1.08	1.27	0.84	0.90	0.49	0.67	0.66	0.22

	3	0.01	-139	-990	1.52	1.77	1.03	1.42	0.40	0.55	0.48	0.12
6%	**1**	0.08	-94	-910	2.68	1.20	1.08	0.70	0.43	0.68	0.82	0.21
	2	0.24	-134	-950	3.21	2.04	1.02	1.24	0.38	0.55	0.53	0.13
	3	0.10	-141	-970	4.33	2.65	1.30	1.51	0.38	0.42	0.52	0.41
12%	**1**	0.55	-138	-900	4.20	1.41	1.21	1.12	0.39	0.61	0.77	0.13
	2	0.50	-135	-944	4.69	2.04	1.38	1.44	0.33	0.51	0.55	0.09
	3	0.70	-136	-870	5.15	2.67	1.77	1.97	0.27	0.44	0.44	0.05
18%	**1**	1.06	-164	-900	4.25	1.43	1.31	1.44	0.39	0.62	0.94	0.24
	2	0.51	-147	-942	5.67	2.32	1.63	1.49	0.34	0.48	0.47	0.08
	3	1.04	-149	-850	6.06	2.88	1.89	2.23	0.28	0.42	0.34	0.04
21%	**1**	1.38	-183	-845	5.75	1.53	1.95	1.53	0.33	0.57	0.85	0.19
	2	1.17	-175	-910	6.16	2.96	1.66	1.53	0.36	0.42	0.48	0.42
	3	1.34	-191	-810	6.15	2.95	1.94	2.48	0.24	0.41	0.37	0.02

Table B-8. Corrosion and film semiconductor data for as-received 316LN bars tested in pore solution, with the N_x and d_x values defined in Figure 6-2.

Chloride addition		**Electronic properties**										
		i_{CORR} (mA/m^2)	E_{CORR} (mV$_{SCE}$)	E_{FB} (mV$_{SCE}$)	N_1 (10^{21} cm^{-3})	N_2 (10^{21} cm^{-3})	N_3 (10^{21} cm^{-3})	N_4 (10^{21} cm^{-3})	d_1 (nm)	d_2 (nm)	d_3 (nm)	d_4 (nm)
0%	**1**	0.01	-148	-920	3.54	2.03	1.37	0.84	0.34	0.50	0.47	0.08
	2	0.01	-161	-1010	5.69	2.62	1.56	1.78	0.34	0.45	0.42	0.13
	3	0.02	-138	-990	4.17	2.21	1.35	1.64	0.36	0.48	0.43	0.12
6%	**1**	0.04	-160	-900	6.39	3.26	2.18	1.76	0.25	0.40	0.46	0.09
	2	0.05	-174	-980	6.28	3.69	2.10	2.62	0.27	0.38	0.34	0.08
	3	0.07	-144	-980	6.29	3.38	2.03	2.43	0.27	0.39	0.35	0.07
12%	**1**	0.55	-166	-870	7.19	4.29	2.42	2.24	0.21	0.34	0.40	0.04

	2	0.25	-201	-970	7.87	4.5	2.45	2.95	0.25	0.35	0.33	0.10
	3	0.53	-152	-950	6.96	4.25	2.39	2.94	0.25	0.35	0.32	0.08
18%	**1**	0.81	-169	-860	7.82	5.07	3.16	3.15	0.19	0.31	0.32	0.01
	2	0.70	-224	-962	8.13	5.03	2.84	3.95	0.22	0.31	0.28	0.05
	3	0.65	-208	-950	8.05	4.89	2.67	3.82	0.22	0.32	0.28	0.04
21%	**1**	1.43	-216	-850	9.15	5.09	3.57	3.17	0.19	0.31	0.34	0.02
	2	1.74	-224	-955	8.44	5.19	3.59	4.02	0.22	0.32	0.28	0.04
	3	1.90	-278	-940	8.39	5.12	3.46	4.22	0.22	0.41	0.26	0.03

Table B-9. Corrosion and film semiconductor data for as-received 24100 bars tested in pore solution, with the N_x and d_x values defined in Figure 6-2. The first replicate was tested between -1 and 0.6 V_{SCE} and, as a result, did not show linear regions to calculate N_1 and N_4.

Chloride addition		**Electronic properties**										
		i_{CORR} (mA/m^2)	E_{CORR} (mV$_{SCE}$)	E_{FB} (mV$_{SCE}$)	N_1 (10^{21} cm^{-3})	N_2 (10^{21} cm^{-3})	N_3 (10^{21} cm^{-3})	N_4 (10^{21} cm^{-3})	d_1 (nm)	d_2 (nm)	d_3 (nm)	d_4 (nm)
0%	**1**	0.03	-155	-1031		1.21	1.28		0.45	0.59	0.65	
	2	0.02	-149	-1111	1.98	2.42	1.83	1.34	0.35	0.47	0.55	0.17
	3	0.03	-134	-1100	2.18	2.75	2.00	1.47	0.32	0.44	0.52	0.16
6%	**1**	0.11	-203	-988		1.47	1.31		0.37	0.53	0.68	
	2	0.21	-180	-1067	1.99	3.27	2.02	1.41	0.33	0.42	0.53	0.15
	3	0.20	-170	-1096	2.00	3.57	2.19	1.70	0.30	0.39	0.48	0.13
12%	**1**	0.36	-219	-980		1.61	1.62		0.32	0.45	0.59	
	2	0.48	-228	-1060	2.12	4.02	2.67	1.79	0.29	0.37	0.46	0.11
	3	0.42	-239	-1050	2.05	4.31	2.74	2.19	0.27	0.34	0.42	0.09
18%	**1**	1.05	-223	-971		2.52	1.76		0.27	0.41	0.52	
	2	1.19	-244	-1063	2.17	4.13	2.80	1.91	0.27	0.36	0.45	0.11
	3	1.41	-248	-1040	2.16	4.53	2.90	2.19	0.27	0.35	0.42	0.10

21%	**1**	2.33	-233	-970		2.96	1.88		0.26	0.43	0.48	
	2	2.91	-256	-1040	2.56	4.66	3.08	2.15	0.26	0.34	0.42	0.10
	3	3.50	-253	-1030	2.48	4.82	3.07	2.43	0.26	0.31	0.40	0.09

Table B-10. Corrosion and film semiconductor data for as-received 2304 bars tested in pore solution, with the N_x and d_x values defined in Figure 6-2. The first replicate was tested between -1 and 0.6 V_{SCE} and, as a result, did not show linear regions to calculate N_1 and N_4.

Chloride addition		**Electronic properties**										
		i_{CORR} (mA/m^2)	E_{CORR} (mV$_{SCE}$)	E_{FB} (mV$_{SCE}$)	N_1 (10^{21} cm^{-3})	N_2 (10^{21} cm^{-3})	N_3 (10^{21} cm^{-3})	N_4 (10^{21} cm^{-3})	d_1 (nm)	d_2 (nm)	d_3 (nm)	d_4 (nm)
0%	**1**	0.03	-104	-880		5.97	2.65		0.26	0.41	0.46	
	2	0.02	-83	-1070	10.40	6.44	3.99	7.51	0.22	0.29	0.20	0.04
	3	0.05	-79	-990	8.83	7.44	3.89	8.74	0.20	0.27	0.18	0.04
6%	**1**	0.12	-169	-860		6.49	3.87		0.24	0.39	0.38	
	2	0.08	-152	-997	10.11	8.73	5.05	7.66	0.18	0.23	0.19	0.03
	3	0.13	-145	-970	11.64	9.66	4.67	9.40	0.16	0.22	0.17	0.03
12%	**1**	0.70	-182	-850		8.63	4.98		0.22	0.37	0.37	
	2	0.55	-171	-990	10.08	11.65	5.51	8.37	0.16	0.21	0.18	0.02
	3	0.80	-166	-960	10.59	12.00	5.37	9.65	0.15	0.20	0.17	0.02
18%	**1**	0.91	-198	-861		9.80	5.29		0.21	0.36	0.35	
	2	1.20	-193	-992	10.98	13.08	6.17	8.66	0.15	0.19	0.15	0.01
	3	1.07	-188	-960	11.41	13.21	6.29	11.21	0.14	0.18	0.13	0.01
21%	**1**	2.14	-242	-840		10.95	6.47	1.22	0.16	0.33	0.29	0.06
	2	2.63	-266	-970	10.91	14.75	6.76	9.60	0.13	0.18	0.15	0.01
	3	2.90	-221	-920	13.41	15.24	7.18	13.63	0.12	0.17	0.13	0.00

Table B-11. Corrosion and film semiconductor data for as-received 2205 bars tested in pore solution, with the N_x and d_x values defined in Figure 6-2.

Chloride addition		**Electronic properties**										
		i_{CORR} (mA/m^2)	E_{CORR} (mV$_{SCE}$)	E_{FB} (mV$_{SCE}$)	N_1 (10^{21} cm^{-3})	N_2 (10^{21} cm^{-3})	N_3 (10^{21} cm^{-3})	N_4 (10^{21} cm^{-3})	d_1 (nm)	d_2 (nm)	d_3 (nm)	d_4 (nm)
0%	**1**	0.04	-139	-1121	7.32	3.94	2.43	3.32	0.20	0.38	0.37	0.49
	2	0.02	-147	-1120	9.25	5.35	2.96	4.00	0.25	0.32	0.28	0.83
	3	0.03	-147	-1140	7.91	4.52	2.52	3.22	0.30	0.37	0.36	0.65
6%	**1**	0.11	-191	-1067	13.37	9.38	4.80	7.06	0.16	0.23	0.22	0.17
	2	0.06	-167	-1070	9.89	5.67	3.24	4.31	0.24	0.31	0.27	0.18
	3	0.06	-180	-1059	9.42	7.71	3.66	5.23	0.21	0.28	0.29	0.15
12%	**1**	0.38	-202	-1022	13.48	9.72	6.08	7.12	0.17	0.22	0.23	0.14
	2	0.31	-183	-1010	10.77	9.06	3.76	5.11	0.26	0.31	0.37	0.13
	3	0.32	-207	-1050	11.47	9.72	4.58	6.21	0.18	0.23	0.21	0.12
18%	**1**	0.41	-216	-1005	15.72	9.98	6.26	7.26	0.17	0.23	0.23	0.14
	2	1.15	-227	-970	12.73	10.63	4.44	6.08	0.17	0.24	0.24	0.15
	3	0.51	-209	-1040	14.48	10.65	4.73	6.51	0.17	0.23	0.23	0.15
21%	**1**	2.56	-273	-1001	19.44	10.24	6.59	7.62	0.17	0.23	0.24	0.14
	2	3.98	-240	-880	15.35	11.12	4.93	7.07	0.17	0.22	0.20	0.16
	3	2.50	-273	-1030	15.53	11.30	5.41	7.60	0.18	0.23	0.23	0.16

Table B-12. Corrosion and film semiconductor data for as-received carbon steel bars tested in pore solution, with the N_x and d_x values defined in Figure 6-2.

Chloride addition		**Electronic properties**										
		i_{CORR} (mA/m^2)	E_{CORR} (mV$_{SCE}$)	E_{FB} (mV$_{SCE}$)	N_1	N_2 (10^{21} cm^{-3})	N_3 (10^{21} cm^{-3})	N_4 (10^{21} cm^{-3})	d_1	d_2 (nm)	d_3 (nm)	d_4 (nm)
0%	**1**	0.19	-161	-694		56	15	7		0.06	0.18	0.022
	2	0.28	-143	-637		67	20	9		0.06	0.11	0.083

	3	0.22	-159	-613		25	13	5		0.11	0.20	0.139
0.6%	**1**	1.01	-170	-710		183	98	34		0.04	0.07	0.025
	2	1.10	-181	-651		328	153	53		0.01	0.04	0.011
	3	1.03	-192	-624		295	132	41		0.02	0.05	0.017
1.2%	**1**	1.39	-252	-713		665	295	99		0.01	0.03	0.004
	2	2.50	-280	-707		551	299	89		0.02	0.04	0.009
	3	2.20	-311	-658		535	246	99		0.01	0.03	0.010
1.8%	**1**	2.4	-352	-701		675	268	103		0.01	0.03	0.006
	2	3.1	-341	-710		771	215	111		0.03	0.04	0.035
	3	3.3	-324	-676		711	321	112		0.01	0.03	0.006
2.4%	**1**	5.2	-391	-704		918	456	145		0.01	0.03	0.004
	2	4.2	-381	-680		1379	551	194		0.00	0.02	0.002
	3	4.5	-367	-684		736	327	124		0.01	0.03	0.009

C. Appendix information from the published journal in Chapter 8

Figures C1 – C6 present the corrosion potentials and current densities of the three batches of UNS S32205 and UNS S32304 bars from all three manufacturers.

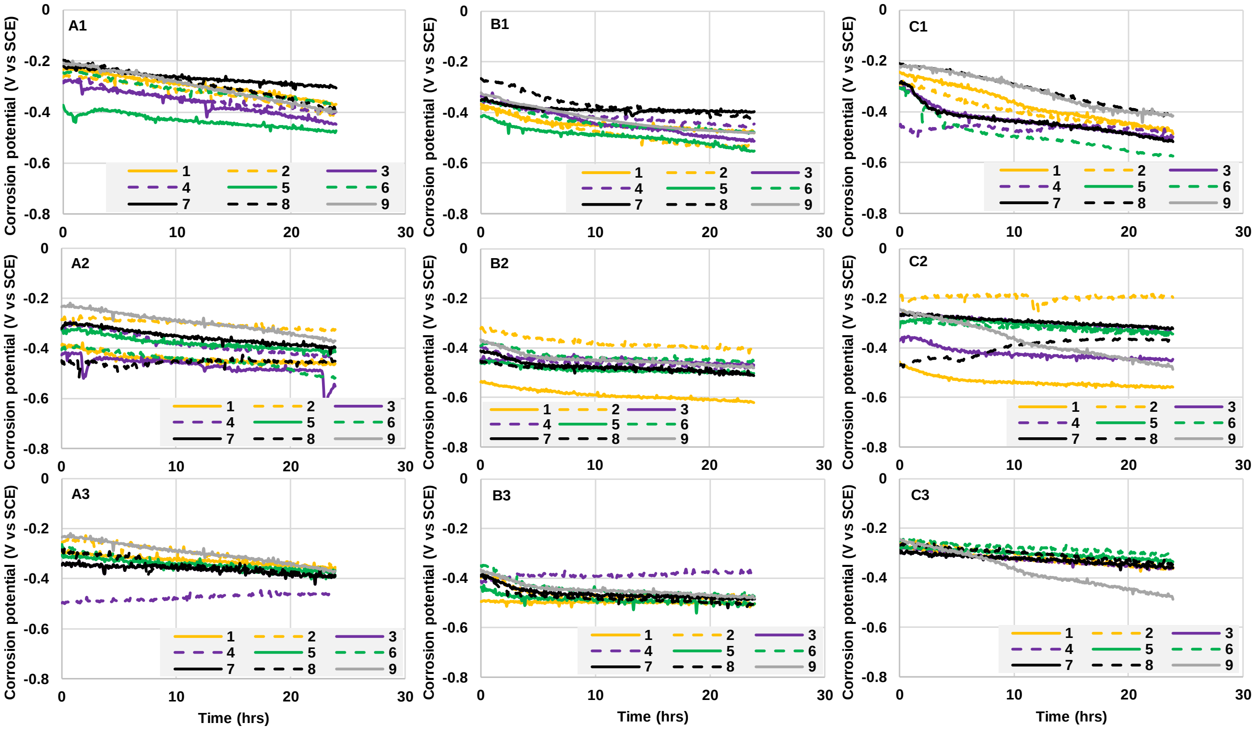

Figure C-1. The corrosion potentials of all batches (1,2,3) of the UNS S32205 alloys from all manufacturers (A, B, C).

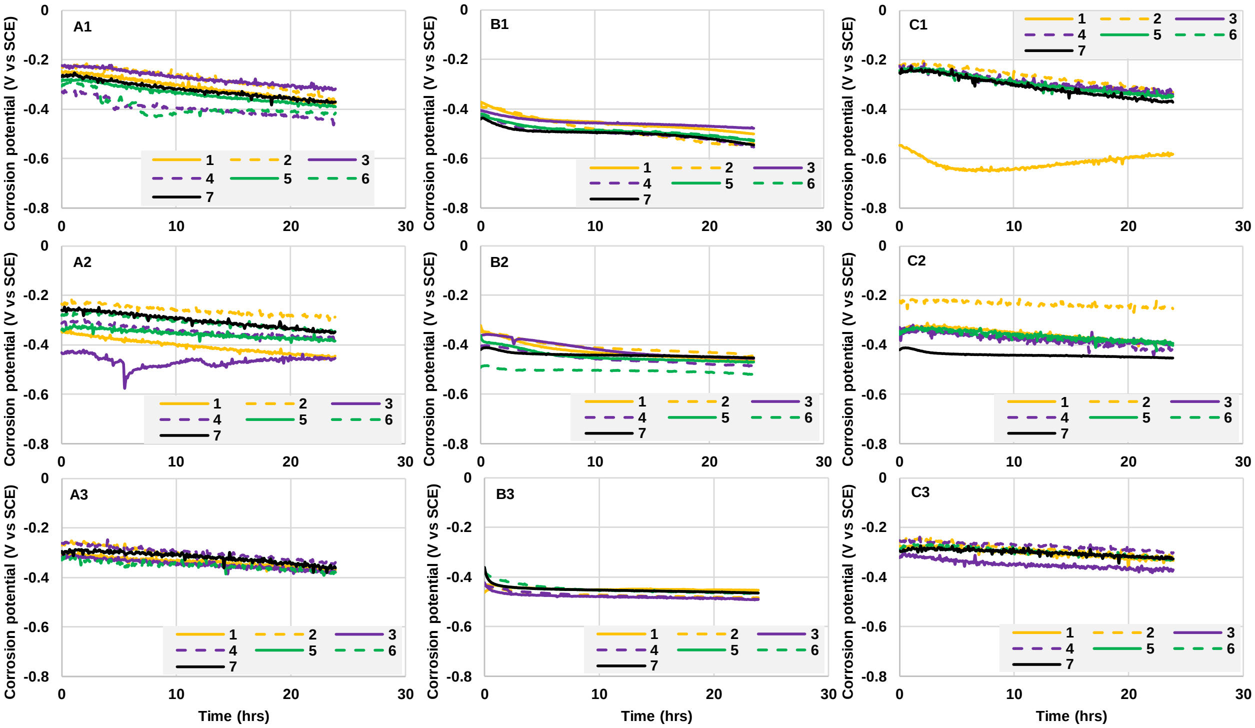

Figure C-2. The corrosion potentials of all batches (1,2,3) of the UNS S32304 alloys from all manufacturers (A, B, C).

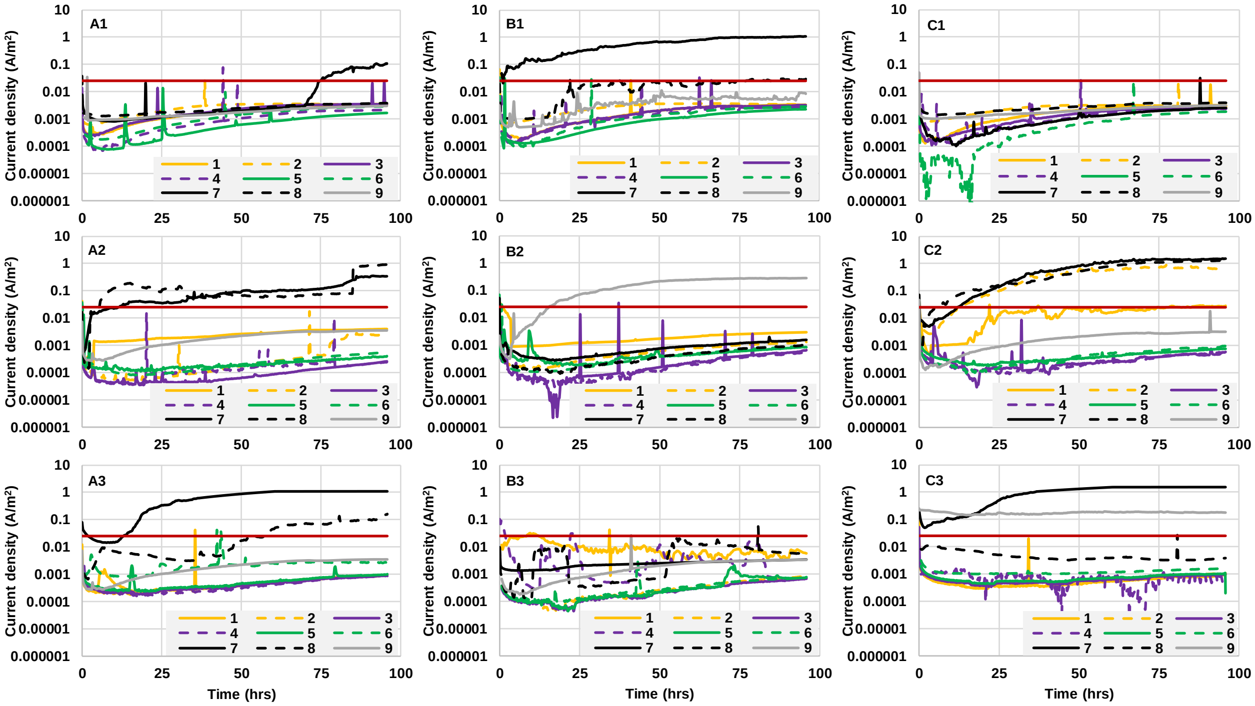

Figure C-3. The current densities of all batches (1, 2, 3) of the UNS S32205 alloys from all manufacturers (A, B, C).

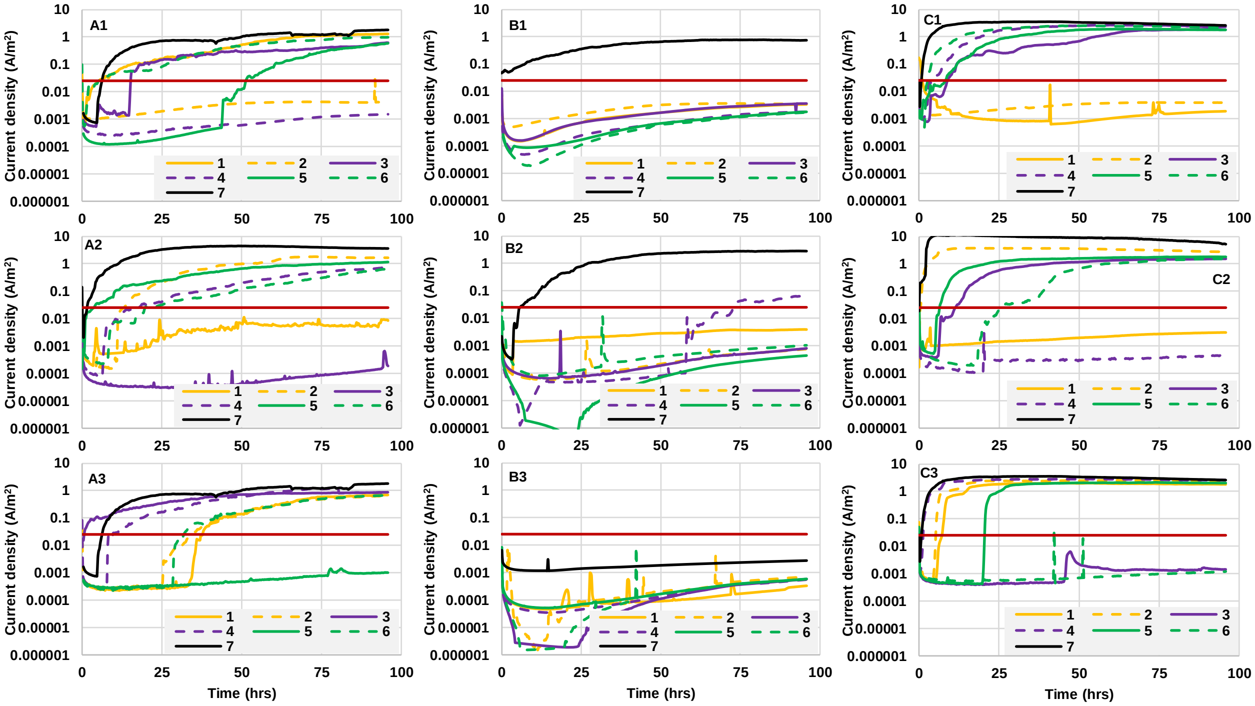

Figure C-4. The current densities of all batches (1, 2, 3) of the UNS S32304 alloys from all manufacturers (A, B, C).